Volume 48 | Number 4 | 21 February 2019 | Pages 965–1230

Chem Soc Rev

Chemical Society Reviews

rsc.li/chem-soc-rev

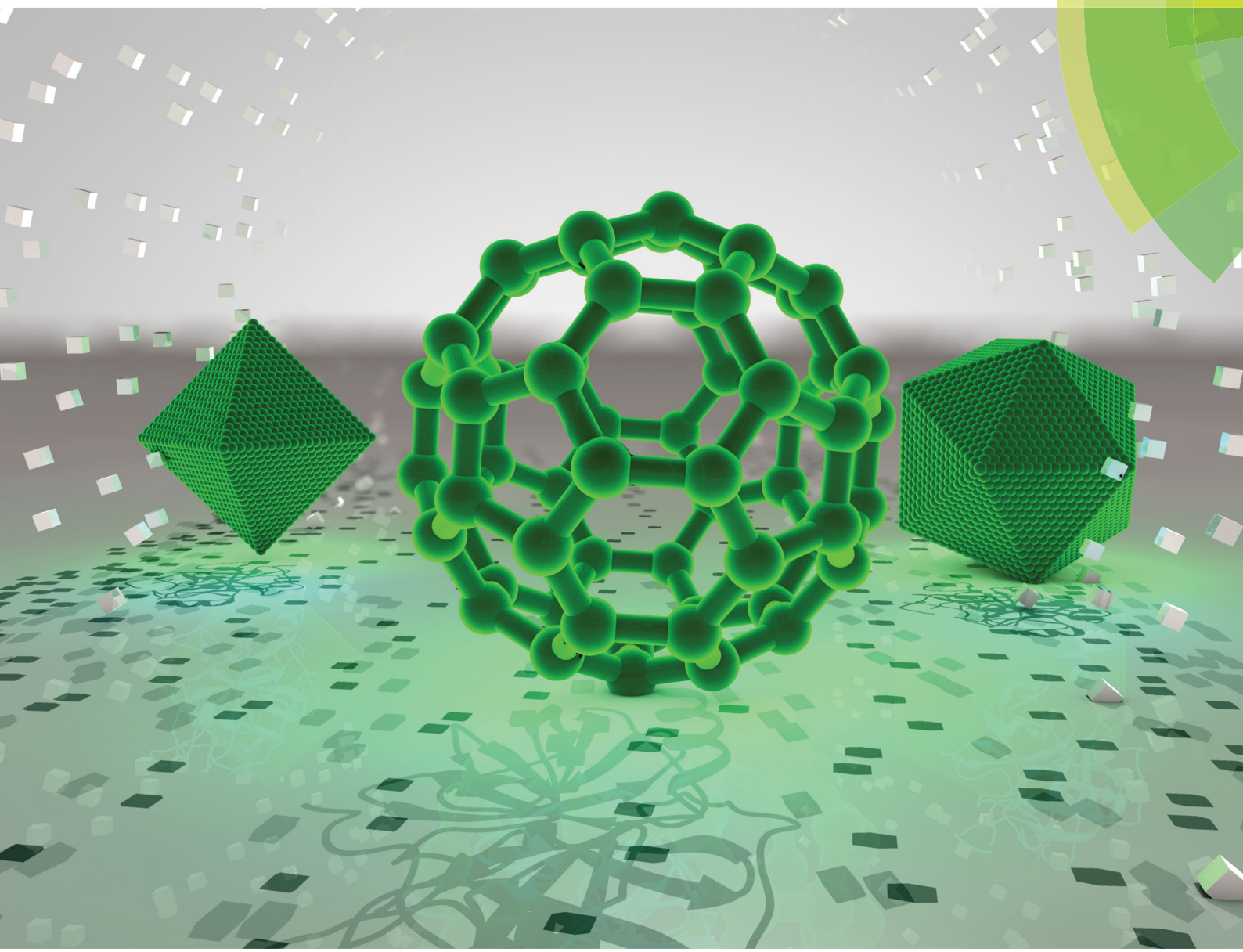

ISSN 0306-0012

ROYAL SOCIETY OF CHEMISTRY | Celebrating IYPT 2019

REVIEW ARTICLE

Hui Wei *et al.*

Nanomaterials with enzyme-like characteristics (nanozymes): next-generation artificial enzymes (II)

Chem Soc Rev

REVIEW ARTICLE

View Article Online
View Journal | View Issue

Cite this: *Chem. Soc. Rev.*, 2019, **48**, 1004

Nanomaterials with enzyme-like characteristics (nanozymes): next-generation artificial enzymes (II)†

Jiangjiexing Wu,[ab] Xiaoyu Wang,[a] Quan Wang,‡[a] Zhangping Lou,‡[a] Sirong Li,‡[a] Yunyao Zhu,‡[a] Li Qin[a] and Hui Wei *[abc]

Received 30th August 2018

DOI: 10.1039/c8cs00457a

rsc.li/chem-soc-rev

Nanozymes are nanomaterials with enzyme-like characteristics (*Chem. Soc. Rev.*, 2013, **42**, 6060–6093). They have been developed to address the limitations of natural enzymes and conventional artificial enzymes. Along with the significant advances in nanotechnology, biotechnology, catalysis science, and computational design, great progress has been achieved in the field of nanozymes since the publication of the above-mentioned comprehensive review in 2013. To highlight these achievements, this review first discusses the types of nanozymes and their representative nanomaterials, together with the corresponding catalytic mechanisms whenever available. Then, it summarizes various strategies for modulating the activity and selectivity of nanozymes. After that, the broad applications from biomedical analysis and imaging to theranostics and environmental protection are covered. Finally, the current challenges faced by nanozymes are outlined and the future directions for advancing nanozyme research are suggested. The current review can help researchers know well the current status of nanozymes and may catalyze breakthroughs in this field.

1. Introduction

The intrinsic limitations (such as high cost, low stability, and difficulty in storage) of natural enzymes have stimulated the emergence and development of various enzyme mimics (also called "artificial enzymes"). Among them, nanozymes have emerged as the next generation of enzyme mimics since the unexpected discovery of magnetic Fe_3O_4 nanoparticles (NPs) with peroxidase-like activities in 2007.[1] "Nanozymes" were defined as "nanomaterials with enzyme-like characteristics" in the first comprehensive review on nanozymes published in 2013.[2] Inspired by nature but advantageous over natural enzymes, nanozymes are generally low-cost, stable, and mass-produced. Moreover, the unique physicochemical properties of nanomaterials not only endow nanozymes with multiple functionalities but also provide more possibilities for rational design and future applications. During the past five years, benefitting from the quick development of nanotechnology, biotechnology, catalysis science, and computational design, significant advances have been achieved in imitating new enzymatic activities with high-performance nanomaterials, regulating the nanozyme activities, elucidating the catalytic mechanisms, and broadening potential applications (Fig. 1). Up to now, there are more than 200 research laboratories around the world working on nanozymes actively, evidencing the importance and impact of the field. Though numerous excellent reviews have been published by other researchers and us since 2013, most of those reviews were mainly focused on certain specific topics of nanozymes while the rest were short ones (such as minireviews or topical reviews).[3–83] Therefore, a comprehensive review is needed to summarize and analyze all the progress, especially the achievements from more than 1100 research papers published in the past five years (Fig. 2). Such an analysis is necessary to help researchers understand nanozymes better and in turn to advance this field. In this review, we intend to cover various types of nanozymes, activity and selectivity regulation of nanozymes, and the applications of nanozymes such as in biomedical sensing, therapeutics, and environmental remediation.

[a] *Department of Biomedical Engineering, College of Engineering and Applied Sciences, Nanjing National Laboratory of Microstructures, Jiangsu Key Laboratory of Artificial Functional Materials, Nanjing University, Nanjing, China. E-mail: weihui@nju.edu.cn; Web: http://weilab.nju.edu.cn; Fax: +86-25-83594648; Tel: +86-25-83593272*

[b] *State Key Laboratory of Coordination Chemistry, School of Chemistry and Chemical Engineering, Nanjing University, Nanjing, China*

[c] *State Key Laboratory of Analytical Chemistry for Life Science, School of Chemistry and Chemical Engineering, Nanjing University, Nanjing, China*

† Electronic supplementary information (ESI) available: (a) Additional tables summarize the current enzyme-mimicking nanomaterials (Tables S1–S5), multi-enzyme-mimicking nanozymes (Table S6), multi-functional nanozymes (Table S7), nanozymes for sensing (Tables S8–S10), and kinetic parameters of nanozymes (Tables S11–S13). (b) Theses on nanozymes are provided in Table S14. (c) References about nanozymes are provided as an EndNote file. (d) A more detailed timeline is available online: http://weilab.nju.edu.cn/research/nanozymetimeline.html. See DOI: 10.1039/c8cs00457a

‡ Q. Wang, Z. Lou, S. Li, and Y. Zhu contributed equally.

Finally, the challenges and future perspectives of nanozymes are also discussed for future investigation in the field. Note: as this review is an update of our first comprehensive review published in 2013, some detailed discussions illustrated before are not covered here, which could refer to the review in 2013.

2. Types of nanozymes

As mentioned in the review in 2013, four types of redox enzymes had been mimicked by nanomaterials, including peroxidase, oxidase, catalase, and superoxide dismutase (SOD). And exploration of new types of nanozymes was brought up as an important topic in the field. Since then, great efforts have been devoted to not only redox reactions but also others such as hydrolysis. Hundreds of nanomaterials have been discovered with enzyme-like activities, and here we only discuss a few representative nanomaterials for each type of enzymatic reactions. Other nanomaterials and their enzyme-like activities are summarized in Tables S1–S5 (ESI†).

2.1 Peroxidase mimics

2.1.1 Iron based. In 2007, the Yan group firstly discovered the intrinsic peroxidase-mimicking properties of Fe_3O_4 magnetic

Jiangjiexing Wu

Jiangjiexing Wu received her bachelor's degree (2009) and PhD degree (2014) from Tianjin University under the supervision of Professors Wei Li and Yi Lu. She then joined Professor Hui Wei's lab as a research scientist. Her research focuses on the design and synthesis of functional nanomaterials (such as nanozymes) and their biomedical applications.

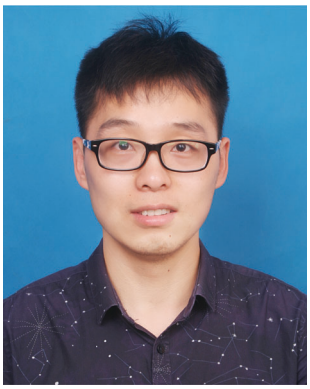

Xiaoyu Wang

Xiaoyu Wang received his bachelor's degree in Materials Science and Engineering from Nanjing Institute of Technology in 2014. Currently, he is a PhD candidate in Professor Hui Wei's group at Nanjing University. His research interests are focused on the rational design of high performance nanozymes and exploiting their wide applications in biomedicine and bioanalysis.

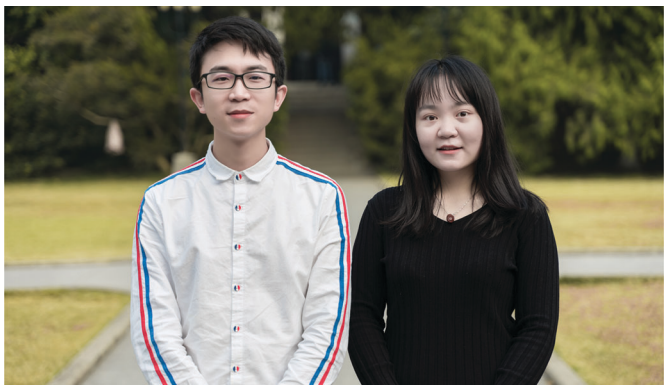

From left to right: Quan Wang and Sirong Li

Quan Wang and Sirong Li are currently pursuing their PhD degree under the supervision of Professor Hui Wei in the College of Engineering and Applied Sciences at Nanjing University. Quan Wang received his BS degree from Wuhan University in 2017, and now his research interests focus on the rational design of nanozymes and discover their potential applications. Sirong Li received her BE degree from Tianjin University in 2016, and carried out undergraduate research with Professor Wenxin Wang at University College Dublin. Now, her research interests focus on the rational design of nanozymes and their biomedical applications.

From left to right: Yunyao Zhu, Li Qin and Zhangping Lou

Zhangping Lou, Yunyao Zhu and Li Qin are currently pursuing their master's degree under the supervision of Professor Hui Wei in the College of Engineering and Applied Sciences at Nanjing University. Zhangping Lou received her Bachelor's Degree from Xiangtan University and carried out the undergraduate research with Dr Yunya Liu in 2016. Now, her current research focuses on carbon-based nanozymes and their biological applications. Yunyao Zhu received her BE degree from Nanjing University in 2017. Now, her research interests focus on the rational design of nanozymes and their biomedical applications. Li Qin received his BS degree in Biomedical Engineering at Nanjing University in 2016. Now, his research interests focus on the rational design of nanozymes and their applications in biosensing.

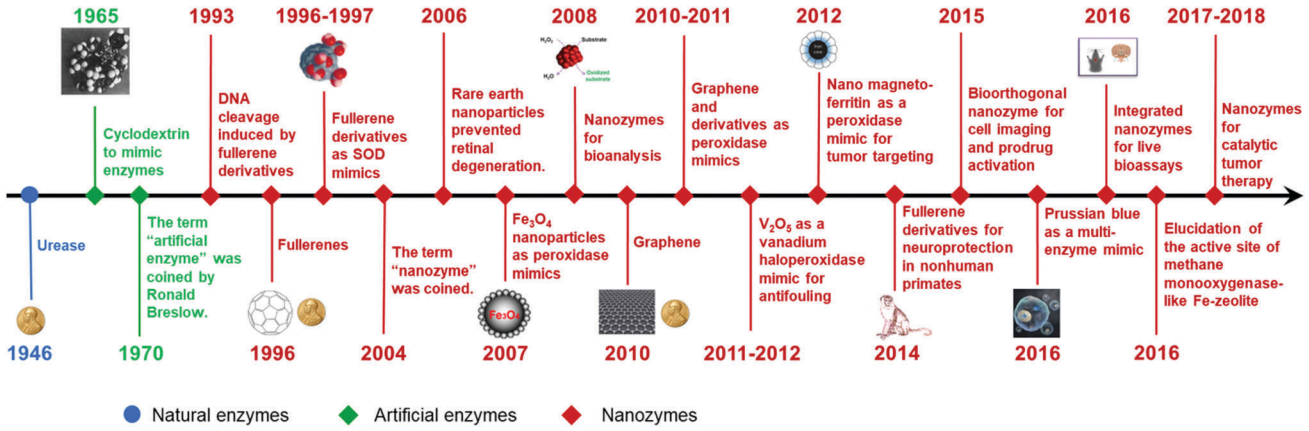

Fig. 1 A brief timeline for the development of nanozymes (natural enzymes and artificial enzymes are listed for comparison). Adapted with permission from ref. 2. Copyright (2013) Royal Society of Chemistry. Note: a more detailed timeline is available online: http://weilab.nju.edu.cn/research/nanozymetimeline.html.

NPs (MNPs), which could oxidize three colorless peroxidase substrates (*i.e.*, TMB (TMB for 3,3′,5,5′-tetramethylbenzidine), diazoaminobenzene, and *o*-phenylenediamine) to their corresponding colored products with the help of H_2O_2. The kinetics studies suggested a ping-pong catalytic mechanism of the MNP nanozymes, and the measured Michaelis–Menten constants indicated higher affinities of the nanozymes to TMB but lower affinities to H_2O_2 than those of horseradish peroxidase (HRP).[1] Later, Wei and Wang applied the Fe_3O_4 MNP-based peroxidase mimics for the detection of both H_2O_2 and glucose.[84] Inspired by the pioneering work, iron oxide-based peroxidase mimics were widely explored and studied, such as Fe_3O_4 (magnetite),[85–101] Fe_2O_3 (hematite),[102–111] and doped ferrites.[112–117] Possible Fenton and/or Haber–Weiss reaction mechanism(s) were proposed for the peroxidase-like iron oxides, where $^{\bullet}OH/HO_2^{\bullet}$ could be involved.[118] By combining the free radicals with the unique magnetic properties of iron oxides, the nanozymes could be used for the degradation of organic pollutants, magnetic resonance imaging, anti-biofouling, and cancer therapy. Thus, during the past five years, the applications of iron oxide nanozymes have been extended from biomedical sensing to environmental remediation and therapeutics, which will be discussed in the Applications section.

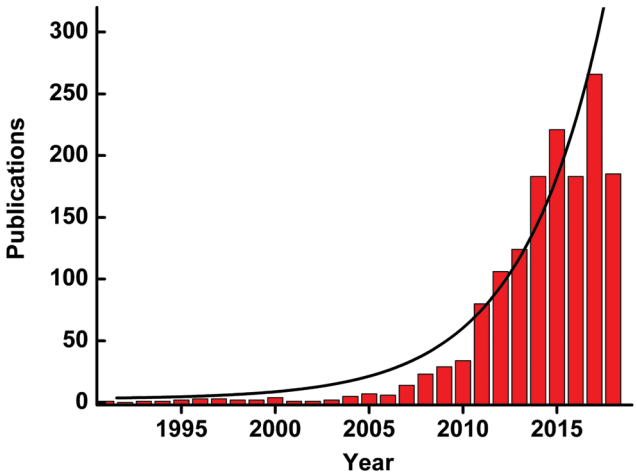

Fig. 2 Number of published papers on nanozymes by the end of May 2018. Data are from the web of science.

Besides the iron oxide nanomaterials, iron chalcogenides (*e.g.*, FeS, Fe_3S_4, FeSe, and FeTe),[119,120] iron phosphates,[121–124] and Prussian blue (PB)[125–128] and its cyanometalate structural analogues (*e.g.*, $Cu_{1.33}[Fe(CN)_6]_{0.667}$, $Fe[Co_{0.2}Fe_{0.8}(CN)_6]$, and $FeCo_{0.67}(CN)_4$)[129] also exhibited excellent peroxidase-like activities. PB ($[Fe(III)Fe(II)(CN)_6]^-$) was an interesting example. In an early study, Karyakin *et al.* compared the catalytic activities of PB and HRP for constructing electrochemical glucose biosensors.[130] Later, they suggested PB as "an artificial peroxidase" in 1998.[131] Recently, the Gu group reported that PB could improve the catalytic activities of Fe_2O_3-based peroxidase mimics through coating.[132] In their further studies, they found that PBNPs themselves also possessed peroxidase-like activities under acidic conditions. The negatively charged PBNPs (zeta potential, −26.1 mV)

Hui Wei

Hui Wei is a Professor at Nanjing University and a Fellow of the Royal Society of Chemistry. He received his BS degree from Nanjing University (advisor: Professor Xinghua Xia) and PhD degree from Changchun Institute of Applied Chemistry, Chinese Academy of Sciences (advisor: Professor Erkang Wang). He then joined Professors Yi Lu's and Shuming Nie's groups for two PostD trainings before he started his independent career at Nanjing University. His research interests are focused on the design and synthesis of functional nanomaterials (such as nanozymes) and the development of new methodologies for analytical and biomedical applications.

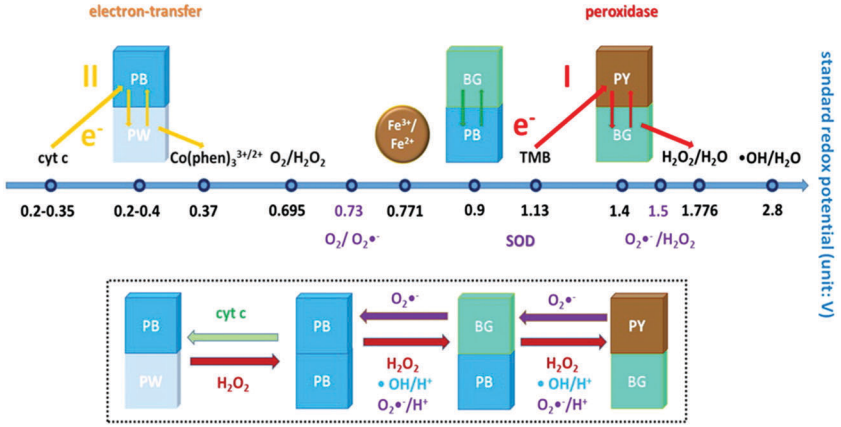

$$H_2O_2 + 2e^- + 2H^+ \rightarrow 2H_2O \quad (1)$$

$$3PB \rightarrow BG + 2e^- \qquad PB \rightarrow PY + e^- \quad (2)$$

$$TMB + H_2O_2 + 2H^+ \xrightarrow{PY} TMB(oxidized) + 2H_2O \quad (3)$$

$$PB + H^+ + {}^{\bullet}OH \rightarrow PY + H_2O \quad (4)$$

Fig. 3 Proposed mechanisms of the multiple enzyme-like activities of PBNPs based on standard redox potentials of different compounds in the reaction systems and reactions involved in peroxidase-mimicking activities. Adapted with permission from ref. 133. Copyright (2016) American Chemical Society.

showed a higher affinity towards TMB than towards ABTS (2,2′-azino-bis(3-ethylbenzothiazoline-6-sulfonic acid)). And with TMB as the substrate, the k_{cat} of PBNPs was 4 times larger than that of Fe_3O_4 NPs. According to the different redox potentials (Fig. 3), the peroxidase-mimicking catalytic mechanisms were illustrated as follows: due to the strong oxidation properties of H_2O_2 under acidic conditions, PY/BG would be first produced through the oxidation of PB by H_2O_2, and then transfer electrons from TMB to H_2O_2 to complete the whole catalytic reaction, as shown in eqn (1)–(3) (PY for Prussian yellow, $[Fe(III)Fe(III)(CN)_6]$; BG for Berlin green, $\{Fe(III)_3[Fe(III)(CN)_6]_2[Fe(II)(CN)_6]\}^-$). An interesting phenomenon was that PB as a peroxidase mimic would scavenge $^{\bullet}OH$ rather than generate $^{\bullet}OH$ *via* the Fenton reaction (eqn (4)). Besides peroxidase-like activities, PB also showed catalase- and SOD-like activities. The multiple enzyme-like activities were mainly dependent on the pH and helpful for therapeutics, and a good case will be provided later in the Applications section.[133]

2.1.2 Vanadium based. In 2011, V_2O_5 nanowire-based peroxidase mimics were first demonstrated by the Tremel group.[134] Later, the particular vanadium haloperoxidase-mimicking activities of V_2O_5 nanowires and their applications in marine anti-biofouling gained a lot of attention.[135] Since then, many studies on peroxidase-like vanadium oxides and vanadium disulfides have been reported.[136–140] And these mimics were used for bioanalysis and therapy. Recently, the glutathione peroxidase (GPx)-like activities of V_2O_5 were discovered by the Mugesh group.[141] They found that monocrystalline V_2O_5 nanowires could eliminate H_2O_2 with the assistance of glutathione (GSH), protecting cells from oxidative damage. Moreover, the GPx-mimicking activities of V_2O_5 nanozymes were not affected by some vanadium haloperoxidase substrates, attributable to the stronger binding affinity and nucleophilic ability of GSH than halides towards the nanozymes. The catalytic activities followed the typical Michaelis–Menten kinetics, with K_m calculated as ~0.11 and ~2.22 mM, and V_{max} of ~0.43 and 0.83 mM min^{-1} for H_2O_2 and GSH, respectively. Further systematic experimental studies speculated the following molecular mechanisms (Fig. 4A): first, the exposed {010} facet of V_2O_5 nanowires may act as the active sites to adsorb and reduce H_2O_2 for generating vanadium peroxido intermediate **1**; then, a second sulfenate-bound intermediate **2** was formed by the nucleophilic attack of GS^- on complex **1**, followed by a quick hydrolytic reaction to convert **2** into glutathione sulfenic acid (**3**, GSOH) and the dihydroxo intermediate **4**; finally, the complex **4** would be oxidized back to intermediate **1** by H_2O_2. If focusing on the GSH participation part, after the aforementioned GS^- attack and GSOH formation, glutathione disulfide (GSSG) would be produced with the help of another GSH. With the addition of glutathione reductase (GR) and nicotinamide adenine dinucleotide phosphate (NADPH), GSSG could be reduced back to GSH. Note, the cleavage of intermediate **2** was similar to the vanadium haloperoxidase-like reaction for removing HOBr from the V–OBr complex, consistent with the previous report by Tremel and co-workers.[135] Moreover, the V_2O_5 nanozymes exhibited a general thiol peroxidase-mimicking activity, catalyzing the

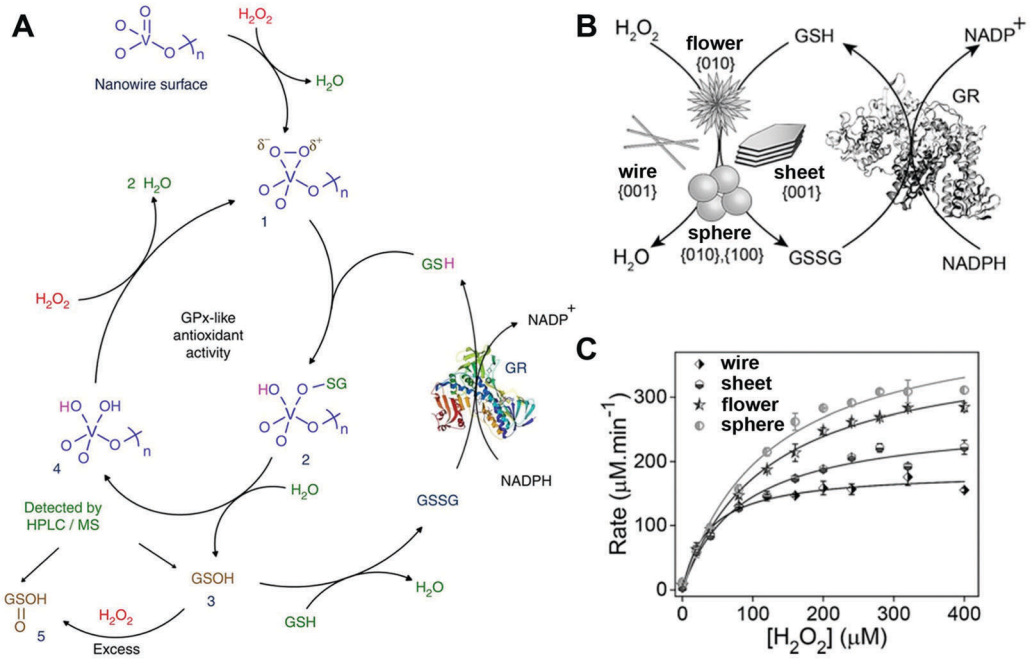

Fig. 4 (A) Proposed molecular mechanism for V_2O_5 nanowires' GPx-mimicking activity. (B) Scheme for GPx-like reaction of four V_2O_5 nanozymes. (C) Michaelis–Menten plot with different concentrations of H_2O_2 for four V_2O_5 nanozymes. (A) Reprinted with permission from ref. 141. Copyright (2014) Nature Publishing Group. (B and C) Adapted with permission from ref. 142. Copyright (2018) John Wiley and Sons.

reduction of H_2O_2 by other thiols such as cysteine, cysteamine, and mercaptoethanol.[141]

In a subsequent study, they identified the catalytic facets on the surface of V_2O_5 nanozymes through a combination of experimental studies and computational simulations. Four different morphologies with different facets of V_2O_5 nanozymes were synthesized, and their GPx-like activities followed the order: only {001} facet bound nanowires < large {001} and minor {010} facets bounded nanosheets < major {010} and minor {001} facets bounded nanoflowers < two major {100}, {010} facets bounded nanospheres (Fig. 4B and C). As mentioned above, interaction with H_2O_2 to form the vanadium peroxido intermediate **1** was the first and crucial step in the whole process, and thus the formation rate of **1** was monitored and compared *via in situ* Raman spectroscopy and theoretical calculations. The results showed that {010} and {100} facets possessed higher catalytic activity than the {001} surface because of the unsaturated coordination of the surface vanadium atoms.[142]

2.1.3 Noble metal based. Many noble metal nanomaterials, such as Au,[143–154] Ag,[155–160] Pt,[161–174] Pd,[175–177] and their multimetallic NPs,[178–193] have been reported as peroxidase mimics and widely used for biosensors, antibiosis, and therapy. For example, Xia, Nie, and co-workers synthesized Pd–Ir NPs with excellent peroxidase-like activities, and the catalytic efficiency was nearly 28 times higher than that of HRP. They further developed an enzyme-linked immunosorbent assay (ELISA) for the detection of disease biomarkers using Pd–Ir nanozymes. A sensitivity at femtogram per mL level for human prostate surface antigen was achieved.[194]

Similar to PBNPs, metal nanomaterials also possess multiple enzyme-like activities under different conditions, such as a peroxidase-like activity under acidic conditions while a catalase-like activity under basic conditions. Detailed computational studies were performed to gain a better understanding of the related mechanisms.[195] Taking Au{111} as an example, the adsorption and decomposition of H_2O_2 under different pH conditions are shown in Fig. 5. In a neutral environment, H_2O_2 could easily adsorb onto the surface without any prevention from H_2O, and then favored a base-like decomposition to H_2O^* and O^* on the surface of metal NPs because of the lowest calculated energies (Fig. 5A). Notably, the high energy barrier of 1.42 eV made O_2 generation from the adsorbed O^* impossible in this condition. For the acidic condition with H pre-adsorbed onto the surface of metal nanomaterials, H_2O_2 could still be adsorbed and take the base-like decomposition pathway to produce adsorbed H_2O^* and OH^*, followed by conversion of OH^* into H_2O^* and O^* on the surface of metal NPs. When the O^* attacked the substrates to abstract H atoms, a peroxidase-mimicking process was completed (Fig. 5B). On the other hand, for the basic condition with OH pre-adsorbed, H_2O_2 would firstly transfer one H to pre-adsorbed OH forming HO_2^* and H_2O^*; subsequently, HO_2^* would give one H to another H_2O_2 and produce H_2O^* and O_2^* at last (Fig. 5C). Therefore, the catalase-like activity could be observed under alkaline conditions. More calculations with other facets of Au (*e.g.*, Au{110} and Au{211}) and other metals (*i.e.*, Ag, Pt, and Pd) demonstrated very similar reaction pathways and pH-dependent enzymatic activities. Both the calculated adsorption energies and activation energies of these noble metals for peroxidase- and

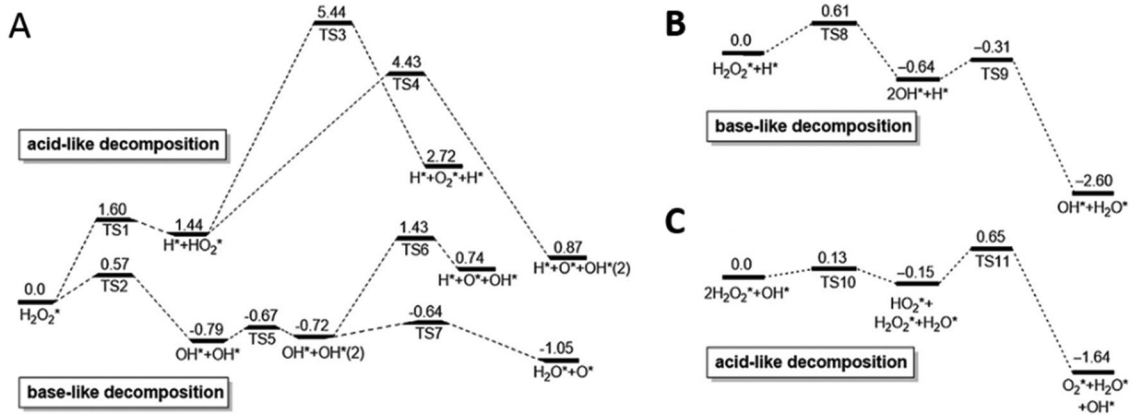

Fig. 5 pH-Switchable enzyme-mimicking activities of noble metals. Calculated reaction energy profiles for H_2O_2 decomposition on the Au{111} surface in neutral (A), acidic (B) and basic (C) conditions are shown as an example (unit: eV). Adapted with permission from ref. 195. Copyright (2015) Elsevier.

catalase-like reactions followed the order Au{111} < Ag{111} < Pt{111} < Pd{111}. Further, they synthesized four nanorods including Au@Ag, Au, Au@Pd, and Au@Pt. They then checked their catalytic activities. The pH-dependent activities of nanorods and the order of Au{111}, Ag{111} < Pt{111}, Pd{111} accorded well with the calculations. Notably, due to the easy oxidation of Ag and the large surface of Pt, the peroxidase-like activities of the nanorods followed the order Au@Ag < Au < Au@Pd < Au@Pt in the experiments.[195]

2.1.4 Carbon based. Another typical nanomaterial as a peroxidase mimic was carbon. Both single-walled carbon nanotubes and graphene oxides were shown to possess peroxidase-like functions in 2010, with pH-, temperature-, and H_2O_2 concentration-dependent activities similar to HRP.[196,197] Inspired by these findings, other carbon-based peroxidase mimics were also explored, such as carbon dots,[198–205] Fe/N-doped carbon,[206–211] carbon nitride,[212–214] and so on.[215–221] For example, graphene quantum dots (GQDs) (*i.e.*, small pieces of graphene) possessed better peroxidase-like activities than large-sized graphene oxides. The GQDs were further used for biological detection. Owing to the generation of •OH during the peroxidase-mimicking catalytic reaction, wound disinfection was carried out with the assistance of GQDs.[222]

As oxygenated functional moieties were needed to help solve the solubility of graphene and derivatives, such as carboxyl groups in nanocarbon oxide, it was necessary to investigate the effect of those functional groups on the peroxidase-mimicking activities.[223,224] Gao, Zhao, and co-workers performed density functional theory calculations and disclosed that the carboxyl groups of nanocarbon oxides were the active sites for decomposing H_2O_2 into •OH, followed by oxidation of peroxidase substrates by •OH.[225] In another study, selective deactivation of functional groups (such as hydroxyl, ketonic carbonyl, and carboxylic groups) was proposed to reveal the roles of the three different groups on GQDs (Fig. 6). Phenylhydrazine (PH), benzoic anhydride (BA), and 2-bromo-1-phenylethanone (BrPE) were used to selectively deactivate the ketonic carbonyl, hydroxyl, and carboxylic groups on GQDs, forming GQD derivatives GQDs-PH, GQDs-BA, and GQDs-BrPE, respectively. According to

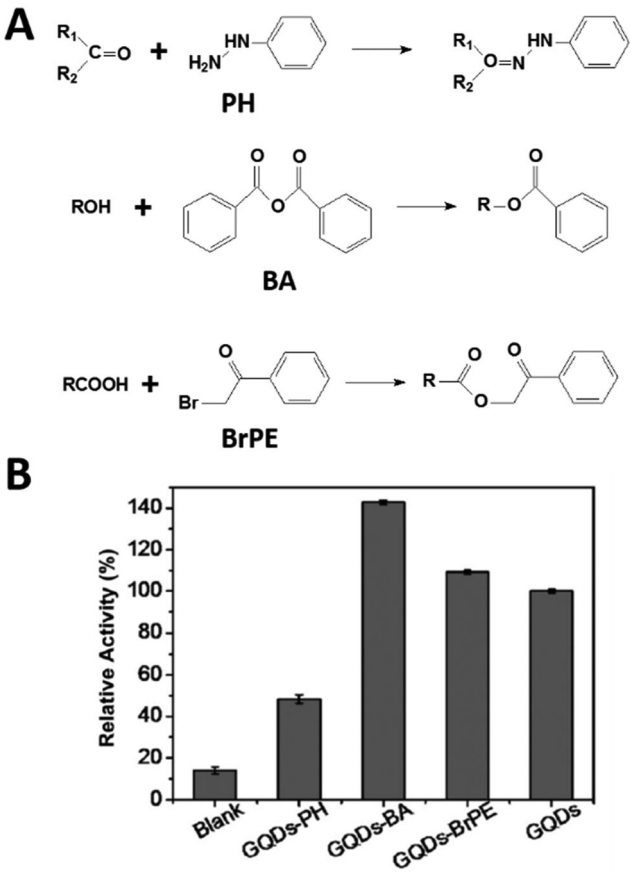

Fig. 6 Deciphering peroxidase-mimicking activities of GQDs. (A) Reactions involved in selectively deactivating functional moieties on GQDs. (B) Relative catalytic activities of GQDs treated with different reagents. Adapted with permission from ref. 226. Copyright (2015) John Wiley and Sons.

the kinetics studies and theoretical calculations of the three GQD derivatives, ketonic carbonyl, carboxylic, and hydroxyl groups were suggested as the catalytic active centers, substrate binding sites, and inhibitors, respectively. Though carboxylic groups could dissociate H_2O_2 to form •OH, the lower catalytic activity for H_2O_2 decomposition but a higher binding affinity to

H_2O_2 than ketonic carbonyl groups made the carboxylic groups as the binding centers.[226] Guided by this principle, in their further studies, the GQDs with abundant carboxyl and carbonyl groups but negligible hydroxyl groups were synthesized from multiwalled carbon nanotubes. As expected, the C=O/COOH-enriched GQDs exhibited five times lower K_m for H_2O_2 and three times higher V_{max} values than those of pristine GQDs. Compared with HRP, the K_m value of the GQDs was one order of magnitude lower, and the V_{max} was comparable.[227] Similar investigations of the three functional groups on carbon nanotubes were also performed, where ketonic carbonyl groups served as active centers, while hydroxyl and carboxylic groups were competitive inhibitors with higher binding affinities to H_2O_2. Owing to the higher binding affinities of carboxylic than hydroxyl groups, the selective deactivation of carboxylic groups with BrPE resulted in the highest peroxidase-like activities of carbon nanotubes.[228]

What's more, numerous studies of carbon-based composites as peroxidase mimics have been reported, such as those involving hemin–graphene, Au nanocluster (NC)–graphene oxide, Au–carbon nitride and so on.[164,229–255] Due to the high stability, large surface area for substrate diffusion and adsorption, and synergistic catalytic activities, these composite nanozymes were widely applied in bioanalysis and therapy (see the Applications section).

2.1.5 Metal–organic framework (MOF) based. Recently, metal–organic frameworks (MOFs) have been widely used as nanozymes for biomedical applications because of their diverse porous structures. By coordinating metal ions/clusters (*e.g.*, Fe and Cu) with organic ligands (*e.g.*, terephthalic acid (H_2BDC) and 1,3,5-benzenetricarboxylic acid (H_3BTC)), MOFs with peroxidase-like catalytic activities could be constructed. Up to now, Material Institute of Lavoisier (MIL) MOFs (*e.g.*, MIL-53, MIL-88, and MIL-101),[256–266] Hong Kong University of Science and Technology (HKUST) MOFs (*e.g.*, HKUST-1),[267] and other MOFs (*e.g.*, Cu-MOFs, Co-MOFs, and Co/2Fe-MOFs)[268–270] have been reported. And the peroxidase-like catalytic process was verified to adopt a Fenton-like mechanism with $^{\bullet}OH$ produced. If the organic linker was replaced by a metalloligand, such as Fe-TCPP (TCPP = tetrakis(4-carboxyphenyl)porphyrin) and hemin, peroxidase-mimicking 3D PCN-222(Fe) (PCN = porous coordination network) MOFs, PCN-600, 2D M-TCPP(Fe) nanosheet MOFs (M = Co, Zn, and Cu) and Cu–hemin MOFs could be fabricated.[268,271–275] For 2D M-TCPP(Fe) MOFs, control experiments using TCPP with other metal ions (such as Zn, Co, Mn, Ni, and Cu) illustrated the important role of Fe in TCPP(Fe) for ensuring the high peroxidase-like activities (Fig. 7A and B). Benefitting from the larger surface area, more exposed active sites, and smaller diffusion barrier, 2D MOFs exhibited higher catalytic activities than the 3D bulk analogues, providing better sensitivity for biomolecule sensing (Fig. 7C).[275]

Another interesting example reported Cu^{2+}-NMOFs (UiO-type MOF NPs, UiO = University of Oslo) as peroxidase mimics. The 2,2′-bipyridine-5,5′-dicarboxylic acid ligand was chosen to bridge Zr^{4+} to form the MOFs. Then bipyridine on the ligand was post-functionalized with Cu^{2+} to provide the catalytic center (Fig. 7D). As shown in Fig. 7E, the dopamine oxidation catalyzed by Cu^{2+} alone or the mixture of Cu^{2+} and bipyridine was much less efficient than that by Cu^{2+}-NMOFs, which evidenced that the catalytic activity was from the synergistic effect of the Cu^{2+}–bipyridine complex. Another possible reason for the elevated activity was the porous structure of the MOF, making dopamine concentrated in the catalytic site.[276] Besides organic ligands, the modifications could also be achieved through the metal nodes. Binding aliphatic diamines onto the unsaturated Fe nodes of MIL-100(Fe) made the surface of MOFs negatively charged, resulting in a higher affinity to positively charged TMB, and thus improved the peroxidase-like activity of the MIL-100(Fe) MOF.[277] Some studies also reported composites of nanoparticles and MOFs as MOF-based nanozymes. On the one hand, the MOF would just serve as a matrix to support nanoparticles, such as PtNPs@UiO-66-NH_2 and AuNPs@MIL-101(Cr),[278–281] and on the other hand, the MOF would not only serve as a support but also catalyze the peroxidase substrate together with nanoparticles, such as Fe_3O_4/MIL-101(Fe) and PdNPs@MIL-88-NH_2(Fe).[282–285] Compared with the individual MOF or the nanoparticles, both cases were demonstrated to enhance the activities of the composites because of the improved stability, stronger adsorption of substrates, and the synergistic effect between the MOF and nanoparticles.

2.1.6 Other nanomaterial based. Besides the representative nanomaterials mentioned above, a large number of other nanomaterials have also been reported to exhibit peroxidase-like activities.[286–343] For example, $Cu(OH)_2$ supercages were reported to mimic peroxidase by the Tan group.[344] With amorphous $Cu(OH)_2$ nanoparticles as the precursors, they added ammonia to transform Cu^{2+} from NPs to 1D nanoribbons, and then assembled nanoribbons into 3D nanocages (Fig. 8A). The high surface area of such a nanocage structure (172 $m^2\ g^{-1}$) made more catalytic sites available for H_2O_2, and thus led to a better affinity to H_2O_2 and a higher V_{max} of the peroxidase-mimicking reaction compared to HRP (Fig. 8C). Further, the pH- and temperature-dependent catalytic activities were measured. The results showed that the catalytic activities of $Cu(OH)_2$ could reach 90% between pH 3 and 5 and temperature 20 and 50 °C, with an optimum condition at pH 4.5 and 25 °C. Moreover, such nanocages could be recycled and retained 75% of the catalytic efficiency after 3 cycles.[344]

In addition, graphene-like 2D layered transition-metal dichalcogenides (such as MoS_2 and WS_2 nanosheets) were also demonstrated as peroxidase mimics.[345–351] Further modification with hemin or some metal nanoparticles (*e.g.*, PtAg, PtCu, and PtAu) would help to improve their catalytic activities and expand the biomedical applications.[352–360]

2.2 Oxidase mimics

Natural oxidases can catalyze the oxidation of a substrate with the assistance of molecular oxygen (or other oxidizing reagents) into oxidized products and $H_2O/H_2O_2/O_2^{\bullet-}$. Up to now, several nanomaterials have been reported to act as oxidases.[361–385] The recent progress in oxidase mimics, especially the exploration of other specific oxidase substrates besides model substrates (*i.e.*, TMB and ABTS), is highlighted below.

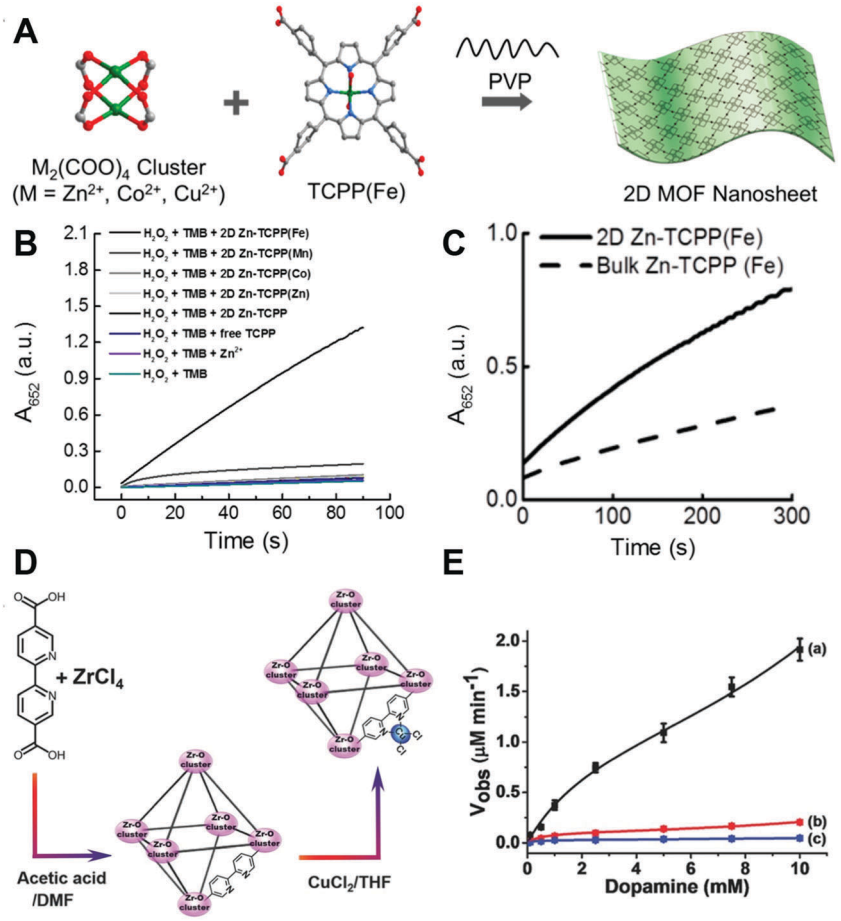

Fig. 7 (A) Scheme showing the surfactant-assisted bottom-up synthesis of 2D MOF nanosheets. (B) Kinetic plots of time-dependent absorbance at 652 nm of reactions catalyzed by different 2D MOFs. (C) Kinetic curves plotting the time-dependent UV-visible absorbance at 652 nm of reactions catalyzed by 2D and 3D bulk Zn-TCPP(Fe) MOFs, showing the different catalytic properties. (D) Synthesis of the Cu^{2+}-functionalized Zr^{4+}-5,5′-bipyridine carboxylate-bridged MOF NPs. (E) Rates of the oxidation of dopamine to aminochrome as a function of dopamine concentration by the Cu^{2+}-NMOFs and the respective control systems: (a) Cu^{2+}-NMOFs 20 μg mL^{-1}, (b) Cu^{2+} ions and the bipyridine ligand, each with a concentration of 17.3×10^{-6} M (at a similar molar ratio to those of the Cu^{2+}/bipyridine ligand present in the NMOFs). (c) Cu^{2+} ions only, 17.3×10^{-6} M. In all experiments 10×10^{-3} M H_2O_2 was used. (A–C) Adapted with permission from ref. 275. Copyright (2017) American Chemical Society. (D and E) Adapted with permission from ref. 276. Copyright (2018) John Wiley and Sons.

2.2.1 Gold based. Though metal nanomaterials were widely used for catalyzing reactions, still the discovery of either carbon-supported gold or unsupported citrate-coated AuNPs (with an average diameter of 3.5 nm) with glucose oxidase (GOx)-mimicking activities was surprising and unexpected.[386,387] Further kinetics measurements suggested an Eley–Rideal mechanism for the AuNP-based oxidase mimics.[388] As shown in Fig. 9A, the hydrated glucose anion first adsorbed onto the surface of gold, forming negative gold species. Then the negative gold species would activate dissolved oxygen through nucleophilic attack, and generate a dioxogold intermediate. Finally, gluconic acids and H_2O_2 were produced. The rate determining step was the oxidation of glucose by oxygen from the liquid phase, and two electron-transfer from glucose to oxygen was supposed to participate.[389] Since the discovery of AuNPs as GOx mimics, other supported gold (*e.g.*, Au/Al_2O_3, Au/TiO_2, and Au/ZrO_2)[390–394] and gold-containing bimetallic/trimetallic nanoparticles[395,396] have also been demonstrated as GOx mimics. For instance, crown-jewel-structured Au/Pd NCs with active Au atoms decorated on PdNCs could catalyze the oxidation of glucose. Such a unique structure endowed Au with a highly negative charge density, facilitating the electron transfer from Au to O_2 with hydroperoxo-like active species generated. The active species were important in glucose oxidation, thus ensuring a greater catalytic activity of crown-jewel-structured Au/Pd NCs than monometallic Au, Pd, and even AuPd alloy.[397]

Recently, the GOx-mimicking catalytic process was monitored through plasmonic imaging of single-particle catalysis (Fig. 9B). A halo-like structure consisting of both 50 nm large AuNPs and 13 nm small AuNPs was fabricated through DNA-directed assembly. Such a structure would not only provide a high catalytic activity but also ensure a strong electromagnetic field at the interface of two adjacent AuNPs, benefiting the monitoring of small AuNPs' change during the catalysis. An initial red-shift of 2.52 nm, a fast blue-shift of 6.88 nm and then a slow red-shift of 3.53 nm were observed corresponding to the

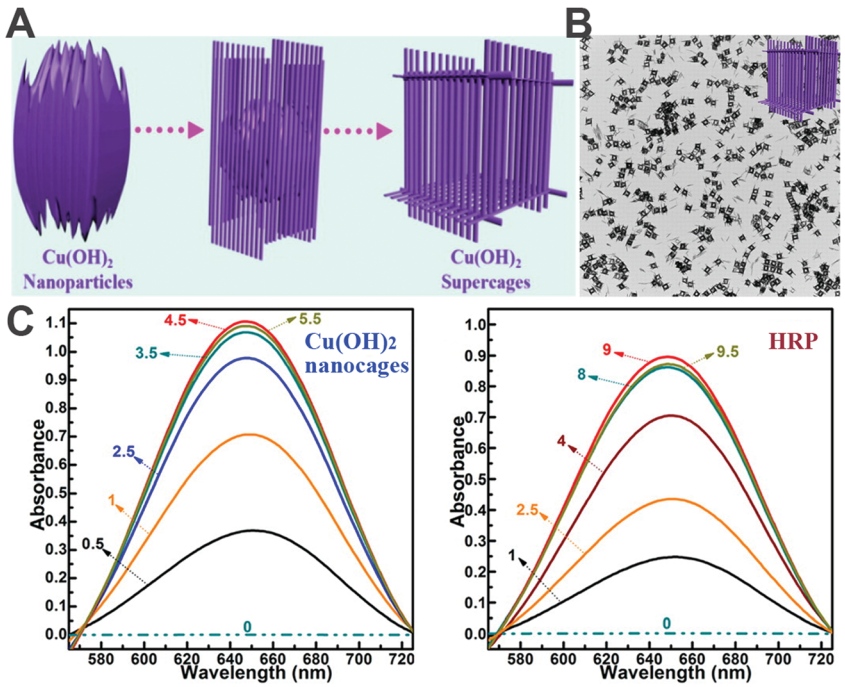

Fig. 8 (A) Schematic illustration of the synthesis process of $Cu(OH)_2$ supercages. (B) Characterization of $Cu(OH)_2$ supercages. (C) Absorption spectra of the oxidation catalysis process (min) of $Cu(OH)_2$ nanocages and HRP. Adapted with permission from ref. 344. Copyright (2015) American Chemical Society.

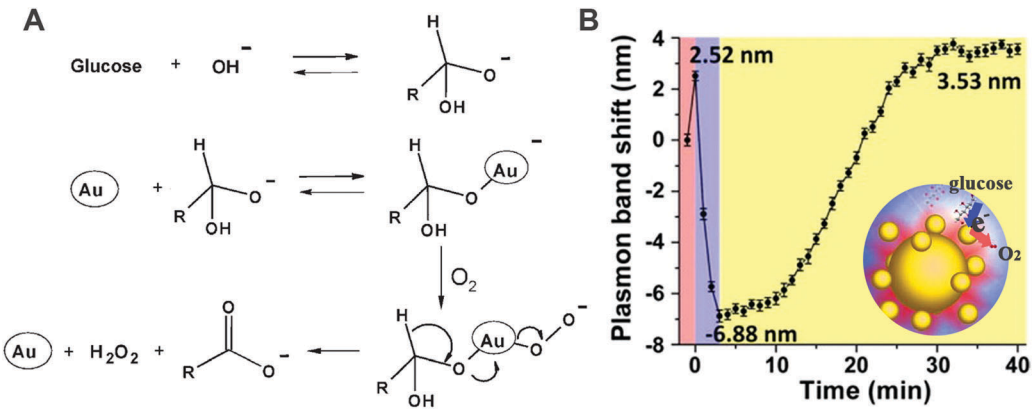

Fig. 9 (A) Proposed molecular mechanism for the GOx-like activity of AuNPs. (B) Plasmonic band peak shifts of one Au nanohalo during the GOx-like catalytic reaction. (A) Reprinted with permission from ref. 389. Copyright (2006) John Wiley and Sons. (B) Adapted with permission from ref. 398. Copyright (2015) American Chemical Society.

first adsorption of glucose, quick charging of small AuNPs, and then retarded discharging of small AuNPs with electrons transferred to O_2. After the dissolved O_2 was dissipated, O_2 in air would redissolve again and diffuse to the surface of small AuNPs, therefore leading to a slow discharging process.[398]

2.2.2 Copper based. Copper containing nanoparticles were also widely explored as oxidase mimics. For instance, GOx-mimicking Cu_2O/polypyrrole composites were reported to catalyze the oxidation of glucose to generate H_2O_2 in basic conditions (0.5 M NaOH). Though high glucose oxidation activities of Cu_2O/polypyrrole composites ensured glucose detection, still the condition for this reaction should be further optimized to a physiological condition for wider applications.[399]

Laccase can oxidize several substrates (*e.g.*, polyphenols, polyamines, and aryl diamines) with oxygen to the oxidized products and H_2O. Since copper ions are the active centers in natural laccase, a few copper-based nanomaterials were designed and synthesized to mimic a laccase. In 2015, Meng, Tang, and co-workers reported one-pot synthesis of copper-containing carbon dots as a laccase mimic. To prepare Cu–carbon dots, the poly(methacrylic acid) sodium salt was chosen to generate carbon dots and to retain copper through a hydrothermal synthesis strategy. The synthesized Cu–carbon dot was around 10 nm, emitted blue fluorescence at 460 nm, and could oxidize the laccase substrate *p*-phenylenediamine (PPD) with oxygen, as shown in Fig. 10A. Comparison of the

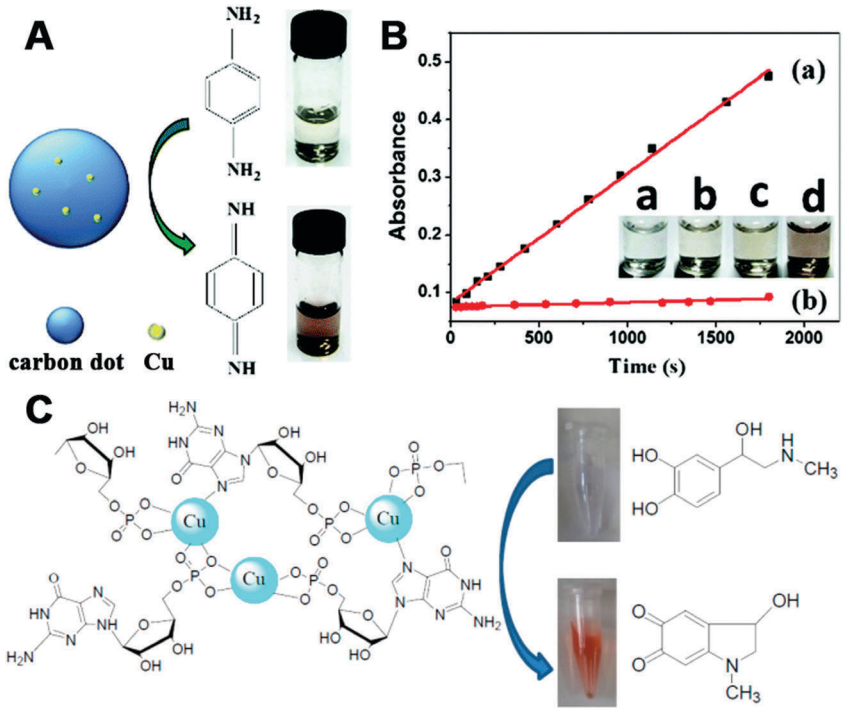

Fig. 10 (A) Schematic illustration of laccase-like catalytic color reaction of Cu–carbon dots with the substrate PPD. (B) Time-dependent absorbance changes at 495 nm of PPD in Cu–carbon dots (a) or carbon dots (b) solutions. Inset: Images of oxidation reaction of PPD. From left to right is Cu–carbon dot solution (a), 10 mM PPD solution (b), 10 mM PPD solution with carbon dots (c) and 10 mM PPD solution with Cu–carbon dots (d). (C) Scheme of Cu^{2+} reacting with GMP to form the laccase mimics. (A and B) Reprinted with permission from ref. 400. Copyright (2015) Royal Society of Chemistry. (C) Adapted with permission from ref. 401. Copyright (2017) American Chemical Society.

catalytic activities between Cu–carbon dots and carbon dots demonstrated the important role of copper in such a catalytic reaction (Fig. 10B). Further applications for PPD removal and hydroquinone detection were performed with the fluorescent Cu–carbon dot nanozymes, which made such a laccase mimic promising in environmental remediation and biological detection.[400]

Another multicopper laccase-mimicking nanozyme was constructed by coordinating nucleotides with copper to form amorphous MOFs, which could catalyze several laccase substrates such as phenol, hydroquinone, naphthol, catechol, and epinephrine (Fig. 10C).[401] Control experiments revealed that three nucleotides including guanosine 5′-monophosphate (GMP), adenosine 5′-monophosphate (AMP), and cytidine 5′-monophosphate (CMP) could be used as the ligands, while only copper ions as metal centers possessed such catalytic activity rather than other metal ions. Among these, Cu/GMP with the best performance was chosen for further mechanism studies and applications. By measuring the catalytic activities of Cu/guanosine and Cu/phosphate, it was suggested that the coordination between Cu and guanosine contributed to the catalytic reaction. Later, thorough kinetics studies of Cu/GMP and laccase with the same mass concentration showed a comparable affinity to the substrate, but a higher catalytic activity of Cu/GMP than that of laccase. And Cu/GMP also showed a better stability over pH 3–9 and temperature 30–90 °C, a high ionic strength of 500 mM NaCl, and long-term storage for 9 days. Finally, the analysis of epinephrine with Cu/GMP was nearly 16 times more sensitive and 2400 times more cost-effective (taking the price of GMP into account) than with laccase. Though some indirect evidence (such as no H_2O_2 generated during the catalysis) was provided, still, more detailed characterization about the four-electron reduction of O_2 to H_2O should be performed to prove laccase-like activity in the future.[401] Notably, non-copper-containing nanomaterials could also possess laccase-mimicking activity. For example, cerium oxide nanoparticles (nanoceria) could catalyze the oxidation of TMB to oxTMB and H_2O without H_2O_2 generation, suggesting the laccase-like activity of nanoceria (Fig. 11).

Besides laccase, cytochrome *c* oxidase (C*c*O) is another interesting enzyme where copper is involved. During the oxidation process, cytochrome *c* (Cyt *c*) would donate electrons to C*c*O and form a complex with C*c*O, accompanied by reduction

$$O_2 + Ce^{3+}(CeO_2) \longrightarrow O_2^{\bullet-} + Ce^{4+}(CeO_2) \quad (1)$$

$$O_2^{\bullet-} + TMB_{red} \longrightarrow H_2O + TMB_{ox} \quad (2)$$

$$CeO_2 + TMB_{red} \longrightarrow Ce_2O_3 + TMB_{ox} \quad (3)$$

$$Ce_2O_3 + O_2^{\bullet-} + 2H^+ \longrightarrow CeO_2 + H_2O \quad (4)$$

Fig. 11 Proposed mechanism for the laccase-like activity of nanoceria. Reprinted with permission from ref. 402. Copyright (2016) American Chemical Society.

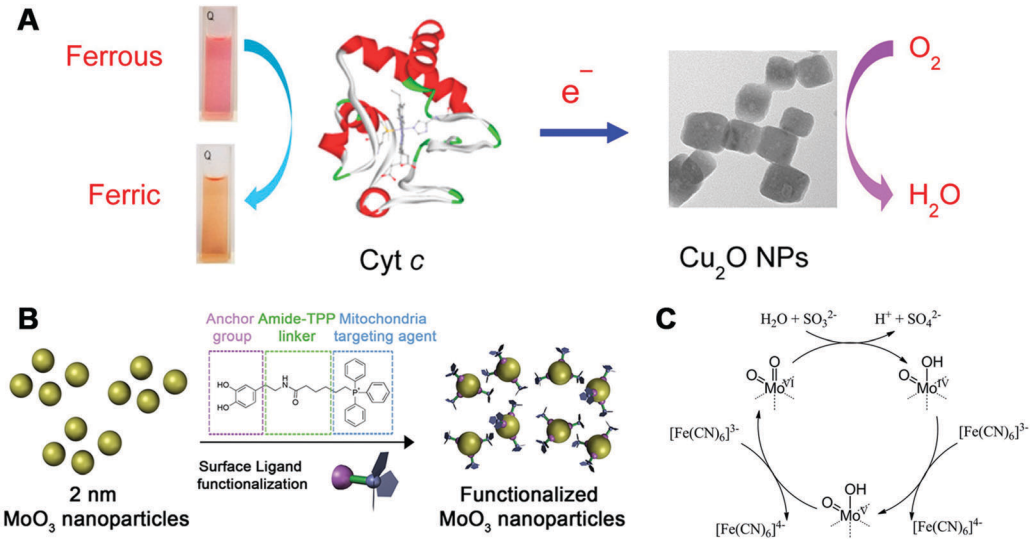

Fig. 12 (A) Schematic illustration of C*c*O-like activity of Cu_2O NPs. (B) Surface functionalization of 2 nm MoO_3 NPs with a ligand containing dopamine as the anchor group and TPP as the mitochondria targeting agent. (C) Proposed catalytic mechanism of sulfite oxidase-mimicking MoO_3 NPs. (A) Reprinted with permission from ref. 403. Copyright (2017) American Chemical Society. (B and C) Reprinted with permission from ref. 404. Copyright (2014) American Chemical Society.

of oxygen to water at the heme-copper center. Lin, Wang, and co-workers found that cuprous oxide nanoparticles (Cu_2O NPs) exhibited C*c*O-mimicking activities, which could catalyze Cyt *c* from the ferrous state to ferric state with the assistance of oxygen (Fig. 12A). Detailed UV-visible spectroscopy, X-ray diffraction, and other experimental studies disclosed the C*c*O-like catalytic mechanisms as follows: first, it was the Cu_2O NPs rather than the leached copper ions that oxidized Cyt *c*; second, neither shape nor valence change was observed for Cu_2O NPs during the oxidation of Cyt *c*; third, oxygen was required and was converted into water at last.[403]

2.2.3 Molybdenum based. Tremel and co-workers reported that molybdenum trioxide nanoparticles (MoO_3 NPs) could mimic sulfite oxidase (SuOx) to convert sulfite to sulfate under physiological conditions.[404] Ultra-small MoO_3 NPs (with an average diameter of 2 nm) were synthesized with high stability in water and serum. Given the fact that SuOx is usually located in the mitochondrial membrane and participates in detoxification processes, the surface of MoO_3 NPs was functionalized through dopamine to link the triphenylphosphonium (TPP) ligand for membrane crossing and mitochondrial targeting (Fig. 12B). The kinetics studies of MoO_3–TPP NPs with SuOx-like activity showed that the K_m value for SO_3^{2-} was 0.59 ± 0.02 mM, which was comparable to those of goat SuOx and human SuOx mutant R160Q, but 1–2 orders of magnitude higher than that of native human SuOx. And the turnover frequency (k_{cat} = 2.78 ± 0.09 s^{-1}) of MoO_3–TPP NPs was similar to that of human SuOx mutant R160Q (k_{cat} = 2.4 s^{-1}), but lower than that of native human SuOx (k_{cat} = 16 s^{-1}). A possible molecular mechanism is proposed in Fig. 12C, where the active Mo(VI) was first reduced to Mo(IV) as a result of sulfite oxidation, and then oxidized back to Mo(VI) *via* two one-electron reduction reactions of ferricyanide. Further studies demonstrated that such low-toxic MoO_3–TPP NPs could selectively accumulate at mitochondria and recover the SuOx activity of SuOx knockdown liver cells, making the MoO_3–TPP NPs promising for therapeutics.[404]

2.2.4 Platinum based. Ferroxidases play a crucial role in transferring and storing iron in cellular environments. Lately, a few studies about PtNPs as ferroxidase mimics to oxidize ferrous ions to ferric ions have been reported. For example, Knez, Zhang, and co-workers utilized light-chain apoferritin as a scaffold to prepare PtNPs. Such a structured nanozyme could regulate the cellular iron homeostasis, which benefited from the ferroxidase-like activities of PtNPs and the ferric ion mineralization ability remaining from the apoferritin.[405] Similarly, instead of using apoferritin as a support, Au nanorods were chosen and Au@Pt nanostructures with PtNPs dispersed on the surface of Au nanorods were synthesized by Wu, Chen, and co-workers. Detailed kinetics studies of Au@Pt-based ferroxidase mimics revealed a slightly lower affinity to Fe^{2+} (K_m = 69.1 ± 3.5 μM) than natural ferroxidase ceruloplasmin (K_m = 22.6 ± 2.6 μM), but a significantly higher catalytic efficiency (k_{cat} = 2.10 × 10^3 s^{-1}) than the natural one (k_{cat} = 1.33 s^{-1}). Further cellular experiments demonstrated that the biocompatible Au@Pt nanozymes could protect cells from oxidative stress.[406]

PtNPs synthesized with oligonucleotides also exhibited laccase-mimicking activities, oxidizing a lot of laccase substrates such as dopamine, catechol, and hydroquinone.[407] Another interesting finding was the oxidation of polyphenols (*e.g.*, quercetin, L-dopa, *r*(−)-epicatechin, and caffeic acid) to their corresponding *o*-quinones through catechol oxidase-mimicking activities of Pt.[408,409] Compared with mushroom tyrosinase, though the affinity of quercetin to PtNPs was lower, the catalytic efficiency of PtNPs was 20 times higher.[409] These results indicated that the possible effect of PtNPs on the

antioxidation activities of polyphenols should be considered in PtNPs' future applications.

Recently, Willner and co-workers reported that in the presence of ascorbic acid and H_2O_2, certain nanomaterials (*e.g.*, CuFe-PB-like NPs, Fe_3O_4 NPs, and AuNPs) could also act as tyrosinase mimics to oxidize L-tyrosine to L-dopa, and subsequently oxidize L-dopa to dopachrome. And the mixture of ascorbic acid and H_2O_2 was evidenced to be essential in the oxidation reaction.[410]

2.3 Catalase mimics

Catalase could efficiently decompose H_2O_2 into water and oxygen. Many nanomaterials such as metals, metal oxides, and PB exhibited catalase-like activities.[411–418] Usually, these reported nanomaterials possessed catalase-like activities along with other enzyme-mimicking activities, and pH or temperature would make certain enzyme-mimicking activity dominant. As discussed in Section 2.1.3, under basic conditions, H_2O_2 would favor the acid-like decomposition into H_2O^* and O_2^* on the surface of metal nanomaterials (*i.e.*, the metal nanomaterials acted as catalase mimics). Moreover, Pt and Pd were demonstrated to possess better catalase-mimicking activities than Au and Ag.[195] Taking advantage of such highly efficient oxygen generation by Pt, biological sensing and photodynamic therapy (PDT) were developed, which will be discussed more in the Applications section.

Similarly, metal oxide nanomaterials (*e.g.*, Co_3O_4 and ZrO_2) and PB also showed catalase-mimicking activities at high pH.[419,420] Wang and co-workers found the weak catalase-like activities of Co_3O_4 NPs when studying the peroxidase-like activities.[421] Further, they demonstrated that the catalase-mimicking properties would be enhanced by changing the pH from acid to neutral and even basic condition. And the in-depth mechanism studies suggested the whole process as the following: on the one hand, Co(II) would activate the adsorbed H_2O_2 to decompose into $^{\bullet}OH$; and on the other hand, OOH^- would be formed *via* the reaction of H_2O_2 and OH^-, and then it would interact with Co(III) to generate $^{\bullet}O_2H$; with the reaction of the two radicals, H_2O and O_2 would be finally produced.[411] Owing to the multiple redox forms of PB and the low redox potential of H_2O_2/O_2 at high pH, H_2O_2 could easily oxidize PB to BG/PY and subsequently reduce PY/BG to PB, accompanied by production of O_2.[133] Inspired by these examples mentioned above, other nanomaterials with peroxidase-like activities could also be investigated to check their catalase-like activities. And the involved molecular mechanisms should be elucidated to further broaden their applications.

2.4 Superoxide dismutase (SOD) mimics

The dysregulated reactive oxygen species (ROS) would cause oxidative damage to living systems. In nature, SOD would eliminate superoxide anion $O_2^{\bullet-}$, one of the ROS, through the dismutation reaction of $O_2^{\bullet-}$ to H_2O_2 and O_2. To overcome the limitations of natural SOD and better combat the oxidative stress, a variety of nanomaterials have been used to mimic SOD.[422–430] Some of them could remove not only $O_2^{\bullet-}$ but also other free radicals, which strengthened the protection from ROS associated injury and inflammation. Several representative nanomaterials are discussed below.

2.4.1 Carbon based. Since the discovery of fullerene as a radical sponge, fullerene and its derivatives have been utilized to scavenge free radicals and protect neurons from oxidative injury.[431–433] In particular, $C_{60}[C(COOH)_2]_3$ with C_3 symmetry (C_{60}-C_3) was proved to possess a better antioxidation activity and provide more effective protection than C_{60}.[434] Such an antioxidation activity was due to the catalytic elimination of superoxide anion $O_2^{\bullet-}$. Further detailed mechanism studies confirmed the non-change of C_{60}-C_3 and the production of oxygen and hydrogen peroxide from $O_2^{\bullet-}$, just like an SOD-catalyzed reaction.[435] The whole process was carried out in two sequential steps: first, the unpaired electron was transferred from $O_2^{\bullet-}$ to C_{60}-C_3, accompanied by oxygen generation; then, another $O_2^{\bullet-}$ came and attracted the electron back, followed by oxidation of C_{60}-$C_3^{\bullet-}$ to its initial state and production of hydrogen peroxide. During the process, the first step where fullerene derivatives accepted the electrons was the rate-determining step. Another study using dendritic C_{60} derivatives also presented the two-step dismutation mechanism as mentioned above. Moreover, engineering the structures of dendritic C_{60} derivatives with higher reduction potentials improved the SOD-like activities. The highest activity from one of the dendritic C_{60} monoadduct derivatives was enhanced by one order of magnitude than that of C_{60}-C_3.[436]

Besides fullerene and its derivatives, the hydrophilic carbon cluster (HCC) has also been demonstrated as an SOD mimic (Fig. 13).[437] The HCC was fabricated by treating single-walled carbon nanotubes with sulfuric acid and nitric acid. Further modification of HCC with poly(ethylene glycol) (PEG) would help to increase the water solubility of HCC. The as-synthesized PEG–HCC could convert $O_2^{\bullet-}$ into oxygen and hydrogen peroxide, but was inert to reactive nitrogen species like nitric oxide ($^{\bullet}NO$) as well as peroxynitrite ($ONOO^-$). Due to many unpaired electrons and the planar structure of PEG–HCC, accepting electrons from $O_2^{\bullet-}$ for PEG–HCC was easier, which made

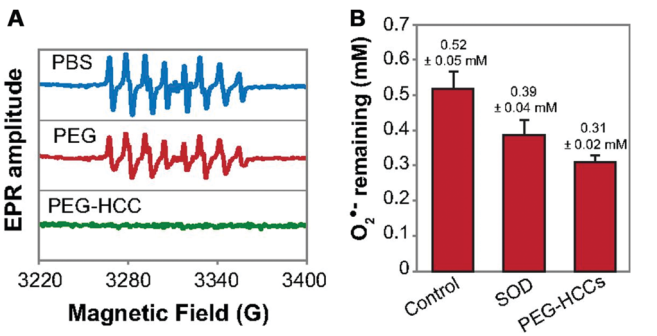

Fig. 13 (A) Effect of PBS (potassium phosphate buffer), PEG, and PEG-HCCs on $O_2^{\bullet-}$ radicals. (B) Comparison of the $O_2^{\bullet-}$ quenching activity of SOD and PEG-HCCs at physiological pH (pH = 7.7); 20 nM each of SOD and PEG-HCCs was used. The error bars are standard error of mean from four repeats. Adapted with permission from ref. 437. Copyright (2015) National Academy of Sciences.

PEG–HCC more efficient. For nanomolar concentration of PEG–HCC, the activity was several orders higher than micromolar concentration of C_{60}-C_3, and was even comparable to CuZn SOD. Such high-performance PEG–HCC would be promising in therapeutics.[437–439] Recently, PEGylated perylene diimides as molecular analogues of PEG–HCC, carbon nitride nanosheets, and nitrogen doped porous carbon nanospheres were reported to possess SOD-like activities as well.[440–442] For some other forms of carbon such as carbon nanotubes and nitrogen doped carbon dots, still, more mechanism studies are needed to check whether their ROS scavenging ability is solely due to the SOD-like activities.[443]

Unlike HCC's inactiveness to $ONOO^-$, hemin functionalized reduced graphene oxide (H-rGO) was capable of scavenging $ONOO^-$.[444] And the mechanisms were proposed to be the synergistic effect of H-rGO on the isomerization and reduction of $ONOO^-$ (Fig. 14). First, $ONOO^-$ would interact with the Fe^{III} center of H-rGO, leading to the formation of Fe^{III}–O–ONO species; second, the Fe^{IV}=O$^{\bullet}NO_2$ intermediate was generated through the homolytic cleavage of the O–O bond in the Fe^{III}–O–ONO species; then, owing to the presence of rGO, an accelerated recombination of the caged radical intermediate formed the Fe^{III}–nitrato complex, which would be hydrolyzed back to the Fe^{III} center, accompanied by the isomerization of $ONOO^-$ to NO_3^-. It was worth noting that the synergistic effect of hemin and rGO could catalyze the reduction of $ONOO^-$ to NO_2^- as well. And the addition of ascorbic acid would enhance the activity by 12%, as the promoted regeneration of the Fe^{III} center from the caged radical intermediate would help in reducing $ONOO^-$ to NO_2^-.[444]

2.4.2 Cerium based. Nanoceria were among the first reported nanomaterials with SOD-mimicking activities, which were attributed to the electron shuttle between their mixed oxidation states (Ce^{3+} and Ce^{4+}).[445,446] Though the detailed mechanism of the superoxide scavenging ability of cerium oxide still needs to be verified, several studies have shown that a higher ratio of Ce^{3+}/Ce^{4+} would result in higher SOD-mimicking activities.[447–449] Considering the association between Ce^{3+} and oxygen vacancies, a reduction in the size of cerium oxide with the formation of more surface oxygen vacancies was utilized to guarantee high Ce^{3+}.[446,450] Therefore, small sized cerium oxides, usually less than 5 nm, were extensively explored as SOD mimics. Further enhancement in the SOD-like activities could be achieved through doping cerium oxide with Zr/La atoms to generate more oxygen vacancies.[451,452]

It is worth mentioning that, different from fullerene-based SOD mimics, the antioxidation properties of cerium oxide were from not only SOD- but also catalase-like activities.[453–458] Moreover, cerium oxide could eliminate $^{\bullet}NO$ and $^{\bullet}OH$ as well.[459–462] The multiple enzyme-mimicking activities of cerium oxide showed promising application in therapeutics, which will be described in the Applications section. For the biological application of cerium oxide, several strategies such as surface coating and hydrogel formation were introduced to improve the stability, dispersity, and location of cerium oxide in a cellular environment.[463–465] The effect of these coating and intracellular molecules on the catalytic activities was also investigated. Most of them had no effect, except the inhibition of activities from phosphate, which was attributed to the specific interaction between Ce^{3+} and phosphate to block the Ce^{3+}/Ce^{4+} shuttling.[466] Another interesting finding was that the larger cerium oxide (larger than 5 nm) could be endowed with SOD-like activities when exposed to native CuZn–SOD or other electron donors (Fig. 15). The electrons transferred from CuZn–SOD/other donors to cerium oxide would help to reduce Ce^{4+} to Ce^{3+}, thereby improving the dismutation of superoxide anions. This unexpected finding was universal to cerium oxides of other sizes and morphologies, which made the regulation and regeneration

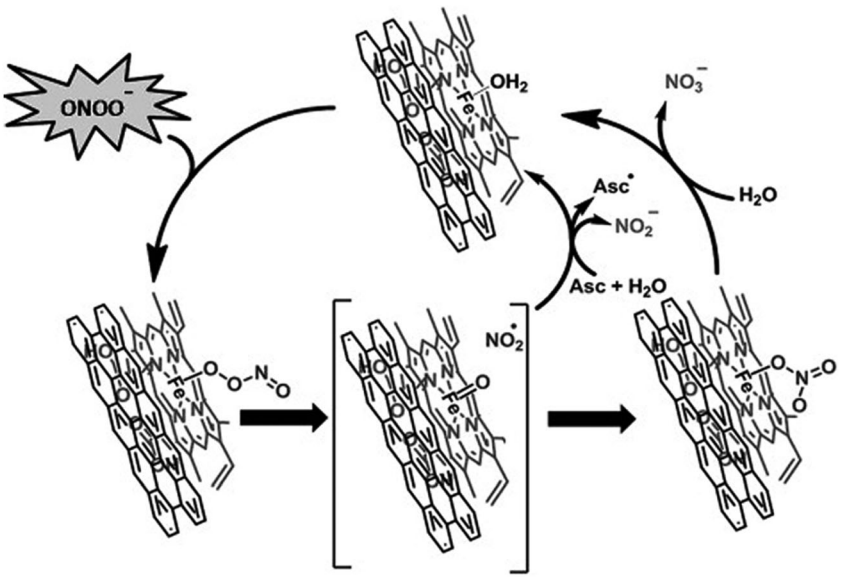

Fig. 14 Proposed mechanism for the isomerization and reduction of peroxynitrite and scavenging of $^{\bullet}NO_2$ by H-RGO hybrid nanosheets. Asc = ascorbic acid. Reprinted with permission from ref. 444. Copyright (2012) John Wiley and Sons.

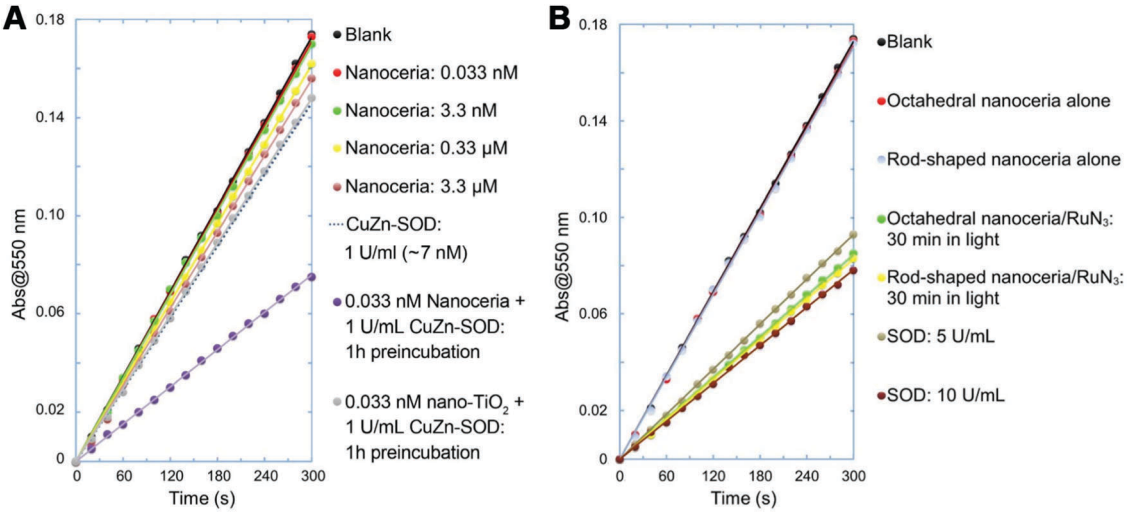

Fig. 15 (A) Nanoceria acquired superoxide-scavenging ability after electron transfer from CuZn-SOD. Titanium oxide nanoparticles (nano-TiO_2) were used as a particle control. (B) SOD-mimicking activities of octahedral nanoceria and rod-shaped nanoceria after activation by an electron donor RuN_3 (RuN_3 for sensitizing dye [$Ru(dcbpy)_2(NCS)_2$]). Adapted with permission from ref. 467. Copyright (2015) John Wiley and Sons.

of Ce^{3+} easier and thus more promising for practical biomedical applications.[467]

2.4.3 Melanin based. Different from the aforementioned SOD mimics, most specific for $O_2^{\bullet-}$, the melanin nanoparticles (MeNPs) with multiple free radical (*e.g.*, $O_2^{\bullet-}$, $^{\bullet}OH$, $^{\bullet}NO$, and $ONOO^-$) scavenging abilities were recently developed by Shi, Lu, and co-workers.[468] The MeNPs were synthesized by mixing dopamine hydrochloride with ammonia in ethanol–water, and then functionalized with amine-terminated PEG to improve their stability. Such PEG–MeNPs (~120 nm in diameter) possessed SOD-like activities for $O_2^{\bullet-}$ scavenging. The scavenging process was suggested to comprise two sequential reactions similar to C_{60}-C_3 (Fig. 16A). As the secondary $^{\bullet}OH$ and $ONOO^-$ converted from $O_2^{\bullet-}$ could also lead to an oxidative injury, an effective antioxidative therapy should benefit from the elimination of these reactive oxygen and nitrogen species as well. As shown in Fig. 16B, PEG–MeNPs could eliminate the $^{\bullet}OH$ produced through Fenton-type reaction between H_2O_2 and Cu^+. Notably, ascribed to the chelating capability of melanin towards Cu^+, the pre-added PEG-MeNPs before H_2O_2 would block $^{\bullet}OH$ from generating (*i.e.*, no signal of $^{\bullet}OH$ generated in reaction (4)). Thanks to the residual functional groups such as catechol of melanin, the PEG–MeNPs could also effectively detoxify $^{\bullet}NO$ and $ONOO^-$ through nitration and nitrosation (Fig. 16C and D). Though the exact molecular mechanisms still need to be verified, the robust multi-antioxidative properties made PEG–MeNPs promising for treating a series of free radical-associated diseases.[468]

2.5 Hydrolase mimics

A hydrolase catalyzes the hydrolysis of a chemical bond. For example, a nucleosidase hydrolyzes the bonds of nucleotides. A phosphatase catalyzes the cleavage of phosphate groups from molecules. Due to the degradative effect on larger molecules, hydrolases play an important role in biological systems and in environmental protection. Up to now, several nanomaterials have been explored to imitate hydrolases,[469–490] and the typical ones are shown in this section.

2.5.1 Carbon based. Besides the aforementioned peroxidase- and SOD-mimicking properties, actually, carbon based nanozymes were firstly discovered to mimic natural nucleases in the 1990s.[491] A water-soluble fullerene functionalized with carboxylic acid moieties, called C_{60}-1, was demonstrated to catalyze the cleavage of the phosphodiester bond of DNA when irradiated by light. Further, by conjugating fullerenes with complementary DNA or DNA intercalators, the cleavage efficiency at a specific site of DNA could be enhanced.[492,493]

In addition to fullerenes, graphene oxides were also used as hydrolase mimics.[494–496] For instance, graphene oxide integrated with peptide nanofibers could hydrolyze cellulose. Systematic studies uncovered that such high polysaccharide hydrolase-mimicking activities of this hybrid were from the fibril structure of peptides, less steric hindrance to the substrate, and the synergistic effect from graphene oxide and peptide nanofibers.[497] Similarly, carbon nanotubes assembled with short peptides could also cleave 4-nitrophenyl acetate.[498]

2.5.2 Monolayer functionalized AuNP based. Among the first nanomaterials as hydrolase mimics, one that deserves to be mentioned is the AuNPs functionalized with catalytic monolayers through Au–S bonds. In 2004, Scrimin, Pasquato, and co-workers assembled alkanethiol ligands bearing a catalytic complex of 1,4,7-triazacyclononane (TACN) and zinc ion onto the surface of AuNPs. Such functionalized AuNPs exhibited RNase-mimicking activities to cleave 2-hydroxypropyl *p*-nitrophenyl phosphate (HPNPP) (Fig. 17A).[499,500] Compared with no catalyst and the unassembled catalytic complex TACN–Zn^{2+}, the reactions with functionalized AuNPs were enhanced by four orders and two orders of magnitude, respectively. Further detailed studies showed that such excellent performance was attributed to the enhanced local concentration of HPNPP,

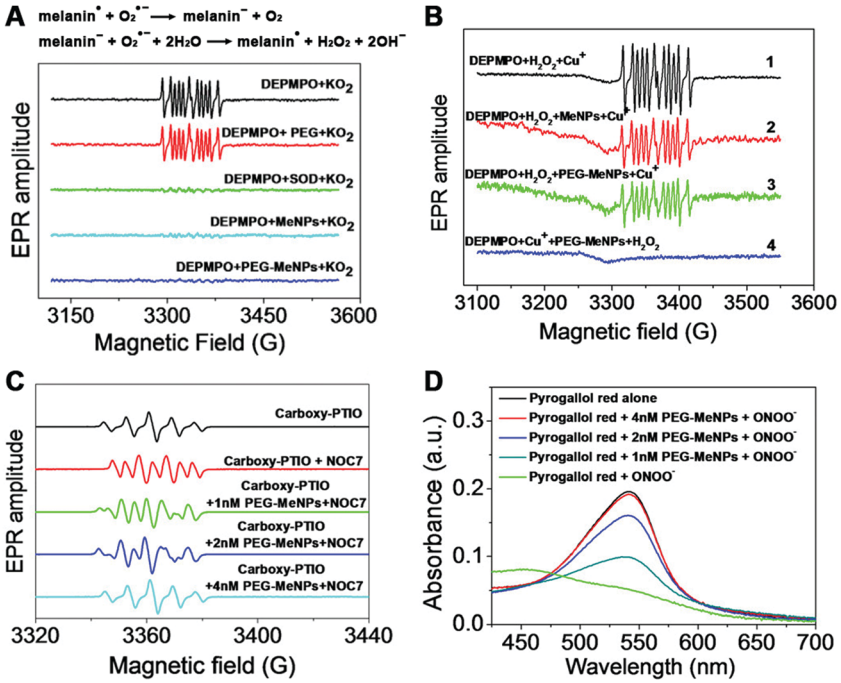

Fig. 16 (A) Effect of PEG, SOD, MeNPs and PEG-MeNPs on $O_2^{\bullet -}$ radicals. And the reactions of SOD-mimicking activities of melanin. (B) Effect of MeNPs and PEG-MeNPs on $^{\bullet}OH$ radicals. The $^{\bullet}OH$ was generated by the Fenton reaction between H_2O_2 and Cu^+ ions. For reactions (2) and (3), MeNPs and PEG-MeNPs were, respectively, added to the mixture of DEPMPO (spin-trap agent 5-diethoxyphosphoryl-5-methyl-1-pyrroline *N*-oxide) and H_2O_2, followed by the addition of Cu^+ ions. In reaction (4), PEG-MeNPs were preincubated with DEPMPO and Cu^+, followed by the addition of H_2O_2. (C) Effect of PEG-MeNPs on $^{\bullet}NO$, where carboxy-PTIO was used as the indicator and NOC7 as the $^{\bullet}NO$ donor. (D) $ONOO^-$ scavenging effect of PEG-MeNPs. Adapted with permission from ref. 468. Copyright (2017) American Chemical Society.

the cooperativity between two or more metal centers, and high stability from the strong Au–S bond.[499–501] More substrates such as RNA dinucleotides ApA, UpU and CpC were also cleaved by the functionalized AuNPs (Fig. 17B).[499] Not surprisingly, such functionalized AuNPs had a high affinity to negatively charged molecules such as peptides, which would thus compete with the binding of HPNPP and decrease the catalytic activities of the RNase mimics. With this in mind, several strategies for activity modulation and subsequently colorimetric sensing of important biological molecules have been reported.[502–504] What's more, the polarity of the alkanethiol ligands could also affect the interaction between the nanozymes and HPNPP, where a lower polarity would enhance the interaction and thus improve the cleavage efficiency (Fig. 17C and D).[505]

Such monolayer functionalized AuNPs were not restricted to the TACN–Zn^{2+} catalytic complex, and others including peptides, lanthanide complex, and guanidine were also reported to assemble onto AuNPs as hydrolase mimics.[508–513] For example, using the complex of bis-(2-amino-pyridinyl-6-methyl)amine and zinc ion as the catalytic moiety, the functionalized AuNPs could catalyze the cleavage of a DNA model substrate bis-*p*-nitrophenyl phosphate and also plasmid DNA.[514] Coating of lanthanides, such as Ce(IV), onto the surface of AuNPs led to a 2.5 million-fold enhanced rate of HPNPP cleavage relative to background hydrolysis. Such a remarkable acceleration was attributed to the same cooperative mechanism as the Zn-based complex. However, there was a difference between free Ce and Zn ions in catalyzing the hydrolytic cleavage, as Ce(IV) rather than Zn(II) could form active oligomeric clusters and thus hydrolyze the substrate efficiently.[509] Moreover, on changing the monolayer to a chiral Zn(II)-based complex (Fig. 17E), enantioselective hydrolysis of RNA model substrates and natural RNA dinucleotides could also be observed with this chiral AuNP nanozyme. In particular, owing to the special preference for uracil, the enantioselective reactivity of UpU was the best among all the RNA dinucleotides.[506]

Unlike the covalent binding mentioned above, some non-covalent assemblies of catalytic moieties onto the surface of alkanethiol protected AuNPs exhibited similar phosphatase-like activities as well (Fig. 17F).[507] Based on such non-covalent assembly, specific activation of pro-drugs could be achieved for therapeutics with minimized toxic side effects of drugs.[515] For more details and applications one could refer to the Applications section.

2.5.3 MOF based. A large number of Zr-based MOFs have been used as phosphotriesterase mimics for cleaving the phosphate ester bond of chemical warfare agents (CWAs) (Fig. 18A).[516–524] The reason was the similarities between the structures of phosphotriesterase catalytic sites (Zn–OH–Zn) and the structures of MOFs where hydroxyl bonds bridge Lewis acidic Zr(IV) centers. The UiO family of MOFs, a representative of Zr-based MOFs, was fabricated by mixing Zr ions with benzene-1,4-dicarboxylate (BDC) and widely explored to mimic phosphotriesterase. For instance, in 2014, Hupp, Farha, and co-workers

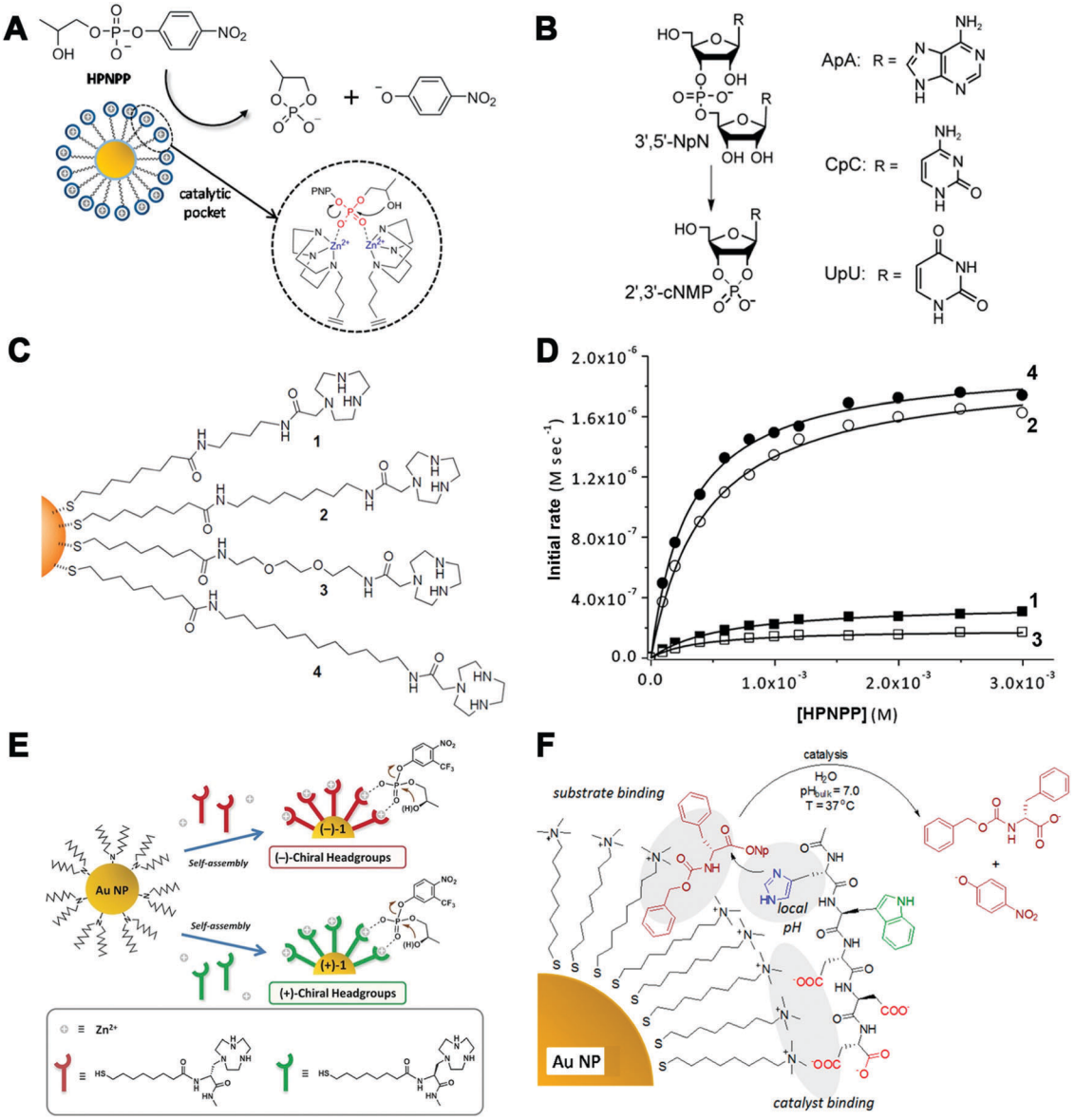

Fig. 17 (A) Transphosphorylation of HPNPP catalyzed by functionalized AuNPs. Two neighboring TACN·Zn(II) complexes in the monolayer create a catalytic pocket in which the two zinc ions cooperatively act on the substrate. (B) Cleavage of RNA dinucleotides (3′,5′-NpN) such as ApA, CpC, and UpU. (C) AuNP-based nanozymes with different polarities. (D) Rate of HPNPP cleavage using nanozymes with different polarities. (E) Schematic representation of the self-assembly of thiols containing chiral head groups on the surface of dioctylamine-passivated AuNPs to form (+)-1 and (–)-1 NPs. (F) Transesterification catalyzed by catalysts non-covalently assembled onto AuNPs. (A) Reprinted with permission from ref. 500. Copyright (2015) American Chemical Society. (B) Reprinted with permission from ref. 499. Copyright (2004) John Wiley and Sons. (C and D) Adapted with permission from ref. 505. Copyright (2014) American Chemical Society. (E) Adapted with permission from ref. 506. Copyright (2016) John Wiley and Sons. (F) Adapted with permission from ref. 507. Copyright (2012) American Chemical Society.

showed that 400 nm UiO-66 could catalyze the hydrolysis of dimethyl-4-nitrophenyl phosphate (DMNP) at room temperature, with a half-life of 45 min. Considering the larger size of the DMNP substrate (11 × 4.5 Å) than the aperture (6 Å), the reaction was suggested to mainly happen on the MOF surface with around 0.75% nodes accessible and a local turnover number (TOF) of 0.4 s^{-1}.[525] Further, they modified the UiO-66 with $-NH_2$ groups, supplying the Zr(IV) centers with proton donor–acceptor centers. Compared with UiO-66, UiO-66-NH_2 shortened the half-life of DMNP (1 min) by 1 order of magnitude, and exhibited a surface TOF with approximately 20-fold enhancement.[526] Besides UiO-66 MOFs, other MOFs (such as NU-1000 and MOF-808) with similar bridging motifs were also synthesized and reported for CWA degradation. Both of them possessed better catalytic activities than UiO-66, which resulted from the less coordination of Zr centers and larger accessible active sites. Instead of 12 and 8 coordinations in UiO-66 and NU-1000, MOF-808 with only 6 coordinations offered the highest hydrolysis efficiency for DMNP, with a half-life of less than 0.5 min and a TOF of larger than 1.4 s^{-1}.[517,527] Later, PCN-777,

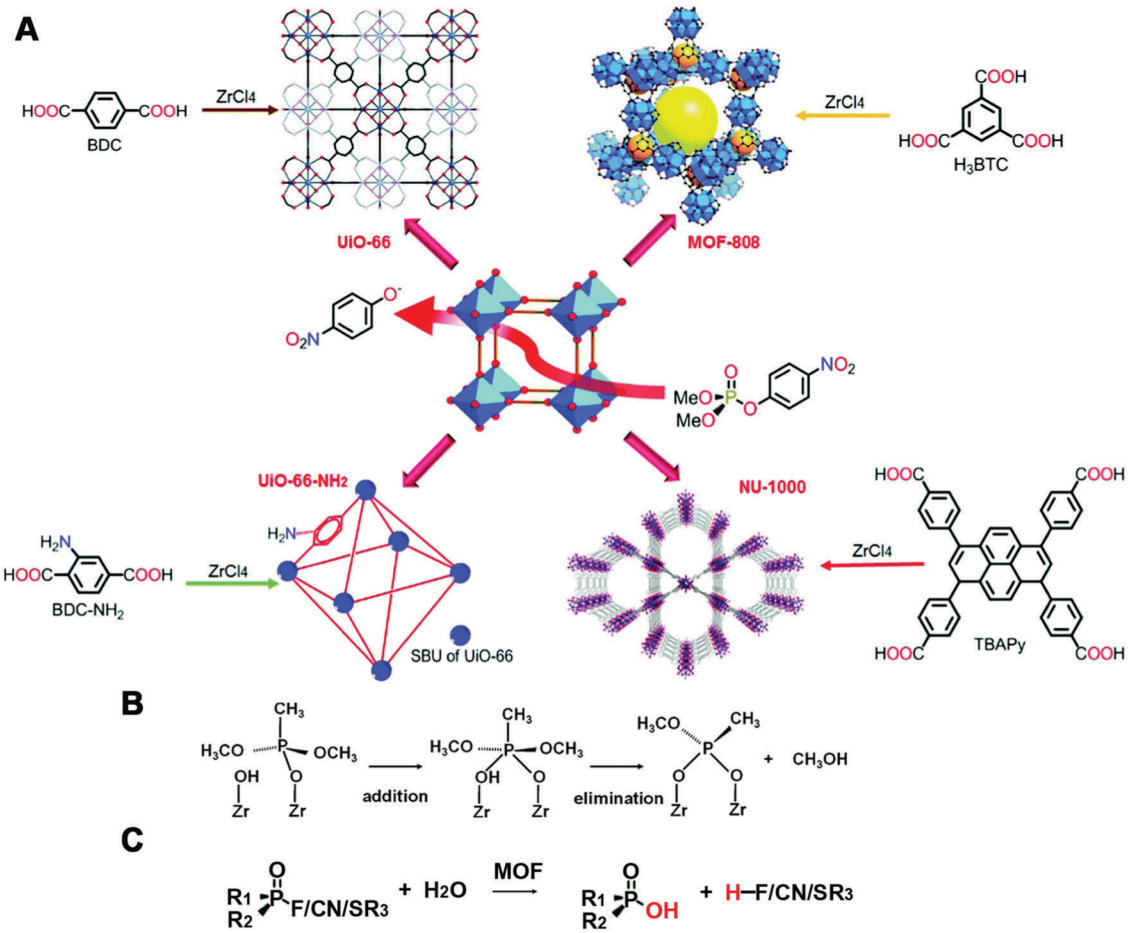

Fig. 18 (A) Illustration of the synthesis and DMNP hydrolysis of phosphotriesterase-mimicking MOFs. (B) Mechanism of dimethyl methylphosphonate decomposition. (C) Scheme for degradation of other CWAs by MOFs. (A) Reprinted with permission from ref. 521. Copyright (2016) Royal Society of Chemistry. (B) Reprinted with permission from ref. 531. Copyright (2017) American Chemical Society.

sharing the same connection but a larger pore size than MOF-808, showed a comparable catalytic activity as MOF-808, verifying that MOFs with less coordination gave better hydrolytic performance. On the other hand, for the effect of the pore size, it was not that significant as the pore size of MOF-808 was already large enough for efficient diffusion.[528] Though some systematic investigations and simulations have been carried out for certain nerve agent simulants, different model systems exhibited different hydrolytic pathways.[529,530] A shared mechanism for this process was that the substrate would bind to the metal center, and then the nucleophilic hydroxyl group would attack the electrophilic phosphorus and complete the cleavage reaction with the release of the leaving group (Fig. 18B).[531] Still, more exact molecular mechanisms for different systems need to be verified through both experiments and calculations in the future.

Besides, MOFs were also studied for degradation of other organophosphate-based CWAs (Fig. 18C), which have been summarized in previous reviews.[528,532–538] For example, Cu-BTC/g-C_3N_4 nanocomposites dispersed on cotton textiles possessed a superior cleavage ability of dimethyl chlorophosphate, due to the high dispersion of composite, large accessible active sites and synergistic promotion from g-C_3N_4.[539] Ce-BDC, similar to the structure of UiO-66, exhibited higher hydrolysis rates for detoxification of DMNP and *O*-pinacolyl methylphosphonofluoridate than UiO-66. Further mixing Ce-BDC with polyethylenimine, consisting of amine groups, could also improve the hydrolysis rate as UiO-66-NH_2 did. They speculated that the underlying cause was an easily attacked intermediate formed from the mixture of Ce(IV) 4f orbitals and P=O orbitals.[540]

In addition to CWAs' cleavage, MOFs have also been utilized for other hydrolytic reactions. For instance, a Cu-MOF with protease-mimicking activity, catalyzing the hydrolysis of peptide bonds in bovine serum albumin (BSA) and casein, was described by Li, Wang, and co-workers. Owing to the large surface and porous structure of the MOF, such Cu-MOFs showed a significantly higher affinity to proteins than natural trypsin and homogeneous artificial metalloprotease Cu(II) complexes. Thus, the obtained Cu-MOF exhibited good hydrolytic activity, stability, and reusability.[541]

2.6 Other enzyme mimics

So far, not only redox and hydrolysis reactions but also other enzymatic reactions have gained a lot of attention.[542–548]

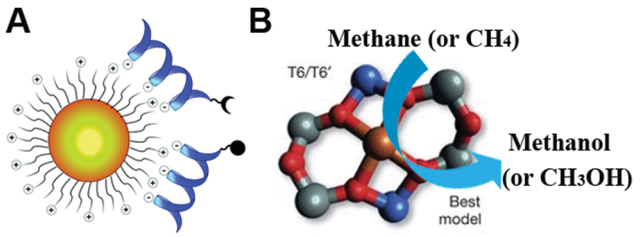

Fig. 19 (A) Peptide ligation catalyzed by catalysts non-covalently assembled onto AuNPs. (B) Computational model of the Fe(II) zeolite-based methane monooxygenase mimic. (A) Reprinted with permission from ref. 553. Copyright (2007) American Chemical Society. (B) Adapted with permission from ref. 554. Copyright (2016) Nature Publishing Group.

For instance, besides peroxidase and hydrolase mimics mentioned earlier, hydrogenase-like activity could also be realized with MOFs, as long as providing MOFs with photon absorption agents (*e.g.*, porphyrin) and proton reducing agents (*e.g.*, PtNPs).[549–551] Moreover, MOFs synthesized with a carbonic anhydrase analogous moiety could mimic carbonic anhydrase to minimize the global warming issues.[552] Great progress has been made in this field of MOF-based enzyme mimics and summarized.[521] Though some issues about MOF-based nanozymes like the large size and dispersity still need to be solved, some good strategies (such as anchoring the catalytic moiety onto MOFs) for designing and expanding the types of enzymatic reactions should be utilized in the future.

In addition, Chmielewski, Rotello, and co-workers reported that the electrostatic assembly of two peptide fragments onto the trimethylammonium functionalized AuNPs would promote ligation of the two peptides, which made the inorganic functionalized nanoparticles promising in the polymerization of biopolymers (Fig. 19A).[553] Morse and co-workers demonstrated that monolayer-functionalized AuNPs could mimic silicatein. When the distance between one hydroxyl functionalized AuNP and another imidazole functionalized AuNP was close enough to form hydrogen bonds, the silica precursor would be hydrolyzed and then condensed to form silica at the interface of two AuNPs.[555]

Moreover, a Fe(II) zeolite-based methane monooxygenase mimic converting methane with nitrous oxide into methanol was studied. The nature of the exact active site was recently disclosed by Solomon and co-workers (Fig. 19B). The extra-lattice active site was determined as a mononuclear, high-spin, square planar Fe(II) site through a site-selective spectroscopic method and magnetic circular dichroism.[554] Not only Fe(II) zeolites but also Cu-exchanged mordenite could convert methane to methanol *via* the pre-oxidized copper-oxo active center.[556]

2.7 Multi-enzyme-mimicking nanozymes

Notably, certain nanomaterials (*e.g.*, Pt and CeO_2) could mimic two or more types of enzymes, and such multiple enzyme-mimicking activities made them more efficient in their further applications.[110,168,557–571] For instance, SOD-, catalase-, peroxidase- and oxidase-like activities of CeO_2 were found. As mentioned in Section 2.4.2, at neutral or high pH, CeO_2 NPs with an excellent antioxidation function were reported due to both SOD- and catalase-like activities. On the other hand, for acidic pH, the catalase-mimicking activities would decrease a lot. Though the SOD-like activity was retained under acidic conditions, the generated excess H_2O_2 without timely elimination would still cause oxidative damage. Moreover, oxidase-like activities of CeO_2 NPs would be enhanced under acidic conditions, and promote the oxidation of those intracellular and extracellular species to kill cells. Therefore, according to different microenvironments, the pH-dependent multi-enzyme-mimicking activities of CeO_2 NPs could be utilized to provide different functions such as a cell protector and a cancer cell killer.[572] Another Mn_3O_4 nanozyme imitating not only SOD and catalase but also GPx was reported to effectively combat cellular oxidative stress.[573] The combination of protease- and SOD-mimicking activities as well as copper-chelating capability made the polyoxometalate-based nanozyme an effective therapeutic agent for the treatment of Alzheimer's disease.[574]

2.8 Multi-functional nanozymes

Besides, the intrinsic magnetic and optical properties of nanomaterials (*e.g.*, Fe_3O_4 and Au) endowed nanozymes with multiple functionalities, ensuring an easy separation process, ultra-sensitive sensing, and in-depth mechanism study.[186,279,575–594] For example, the Wei group developed versatile bioassays based on AuNPs with both peroxidase-like activities and surface enhanced Raman scattering properties. An additional growth of suitable Pt shells (2.5%) would enhance the activities of nanozymes while retaining the Raman properties of AuNPs, leading to 1–2 orders of magnitude enhancement of sensitivity and shortening of the detection time.[595] Moreover, the optical properties of Au and the magnetic properties of iron could also be used for imaging, which will be discussed in the Applications section. To highlight such categories, nanomaterials with multiple enzyme activities and multiple functionalities are summarized in Tables S6 and S7 (ESI†), respectively.

3. Engineering nanozyme activity and selectivity

To make nanozymes better alternatives to natural enzymes, engineering their activity and selectivity should be prioritized. So far, most studies focused on the activity regulation and only a few on selectivity. Several important factors inspired by the intrinsic properties of nanomaterials or natural enzymes are summarized as below.

3.1 Size

Since nanomaterials with a smaller size would expose more active sites due to the higher surface to volume ratio, most studies have demonstrated that a better catalytic activity came along with smaller sized nanomaterials.[419,516,596–599] Moreover, some specific properties could appear only when the size was shrunk to a certain extent. For example, Ce^{3+}, helpful for SOD-mimicking activities of nanoceria, would become stable in the

nanoparticles with size less than 5 nm.[446,450] Similarly, the high-energy facet {211}, which was responsible for the oxidase-like activity of AuNPs, became abundant only when the size decreased to 3–5 nm.[195]

However, it is notable that a larger size would sometimes behave better than a smaller one. For instance, guanine-rich oligonucleotide capped 1.8 nm Pt nanozymes showed a lower peroxidase-like activity than cytosine-rich oligonucleotide capped 2.9 nm Pt. The underlying reason was that 2.9 nm Pt contained more metallic Pt^0 for enzyme-like catalysis, while 1.8 nm Pt had more Pt^{2+} but less Pt^0.[600]

3.2 Shape and morphology

It is well known that the shape and morphology of nanomaterials play a critical role in their catalytic properties.[599,601–613] For instance, Mugesh, D'Silva, and co-workers compared the catalase-, GPx- and SOD-like activities of different shaped Mn_3O_4 NPs (*e.g.*, nanoflowers, flakes, cubes, polyhedra, and hexagonal plates). They found that the flower-shaped Mn_3O_4 exhibited the highest catalytic activities for the three types of reactions, whereas other morphologies only showed SOD-like activities. Thus, the flower-shaped Mn_3O_4 NPs were chosen for further neuroprotection application.[573] The morphology-dependent oxidase-like activity of $MnFe_2O_4$ was investigated by changing the synthetic conditions. Owing to different morphologies with different facets, the nanooctahedra bound by {111} planes exhibited a better oxidase-like activity than nanosheets and nanowires.[614] Yin, Chen, Gao, and co-workers reported that {111}-faceted Pd octahedra possessed both better catalase- and SOD-like activities to scavenge ROS than {100}-faceted Pd cubes. The scavenging reactions of ROS like H_2O_2 and $O_2^{\bullet-}$ on these two facets and the reaction energy (E_r) of the rate-determining step were calculated, where more negative E_r evidenced higher activity. As shown in Fig. 20, the scavenging abilities of H_2O_2 and $O_2^{\bullet-}$ on the {111} facet (E_r equaled −2.81 and −0.60 eV, respectively) were stronger than those on the {100} facet (E_r equaled −2.64 and −0.13 eV, respectively).[615] On the other hand, for their abilities of generating ROS, a recent study observed that {100}-faceted Pd cubes exhibited higher oxidase-like and peroxidase-like activities than those of {111}-faceted Pd octahedra. Similarly, theoretical simulations of O_2 and H_2O_2 dissociation in their corresponding oxidase- and peroxidase-mimicking reactions were carried out. The lower energy barriers of O_2 and H_2O_2 dissociation on the {100} facet indicated that these processes were energetically more favorable than on {111}, thus agreeing with the aforementioned observation.[616]

3.3 Composition

An economic and efficient method to regulate the activity was growing with a (more) active nanomaterial or doping another element. A widely explored strategy was growing less active nanomaterials (*e.g.*, Au and Ag) with another higher active one (*e.g.*, Pt and Ir), which would not only improve the enzymatic activities but also make effective utilization of these noble metals.[414,617–621] For example, as shown in Fig. 21A, the coating of a few atomic Ir layers on Pd cubes would enhance the catalytic efficiency by at least 20- and 400-fold than Pd cubes and HRP.[622] The Wei group synthesized high-performance Au@Pt multi-functional nanozymes *via* a seed-mediated method for H_2O_2 detection. Compared with previous reports, such a structure possessed simultaneous plasmonic properties from the Au core and enzymatic activity from the Pt shell, shortening the detection time and improving the sensitivity by 1–2 orders of magnitude (Fig. 21B).[595] To further improve the activity, sometimes, the less active core would be selectively etched after growing the higher active one. For example, after etching the Pd core, Pd–Pt core-frame nanodendrites were transferred to Pt hollow nanodendrites, accompanied by more active sites and high-index facets exposed for enhancing the peroxidase-like activity.[623]

Doping was another effective strategy to regulate the activities of nanozymes benefited from the change of the electronic structure.[452,624–632] For example, considering the requirement for excellent SOD-like activity of ceria nanoparticles, Zr^{4+} with smaller ionic radius (0.084 nm) was chosen to promote high Ce^{3+}/Ce^{4+} and fast regeneration of Ce^{3+}, as the lattice strain of

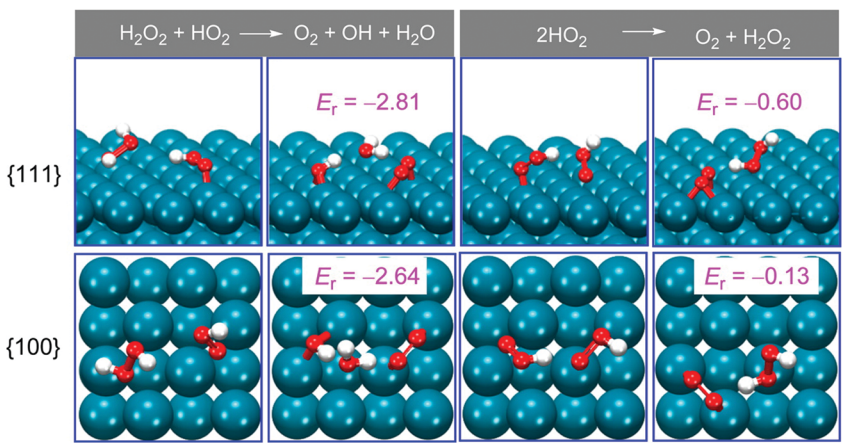

Fig. 20 Lowest-energy adsorption structures and reaction energies (in eV) for the reactions on structures having either Pd{111} or {100} facets. Reprinted with permission from ref. 615. Copyright (2016) American Chemical Society.

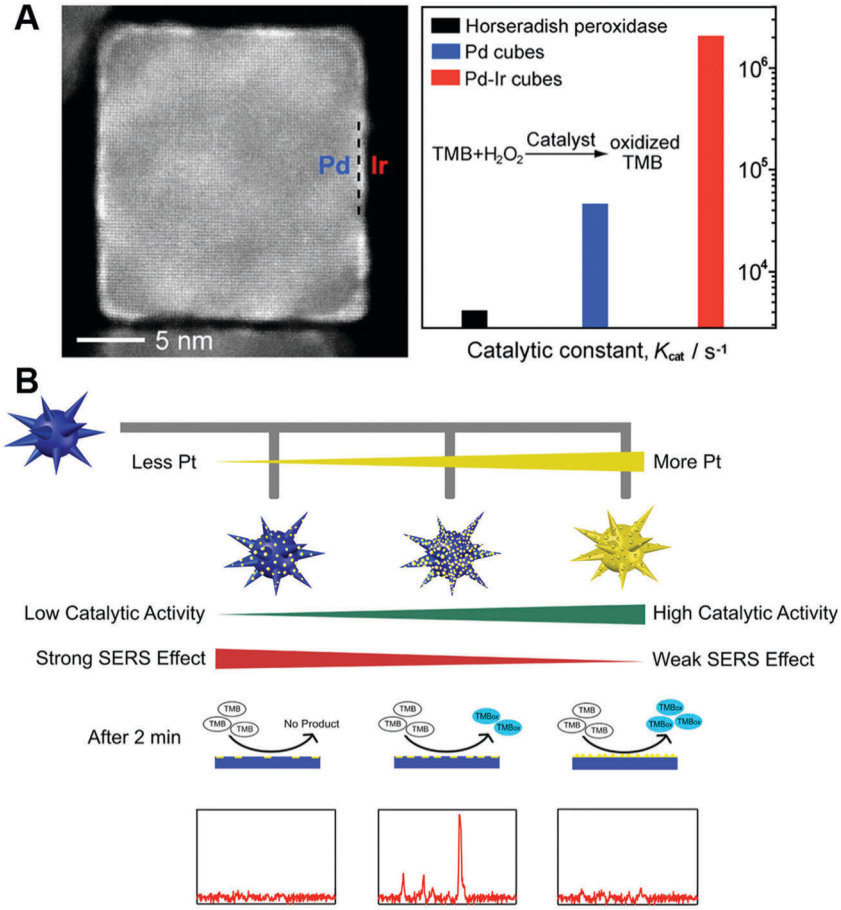

Fig. 21 (A) Pd–Ir core–shell nanocubes as efficient peroxidase mimics. (B) Rational design of high-performance Au@Pt NP bifunctional nanozymes by controlling the Pt amount. (A) Reprinted with permission from ref. 622. Copyright (2015) American Chemical Society. (B) Reprinted with permission from ref. 595. Copyright (2018) American Chemical Society.

Ce^{4+} (0.097 nm) to Ce^{3+} (0.114 nm) could be released from the smaller Zr^{4+}.[451] Besides, Qu, Ren, and co-workers reported that Fe^{3+} doped mesoporous carbon nanospheres could improve the peroxidase-like activities as a result of containing both catalytic sites (*e.g.*, Fe^{3+}) and binding sites (*e.g.*, carboxyl groups in carbon).[633]

3.4 Forming complexes or hybrids

Numerous studies have shown that conjugating several nanomaterials to form hybrids would improve the catalytic activity as a result of the synergistic effect.[108,306,321,634–665] For example, assembling Pt@CuMOFs with hemin/G-quadruplex showed an elevated peroxidase-like activity from the two catalysts.[666] An interesting $Pt_{48}Pd_{52}$–Fe_3O_4 dumbbell structure as a peroxidase mimic exhibited the highest V_{max} among the $Pt_{48}Pd_{52}$ and Fe_3O_4 mixture (4.44×10^{-8} M s^{-1}), individual $Pt_{48}Pd_{52}$ (2.56×10^{-8} M s^{-1}), individual Fe_3O_4 (3.46×10^{-8} M s^{-1}), and $Pt_{48}Pd_{52}$–Fe_3O_4 dumbbell structure (9.36×10^{-8} M s^{-1}).[667] Moreover, a series of studies using the hybrid of certain nanozymes (*e.g.*, MoS_2, CuO, and Pt) with graphene demonstrated a higher catalytic activity than that of the individual catalysts due to the high conductivity, good dispersity, and synergistic interaction.[104,668–684] For example, AuNCs on graphene oxide possessed high peroxidase-like activity over a broad pH range, especially a comparable catalytic efficiency to HRP at neutral pH.[231]

Recently, integrating two or more nanozymes together to enhance the cascade reaction catalytic efficiency has been widely explored.[279,685–689] Such an integration would have confinement effects (or nanoscale proximity effects) to provide a high local concentration of the substrate, enable efficient transfer, and minimize the decomposition of intermediates. For instance, as shown in Fig. 22, the Wei group synthesized the GOx/hemin@ZIF-8 integrate by adding GOx and hemin during the assembly of Zn^{2+} and 2-methylimidazole. They confirmed this integration through the element mapping of Zn in ZIF-8, Fe in hemin and fluorescence labelling of GOx. Compared with the mixture of GOx@ZIF-8 and hemin@ZIF-8, nearly 600% improvement of the overall catalytic efficiency was achieved with GOx/hemin@ZIF-8.[690] And it was worth noting that such a strategy was applicable to other systems (*e.g.*, GOx/NiPd@ZIF-8).[281,691] Even for three biocatalysts, invertase/GOx/hemin@ZIF-8, a stable integrate could also be constructed and improved the efficiency by 700% compared to the mixture of invertase@ZIF-8, GOx@ZIF-8, and hemin@ZIF-8.[690] Instead of using MOFs as a host, porous carbon or silica could serve for integrating several nanozymes as well.[692–694] Besides, an additional

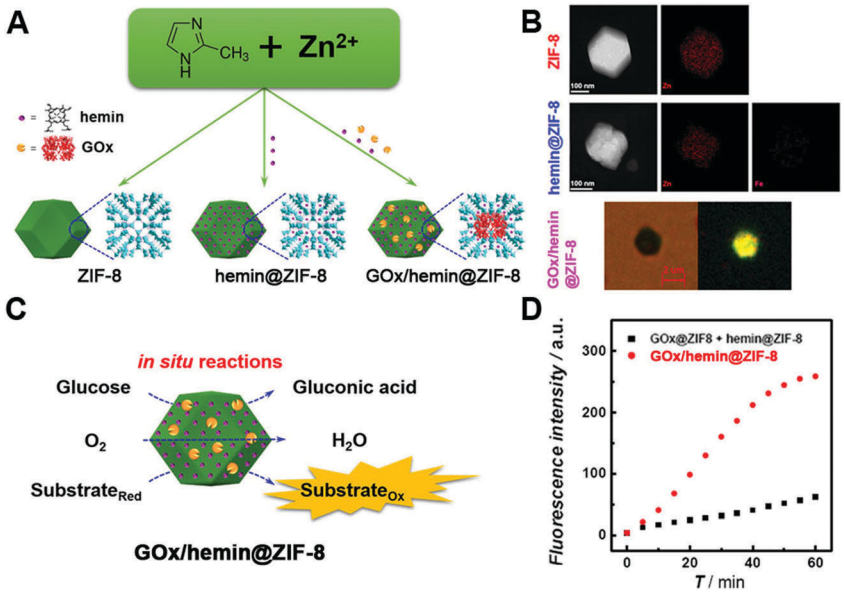

Fig. 22 (A) Schematic illustration of GOx/hemin@ZIF-8. (B) TEM images and the corresponding element mapping of ZIF-8 and hemin@ZIF-8, as well as bright field and the corresponding fluorescence images of GOx-FITC/hemin@ZIF-8 (λ_{ex} = 436 nm; FITC, fluorescein isothiocyanate isomer I). (C) Schematic illustration of reactions catalyzed by GOx/hemin@ZIF-8. (D) Kinetic plots of the time-dependent fluorescence intensity of GOx/hemin@ZIF-8 or the mixture of hemin@ZIF-8 and GOx@ZIF-8. Adapted with permission from ref. 690. Copyright (2016) American Chemical Society.

host became unnecessary when fabricating integrates through layer-by-layer deposition, such as directly depositing AuNPs onto the surface of V_2O_5 nanorods or 2D MOFs.[695,696] Notably, the 2D MOFs used here provided peroxidase-like activities, which were different from those of the inactive ZIF-8 host.

Meanwhile, it was noteworthy that when coupling with natural enzymes, not only the catalytic activity but also the selectivity of the integrate was improved. As a result, the detection of glucose or lactase with the assistance of GOx or lactate oxidase could be achieved, which will be discussed in Section 4.1.2.[281,690]

3.5 Surface coating and modification

Most reactions take place on the surface of nanozymes. An additional surface coating or modification of nanozymes would affect their activities through the change of surface charge and microenvironment, as well as the exposure of active sites. Normally, the extra coating or modification would shield the active sites and thus decrease the catalytic activities. For instance, the coating of DNA or other biomolecules has been reported for inhibiting the activities of nanozymes.[148,169,695,697–701] And then the corresponding sensing of these molecules was developed on the basis of activity modulation. However, in some cases, a coating or modification would form a favorable environment to improve the total catalytic activities.[702–708] For example, coating with an active surface would help to enhance the entire activity, such as with Fe_2O_3@PB.[132] Due to the negative charge of DNA, many researchers have reported enhanced affinities and improved activities to positively charged TMB with the assistance of DNA.[157,709–712] Likewise, Fu, Hu, and co-workers found that coating AuNCs with heparin could endow AuNCs with negative charges and thus enhance the peroxidase-like activity towards TMB by 25-fold at neutral pH.[713] Another interesting finding was that coating ferric oxide nanoparticles with the cetyl trimethyl ammonium bromide surfactant changed their structures and catalytic activities. Different from pristine spherical ones, rod-shaped nanoparticles with a more porous structure and higher peroxidase-like activities were formed after surfactant coating.[714]

Notably, when charged monomers are combined with molecular imprinting, certain substrate binding pockets would be created on the surface of nanozymes, leading to significant enhancements of both activity and selectivity.[95,715–718] As shown in Fig. 23, a specific binding pocket to TMB was formed on the surface of Fe_3O_4 NPs. As a result, around 15-fold catalytic efficiency and 98-fold specificity were achieved with the imprinted substrate TMB over ABTS. Such a strategy was applicable to other nanozymes (*e.g.*, AuNPs and CeO_2 NPs).[719] Additionally, taking advantage of the chiral structures of amino acids or others

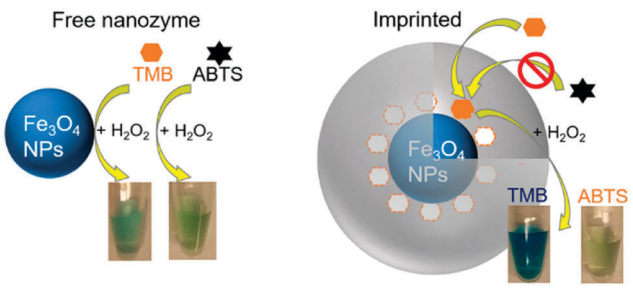

Fig. 23 Fe_3O_4 peroxidase-mimicking nanozyme has a similar activity for TMB and ABTS. After imprinting with TMB, its selectivity for TMB is drastically improved. Reprinted with permission from ref. 719. Copyright (2017) American Chemical Society.

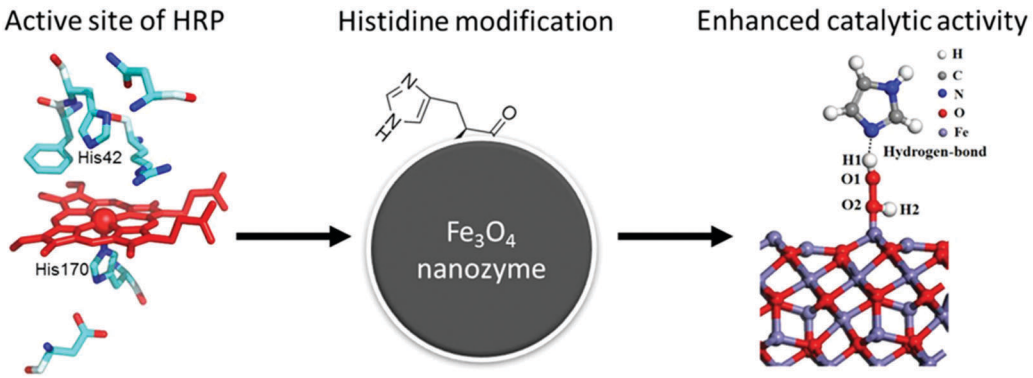

Fig. 24 Mimicking the active site of natural enzymes to improve the peroxidase-like activity of Fe_3O_4 NPs. Adapted with permission from ref. 724. Copyright (2017) Royal Society of Chemistry.

(*e.g.*, secondary structures of DNA and zinc-finger-protein like chiral supramolecular complex) as surface coating, the chirality of surface coating could also help to improve selectivity and realize enantioselective discriminations.[720–723]

Inspired by natural peroxidases, Yan, Gao, and co-workers modified Fe_3O_4 NPs with histidine to form a similar microenvironment to natural enzymes (Fig. 24). Compared with naked Fe_3O_4 NPs, such modification improved the affinity towards H_2O_2 by at least 10-fold, as a hydrogen bond would form between the side-chain imidazole group of histidine and H_2O_2. Therefore, more than 20-fold increase of the peroxidase-like catalytic efficiency was obtained with histidine-modified Fe_3O_4 NPs. Benefitting from the significantly improved affinity to H_2O_2, the catalase-like activity could also be enhanced.[724]

Another interesting example of surface modification was that amine-terminated dendrimer-encapsulated AuNCs (AuNCs-NH_2) could selectively decrease the peroxidase-like activities while maintaining their catalase-like activities. When blocking most amines (1°- and 3°-amines) of AuNCs-NH_2 *via* methylation, significantly recovered peroxidase-mimicking activities could be observed, indicating the importance of amines in inhibiting the peroxidase-like activities. A similar suppression of peroxidase-mimicking activities was also found in AuNCs-OH (hydroxyl-terminated, containing 3°-amines inside the backbone), which further evidenced the role of 3°-amines. And the possible mechanism was speculated to be the competitive consumption of $^{\bullet}OH$ through easy oxidation of 3°-amines.[725] In their following study, catalase-mimicking AuNCs-NH_2 with O_2 self-supplied was used for cancer PDT to overcome hypoxia.[726]

3.6 Promoters and inhibitors

Inspired by coenzymes, Qu and co-workers reported that with the addition of nucleoside triphosphates, the oxidase-mimicking activities of CeO_2 would be enhanced in the following order: guanosine triphosphate > adenosine triphosphate > uridine triphosphate > cytidine triphosphate. Unlike natural coenzymes, they suggested that this increase was due to the energies released from the hydrolytic reaction of nucleoside triphosphates catalyzed by CeO_2.[727] In another study, the Wei group found that adenosine triphosphate exhibited a positive effect to enhance the oxidase-like activity of CeO_2 at first, but an inhibitory role under longer reaction time. The formation of the Ce–PO_4 complex was speculated for shielding the active sites of CeO_2.[402] More in-depth mechanisms for the complicated roles of adenosine triphosphate in the catalytic activities of CeO_2 should be further investigated. Several ions or molecules were also reported to improve the enzymatic activities of nanomaterials.[155,366,728–737] For example, Lu *et al.* found that Hg^{2+} could significantly enhance the peroxidase-like activity of rGO/PEI/Pd nanohybrids and Liu *et al.* demonstrated that the oxidase-like activity of nanoceria could be enhanced by over two orders of magnitude in the presence of fluoride.[738,739] However, in some cases, certain ions (*e.g.*, Ag^+ and Hg^{2+}) and other molecules could react with the nanozymes to inhibit their catalytic activities.[144,160,163,164,187,371,373,740–749] Accordingly, owing to the specific inhibition, the sensing of these inhibitors with good selectivity and sensitivity was developed.

Another interesting phenomenon was that certain inhibitors could selectively inhibit certain enzymatic activities. For instance, NaN_3 only decreased the catalase-like activity of ferritin-PtNPs while 3-amino-1,2,4-triazole inhibited both SOD- and catalase-like activities of ferritin-PtNPs. The reason was that singlet oxygen generated from superoxide was involved in the SOD-like reaction but not in the catalase-like reaction. And as a strong quencher of singlet oxygen, NaN_3, rather than 3-amino-1,2,4-triazole, would be removed from the PtNP surface *via* the reaction with singlet oxygen. Therefore, NaN_3 only selectively suppressed the catalase-like activity.[750]

3.7 pH and temperature

Similar to natural enzymes, the activities of nanozymes are normally pH and temperature dependent.[300,319,353,606,751–756] As we elucidated above, an acidic condition would be suitable for a peroxidase-mimicking activity, whereas neutral and alkaline pH promote SOD- and catalase-like properties.[168,195,559,757] Most studies provided a systematic investigation of the effects of pH and temperature on the nanozyme activity, and then optimal pH and temperature would be found, such as pH 4.5 at 55 °C for $LaNiO_3$ perovskite nanocubes as peroxidase mimics.[758] As a result of the stabilization effect on the final products,

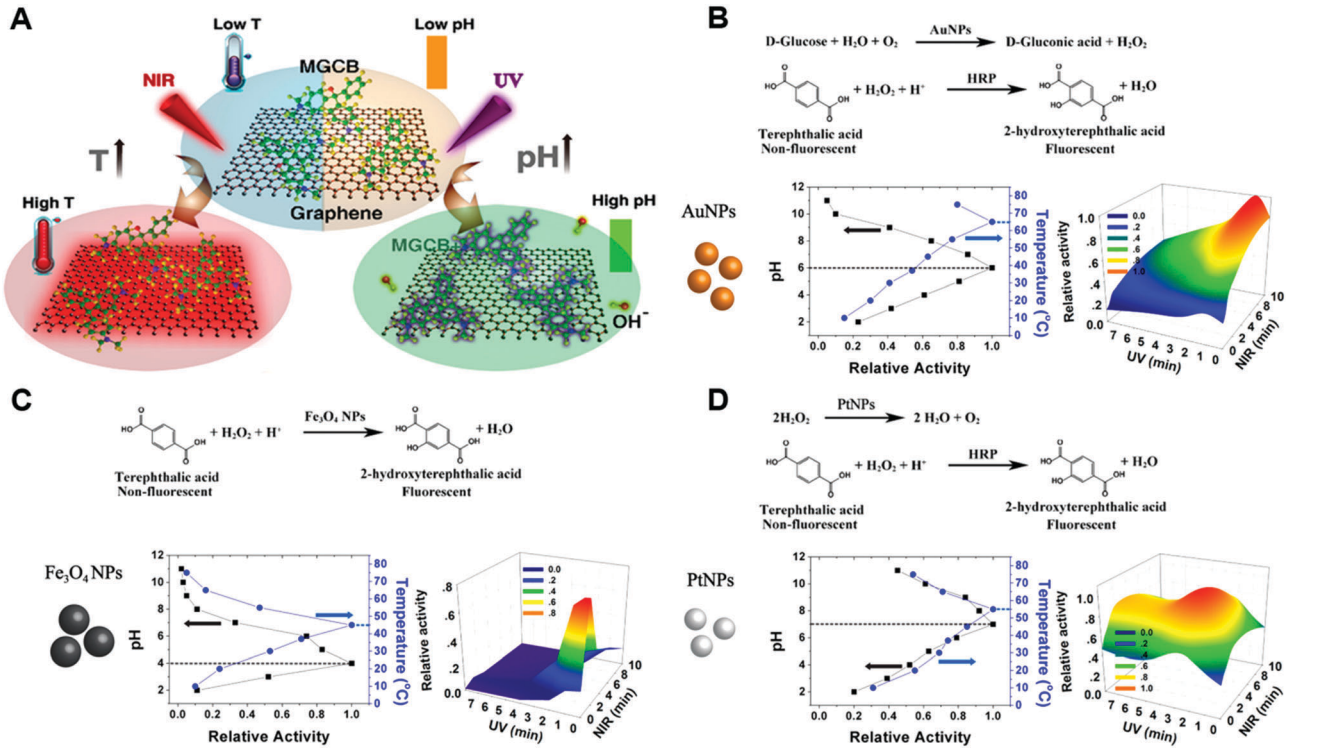

Fig. 25 (A) Photothermal effect of graphene and light-induced pH changes by MGCB. (B) The illustrations of reaction equations used to determine the activity and light-controlled AuNP activity maps obtained by varying the light irradiation time. (C) The illustrations of reaction equations used to determine the activity and light-controlled Fe_3O_4 NP activity maps obtained by varying the light irradiation time. (D) The illustrations of reaction equations used to determine the activity and light-controlled PtNP activity maps obtained by varying the light irradiation time. Adapted with permission from ref. 761. Copyright (2017) American Chemical Society.

ionic liquids and adenosine triphosphate were reported to help peroxidase-mimicking nanozymes realize high-temperature reactions.[759,760] Besides, some interesting research studies based on pH and temperature modulation were performed.[402,720,761] An *in situ* modulation of pH was demonstrated by the Wei group through proton-producing or consuming bioreactions.[402] Another photoregulation of pH and temperature was carried out with the hybrids of photobase reagent malachite green carbinol base (MGCB) and graphene oxide. Upon irradiation of ultraviolet and near-infrared light, OH^- from MGCB and high temperature from graphene oxide would be generated, respectively. Therefore, a wide range of both pH and temperature could be adjusted upon irradiation, and the catalytic activities would be tuned accordingly (Fig. 25A). For instance, for GOx-mimicking AuNPs, the optimal pH 6 at 65 °C could be achieved with ultraviolet and near-infrared light irradiation for ~1 min and ~10 min, respectively (Fig. 25B). Likewise, as shown in Fig. 25C and D, the optimal pH and temperature for peroxidase-mimicking Fe_3O_4 NPs and catalase-mimicking PtNPs could be regulated as well.[761]

3.8 Light

Due to non-pollution to the environment and efficient control with spatial and temporal precision, light has been widely used as an ideal external stimulus for reactions.[762–767] Besides the pH/temperature dual photoresponsive example mentioned above, light-induced *trans–cis* and *cis–trans* isomerization was reported by Prins and co-workers to reversibly regulate the AuNP-catalyzed hydrolysis of HPNPP (Fig. 26A). A higher affinity of *trans* isomerization to the monolayer functionalized AuNPs would inhibit the adsorption of substrate HPNPP, therefore reducing the hydrolysis activity. Upon irradiation at 365 nm, *trans–cis* isomerization would happen. Meanwhile, the *cis* isomer with a lower affinity to the NP surface would help up-regulate the transphosphorylation rate of HPNPP. Further irradiation at 465 nm and 365 nm would repeat the *cis–trans* and *trans–cis* isomerization cycle and the down- and up-regulation.[768] Likewise, the catalytic activity of the azobenzene modified Pd nanozyme could be controlled by light induced isomerization, where cyclodextrin was present in the system. *trans*-Azobenzene binding to cyclodextrin *via* a host–guest interaction could prevent the substrates from active sites and thus inhibit the catalytic activity of Pd nanozymes. However, upon UV light irradiation, transformation from *trans* to *cis* would cause the dissociation of cyclodextrin and recover the activity with the exposed catalytic sites. Further application of such light-gated nanozymes will be demonstrated in the Applications section.[769]

Moreover, under a visible light ($\lambda \geq 400$ nm) trigger, the intrinsic enzyme-mimicking activities of 2 nm AuNCs templated by BSA could be enhanced. Careful mechanism studies disclosed that light stimulated BSA–AuNCs to generate electron–hole pairs, which would then activate oxygen or water to

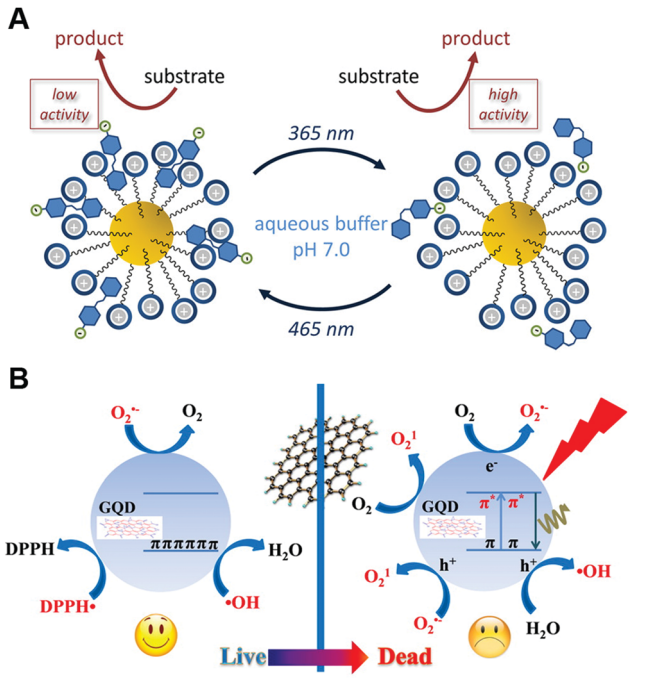

Fig. 26 (A) Light-induced *cis–trans* isomerization changes the affinity for AuNPs, which affects the transphosphorylation rate of HPNPP. (B) Light-induced crossover between anti- and pro-oxidant activities of graphene quantum dots. (A) Reprinted with permission from ref. 768. Copyright (2017) American Chemical Society. (B) Reprinted with permission from ref. 770. Copyright (2016) American Chemical Society.

produce $^{\bullet}OH$ and $O_2^{\bullet-}$ for TMB oxidation.[771] Likewise, the Xia group found that elevated peroxidase-like activities of 15 nm AuNPs could be obtained under visible light (532 nm) irradiation.[772] In addition to AuNPs, GQDs were also reported to accelerate the oxidation of ascorbate and glutathione, as well as to promote the lipid peroxidation in liposomes upon exposure to blue-violet light at 405 nm. The underlying reason was the light-induced regulation of anti- and pro-oxidant activities of GQDs (Fig. 26B).[770] In a common condition without any light, the as-synthesized 3–6 nm GQDs were capable of eliminating several free radicals like $^{\bullet}OH$, $O_2^{\bullet-}$ and DPPH$^{\bullet}$ (nitrogen-centered free radical), ascribed to the presence of surface unpaired electrons of GQDs and the intrinsic properties of π-conjugated GQDs for charge transfer and electron storage. However, upon light irradiation, instead of protecting cells from anti-oxidative damage, GQDs would generate more free radicals and thus cause cellular toxicity. The photo-induced free radicals were experimentally verified to be $^1O_2$, $^{\bullet}OH$ and $O_2^{\bullet-}$. Further systematic mechanism studies elucidated the origin of these free radicals: for $^1O_2$ generation, both energy-transfer and electron-transfer pathways *via* GQDs were proposed. The authors speculated that $O_2^{\bullet-}$ was also involved in producing $^1O_2$. Therefore, besides the previous report of energy-transfer to oxygen, the electron-transfer pathway was also followed. For $^{\bullet}OH$ and $O_2^{\bullet-}$, the generation process was similar to light-stimulated BSA–AuNC systems mentioned above.[770]

3.9 Other strategies

Considering the oxygen vacancy-dependent catalytic activities of nanoceria (elucidated in Section 2.4.2), some interesting methods were reported using small molecules (*e.g.*, H_2O_2) to directly prepare vacancy-rich ceria nanozymes rather than doping. Thanks to the unique chemical structure of vacancies as catalytic hotspots, substrates could be selectively bound to exposed Ce^{4+} and Ce^{3+} and then facilitate the whole reaction process.[773] For the special porous structure of MOFs, general engineering of linkers and nodes for topologies with more active sites accessible would elevate the catalytic rate.[521,774] Given the Lewis acidic active site for hydrolysis reaction, other cofactors such as NH_2 modification would promote the proton transfer, just like the aspartate and histidine residues in a natural phosphotriesterase.[775] Another strategy for speeding up the catalysis of water insoluble substrates was developed with Pickering emulsions. AuNPs functionalized with catalytic groups were loaded on mesoporous silica to form a surface-active nanozyme, followed by assembling at the Pickering emulsion droplet interface to improve the catalysis of two phase separated substrates.[776]

4. Applications

With the expanded types of nanozymes and engineered high performance, outstanding applications have been accomplished and discussed as follows.

4.1 *In vitro* sensing

4.1.1 H_2O_2 detection. H_2O_2 detection based on nanozymes, especially peroxidase mimics, has been extensively studied ever since Wang and Wei's report of a colorimetric assay for H_2O_2 detection by using Fe_3O_4 MNPs as peroxidase mimics.[84,93,94,146,183,209,215,220,236,311–317,347,354,580,777–829] The general principle is monitoring the signal change of a substrate which is oxidized by H_2O_2 with the assistance of a peroxidase-like nanozyme (Fig. 27). Due to the various types of substrates, different assays based on colorimetric, fluorescence, electrochemical, and Raman signals could be designed (Table S8, ESI†). In addition, the signals for sensing could also be generated by multi-functional peroxidase mimics. For instance, Chen and

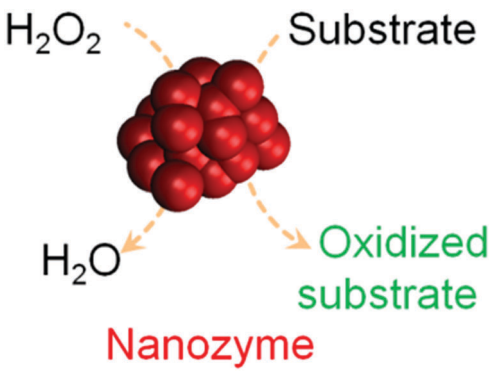

Fig. 27 Nanozyme as a peroxidase mimic for H_2O_2 detection. Reprinted with permission from ref. 29. Copyright (2016) Royal Society of Chemistry.

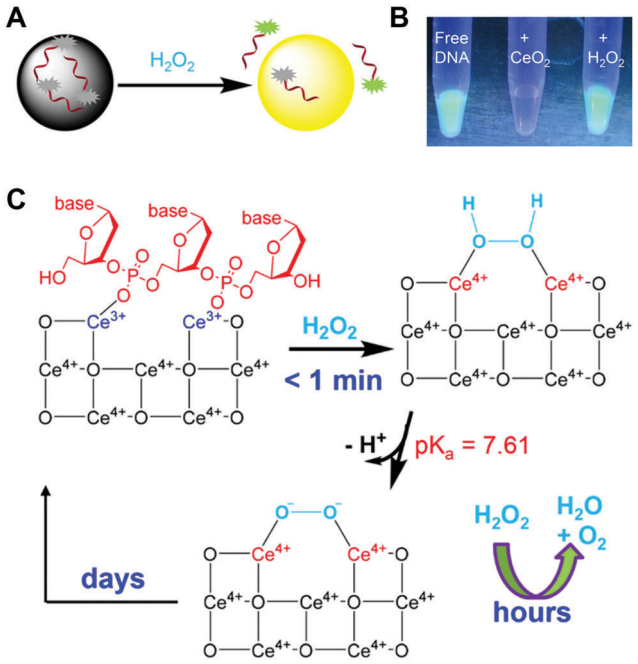

Fig. 28 (A) Sensing H_2O_2 by displacing the adsorbed fluorescent DNA from the nanoceria surface. (B) A fluorescence photo of free FAM-A_{15} DNA, after adding CeO_2 and then adding H_2O_2. (C) A proposed mechanism of H_2O_2 induced DNA release by capping the nanoceria surface. Adapted with permission from ref. 831. Copyright (2015) American Chemical Society.

co-workers fabricated a peroxidase-mimicking MOF containing catalytic Cu^{2+} and luminescent Tb^{3+}. In the presence of H_2O_2, ascorbic acid was catalyzed by the MOF to diketohexanoic acid, which would then sensitize Tb^{3+} to produce strong luminescence. Based on this multi-functional nanozyme, a luminescence sensing assay of H_2O_2 with high selectivity and sensitivity was built.[830]

Recently, Liu *et al.* found an interesting phenomenon that instead of oxidative DNA cleavage, H_2O_2 would prefer to displace fluorophore-labeled DNA from the surface of CeO_2 with over 20-fold fluorescence recovery. Therefore, a sensitive H_2O_2 sensor was developed with a detection limit of as low as 130 nM (Fig. 28). And the possible sensing mechanism is proposed in Fig. 28C. The interaction between the phosphate group of DNA and the Ce^{3+} resulted in the adsorption of dye-labeled DNA, accompanied by fluorescence quenching. Due to the fast oxidation of Ce^{3+} into Ce^{4+} by H_2O_2, the adsorbed DNA would be released from the surface and return back to a fluorescent state. On the other hand, for bound H_2O_2, it would be finally decomposed into H_2O and O_2 under the catalase-like catalysis of CeO_2 NPs.[831]

Another interesting H_2O_2 detection was demonstrated by Sotiriou *et al.* with rationally designed enzyme-mimicking luminescent NPs. By doping Eu^{3+} into CeO_2, the as-prepared catalase-like luminescent NPs could efficiently decompose H_2O_2 into O_2, which would in turn quench the luminescence of these NPs. Based on the change of the luminescence, a detection limit of 150 nM H_2O_2 was achieved.[832]

4.1.2 Detection of glucose and other oxidase substrates. Some substrates can be oxidized by their corresponding oxidases to generate H_2O_2. Therefore, taking advantage of the aforementioned H_2O_2 detection, a combination of these oxidases with H_2O_2 detection assay would help a further sensing of the oxidase substrates (*e.g.*, glucose,[150,170,184,185,209,220,233,260,309–311,598,642,702,778,779,833–883] lactate,[884–886] cholesterol,[244,288,887–897] choline,[277,898,899] and xanthine[214,246,351,797,900]). A summary of all oxidase substrates is listed in Table S9 (ESI†). For example, glucose in drinks and biological samples (such as blood and urine) has been detected by combining GOx and nanozymes with peroxidase-like activities. However, there were some issues with this combination such as low diffusion efficiency and unstable intermediates, which would result in limited catalytic efficiency of the cascade reaction. Recently, integrated nanozyme GOx/hemin@ZIF-8 with nanoscale proximity effect was developed by Wei and co-workers to fill this gap, as mentioned in Section 3.4 and Fig. 22. Attributed to the significantly enhanced efficiency, high sensitivity and specificity of 1.7 μM glucose were achieved.[690] Likewise, other nanozymes such as AuNPs as GOx mimics and NiPd/V_2O_5/2D MOF as an alternative to hemin were also used to construct the integrated nanozymes, respectively.[691,695,696] For example, Zhang *et al.* developed a colorimetric method for glucose detection by using the AuNPs/Cu–TCPP(M) (M = Fe, Co) composite (Fig. 29A), with a detection limit of 8.5 μM. The composite nanozyme was prepared with AuNPs directly grown onto the 2D MOF nanosheet.[696] Further considering the multiple enzymatic activities of AuNPs, a three-in-one nanoplatform (*i.e.*, sensing, self-assembly, and cascade catalysis) was fabricated by Xia *et al.* and the glucose detection could be achieved using the sole AuNP catalyst, as shown in Fig. 29B.[901]

4.1.3 Nucleic acid detection. Nucleic acid (*e.g.*, DNA and RNA) detection plays a vital role in the fields of human genetics, clinical diagnosis, cytology, *etc.* Therefore, a variety of methods with nanozymes for nucleic acid detection (most for DNA detection) were developed along with the huge achievements

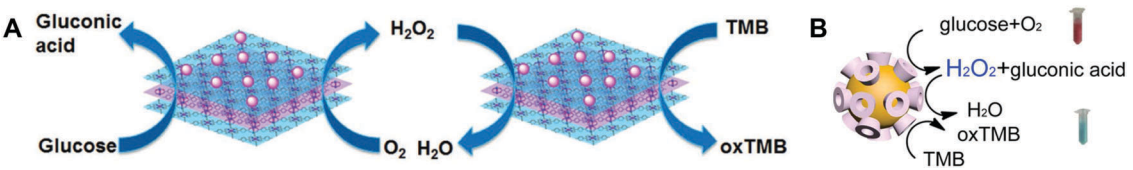

Fig. 29 Schematic illustration of the enzyme-mimicking cascade reaction catalyzed by (A) AuNPs/Cu–TCPP(M) (M = Fe, Co) and (B) Au nanozymes. (A) Reprinted with permission from ref. 696. Copyright (2017) John Wiley and Sons. (B) Reprinted with permission from ref. 901. Copyright (2016) American Chemical Society.

made in the nanozymes field. The present methods could be mainly classified into two types: (1) nanozymes as tags to label nucleic acids for signaling and (2) nucleic acid detection by tuning nanozymes' activities.

For the first type, various studies have demonstrated the detection of target DNA through the conjugated nanozymes for signaling.[273,902–904] For example, Ju and co-workers developed a streptavidin-functionalized complex of graphene loaded ferric porphyrin with a peroxidase-mimicking activity for specific recognition of biotinylated molecular beacon. In the presence of target DNA, the pre-immobilized hairpin structure could be opened, followed by the binding of streptavidin-functionalized nanozyme through the interaction between streptavidin and biotin. Then, the nanozyme could catalyze the oxidation of *o*-phenylenediamine into oxidized *o*-phenylenediamine in the presence of H_2O_2, which in turn produced electrochemical signals for quantification of DNA. With the electrochemical detection platform, a detection limit of attomolar levels could be achieved.[905] Likewise, global DNA methylation in colorectal cancer cell lines was successfully detected using peroxidase-mimicking mesoporous Fe_2O_3 (Fig. 30A). The extracted and denatured ssDNA (single-stranded DNA) from colorectal cancer cell lines was adsorbed on a bare screen-printed gold electrode surface. Fe_2O_3 nanozymes, modified with the 5-methylcytosine antibody, could specifically recognize the methylcytosine groups on target DNA. Therefore, either an electrochemical signal or a colorimetric signal could be used for detection by catalyzing the oxidation of TMB in the presence of H_2O_2. As low as 10% difference in the global DNA methylation level was detected.[906]

Besides DNA, microRNA detection was also reported. In their platform, Wang and co-workers used two nanozymes (Fe_3O_4 and planar Cu(II) complex) and the hybridization chain reaction protocol for signal amplification. In the presence of microRNA, the hybridization chain reaction could be triggered by the hairpin capture probe on Fe_3O_4 NPs. Then the planar Cu(II) complex intercalated into the formed DNA duplex structure. Such a complex with binanozymes (Fe_3O_4 and planar Cu(II) complex) could be enriched on the surface of magnetic glassy carbon electrode. Similar to the DNA detection platform mentioned above, both electrochemical and colorimetric signals were generated for sensing, with a detection limit of as low as 33 aM (with the electrochemical method).[907]

The second type was mainly based on the activity regulation by nucleic acids, as elucidated in Section 3.5.[148,169,284,695,727,908–910] For instance, Park *et al.* reported a colorimetric method for DNA detection by coupling oxidase-mimicking CeO_2 NPs with polymerase chain reaction (PCR) technology. As shown in Fig. 30B, without the target DNA, colorless substrates could be oxidized to dark blue. On the other hand, in the presence of the target DNA, amplified DNA could be quickly formed by PCR technology,

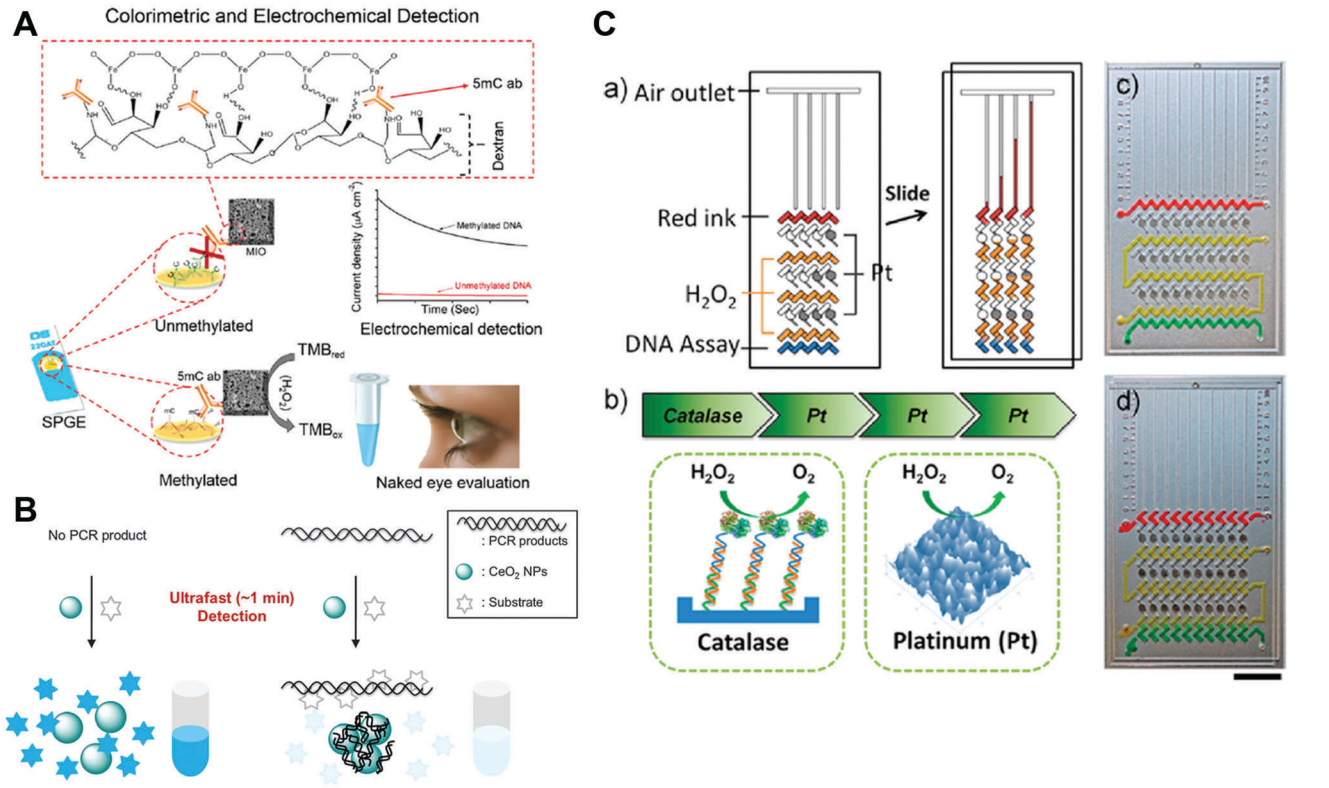

Fig. 30 (A) Schematic representation of the colorimetric and electrochemical detection of global DNA methylation by using mesoporous Fe_2O_3 nanozymes. (B) Combining oxidase-mimicking CeO_2 NPs with PCR technology for colorimetric detection of target DNA. (C) Catalase-mimicking Pt films for constructing a multistage propelled volumetric bar chart chip for sensitive detection of DNA. (A) Adapted with permission from ref. 906. Copyright (2018) Royal Society of Chemistry. (B) Reprinted with permission from ref. 911. Copyright (2014) Royal Society of Chemistry. (C) Reprinted with permission from ref. 912. Copyright (2013) American Chemical Society.

which then significantly inhibited the activity of the CeO_2 nanozyme by shielding its surface. Moreover, the potential clinical utility of this sensing platform was successfully demonstrated by detecting model target nucleic acids from *Chlamydia trachomatis* using a human urine sample.[911]

Besides, another innovative concept for DNA detection was reported by using catalase-mimicking Pt films with a multistage propelled volumetric bar chart chip. As shown in Fig. 30C, the presence of the target DNA formed a sandwich DNA hybrid, which would induce the decomposition of H_2O_2 to generate O_2 by catalase (note, the catalase was conjugated onto a probe ssDNA). Subsequently, with the assistance of the produced oxygen, the fuel (*i.e.*, H_2O_2) would be propelled to react with catalase-like Pt films to produce additional oxygen gas for signal amplification. After three amplified rounds, the red ink bar charts could be pushed to a long distance, which would be used for the quantification of DNA, with a detection limit of as low as 20 pM.[912]

4.1.4 Protein detection. For protein detection, a widely used technology is immunoassay, taking advantage of the unique recognition between an antibody and an antigen.[166,171,180,182,368,621,913–948] In the seminal study of nanozymes, Yan *et al.* reported two interesting immunoassays for protein detection using peroxidase-mimicking Fe_3O_4 MNPs.[1] Since then, numerous immunoassays have been developed with antibody conjugated nanozymes. In their subsequent study, Yan *et al.* developed a nanozyme-strip for Ebola diagnosis using peroxidase-mimicking Fe_3O_4 MNPs (Fig. 31B). Compared with a standard colloidal gold strip, the nanozyme-strip could amplify the signal by catalyzing the oxidation of peroxidase substrates in the presence of H_2O_2, which significantly enhanced its detection sensitivity by 100-fold, with a detection limit of as low as 1 ng mL^{-1} for the glycoprotein of Ebola virus (EBOV) (Fig. 31C and D). If utilizing the magnetic separation property of MNPs to enrich targets, another 10-fold enhancement could be achieved, as shown in Fig. 31E. Furthermore, the clinical samples could be diagnosed within 30 min and the detection accuracy was comparable to ELISA. These results demonstrated that the nanozyme-strip could provide a much faster and simpler platform for diagnosis of infection in Ebola-stricken areas.[949]

Instead of Fe_3O_4 MNPs, Xia *et al.* used Pd–Ir cubes with peroxidase-like activities for immunoassays of human prostate-specific antigen (PSA). Compared with conventional immunoassays, the Pd–Ir nanozyme based ELISA exhibited 110-fold lower limit of detection.[622] To further enhance the detection sensitivity of immunoassays, they developed gold vesicle encapsulated Pd–Ir NPs as peroxidase mimics in their following study. As shown in Fig. 32, numerous Pd–Ir NPs could be released from the gold vesicles upon heating, resulting in a signal amplification platform for immunoassays. This method achieved a detection limit of femtogram per mL for PSA, which was three orders of magnitude lower than that of the conventional immunoassays.[194]

The unique recognition could come not only from an antigen and an antibody, but also from an aptamer and its corresponding target.[646,950–956] For example, Yang *et al.* developed a label-free colorimetric method for thrombin detection. One anti-thrombin aptamer was first immobilized onto the 96-well microplates by biotin–streptavidin interaction. Another ssDNA contained one part of anti-thrombin aptamer and another part of template DNA for Ag/Pt NC preparation. In the presence of target thrombin, the two aptamers would be conjugated to form a sandwich structure. Then, the DNA-templated Ag/Pt bimetallic nanoclusters would catalyze the oxidation of TMB to oxTMB for colorimetric signaling. A detection limit of 2.6 nM was obtained for thrombin.[181] Besides, based on the recognition between Zr^{4+} and phosphate, Song and co-workers synthesized Zr^{4+}-functionalized Pt/carbon dots as peroxidase mimics to recognize and detect phosphoproteins.[957]

In addition, colorimetric cross-reactive sensor arrays (the so-called "chemical noses/tongues") were also reported for protein discrimination. The detection principle was that the differential interactions between proteins and the layers on nanozymes would modulate the catalytic activities of nanozymes to varying degrees, thus generating differential colorimetric signals for protein discrimination. Both Fe_3O_4 NPs functionalized with cationic monolayers and AuNPs–ssDNA conjugates have been utilized to construct sensor arrays for protein discrimination. And the two arrays could differentiate ten proteins at 50 nM and seven proteins at 10 nM, respectively. When processing with unknown samples, 95% and 100% accuracy was achieved with the Fe_3O_4 NP and AuNP based arrays, respectively.[958,959]

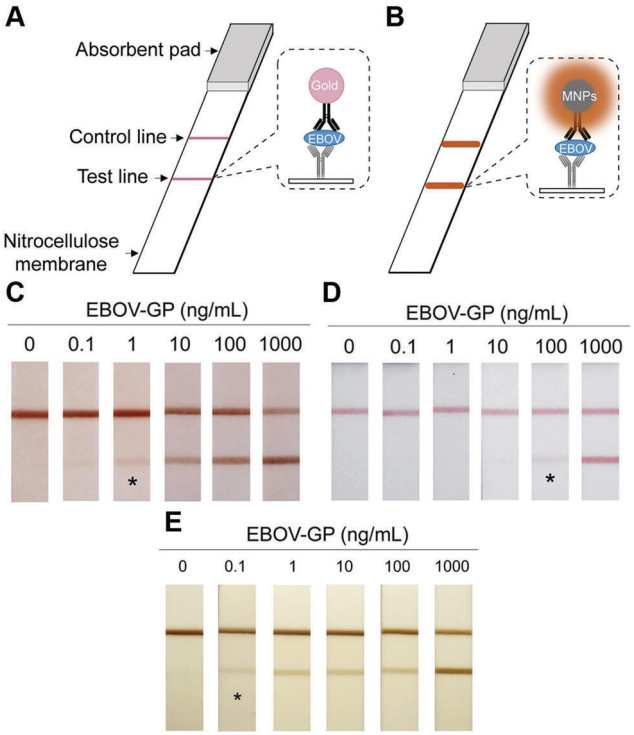

Fig. 31 (A) Standard AuNP-based strip. (B) Nanozyme-strip employing Fe_3O_4 MNPs in place of AuNPs. (C) Nanozyme-strip, (D) standard colloidal gold strip and (E) nanozyme-strip combined with magnetic enrichment for EBOV-GP detection. The asterisk (*) indicates the limit of visual detection of the test line in strips. Adapted with permission from ref. 949. Copyright (2015) Elsevier.

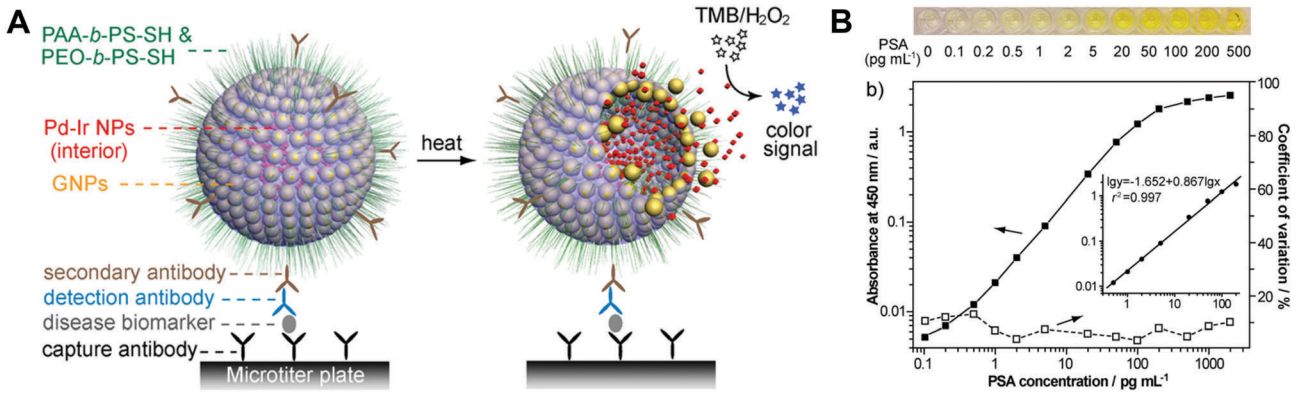

Fig. 32 (A) ELISA for ultrasensitive detection of disease biomarkers by using gold vesicle encapsulated Pd–Ir NPs for signal amplification. (B) Gold vesicle encapsulated Pd–Ir NP based ELISA for detection of PSA. Reprinted with permission from ref. 194. Copyright (2017) American Chemical Society.

4.1.5 Cell (cancer markers on cell surface) detection. Overexpressed proteins on cell surface could be used as biomarkers for early cancer diagnosis.[179,231,259,283,290,370,960–966] Therefore, the aforementioned detection methods for proteins would give a hint for sensing cancer cells. For example, Gao *et al.* developed a sensitive and selective nanoprobe for precisely quantifying the expression level of integrin GpIIb/IIIa on the human erythroleukemia (HEL) cell line (Fig. 33A). The peptide conjugated AuNP nanoprobe could specifically recognize the integrin through an integrin specific peptide and generate a colorimetric signal by catalyzing the oxidation of TMB in the presence of H_2O_2. About 6.4×10^6 integrin receptors could be detected on a single HEL cell using the nanozyme detection platform.[967]

Trau, Wang, and co-workers established a circulating tumor cell (CTCs) detection platform with Fe_3O_4 MNPs. The MNPs were modified by anti-melanoma-associated chondroitin sulfate

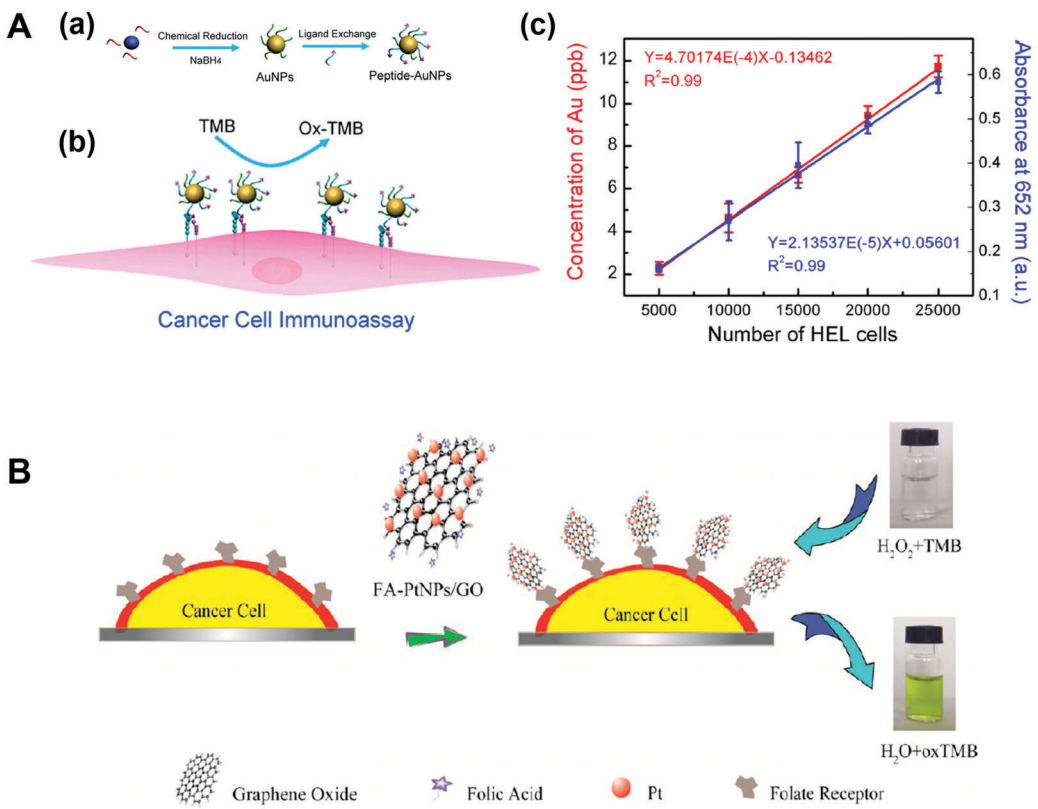

Fig. 33 (A) Peptide–AuNP conjugates for cancer cell immunoassay. (a) Preparation of peptide conjugated AuNPs by chemical reduction and ligand exchange. (b) Peptide–AuNP mediated cancer cell immunoassay by catalyzing the oxidation of TMB in the presence of H_2O_2. (c) Linear regression plotting HEL cell number *versus* Au concentration (red curve) and absorbance at 652 nm (blue curve). (B) Schematic of colorimetric detection of cancer cells by using folic acid functionalized PtNPs/GO nanocomposites. (A) Reprinted with permission from ref. 967. Copyright (2015) American Chemical Society. (B) Reprinted with permission from ref. 971. Copyright (2014) American Chemical Society.

proteoglycan (MCSP) antibodies for recognizing MCSP expressed on melanoma CTCs. The MNPs exhibited bi-functionalities, including peroxidase-like activity and magnetic property. The peroxidase-like activity was used for signaling, while the magnetic property was used for CTC isolation and enrichment. On the basis of this detection platform, 13 melanoma CTCs per mL could be successfully detected within 50 min.[968] Similarly, over-expressed mucin 1 proteins (MUC-1) on MCF-7 CTCs were recognized by the anti-MUC-1 aptamer functionalized copper oxide nanozymes or Fe_3O_4 nanozymes. With signal amplification, as low as 27 and 6 cells mL^{-1} could be successfully detected, respectively.[969,970]

Chen *et al.* developed folic acid modified platinum NPs/graphene oxide (PtNPs/GO) nanocomposites for specific cancer cell detection (Fig. 33B). The PtNPs/GO exhibited an enhanced peroxidase-like activity, which could catalyze the oxidation of TMB in the presence of H_2O_2 for signaling. When modified by folic acid, the nanocomposites could target cancer cells *via* over-expressed folic acid receptors on the cell membrane. The detection platform based on peroxidase-mimicking PtNPs/GO nanocomposites showed high sensitivity for cancer cells. Even 125 cells could be detected by naked eyes.[971] Besides protein receptors, other over-expressed molecules such as glycans and epithelial cell adhesion molecule (EpCAM) have also been utilized for cancer cell detection by coupling with their bio-recognition ligands like lectin and an anti-EpCAM aptamer (SYL3C).[675,972]

4.1.6 Ion detection. As discussed in Section 3.6, several ions could be used for tuning nanozymes' activities. Therefore, on the basis of their inhibitory or enhanced effects on nanozymes' activities, several metal ions, such as Cu^{2+}, Hg^{2+}, and Ag^{+}, have been detected with nanozymes.[143,199,242,366,740,973–980] For instance, as shown in Fig. 34, Xia and co-workers demonstrated that PVP-capped Pt nanocubes as peroxidase mimics could catalyze the oxidation of TMB to generate a colorimetric signal. However, if Ag^{+} existed in the system, it would adsorb on the surface of PtNPs and block the access of catalytic active sites, leading to the inhibition of the PVP-capped Pt cubes' activity. Based on this principle, a biosensor was constructed for Ag^{+} detection. The biosensor had a linear range of 10^{-2}–10^{4} nM with a detection limit of 80 pM.[981] Likewise, Chen *et al.* found that the peroxidase-like activity of 2.5 nm citrate-capped PtNPs could be evidently inhibited because of the Hg–Pt interaction. Therefore, they fabricated a sensitive and selective biosensor for Hg^{2+} based on this principle. The detection limit of this biosensor was as low as 8.5 pM.[163] In contrast to inhibition of the activity, Lu *et al.* reported that Hg^{2+} could significantly improve the peroxidase-like activity of rGO/PEI/Pd nanohybrids because the physicochemical property of PdNPs was changed after forming a Pd–Hg thin amalgam layer. According to this phenomenon, an assay for detecting low concentrations of Hg^{2+} was designed with the rGO/PEI/Pd nanozyme. As low as ~10 nM Hg^{2+} in wastewater or serum was detected by the naked-eye-based

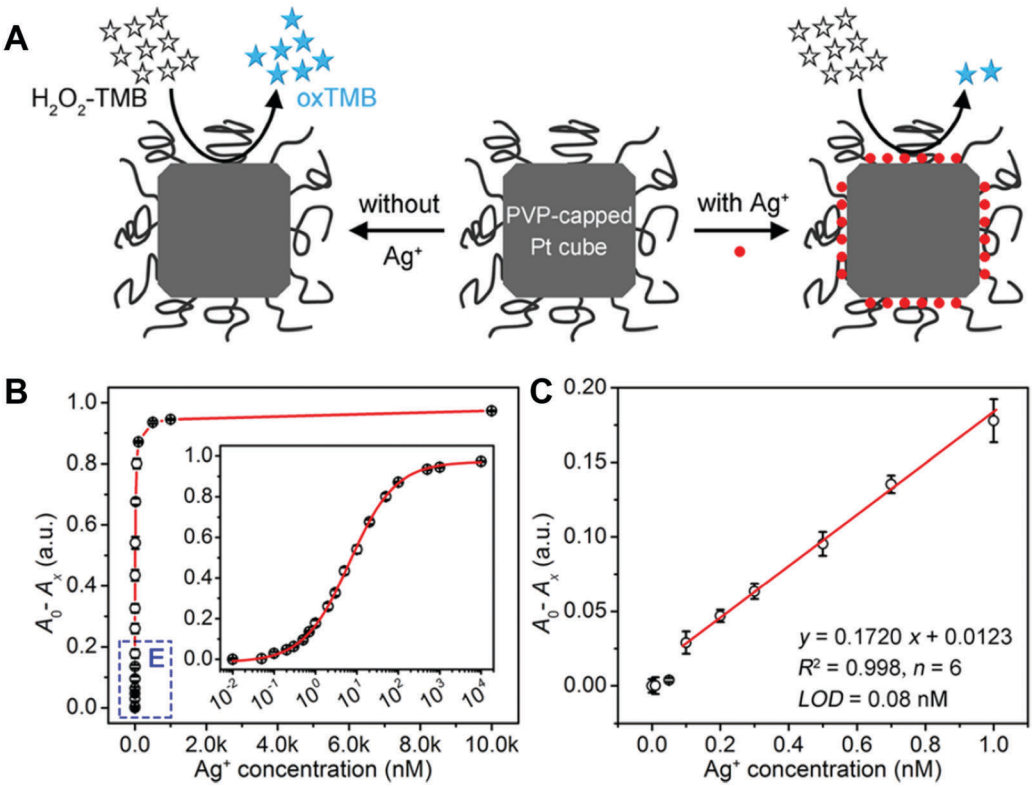

Fig. 34 PVP-capped Pt cubes with peroxidase-like activity for Ag^{+} detection. (A) Schematic of the detection principle. (B) Calibration curve obtained by plotting the decreased absorbance at 653 nm ($A_0 - A_x$) *versus* Ag^{+} concentration. (C) Linear range of the calibration curve shown in panel B. Reprinted with permission from ref. 981. Copyright (2017) American Chemical Society.

colorimetric method, demonstrating its potential applications in environmental monitoring, clinical diagnosis, *etc.*[738]

Several anions, such as F^-, S^{2-}, and CN^-, were detected by using nanozymes.[365,422–424,741,982–988] For example, Liu *et al.* found that the oxidase-like activity of nanoceria could be enhanced by over two orders of magnitude after capping with fluoride. Their study suggested that surface charge modulation and facilitated electron transfer were responsible for boosting the oxidase-like activity of nanoceria after modified with F^-. On the basis of this principle, sensitive detection of F^- was achieved with a detection limit of 0.64 μM (Fig. 35). Moreover, other common anions showed no interference with this colorimetric sensor, which allowed for selective detection of F^-.[739] Guo *et al.* demonstrated that S^{2-} detection can be achieved based on its switching effect on the peroxidase-like activity of Pt nanozymes.[985] Huang and co-workers' study suggested that CN^- can effectively inhibit the peroxidase-like activity of cobalt hydroxide/oxide modified graphene oxide (CoO_xH–GO), which allowed for the construction of a sensing platform for detecting CN^-. Moreover, by coating CoO_xH–GO on the nylon membrane, a membrane-based sensing platform was fabricated for detection of CN^- in wastewater samples.[989]

Another interesting example about a colorimetric aptasensor for K^+ detection was demonstrated by Li *et al.* with peroxidase-mimicking AuNPs and K^+ specific binding aptamers. In the presence of aptamers, the peroxidase-like activity of AuNPs was significantly improved because of the enhanced affinity between aptamer-modified AuNPs and TMB. The presence of target K^+ would convert aptamers to form a G-quadruplex structure, resulting in the inhibition of the peroxidase-like activity of AuNPs. As low as 0.06 nM K^+ could be detected by the colorimetric aptasensor.[990] Recently, the Wei group demonstrated that five phosphates could be discriminated using 2D MOF nanozyme sensor arrays. More encouragingly, real-time biologically related events involving the hydrolytic processes of ATP and pyrophosphate could be probed by the as-designed nanozyme sensor arrays.[991]

4.1.7 Others. Besides the above mentioned analytes, several other targets were also successfully detected by regulating the catalytic activities of nanozymes.[86–88,145,156,157,175,181,186,241,257,294,304,369,414,578,581,605,673,729,742,992–1035] For example, as we mentioned in Section 3.7, an *in situ* modulation of pH was demonstrated by the Wei group through proton-producing or consuming bioreactions (Fig. 36A). Therefore, the proton-producing/consuming enzyme acetylcholinesterase (AChE)/urease could be detected based on the enhanced/decreased activity of CeO_2. Similarly, other important targets (such as nerve agents, drugs, and ions) which could cooperatively regulate nanoceria's catalytic activity were also detected.[402]

Melamine was detected by a colorimetric method based on its enhancement of AuNPs' peroxidase-like activity.[1036] GSH and L-cysteine were detected on the basis of their competitive inhibition of nanozymes' catalytic reaction.[164,200,216,307,1037–1047] For example, Fu *et al.* found that biothiols, such as L-cysteine and homocysteine, could effectively inhibit the oxidation of TMB in the presence of bimetallic Au_xPt_y nanozyme and H_2O_2.

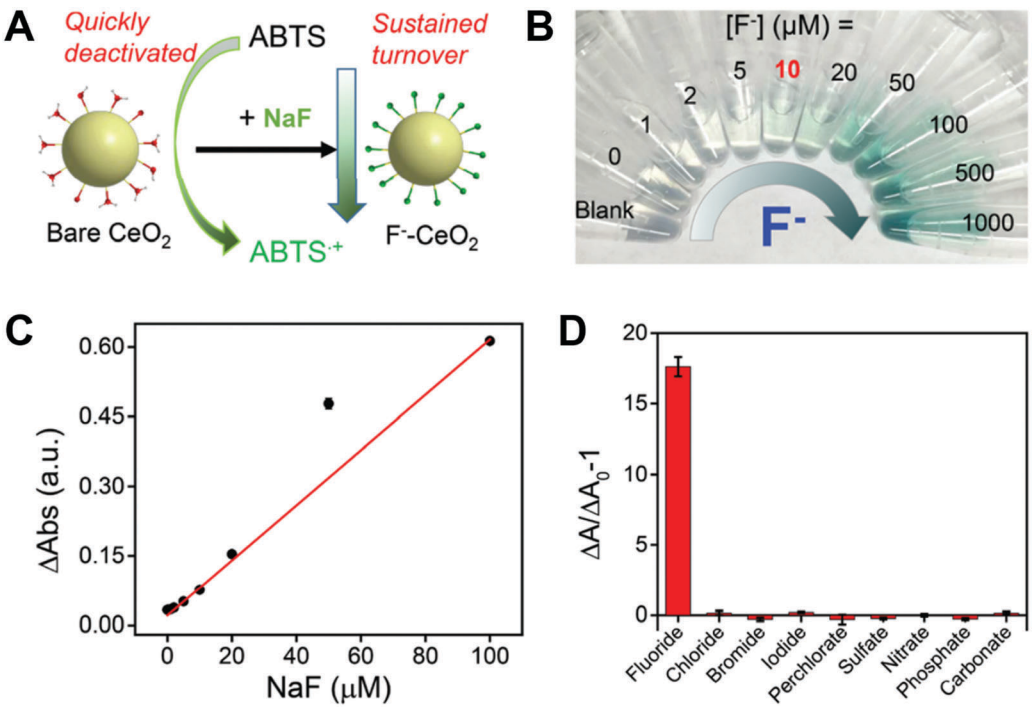

Fig. 35 Detection of F^- by boosting the oxidase-mimicking activity of nanoceria. (A) Schematic of boosting the oxidase-like activity of nanoceria by capping with F^-. (B) Photographs of the F^- concentration dependent sensor color change. (C) Calibration curve by plotting the relative change of absorbance (ΔAbs) as a function of F^- concentration. (D) Selective detection of F^- against various common anions. Reprinted with permission from ref. 739. Copyright (2016) Royal Society of Chemistry.

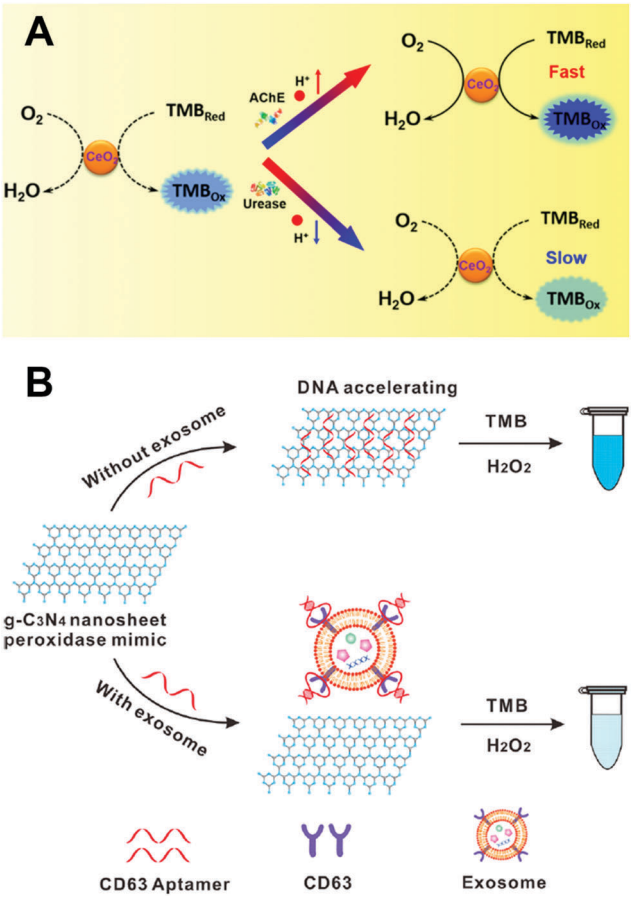

Fig. 36 (A) Self-regulated bioassays by rationally modulating the oxidase-like activity of nanoceria for probing enzyme activity and other related targets. (B) Tailoring the peroxidase-like activity of g-C_3N_4 nanosheets with an aptamer for the detection of exosomes. (A) Reprinted with permission from ref. 402. Copyright (2016) American Chemical Society. (B) Reprinted with permission from ref. 1048. Copyright (2017) American Chemical Society.

Based on this phenomenon, as low as 3.5 nM L-cysteine was detected by the as-designed biosensor.[187] Likewise, the detection of bacteria with a detection limit of 10^2 cfu mL^{-1} was achieved based on the inhibition of catalytic activity of dopamine coated Fe_3O_4 nanozymes by bacteria.[1020] Another interesting finding was that heparin could significantly enhance the peroxidase-like activity of Au clusters at neural pH, which allowed for colorimetric detection of heparin and the corresponding heparinase at pH 7.[713]

Further combination of nanozymes with aptamers, bacteria (*Salmonella typhimurium*),[1049] pesticides (acetamiprid),[148,1050] antibiotics (kanamycin, sulfadimethoxine, and so on),[1051–1054] and exosomes[1048] could be tested based on highly sensitive "turn off/turn on" biosensing platforms. For example, Zhong, Jiang, and co-workers developed a colorimetric method for exosome detection in human serum. Exosomes act as extracellular vesicles for carrying cellular cargoes such as proteins and nucleic acids, which play vital roles in disease diagnosis. As shown in Fig. 36B, the peroxidase-like activity of g-C_3N_4 nanosheets could be significantly improved by ssDNA (*i.e.*, CD 63 specific aptamer), attributed to the stronger adsorption of TMB. However, the presence of exosomes carrying CD 63 would promote the release of ssDNA from the surface of g-C_3N_4 nanosheets, thus decreasing the catalytic activity. Quantification of exosomes could be achieved by the naked eye or UV-visible spectroscopy. Moreover, the colorimetric method could discriminate the expression of CD 63 on the surface of exosomes collected from breast cancer patients and healthy controls, demonstrating its practicability in clinical diagnosis.[1048] Likewise, single-walled carbon nanotubes as peroxidase mimics were also used to construct a platform for exosome detection.[1055] Note: except H_2O_2 and oxidase substrates, detection of other targets based on nanozymes is presented in Table S10 (ESI†).

4.2 *In vivo* sensing

Several studies of nanozymes for *in vivo* sensing were developed by the Wei group. As elucidated in Section 4.1.2, the nanoscale proximity effect of integrated nanozyme GOx/hemin@ZIF-8 enabled high sensitivity and specificity for *in vitro* glucose detection. Such a low detection limit of 1.7 μM and the obtained dynamic linear range of glucose from 0 to 250 μM offered the possibilities for sensing cerebral glucose in living brains. With the assistance of *in vivo* microdialysis, an off-line detection platform for cerebral glucose was developed. By mixing the microdialyzed samples with GOx/hemin@ZIF-8 and peroxidase substrates, the corresponding signals of products catalyzed by nanozymes would be generated (Fig. 37A). When choosing ABTS and Ampliflu red as peroxidase substrates, green color and fluorescence were produced for signaling, respectively.[690] Likewise, Wei and co-workers further developed another integrative nanozyme for analyte detection by Raman signals, where hemin@ZIF-8 was replaced by peroxidase-mimicking AuNPs@MIL-101. Herein, the AuNPs could not only exhibit peroxidase-like activities for catalyzing the oxidation of Raman inactive receptors into Raman active ones but also possess plasmonic properties to enhance the Raman reporters' signals. They demonstrated that after global cerebral ischemia, the blockage of cerebral blood flow would enhance anaerobic respiration, leading to a decreased glucose level. Further, the integrated nanozyme with AuNPs@MIL-101 was applied for evaluating the therapeutic efficacy of an anti-oxidation drug candidate (*i.e.*, astaxanthin (ATX)) for stroke. As shown in Fig. 37B and C, the ischemic stroke led to a decrease in the striatum glucose level and an increase in the lactate level. With the treatment of ATX, fluctuations in the glucose and lactate level were suppressed, proving ATX to be a promising drug candidate for treatment of cerebral ischemic injuries. Besides, discrimination of abnormal metabolism in tumors from that in normal tissues could also be realized with this bioassay by measuring their corresponding glucose and lactate level.[281]

In their subsequent study, they developed a series of 2D MOFs with peroxidase-like activities for monitoring the elimination process of heparin in live rats. Heparin-specific AG73 peptides would block the access of active sites after adsorbing onto the 2D MOF, which in turn decreased the catalytic activity. In the presence of heparin, the activity of 2D MOFs would

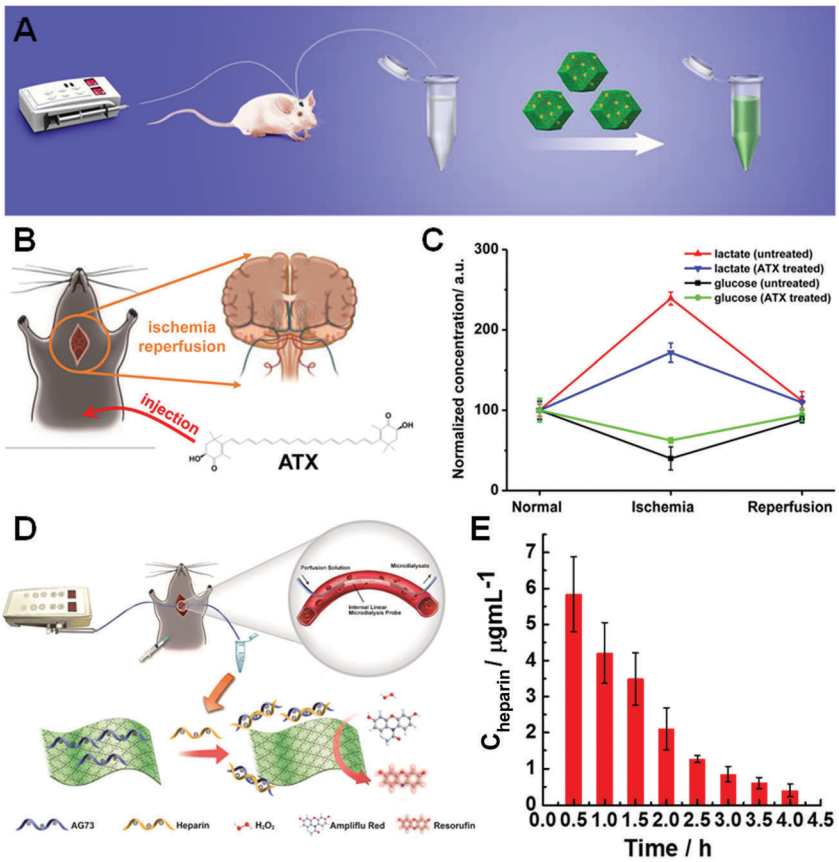

Fig. 37 (A) Schematic illustration of off-line measurement of glucose in the brain of living rats *via* the INAzyme-catalyzed cascade reactions. (B) Schematic illustration of global cerebral ischemia/reperfusion and treatment with ATX. (C) Dynamic changes of glucose and lactate following ischemia and reperfusion with and without ATX pretreatment. The glucose and lactate levels before ischemia were normalized as 100. (D) Scheme showing the monitoring of the heparin elimination process in live rats using 2D MOF nanozymes. (E) Dynamic changes of heparin concentrations in the artery of live rats over 4 h following the administration of heparin. A fitting of the data indicates an exponential decay. Error bars indicate standard deviations of three independent measurements. (A) Reprinted with permission from ref. 690. Copyright (2016) American Chemical Society. (B and C) Reprinted with permission from ref. 281. Copyright (2017) American Chemical Society. (D and E) Adapted with permission from ref. 275. Copyright (2017) American Chemical Society.

be restored. Therefore, a heparin sensing platform could be constructed with the 2D MOF. As discussed in Section 2.1.5, 2D MOFs possessed a greater catalytic activity than the bulk ones. Such an excellent activity ensured a linear range from 0.1 to 10 μg mL^{-1} and a detection limit of 15 ng mL^{-1}, thus meeting the requirements of heparin detection in clinical samples. Before *in vivo* monitoring, the high selectivity to heparin over other interfering species was also evaluated. Then the elimination process of heparin was performed with *in vivo* microdialysis technology, as shown in Fig. 37D. As the fluorescence signals indicated, an exponential decrease of heparin suggested depolymerization of heparin by the reticuloendothelial system or urine from the renal route, which was consistent with previous pharmacokinetic studies (Fig. 37E).[275]

Despite the achievement in effective *in vivo* detection of glucose and heparin, there still existed a poor temporal resolution issue for off-line sensing. To solve this problem and advance the future practical application, an online monitoring platform was constructed by immobilizing nanozymes into the channel of the microfluidics chip, as shown in Fig. 38A. Benefiting from the online platform, the dynamic changes of cerebral glucose could be monitored. In Fig. 38B, a decrease to 49.1 ± 12.7% after global ischemia was observed, matching well with the off-line results of 50.2 ± 8.3%. Further reperfusion led to a recovery back to 98.4 ± 10.1% of the basal level. Such an online detection platform demonstrated its practical applications for *in vivo* sensing and may help explore the mechanism of an unclear illness.[690]

Recently, Guo, Fang, and co-workers fabricated a needle-type microelectrode by layer-by-layer deposition of Cu nanoflowers, GOx, and polyurethane. The large surface area of Cu nanoflowers ensured an excellent catalytic activity and the mass transport limited by polyurethane membrane made the sensor stable. Such an integrated microelectrode was then implanted under the skin of cervical dorsal of anesthetized rats. A real-time detection of the change of blood glucose level was realized, and the detection results were consistent with those obtained from a glucose meter.[1056] Andreescu and co-workers used Pt-doped nanoceria and lactate oxidases as electrochemical microbiosensors to realize *in vitro* detection of lactate and

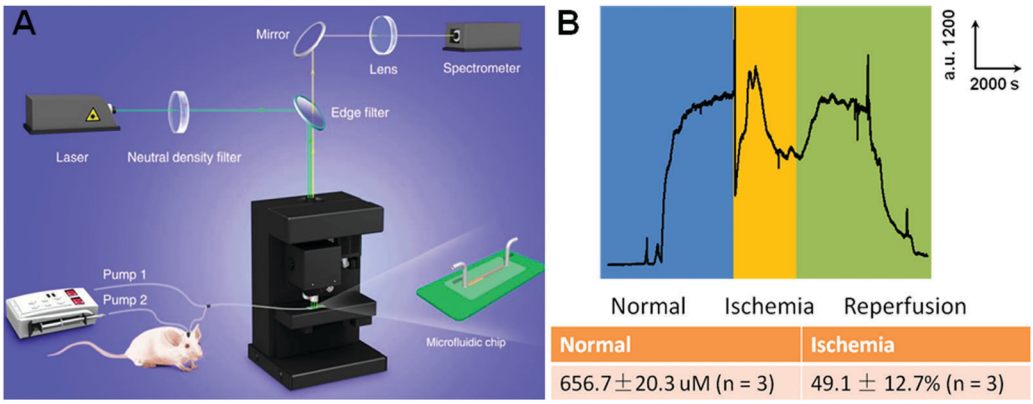

Fig. 38 (A) The INAzyme-based integrative fluorescence sensing platform for continuous *in vivo* measurement of neurochemicals (glucose as an example here) in living rats. The platform mainly consisted of three parts: (a) the microdialysis device, which included two pumps with syringes, a microdialysis probe (inserted in the rat's brain), and a T-junction, connected with tubing; (b) the fluorescence microscope, which included the excitation laser and a spectrometer; and (c) the microfluidic chip, which was connected with the microdialysis device *via* the tubing and had the INAzyme immobilized in its microchannel. The 532 nm laser through the microscope was focused onto the sample within the microchannel with a distance of 2 mm far from the outlet. The resultant fluorescence spectra of the sample were continuously collected. (B) Continuously monitoring the dynamic changes of glucose level in the striatum of a living rat brain following global ischemia/reperfusion with the INAzyme-based sensing platform. Adapted with permission from ref. 690. Copyright (2016) American Chemical Society.

further *in vivo* monitoring of lactate levels in anesthetized rats continuously for 2 h ischemia and reperfusion.[1002]

4.3 Imaging

Several studies have demonstrated the applications of nanozymes for imaging.[117,1057–1059] Benefiting from the intrinsic properties (*e.g.*, magnetism of Fe, X-ray absorption ability of Ir, and optics of Au), magnetic resonance imaging, computed tomography imaging, and optical imaging could be utilized for tracking the *in vivo* behaviors of nanozymes, which will be discussed in Section 4.4.5. Besides, taking advantage of the catalytic properties of nanozymes, several colored or fluorescent products could also be generated for imaging. A seminal study was reported by Yan and co-workers (Fig. 39). They prepared magnetoferritin NPs (M-HFn) by encapsulating peroxidase-mimicking MNPs inside recombinant human heavy-chain ferritin shells. The HFn shells could target tumor tissue *via* over-expressed transferritin receptors onto tumor cell surface without additional recognition ligands. Meanwhile, the iron oxide cores catalyzed the oxidation of a peroxidase substrate to produce a colored product for visualizing tumor tissues. In the presence of H_2O_2 and diazoaminobenzene, M-HFn showed an intense brown color for visualizing the tumor tissues. To further demonstrate the high specificity, sensitivity and accuracy of the M-HFn-based staining platform, 474 clinical specimens from patients with nine types of cancer were tested (note: in total, more than 1400 clinical specimens with ten types of cancer have been tested so far). Their results showed that the nanozyme imaging platform can discriminate cancerous cells from normal cells with 98% sensitivity and 95% specificity.[1060] Likewise, Gu *et al.* used avastin antibody functionalized Co_3O_4 NPs with peroxidase-like activities for immunohistochemical staining, and their staining ability was comparable to that of natural HRP.[559]

Another example was demonstrated with bioorthogonal nanozymes. For instance, Rotello and co-workers developed charge switchable nanozymes by encapsulating transition metal catalysts in pH responsive NPs for specific biofilm imaging. As shown in Fig. 40, the zwitterionic NPs would switch to a cationic state in the acidic microenvironments of bacterial biofilms, resulting in a higher uptake by biofilms. And then imaging of biofilms could be achieved by catalyzing the pro-fluorophores with the uptaken nanozymes inside the biofilm.[1061] More examples about bioorthogonal nanozymes will be discussed in Section 4.4.5.

Several studies also demonstrated that nanozymes were able to improve the imaging sensitivity. Tremel, Tahir, and co-workers found that manganese oxide (MnO) with an intrinsic SOD-mimicking activity can enhance its MRI contrast when exposed to $O_2^{\bullet-}$. The enhanced MRI contrast was attributed to the temporary change of the oxidation states of manganese ions in the $O_2^{\bullet-}$ scavenging process.[1062] In another study, Jiang, Tian, and co-workers found that catalase-mimicking BSA–IrO_2 NPs catalyzed the dismutation of H_2O_2 to O_2 for enhancing its photoacoustic signal by oxygen-induced inertial cavitation.[1059] And the aforementioned H_2O_2 sensor (Fig. 28), based on displacing fluorophore-labeled DNA from the nanoceria surface, was further used for fluorescence imaging of wound-induced H_2O_2 in zebrafish larvae.[1063]

4.4 Therapeutics

4.4.1 Neuroprotection. Owing to the SOD-mimicking activities of carboxyfullerenes, some pioneering works on their role in protecting neural cells from radical damage were demonstrated by Dugan and co-workers.[431,1064] Further, they demonstrated that C_{60}-C_3 may offer therapeutic effects on familial amyotrophic lateral sclerosis (ALS). ALS, a neurodegenerative disorder, is associated with several genetic mutations, such as

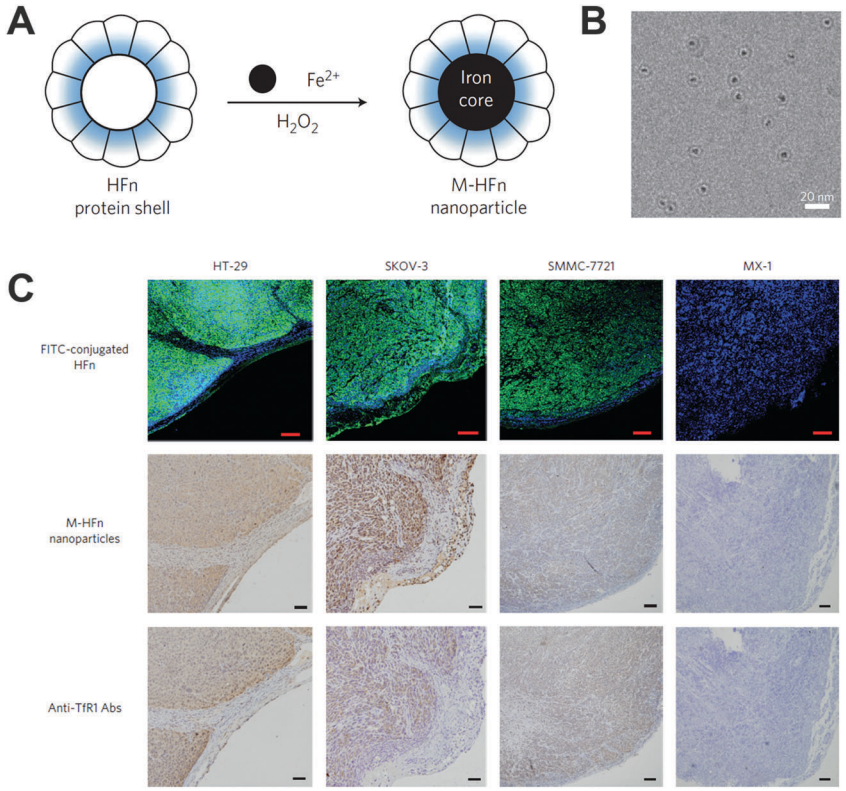

Fig. 39 M-HFn staining of tumor tissues. (A) Schematic illustration of the synthesis of M-HFn. (B) TEM images of M-HFn. (C) M-HFn as a peroxidase mimic for targeting and visualizing tumor tissues. Adapted with permission from ref. 1060. Copyright (2012) Nature Publishing Group.

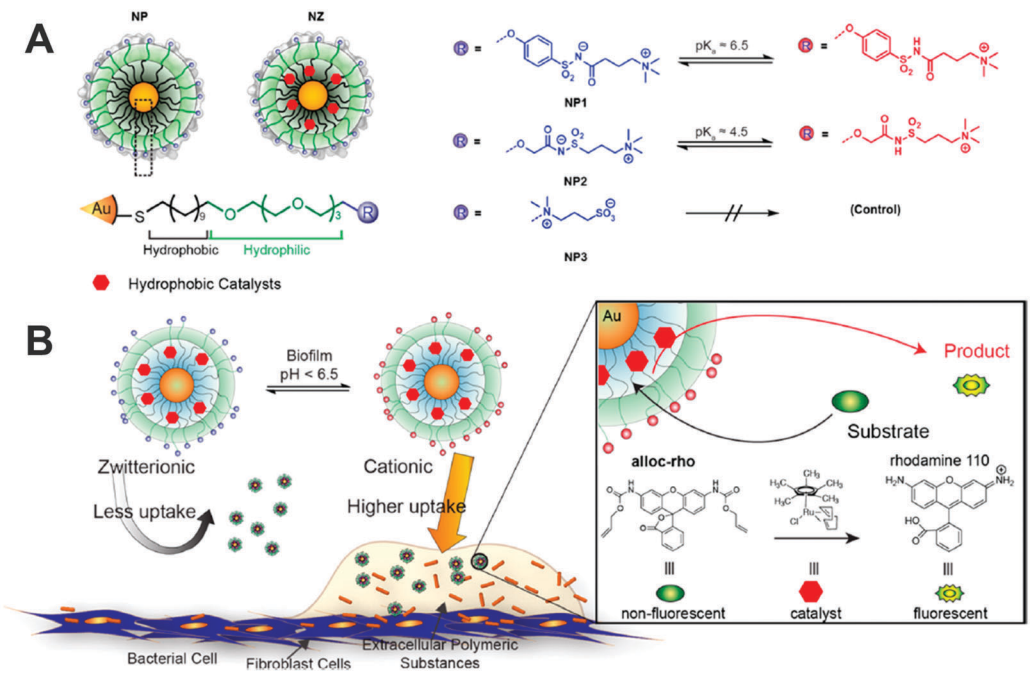

Fig. 40 Charge switchable nanozymes for specific biofilm imaging. (A) Molecular structures of pH-switchable and control ligands on AuNPs. (B) Schematic showing selective targeting of biofilm infections using pH-responsive NPs. Reprinted with permission from ref. 1061. Copyright (2018) American Chemical Society.

the missense mutations in SOD1 for familial ALS. If transgenic mice carrying a human disease gene for familial ALS were treated with C_{60}-C_3, a 10 day delay in symptom onset and an 8 day improvement in survival could be observed.[434]

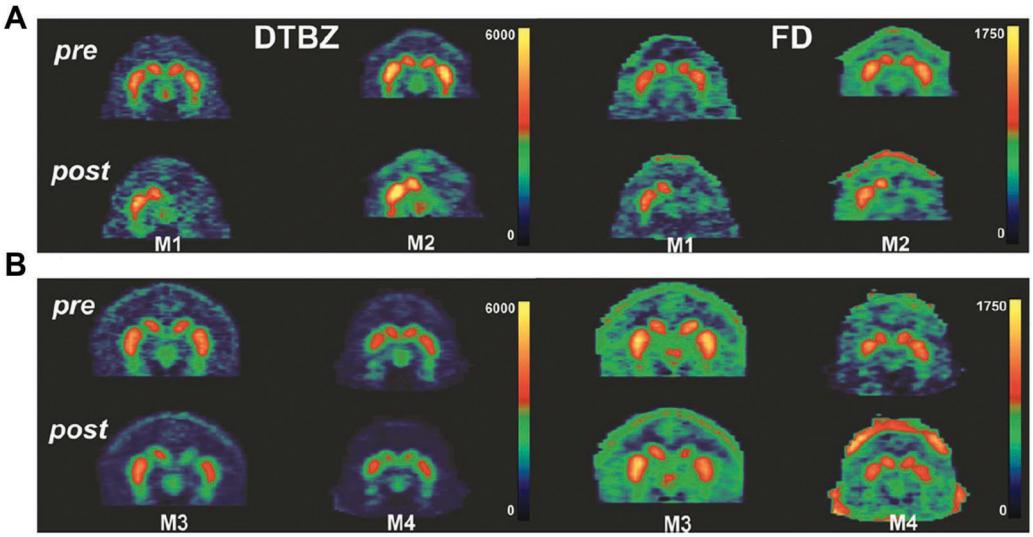

Fig. 41 Representative PET images for placebo-treated (A) and C_{60}-C_3-treated monkeys (B) just prior to MPTP and at the end of 2 months of treatment. PET images were taken with DTBZ and FD tracers, respectively. Note the bilateral uptake of each tracer pre-MPTP, showing the teardrop-shaped substantia nigra bilaterally for all 4 monkeys. However, at the end of the study, there was significantly less uptake of both tracers on the lesioned side in placebo-treated monkeys compared to C_{60}-C_3-treated ones, or conversely, there was preservation of DTBZ and FD in C_{60}-C_3-treated monkeys. Reprinted with permission from ref. 1065. Copyright (2014) American Neurological Association.

Most encouragingly, C_{60}-C_3 was proved to be capable of treating Parkinsonian nonhuman primates. In the study, Dugan, Perlmutter, and co-workers systematically treated MPTP-induced Parkinson's disease model of *Macaca fascicularis* monkeys with C_{60}-C_3 for two months (MPTP is 1-methyl-4-phenyl-1,2,3,6-tetrahydropyridine). The therapeutic outcomes were evaluated by using (1) *in vivo* behavioral measures of motor function, (2) *ex vivo* quantification of striatal dopamine, and (3) positron emission tomography (PET) imaging of 6-[^{18}F]fluorodopa (FD, reflecting dopa decarboxylase), [^{11}C]dihydrotetrabenazine (DTBZ, reflecting vesicular monoamine transporter type 2), *etc.* These results demonstrated that the C_{60}-C_3 treatment could significantly reduce striatal injury and improve motor function (Fig. 41). And it should be noted that C_{60}-C_3 treatment did not show any toxicity.[1065]

Nanoceria, one creditable ROS scavenger, have also been extensively studied for neuroprotection.[1066–1069] ROS, generated and accumulated during the ischemic process, would induce oxidative damage, resulting in ischemic injury and stroke-related cell death. Hyeon, Lee, and co-workers established that nanoceria could eradicate ROS to protect against ischemic stroke *in vivo* (Fig. 42). Animal experiments showed that nanoceria with optimal doses at 0.5 and 0.7 mg kg^{-1} significantly reduced the brain infarct volume.[463] In their following study, triphenylphosphonium-conjugated nanoceria (TPP–nanoceria) were developed as the ROS scavenger to protect mitochondria against oxidative stress in Alzheimer's disease. Therapeutic effects of TPP–nanoceria were evaluated using a 5XFAD transgenic Alzheimer's disease mouse model, where TPP–nanoceria could target mitochondria and reduce neuronal death. Moreover, *in vivo* experiments showed that TPP–nanoceria could relieve reactive gliosis and mitochondria damage, demonstrating their potential application for protecting mitochondria against oxidative stress in Alzheimer's disease.[1070] In another interesting study on the treatment of Parkinson's disease, three different types of nanoceria, including nanoceria, TPP–nanoceria, and clustered nanoceria, were prepared for selectively scavenging intracellular, mitochondrial, and extracellular ROS, respectively. By scavenging mitochondrial and intracellular ROS, the microglial activation and lipid peroxidation could be suppressed while the expression level of tyrosine hydroxylase could be enhanced in the striata of Parkinson's disease model mice. The above results demonstrated the critical importance of mitochondrial and intracellular ROS in the development and progression of Parkinson's disease. Therefore, the function of ROS in different cellular localizations in some diseases could be evaluated through these three types of nanoceria.[1071] Nanoceria could also be combined with polyoxometalates to effectively scavenge ROS and degrade amyloid-β (Aβ) aggregates. Based on the proteolytic and SOD activities, nanoceria/polyoxometalates could not only inhibit Aβ-triggered BV2 microglial cell activation but also improve PC12 cell proliferation, demonstrating their potential applications for treatment of neurotoxicity of Aβ peptide in neurodegenerative disease progression.[1072]

Though substantial success was achieved for neuroprotection using nanoceria, nanoceria could only cross the blood brain barrier (BBB) by targeting the damaged area of the BBB, which resulted in very limited accumulation of CeO_2 in brain lesions. To address this challenge, Shi *et al.* developed a nanoceria-based neuroprotection agent (E-A/P-CeO_2), which was loaded with edaravone and further functionalized with Angiopep-2 and PEG. Since Angiopep-2 could target the brain lesions *via* receptor-mediated transcytosis, an effective BBB crossing and much higher accumulation of E-A/P-CeO_2 NPs could be observed (Fig. 43B). And combined with the synergistic SOD-mimicking activities of both nanoceria and edaravone, E-A/P-CeO_2 was demonstrated to be the most

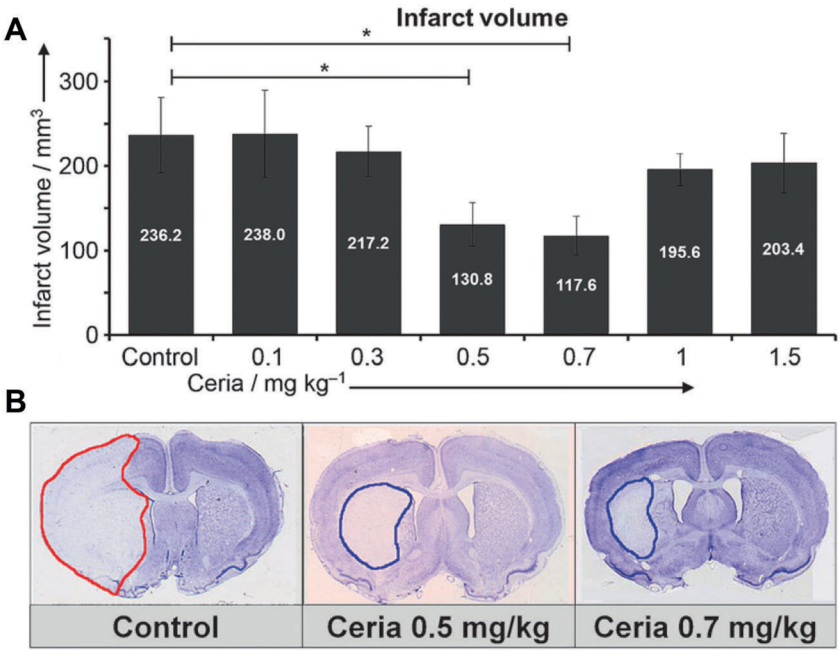

Fig. 42 Nanoceria protect against ischemic stroke. (A) Brain infarct volume in rats treated with various doses of nanoceria during the stroke process. (B) Representative brain slices of the control and nanoceria treated groups. The brain slices were stained with Nissl – the infarcts are shown as pale blue-colored lesions while the undamaged region is stained deep blue. Adapted with permission from ref. 463. Copyright (2012) John Wiley and Sons.

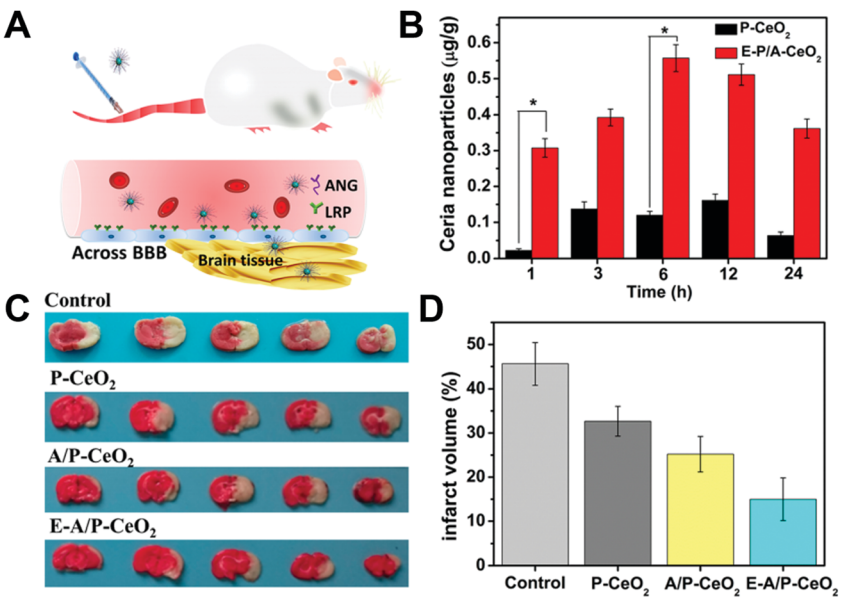

Fig. 43 (A) Schematic illustration of Angiopep-2 (ANG) targeting the overexpressed lipoprotein receptor-related protein (LRP) on brain capillary endothelial cells, which facilitates the BBB crossing of E-A/P-CeO_2 into brain tissue for stroke treatment. (B) Time-dependent concentrations (μg Ce per g brain tissue) of nanoceria in normal brain tissue after administrating 0.5 mg kg^{-1} of nanoceria (*$P < 0.05$). (C) Digital photograph of the representative 2,3,5-triphenyltetrazolium chloride-stained brain in each group within 24 h of stroke. (D) The volume proportion over the whole brain analyzed by using Image-Pro Plus at 0.6 mg kg^{-1} of nanoceria. Reprinted with permission from ref. 1073. Copyright (2018) American Chemical Society.

efficient protection against brain injury in stroke (Fig. 43C and D).[1073] In another study, the in-depth mechanism of nanoceria's neuroprotection effect was deciphered by Li and co-workers. They found that nanoceria could covert microglial polarization from a pro-inflammatory phenotype into an anti-inflammatory phenotype, which may be responsible for their neuroprotective effect.[1074]

Besides carboxyfullerenes and nanoceria, other nanomaterials were also used for neuroprotection.[1075,1076] For example, as mentioned in Section 2.4.3, PEG–MeNPs with ROS/RNS (RNS for reactive nitrogen species) scavenging abilities could provide an effective protection against ischemic brain injury with negligible side effects. Compared to the control group with

around 32% infarct area, the treatment of PEG–MeNPs significantly reduced the infarct area by half (~14%).[468] Mugesh *et al.* demonstrated that flower-like Mn_3O_4 nanozymes mimicked three antioxidation enzymes, including SOD, catalase as well as GPx. The therapeutic effect of Mn_3O_4 nanozymes was demonstrated using an experimental model of Parkinson's disease. Their results suggested that Mn_3O_4 nanozymes could provide neuroprotective effects for cells, demonstrating their potential for treating ROS-mediated neurodegenerative disorders.[573]

4.4.2 Cytoprotection. Recently, a variety of nanozymes have also been demonstrated as antioxidants for cytoprotection.[443,561,1077–1091] For example, Mugesh *et al.* found that V_2O_5 nanowires exhibited an interesting GPx-like activity, catalyzing the conversion of H_2O_2 into H_2O in the presence of GSH (Fig. 44). Therefore, V_2O_5 nanowires provided the cytoprotective effect by scavenging H_2O_2. Cell experiments showed that V_2O_5 nanowires could eliminate not only extrinsic H_2O_2 but also intrinsic cellular peroxide induced by $CuSO_4$, demonstrating V_2O_5 nanowires as efficient antioxidants for cytoprotection.[141] The detailed mechanism of GPx-like activity of V_2O_5 nanowires is presented in Section 2.1.2.

Another interesting example was directly growing MnO_2-nanozyme shells *via* mineralization for long-term cytoprotection of yeast cells. Owing to the SOD- and catalase-like activities of MnO_2 nanozymes, the cellular resistance against harmful H_2O_2 was enhanced. Over 65% of yeast cells@MnO_2 could survive after incubating with H_2O_2 for 48 h, while only 5% of native cells remained viable. The robust MnO_2 shell provided improved cytoprotection against not only H_2O_2 but also other stressors such as lytic enzymes and UV radiation. And this protection was general to other living cells as well. It was worth noting that such a protection could be biodegraded and thus recover the functions of cells. However, the potential toxicity of released Mn ions should also be considered in the future application.[1092]

Besides, Se-based nanozymes such as GO–Se nanocomposites and Se@polydopamine with GPx-like activities were also reported to eliminate H_2O_2 for cytoprotection.[1093,1094] Recently, a robust synthesis of fluorescent Se-doped carbon dots *via* hydrothermal treatment of selenocystine at 60 °C was reported by Xu *et al.* A further study demonstrated that the obtained Se-doped carbon dots could effectively eliminate •OH for cell protection. And the distribution of Se-doped carbon dots in cells was verified by confocal microscopy imaging, which showed a random location at cell nuclei, lysosomes, mitochondria, and cytoplasm.[1095]

4.4.3 Anti-inflammatory agents. Numerous studies have demonstrated that nanozymes with multiple enzymatic activities were outstanding anti-inflammatory agents. For example, ceria nanozymes with SOD- and catalase-like activities exhibited excellent repetitive ROS scavenging ability due to their autocatalytic properties. As a result, several studies reported biocompatible nanoceria for *in vitro* and *in vivo* anti-inflammation.[1096,1097] To further enhance the ROS removal efficiency, a doping method was chosen. As discussed in Section 3.3, nanoceria with Zr^{4+} doping (CZ NPs) possessed higher activities than nanoceria due to the higher Ce^{3+}/Ce^{4+} ratio as well as faster recovery from Ce^{4+} to Ce^{3+}. Two representative sepsis models (*i.e.*, LPS-induced

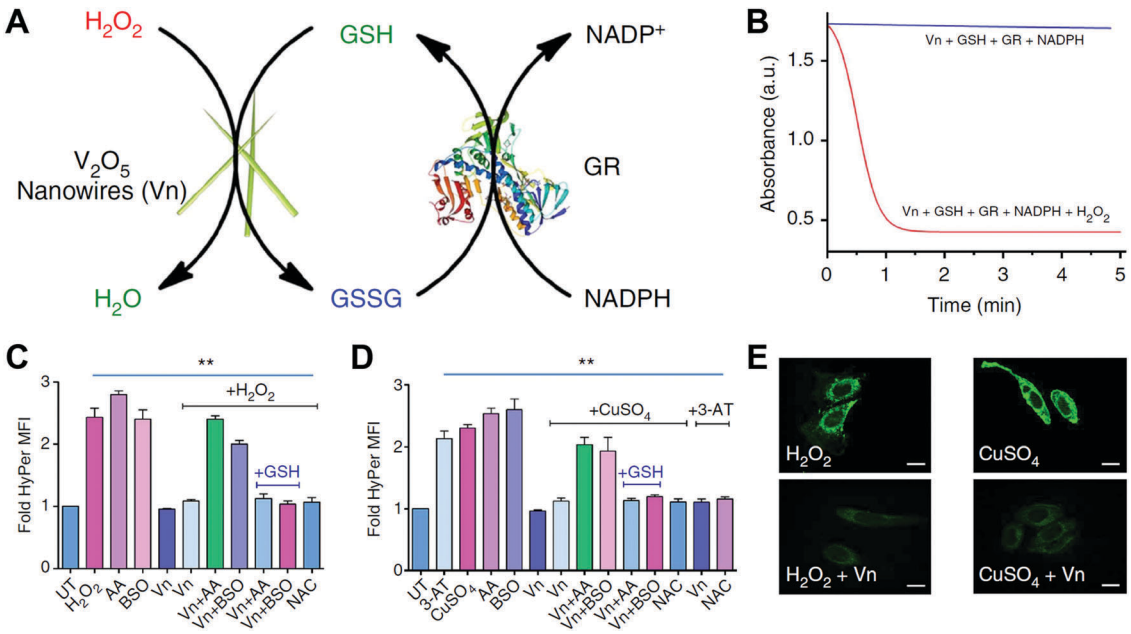

Fig. 44 V_2O_5 nanowires as a GPx mimic for cytoprotection. (A) Schematic showing the GPx-like antioxidant activity of V_2O_5 nanowires and GSH recycling by GR. (B) Plot of absorbance *versus* time revealing the activity of V_2O_5 nanowires in the presence of V_2O_5 nanowires, GSH, NADPH, GR, and H_2O_2 in phosphate buffer at 25 °C. The scavenging ability of V_2O_5 nanowires for extrinsic H_2O_2 (C) and intrinsic cellular peroxide induced by $CuSO_4$ (D) was measured by using genetically encoded H_2O_2-specific probe HyPer in HEK293T cells. (E) HeLa cells were treated with V_2O_5 nanowires before the treatment with H_2O_2 or $CuSO_4$ and then stained with 15 μM DCFA-H2 dye. Adapted with permission from ref. 141. Copyright (2014) Nature Publishing Group.

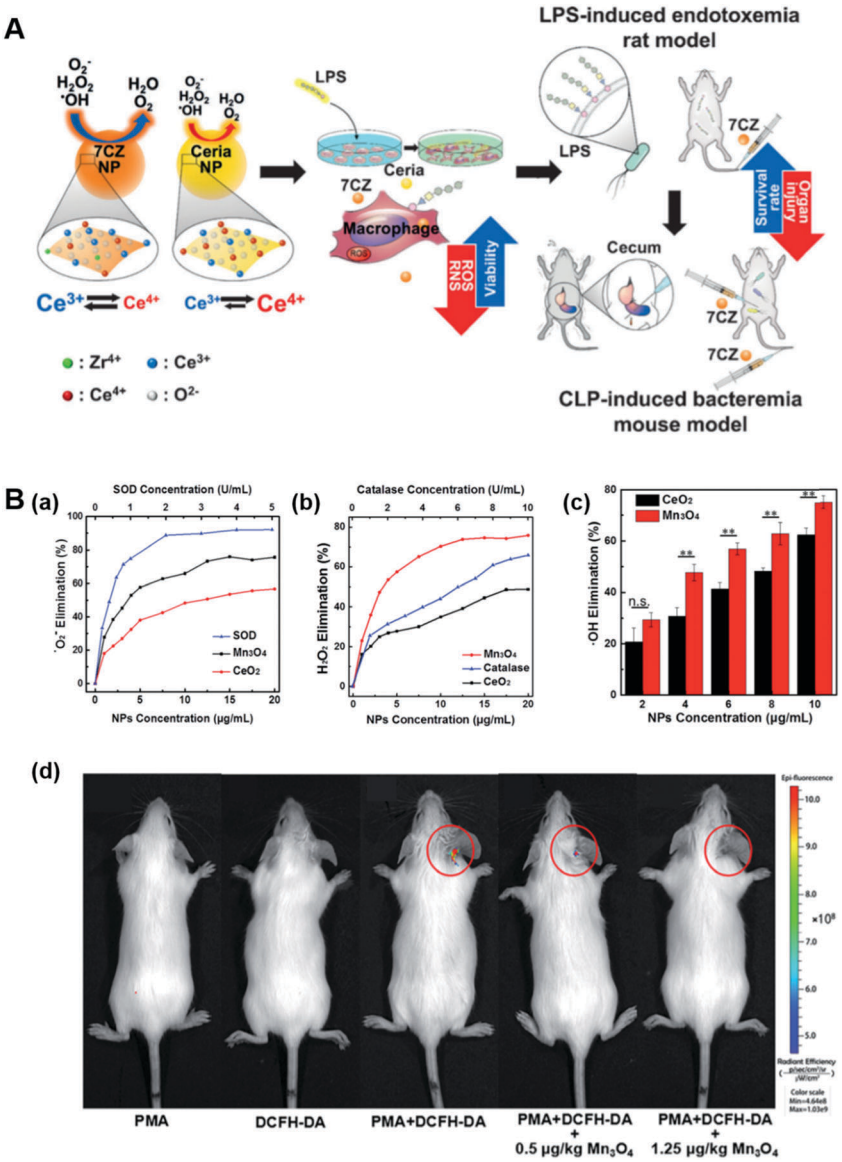

Fig. 45 (A) Schematic illustration of ceria and CZ NPs used as therapeutic nanomedicine in models of *in vitro* inflammation and *in vivo* sepsis. (B) Mn_3O_4 nanozymes for *in vivo* anti-inflammation. Dependence between the elimination of (a) $O_2^{\bullet -}$ and (b) H_2O_2 and concentrations of Mn_3O_4 NPs, CeO_2 NPs, and the corresponding natural enzymes. (c) Dependence between the elimination of $^{\bullet}OH$ and concentrations of Mn_3O_4 NPs and CeO_2 NPs. (d) *In vivo* fluorescence imaging of mice with PMA-induced ear inflammation after treatment under different conditions (PMA, phorbol 12-myristate 13-acetate). (A) Reprinted with permission from ref. 451. Copyright (2017) John Wiley and Sons. (B) Adapted with permission from ref. 1100. Copyright (2018) Royal Society of Chemistry.

endotoxemia rat model and CLP-induced bacteremia mouse model) were used to demonstrate the *in vivo* anti-inflammatory effect of CZ NPs (Fig. 45A). Compared with the control group, the median survival rate was improved by 2.5 times with CZ NP administration, demonstrating CZ NPs as a novel therapeutic agent for systematic inflammation.[451]

Besides, PB was also used as a ROS scavenger on the basis of its catalase- and SOD-like activities under physiological conditions. The detailed mechanism of its multiple enzyme-like activities is discussed in Section 2.1.1. The *in vitro* inflammatory model of RAW264.7 cells and *in vivo* liver inflammation model of rats suggested that PB with ROS scavenging ability could protect against oxidative damage and alleviate inflammatory response.[133] Another *in vitro* inflammatory model of A549 cells and *in vivo* pulmonary inflammation model of mice exposed to cigarette smoke successfully demonstrated the inhibition of pulmonary inflammation with SOD- and catalase-mimicking PtNPs as antioxidants.[1098] Later, instead of intranasal administration, glycine-functionalized copper(II) hydroxide NPs with SOD-mimicking activities were directly put into cigarette filters, which also exhibited antioxidant abilities and protected the A549 cells from oxidative stress. Such a strategy might be a direct way for the anti-pulmonary inflammation of smokers in the future.[1099]

Recently, Wei *et al.* have demonstrated that Mn_3O_4 NPs could act as promising anti-inflammation agents because of their ROS scavenging ability for not only $O_2^{\bullet-}$ and H_2O_2 but also $^{\bullet}OH$ (Fig. 45B). Notably, Mn_3O_4 NPs exhibited superior ROS removal efficiency compared to nanoceria and better stability than natural enzymes. Further *in vitro* and *in vivo* experiments proved the anti-inflammatory therapeutics of ROS-scavenging Mn_3O_4 nanozymes.[1100]

Another innovative example was developing an interesting multi-antioxidant enzyme synergetic platform (*i.e.*, V_2O_5@PDA@MnO_2 nanocomposites; PDA, polydopamine) to imitate the intracellular antioxidation defense process involving SOD, catalase, and GPx. The obtained hybrid nanocomposites exhibited multi-antioxidation enzyme activities, where V_2O_5 served as a GPx mimic and MnO_2 as a SOD and catalase mimic. Even for PDA, a synergetic efficient antioxidative effect was also found. Encouraged by the excellent ROS scavenging ability, later, they constructed a PMA-induced ear inflammation model, demonstrating the potential application of V_2O_5@PDA@MnO_2 for *in vivo* anti-inflammation.[1101]

Besides SOD and catalase mimics, hydrogenase-like nanozymes with H_2 production were also reported for anti-inflammation. Sung, Chia, and co-workers fabricated a liposomal hybrid containing a photosensitizer chlorophyll *a*, an electron donor ascorbic acid and a photo-reducing AuNP as a hydrogenase-like nanozyme. Activated by a 660 nm laser, H_2 would be generated to reduce $^{\bullet}OH$ to H_2O, therefore alleviating tissue inflammation.[547]

4.4.4 Combating bacteria. Unlike the aforementioned ROS elimination, the oxidase- or peroxidase-like activity for converting O_2 or H_2O_2 into ROS would endow nanozymes with antibacterial activities.[1102–1107] Excellent reviews summarizing nanozymes' antibacterial applications are available.[79,1108] Herein, we will discuss some representative examples. For example, Qu *et al.* synthesized AuNPs loaded on mesoporous silica (MSN-AuNPs) with oxidase- and peroxidase-like activities for combating bacteria. And these catalytic activities of MSN-AuNPs could be retained over a broad pH range even at neural pH, which allowed for killing bacteria under physiological conditions. They demonstrated that the peroxidase-like activity of MSN-AuNPs was attributed to the generation of $^{\bullet}OH$ in the presence of H_2O_2, while the oxidase-like activity was from several ROS, including $^1O_2$, $^{\bullet}OH$, and $O_2^{\bullet-}$. Therefore, the MSN-AuNPs could generate excessive ROS in the presence of O_2 or H_2O_2, resulting in considerable antibacterial properties. Further antibacterial experiments were performed with both Gram-positive bacteria *Staphylococcus aureus* (*S. aureus*) and Gram-negative bacteria *Escherichia coli* (*E. coli*). Compared with the control group, the MSN-AuNPs exhibited highly effective inhibition of the proliferation of both bacterial strains.[1109] Besides, other peroxidase-mimicking nanomaterials, such as carbon nanotubes, Pt hollow nanodendrites, and AuNPs/g-C_3N_4, were also reported to effectively generate $^{\bullet}OH$ for killing both Gram-positive and Gram-negative bacteria.[228,253,1104]

Recently, Zhou, Ge, and co-workers found that Pd-nanocrystal facets showed different antibacterial activities against Gram-positive and Gram-negative bacteria (Fig. 46). Their study suggested that the oxidase- and peroxidase-like activities of Pd nanocrystals exhibited facet-dependence, where {100}-faceted Pd cubes possessed greater catalytic activities than {111}-faceted Pd octahedra. According to a previous report, the antibacterial activity against bacteria was expected for Pd cubes rather than Pd octahedra. As shown in Fig. 46A, the survival rate and the scanning electron microscopic (SEM) images of *S. aureus* did evidence the higher antibacterial activity of Pd cubes compared to Pd octahedra. On the other hand, for Gram-negative bacteria *E. coli*, an opposite result was observed. More effective antibacterial properties were from Pd octahedra instead of Pd cubes (Fig. 46B). Further experiments and molecular dynamics simulations suggested that a stronger membrane penetration of Pd octahedra promoted the antibacterial activity against *E. coli*, as shown in Fig. 46C and D.[616]

Besides, other therapies (such as photothermal therapy) have also been utilized together with $^{\bullet}OH$ for combating bacteria.[1110–1112] For instance, Zhao, Gu, and co-workers found that peroxidase-mimicking PEG–MoS_2 nanoflowers could rapidly and effectively kill bacteria (*e.g.*, *E. coli* and *Bacillus subtilis*) through a synergistic effect of catalysis and photothermal therapy. The synergistic processes were as below: first, PEG–MoS_2 nanoflowers would decompose H_2O_2 to produce $^{\bullet}OH$ for damaging cell walls and membranes, making cells vulnerable to heat; then, PEG–MoS_2 nanoflowers with near-infrared absorption could cause hyperthermia under 808 nm irradiation for photothermal therapy. Meanwhile, the hyperthermia improved the oxidation of GSH, further helping to accelerate the whole antibacterial outcome. Notably, a catalysis-induced damage to cells could shorten the irradiation time and minimize the side effects of photothermal therapy.[1113]

4.4.5 Cancer therapy. ROS could also do harm to cancer cells. According to the different ways of ROS generation (mechanisms), nanozymes for cancer therapeutics could be roughly classified into two types: (1) nanozymes as peroxidase or oxidase mimics with ROS generation during catalysis; (2) ROS produced under light irradiation in the presence of photosensitizers and catalase mimics, where the key role of nanozymes is to generate O_2 to enhance the PDT efficiency.

The principle of the first type was similar to the above-mentioned antibacterial activity.[1114–1120] Recently, Shi *et al.* proposed and demonstrated the concept of catalytic nanomedicine. As shown in Fig. 47, the GOx–Fe_3O_4@DMSNs nanocatalyst was fabricated by encapsulating GOx and ultrasmall Fe_3O_4 NPs in the dendritic mesoporous silica NPs (DMSNs). After being taken up by cancer cells, the GOx could deplete glucose in tumor cells, which would not only starve cancer cells but also produce considerable concentration of H_2O_2 for downstream reaction. Subsequently, the abundant H_2O_2 would be *in situ* catalyzed by ultrasmall Fe_3O_4 NPs *via* Fenton-like reaction to produce toxic $^{\bullet}OH$, which in turn induced the apoptosis and death of tumor cells. The biodegradation behavior and pharmacokinetics of GOx–Fe_3O_4@DMSNs were also studied. Encouragingly, the structure of GOx–Fe_3O_4@DMSNs could be degraded in cancer cells upon 7 day incubation. And no significant effect on Kunming mice growth proved the high

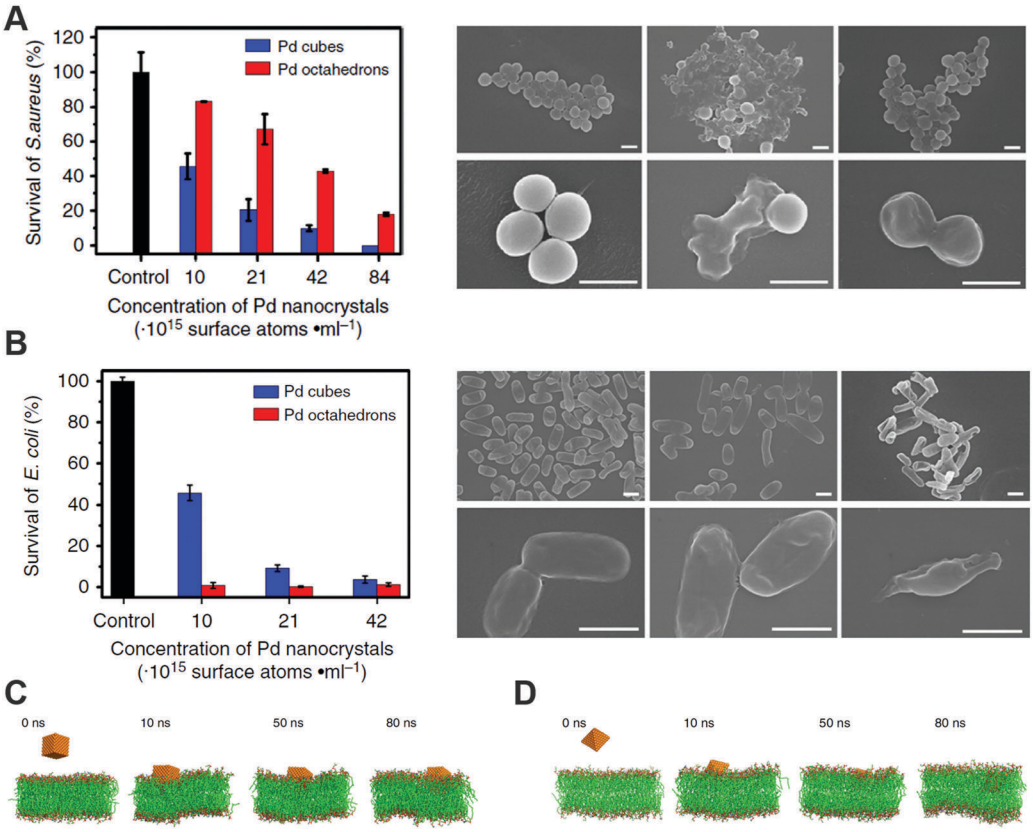

Fig. 46 (A) Survival rates and typical SEM images of *S. aureus* cells exposed to various treatments of Pd nanocrystals. (B) Survival rates and typical SEM images of *E. coli* cells exposed to various treatments of Pd nanocrystals. (C and D) Membrane penetration of Pd nanocrystals from simulations. Adapted with permission from ref. 616. Copyright (2018) Nature Publishing Group.

biosafety of GOx–Fe_3O_4@DMSNs. Besides, *in vivo* behaviors (such as distribution kinetics in the whole blood and the 2.65 h circulating half-life of GOx–Fe_3O_4@DMSNs in the bloodstream) further demonstrated an improved pharmacokinetics. On the basis of the biodegradation behavior and the high biocompatibility, the GOx–Fe_3O_4@DMSNs were applied for *in vivo* tumor catalytic therapeutics, which exhibited satisfactory tumor suppression effects for 4T1 and U87 tumor xenografts.[1121]

Likewise, Yan *et al.* reported that nitrogen doped porous carbon nanospheres (N-PCNs) exhibited four enzyme-like activities including oxidase, peroxidase, catalase, and superoxide dismutase, which could regulate ROS *in vivo*. Further modification of N-PCNs with ferritin helped targeted-delivery into lysosomes *via* receptor-mediated endocytosis. Then, the acidic environment of lysosomes facilitated the N-PCNs performing peroxidase- and oxidase-mimicking activities to generate ROS and consume oxygen, resulting in the toxic effect and hypoxia for tumor cells (Fig. 48). Moreover, the results of their animal experiments showed that the N-PCNs could efficiently reduce the tumor volume and improve the survival rate of tumor-bearing mice.[442]

For the second type, nanozymes with catalase-like activities were normally used for producing more oxygen to enhance the PDT efficacy.[65,726,1122–1124] In the PDT processes, O_2 would be converted into ROS by light-activated photosensitizers. However, the hypoxic microenvironment of cancer cells has limited the therapeutic effects, which provides an opportunity for nanozymes with catalase-like activities because they could *in situ* decompose H_2O_2 into O_2 and H_2O. For example, Hyeon *et al.* developed biocompatible manganese ferrite NP-anchored mesoporous silica NPs (MFMSNs) for improving the PDT efficiency (Fig. 49). Continuously generated O_2 from MFMSNs and ROS under laser irradiation relieved the hypoxia cancer microenvironment and enhanced the therapeutic efficacy. Moreover, as a contrast agent for magnetic resonance imaging, MFMSNs could be tracked *in vivo*.[1122]

Similarly, other nanomaterials (such as Pt decorated photosensitive MOFs and BSA–IrO_2) were also demonstrated to improve the therapeutic efficacy by producing O_2.[1059,1123,1125] In certain cases, several approaches were applied together for cancer treatment.[1125–1129] For example, the BSA–IrO_2 NP was promising for cancer theranostics because of its excellent photothermal conversion efficiency and photocatalytic activity, as well as high X-ray absorption ability for computed tomography imaging. More importantly, BSA–IrO_2 NPs with catalase-mimicking activity could not only supply O_2 for overcoming tumor hypoxia and enhancing photoacoustic imaging but also act as self-anti-inflammatory agents for protecting normal cells against H_2O_2-induced oxidative stress.[1059]

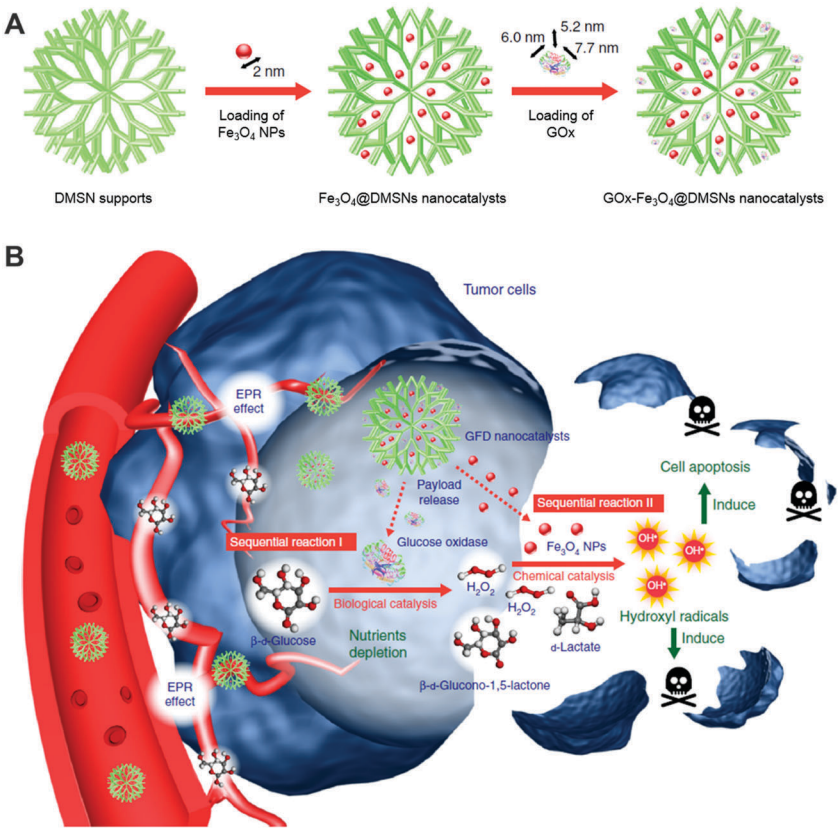

Fig. 47 (A) Schematic showing the synthetic procedure of Fe_3O_4@DMSNs nanocatalysts and GOx-Fe_3O_4@DMSNs nanocatalysts. The sizes of the prepared Fe_3O_4 NPs and adopted GOx are indicated in the scheme. (B) Scheme of the sequential catalytic-therapeutic mechanism of GOx-Fe_3O_4@DMSNs (GFD) nanocatalysts in the generation of hydroxyl radicals for cancer therapy. Adapted with permission from ref. 1121. Copyright (2017) Nature Publishing Group.

Besides ROS, in some recent research studies, bioorthogonal nanozymes have also been used in pro-drug activation for cancer therapeutics by converting a pro-drug into the toxic drug. For instance, first, non-covalent encapsulation of the transition metal catalyst (*e.g.*, Ru complex or Pd complex) in the alkanethiol monolayers on AuNP cores was performed. Then, additional capping of the cucurbit[7]uril (CB[7]) to the head groups of monolayers would protect the catalyst from release, meanwhile blocking the access to catalytic active sites, leading to the deactivation of the bioorthogonal nanozymes. When adding a competing guest molecule (*i.e.*, 1-adamantylamine (ADA)), the CB[7] would be taken away from the bioorthogonal nanozymes, resulting in the exposure of active sites (Fig. 50A). Therefore, the catalytic activity of bioorthogonal nanozymes could be reversibly modulated by such supramolecular interaction between ADA and CB[7]. As shown in Fig. 50B, the propargyl group of pro-5FU was only cleaved with exposed active catalysts to produce the toxic 5-FU, which demonstrated future therapeutics at the site of action with minimized side effects of 5-FU.[515] Likewise, a light-controlled bioorthogonal nanozyme was prepared with azobenzene isomerization and cyclodextrin instead of ADA and CB[7]. With light-induced structural changes of azobenzene, cyclodextrin would be released for pro-5FU activation, demonstrating its potential application for cancer therapeutics. Further, instead of using pro-drug for cancer therapeutics, pro-fluorophore was chosen to demonstrate the cell imaging ability of the bioorthogonal nanozymes.[769]

4.4.6 Others. Several studies have also demonstrated nanozymes' broad applications in disease therapeutics.[453,454,1124,1130–1141] For example, Song, Fan, and co-workers demonstrated that catalase-like dietary Fe_3O_4 NPs delayed aging and protected against neurodegeneration *in vivo*. A *Drosophila* model was selected to evaluate the effects of Fe_3O_4 NPs on aging and life span. Aged *Drosophila* (six weeks old) exhibited increased ROS levels and decreased climbing ability (0.43 cm s^{-1}). Compared with the control group, the ROS levels were significantly reduced and the climbing ability (0.6 cm s^{-1}) was enhanced when the flies daily ingested 200 μg mL^{-1} Fe_3O_4 NPs. More encouragingly, the median life span (t_{50}) was improved from 49 to 57 days by ingestion of Fe_3O_4 NPs. Moreover, they found that dietary Fe_3O_4 NPs could relieve neurodegeneration in a *Drosophila* Alzheimer's disease model. After administrating dietary Fe_3O_4 NPs, the level of apoptosis in the brain was reduced and the median life span was extended by 16%, demonstrating that dietary Fe_3O_4 NPs could protect against neurodegeneration in a *Drosophila* Alzheimer's disease model.[1142] Besides, PAPLAL, a mixture of Pd and Pt NPs used in Japan over the past 60 years,

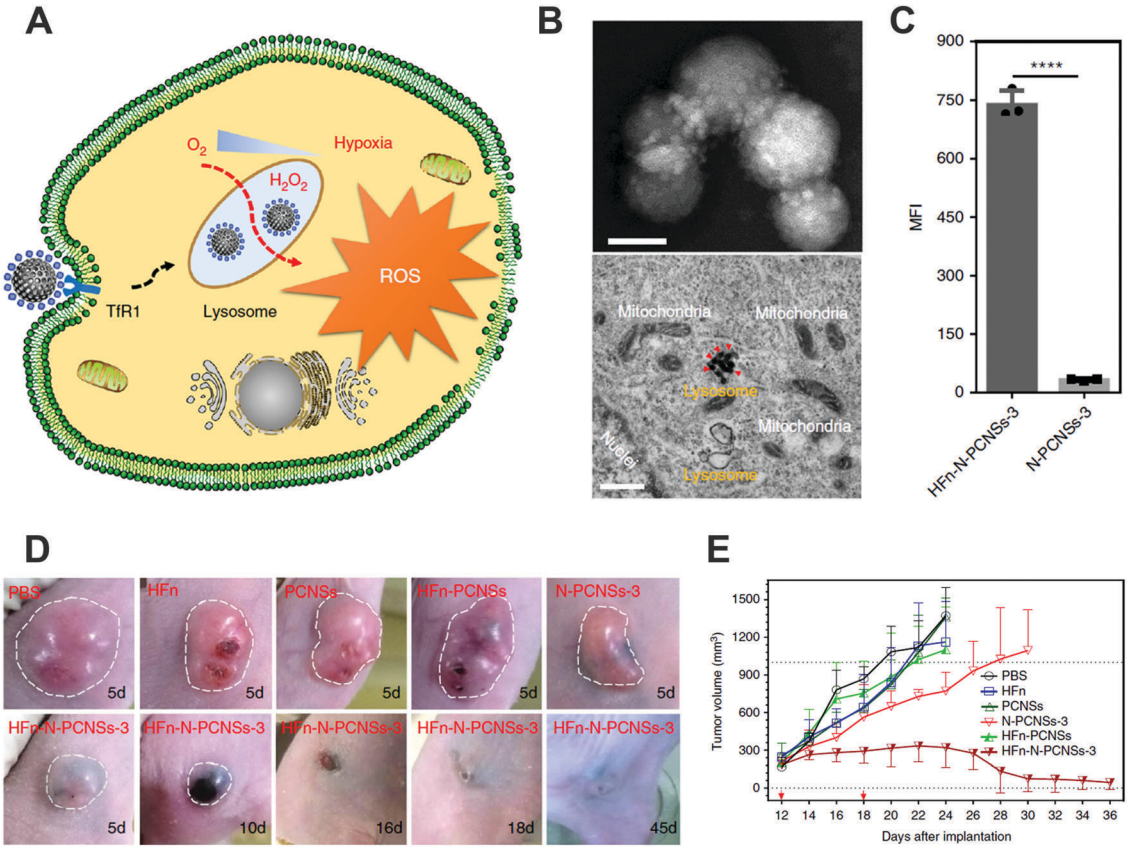

Fig. 48 (A) Schematic illustration of N-PCN induced tumor cell destruction *via* ferritin-mediated specific delivery. PCNs, porous carbon nanospheres. (B) TEM images of ferritin assembled onto N-PCNs and cancer cells treated with ferritin-PCNs. (C) Quantification of ferritin-enhanced internalization of N-PCNs by flow cytometry analysis (n = 3). (D) Tumor morphology and progress with ferritin-N-PCN treatment (n = 5). (E) Tumor volume after intratumoral treatment with ferritin-N-PCNs (n = 5). Adapted with permission from ref. 442. Copyright (2018) Nature Publishing Group.

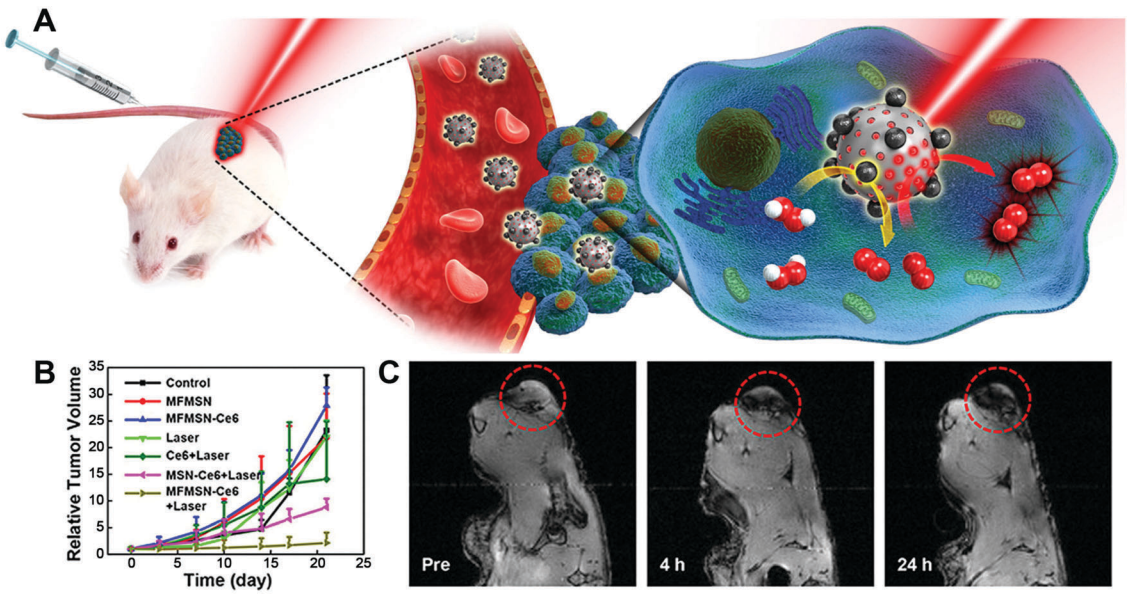

Fig. 49 (A) Schematic illustration of MFMSNs for efficient PDT in hypoxic cancer. (B) Tumor volume changes of each group after 3 weeks. (C) *In vivo* T_2-weighted magnetic resonance imaging tracking of a tumor-bearing mouse at various time periods. Tumors are circled with red dashed lines. Adapted with permission from ref. 1122. Copyright (2017) American Chemical Society.

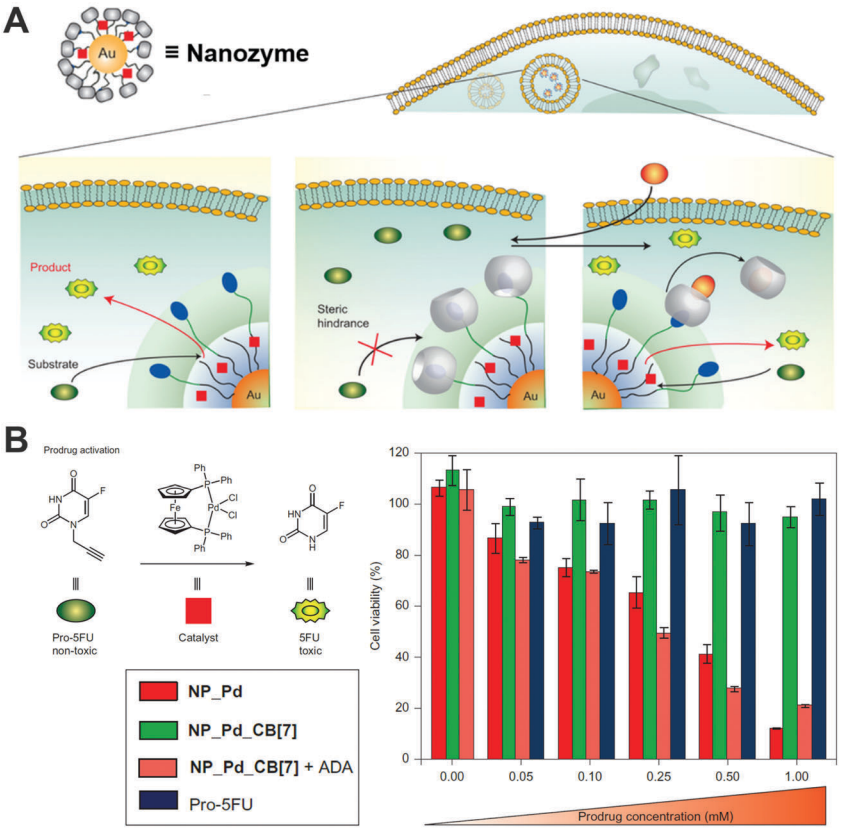

Fig. 50 (A) Schematic of the nanozyme and its regulation after cellular uptake. (B) Prodrug activation in live cells using bioorthogonal nanozymes. Adapted with permission from ref. 515. Copyright (2015) Nature Publishing Group.

has also been studied by Shimizu and co-workers for treating oxidative-induced aging-related skin diseases. Such an effect was due to the SOD- and catalase-mimicking activities of Pd and Pt NPs.[1143]

4.5 Others

4.5.1 Environmental protection. As discussed above, nanozymes have exhibited broad applications in detecting toxic pollutants, such as Hg^{2+}, Ag^{+}, and pesticides.[86,160–162,1028,1144–1149] Moreover, various studies demonstrated that nanozymes could remove pollutants for water treatment and environmental protection *via* a Fenton-like reaction.[235,302,320,838,1150–1160] A widely explored nanozyme was based on iron, which could not only degrade pollutants through the peroxidase-like catalytic process, but also be recycled for sustainable usage.[97,98,102,671,1161–1183] Besides the Fenton-like reaction, the oxidation reaction catalyzed by polyphenol oxidase mimics was also helpful for removing another type of pollutants (*i.e.*, phenols) from the environment.[400,401,410]

In a recent study, Mugesh *et al.* developed vacancy engineering nanoceria as phosphotriesterase mimics to hydrolyze the organophosphorus-based nerve agents. A mechanism study showed that Ce^{3+} and Ce^{4+} ions in the hotspots played a vital role in effectively catalyzing the hydrolysis of nerve agents.[773] By using phosphotriesterase-mimicking nanoceria, some environmentally harmful nerve agents, such as paraoxon, could be effectively degraded.[479,1184,1185] In addition to nanoceria, MOF-based nanomaterials, such as UiO-66, could also cleave organophosphate bonds of CWAs for environmental protection and national security.[534,1186–1189] A detailed discussion of MOF-based nanomaterials for phosphotriesterase mimics is presented in Section 2.5.3. Given the low hydrolysis efficiency of sulfur mustard, further combination of porphyrin linker-based or polyoxometalate-based oxidation in MOFs was used to detoxify sulfur mustard (*e.g.*, 2-chloroethyl ethyl sulfide).[1190]

4.5.2 Anti-biofouling. Tremel *et al.* demonstrated that V_2O_5 nanowires could act as vanadium haloperoxidase mimics. When the bromide ions and hydrogen peroxide were present, the V_2O_5 nanowires could catalyze the oxidation of bromide ions to form HOBr, which endowed them with a strong anti-biofouling activity.[134] In their subsequent study, they developed CeO_{2-x} nanorods as haloperoxidase mimics due to the existence of the Ce^{4+}/Ce^{3+} redox couple. Density functional theory calculations suggested that the Ce^{3+} defect may be responsible for its haloperoxidase-like activity. Similarly, bromide ions could be oxidized by CeO_{2-x} nanorods to form HOBr in the presence of H_2O_2. Subsequently, the reactive HOBr reacted with signaling molecules involved in bacterial quorum sensing (*i.e.*, *N*-(3-oxoacyl)homoserine lactone) to form a halogenated product, leading to the final anti-biofouling (Fig. 51A).[1191]

Nanozymes with peroxidase-like activities can also be used for combating biofouling. Gao *et al.* demonstrated that peroxidase-mimicking Fe_3O_4 NPs with H_2O_2 could effectively improve the

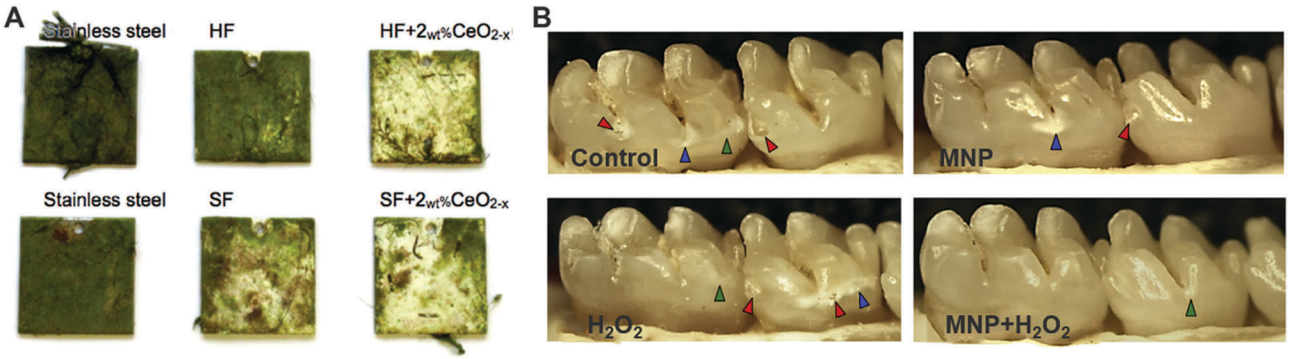

Fig. 51 (A) Selected samples after seven and half weeks of static field immersion. The plates were fixed statically to a boat bridge (HF, hard formulation; SF, soft formulation). (B) Dental caries prevention with MNPs. The green arrows indicate the initial lesion formation where the areas of the enamel are demineralized and have become white; the blue arrows show moderate carious lesions where the areas of enamel are white-opaque or damaged. In some areas, the enamel is eroded leading to cavitation, which are the most severe carious lesions (red arrows). (A) Adapted with permission from ref. 1191. Copyright (2017) John Wiley and Sons. (B) Adapted with permission from ref. 1192. Copyright (2016) Elsevier.

oxidative cleavage of biofilm components (*i.e.*, nucleic acids, proteins, and oligosaccharides). Moreover, the Fe_3O_4–H_2O_2 system could not only degrade the existing biofilm but also prevent the formation of a new biofilm.[1193] Later, Gao, Koo, and co-workers developed a method for dental biofilm elimination by using Fe_3O_4 MNPs with a peroxidase-like activity. Their results illustrated that Fe_3O_4 MNPs could catalyze H_2O_2 to generate $^{\bullet}OH$, which resulted in the degradation of the biofilm matrix and the death of bacteria in a short time. Furthermore, by using a rodent model, *in vivo* studies demonstrated that the Fe_3O_4–H_2O_2 system could effectively suppress dental caries (Fig. 51B).[1192] Likewise, ferumoxytol, which was approved by the U.S. Food and Drug Administration for treatment of iron deficiency, was used as a peroxidase mimic by Koo and co-workers to disrupt oral biofilms and prevent tooth decay in the presence of low concentrations of H_2O_2. Moreover, they performed microbiome and histological analyses and demonstrated the negligible adverse effects of ferumoxytol on oral microbiota diversity and gingival and mucosal tissues.[1194]

Besides peroxidase-mimicking nanozymes, an anti-biofilm DNase-mimicking nanozyme was also reported by Qu and co-workers. They synthesized Fe_3O_4/SiO_2 nanoparticles as the core to confine AuNPs on the surface, followed by functionalizing AuNPs with the Ce(IV) complex as the catalytic monolayers. Such a DNase-mimicking nanozyme could effectively cleave the extracellular DNA in extracellular polymeric substances, thus inhibiting the biofilm formation and dispersing the formed biofilms. Because of the high stability and easy separation with an external magnetic field, the as-synthesized nanozyme could be reused for five rounds. Moreover, hydrolysis-induced disruption of the integrated extracellular polymeric substance helped the traditional antibiotics to eradicate the bacterial biofilms.[1195]

4.5.3 Logic gates. Various studies used nanozymes to construct logic gates.[1196–1202] For example, Qu and co-workers developed label-free, resettable, colorimetric logic gates, including "AND", "OR", and "INHIBIT", by combining natural enzymes with thermally responsive ceria nanozymes.[1203] As shown in Fig. 52, the colorless nanoceria would turn into a yellow colored

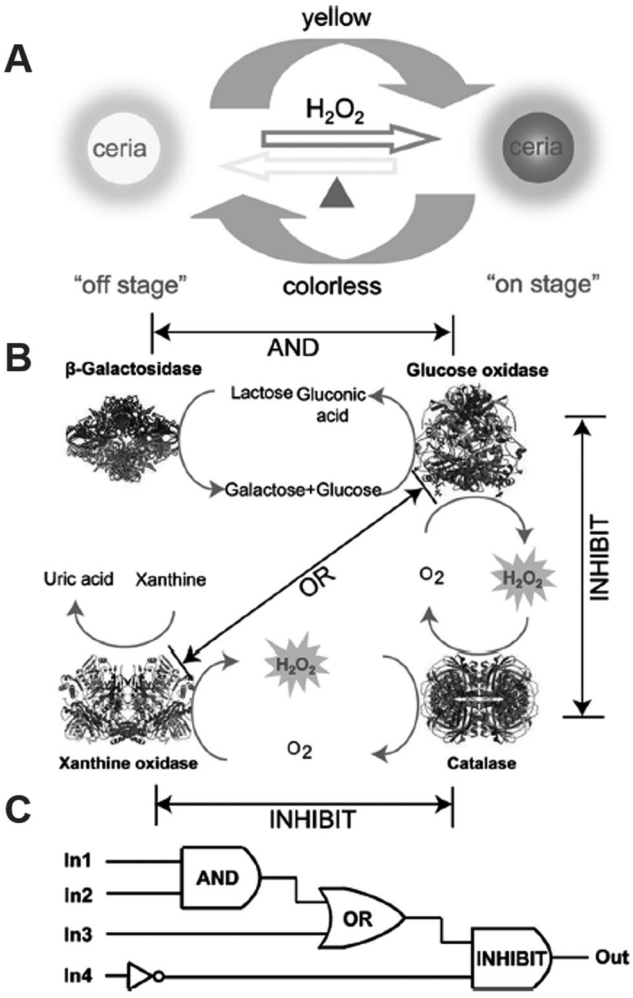

Fig. 52 (A) Schematic illustration of a thermally responsive switch based on nanoceria. (B) The operation of logic gates based on biocatalytic reactions. (C) Logic circuitry for the integrated logic system. In1 = β-galactosidase, In2 = GOx, In3 = xanthine oxidase, In4 = catalase. Reprinted with permission from ref. 1203. Copyright (2012) John Wiley and Sons.

one in the presence of H_2O_2 because of the change in the dominant oxidation state from Ce^{3+} to Ce^{4+} on nanoceria's surface. On the basis of nanoceria's color change, various logic gates were constructed by combining with several bioreactions. When employing β-galactosidase and GOx as inputs and nanoceria's color as output, an ''AND'' logic gate could be achieved. Similarly, when using GOx and xanthine oxidase as inputs, an ''OR'' logic gate was constructed. When combining catalase with GOx or xanthine oxidase, two ''INHIBIT'' logic gates were formed. Interestingly, these logic gates could be reset because the yellow colored nanoceria could turn into a colorless one on heating at 85 °C. Finally, practical logic sensing applications were demonstrated by using the proposed platform for multiplex detection.[1203]

Another example was reported by Chang *et al.* They used functional logic gates for selective detection of Pb^{2+} and Hg^{2+} by tailoring AuNPs' peroxidase-like activity with metal ions. They found that Pt^{4+} and Pb^{2+} could significantly enhance the peroxidase-like activity of AuNPs when depositing on the surface. On the basis of this phenomenon, an ''AND'' logic gate could be constructed when Pt^{4+} and Pb^{2+} were employed as inputs and the catalytic activity of AuNPs as output. Even though Bi^{3+} could enhance the peroxidase-like activity of AuNPs, the presence of both Bi^{3+} and Pb^{2+} exhibited an inhibition effect. Therefore, an ''INHIBIT'' logic gate could be achieved by using Bi^{3+} and Hg^{2+} as inputs.[1204] Besides ''AND'' and ''INHIBIT'' logic gates, others, such as ''OR'' and ''XOR'', were also constructed by tuning the AuNPs' catalase- or oxidase-like activity with various metal ions. Based on these logic gates, various metal ions were successfully detected.[1196]

Very recently, Dong and co-workers developed an ''INHIBIT'' logic gate for sensitive GSH detection. They found that MnO_2 nanosheets could effectively quench Scopoletin's fluorescence while enhancing Ampliflu Red's fluorescence by oxidation reaction. In the presence of GSH, the MnO_2 nanosheets would be decomposed into Mn^{2+}, resulting in the restored fluorescence of Scopoletin and decreased fluorescence of Ampliflu Red. Therefore, a ratiometric fluorescence signal could be obtained for GSH sensing. Accordingly, an ''INHIBIT'' logic gate could be constructed by using MnO_2 nanosheets and GSH as inputs and the ratiometric fluorescence signal as output.[380]

5. Conclusions, challenges, and perspective

Herein, we summarize recent advances in expanding the types of nanozymes, deepening the understanding of reaction mechanisms, and regulating their catalytic properties. With these advances, great achievements in applications such as biomedical sensing, therapeutics, and environmental remediation are discussed. Despite the remarkable progress that has been made since the first comprehensive review in 2013, there still remains plenty of room for advancing future research of nanozymes.

(1) *Rational design of nanozymes.* Up to now, most of nanozymes have been prepared *via* a trial-and-error strategy. To guide the synthesis of high-performance nanozymes with desired properties, the following studies might be considered. First, a better understanding of the catalytic mechanism of a nanozyme should be achieved to reveal the structure–activity relationship. Second, both experimental and computational studies should be combined together to elucidate the catalytic mechanisms. Third, the concepts of single atom (active site) nanozymes and single nanozyme catalysis should be introduced into the field. Fourth, machine learning and other artificial intelligence techniques should be explored to search for the best nanozyme candidates.

(2) *Sabatier principle and descriptors of nanozyme activities.* The Sabatier principle qualitatively states that an optimal catalyst for a given reaction should interact with the reactants neither too strongly nor too weakly.[1205,1206] The principle results in ''a volcano-type relationship between activity and bond strength''.[1206] Based on the Sabatier principle and the more quantitative scaling relationships, descriptors of catalytic activities can be identified and the corresponding activity (and selectivity) maps can be obtained. The Sabatier principle has been successfully used to search for catalysts for heterogeneous catalysis (such as in ammonia synthesis and electrocatalysis).[1205,1206] Inspired by such success and encouraged by our recent results, here we propose that general design rules for high-performance nanozymes can be established from the electronic point of view by identifying suitable descriptors of activities. These descriptors can be the adsorption (binding free) energy of a reactant (intermediate) on catalysts; the dissociation energy of a reactant (intermediate) on catalysts; d band for transition metal; e_g occupancy, O p band center, metal–oxygen hybridization (bond strength), and charge-transfer gap for transition metal oxides; *etc.*

(3) *Mimics of the protein scaffold (and native microenvironment) of an enzyme*. The current studies are mostly focused on the active sites of enzymes of interest. The mimics of the protein scaffold of an enzyme, which is important for the selectivity and efficiency of an enzymatic reaction, have largely not been studied yet.[1207] Moreover, some enzymes act properly only in their native environments (such as residence within a lipid membrane). The mimics of such an environment were rarely reported. Therefore, new strategies should be explored to address these challenges in the future study of nanozymes.

(4) *Expanding the types of nanozymes and beyond*. Currently, the types of reactions catalyzed by nanozymes have been expanded from redox to hydrolysis and a few others. But they are still not wide enough to cover all the important enzymatic reactions. To further increase the types of nanozymes, a fast and possible method is to create the analogues of active centers in natural enzymes, and then incorporate them into MOFs or other nanomaterials for mimicking the catalytic activities.

For an even wider view, the fabrication of organelle and cell mimics should be considered for future studies.[1208] The study of the potential implications of nanozymes in prebiotic chemistry and origin of life would be another challenging but rewarding research area.[29]

(5) *Specific nanozymes versus multi-enzyme mimicking nanozymes*. Another critical issue is the low substrate specificity of

nanozymes, with specificity being a fundamental property of natural enzymes. Although the combination of natural enzymes and nanozymes together could partially solve this problem, the stability and cost of the whole catalyst system were sacrificed because of the natural enzymes. Thus, by learning from nature, incorporating certain recognition mechanisms such as building protein-like (or aptamer-like) binding pockets and molecular imprinting of selective substrate pockets should be promising approaches to nanozymes with high specificity.[719,724,1209] Constructing asymmetric nanomaterials or using bioorthogonal nanozymes could also be considered as an optional choice in the future. Fine-modulation of the interaction of substrates with nanozymes by engineering the nanomaterials could be an alternative way to fabricate specific nanozymes.[1210,1211]

On the other hand, some nanozymes have multi-enzymatic activities, which have been demonstrated to be helpful for therapeutics in the Applications section. However, in certain cases, one unavoidable type of catalytic properties would cause some potential side effects, which should be carefully investigated to obtain an effective window for therapy.

(6) *Multi-functional nanozymes*. Taking advantage of the physiochemical properties of nanomaterials, the development of multi-functional nanozymes should be another interesting and challenging topic in the future.[68] Besides catalysis, nanomaterials endow nanozymes with more functions including magnetic, optical, and thermal properties, allowing more potential applications for ultra-sensitive sensing, sustainable chemistry, and multi-modality therapy.

(7) *Bioeffects of nanozymes*. To advance nanozymes for translational applications, both the benefits and risks of them should be systematically evaluated. Such studies would include but not be limited to assessments of cellular fate of nanozymes, clinical toxicity, pharmacokinetics, immunogenicity, *etc.* A further conjugation with ligands may help to decrease the toxicity and guide the targeting, but the accompanying influence on the catalytic activities and the subsequent metabolism of nanozymes come up. The long-term effects on the environment should also be considered.

(8) *Standardization of nanozyme research*. As summarized in Tables S11–S13 (ESI†), one type of nanomaterials has several different kinetics parameters. For a fair evaluation of different nanozymes, standards should be established to quantitatively determine their catalytic activities. Recently, Yan, Liang, and co-workers proposed standardized assays for peroxidase-like nanozymes, which would promote the development of peroxidase-like nanozyme based bio-detection.[1212] In the future study, we expect standards for other types of nanozymes to be set as well. Notably, the specific surface area, a unique characteristic of nanomaterials, plays an important role in the catalytic activities of nanozymes, especially for those with porous structures. Therefore, it is necessary to take the specific surface area into account when setting the standards.

(9) *Killer applications*. With the enormous development of nanozymes, we expect to see more practical applications, such as stem cell promotion, drug screening, and even some biomedical devices. Not only biomedicine, but also environment, agriculture, forensic science, and even national security fields are full of expectation as well. However, to gain long-term support for the nanozyme research, nanozymes have to find their unique applications in some specific niches.

Abbreviations

ΔAbs	The relative change of absorbance
Aβ	Amyloid-β
ABTS	2,2′-Azino-bis(3-ethylbenzothiazoline-6-sulfonic acid)
AChE	Acetylcholinesterase
ADA	Adamantylamine
ALS	Amyotrophic lateral sclerosis
AMP	Adenosine 5′-monophosphate
ATX	Astaxanthin
AuNCs-NH_2	Amine-terminated dendrimer-encapsulated AuNCs
AuNCs-OH	Hydroxyl-terminated, containing 3°-amines inside the backbone
BA	Benzoic anhydride
BBB	Blood brain barrier
BDC	Benzene-1,4-dicarboxylate
BrPE	2-Bromo-1-phenylethanone
BSA	Bovine serum albumin
C_{60}-C_3	$C_{60}[C(COOH)_2]_3$ with C_3 symmetry
CB	Cucurbit
C*c*O	Cytochrome *c* oxidase
CMP	Cytidine 5′-monophosphate
CoO_xH–GO	Cobalt hydroxide/oxide modified graphene oxide
CTC	Circulating tumor cell
Cu_2O NP	Cuprous oxide nanoparticle
CWA	Chemical warfare agent
Cyt *c*	Cytochrome *c*
CZ NPs	Ceria NPs with Zr^{4+} doping
DMNP	Dimethyl-4-nitrophenyl phosphate
DMSN	Dendritic mesoporous silica NP
DTBZ	Dihydrotetrabenazine
E-A/P-CeO_2	CeO_2 NP based neuroprotection agent
EBOV	Ebola virus
E. coli	*Escherichia coli*
ELISA	Enzyme-linked immunosorbent assay
EpCAM	Epithelial cell adhesion molecule
E_r	Reaction energy
FD	Fluorodopa
GMP	Guanosine 5′-monophosphate
GOx	Glucose oxidase
GPx	Glutathione peroxidase
GQD	Graphene quantum dot
GR	Glutathione reductase
GSH	Glutathione
GSOH	Glutathione sulfenic acid
GSSG	Glutathione disulfide
H_2BDC	Terephthalic acid
H_3BTC	1,3,5-Benzenetricarboxylic acid

HCC	Hydrophilic carbon cluster
HEL	Human erythroleukemia
HKUST	Hong Kong University of Science and Technology
HPNPP	2-Hydroxypropyl *p*-nitrophenyl phosphate
H-rGO	Hemin functionalized reduced graphene oxide
HRP	Horseradish peroxidase
MCSP	Anti-melanoma-associated chondroitin sulfate proteoglycan
MeNP	Melanin nanoparticle
MFMSN	Manganese ferrite NP-anchored mesoporous silica NP
MGCB	Malachite green carbinol base
M-HFn	Magnetoferritin NPs
MIL	Material Institute of Lavoisier
MNP	Magnetic nanoparticle
MOF	Metal–organic framework
MoO_3 NP	Molybdenum trioxide nanoparticle
MPTP	1-Methyl-4-phenyl-1,2,3,6-tetrahydropyridine
MSN-AuNPs	AuNPs loaded on mesoporous silica
MUC-1	Mucin 1 protein
NADPH	Nicotinamide adenine dinucleotide phosphate
NC	Nanocluster
$^{\bullet}NO$	Nitric oxide
NP	Nanoparticle
N-PCN	Nitrogen doped porous carbon nanosphere
$ONOO^-$	Peroxynitrite
PAPLAL	A mixture of Pd and Pt NPs used in Japan
PB	Prussian blue
PCR	Polymerase chain reaction
PDA	Polydopamine
PDT	Photodynamic therapy
PEG	Poly(ethylene glycol)
PET	Positron emission tomography
PH	Phenylhydrazine
PMA	Phorbol 12-myristate 13-acetate
PPD	*p*-Phenylenediamine
PSA	Prostate-specific antigen
PtNPs/GO	Platinum NPs/graphene oxide
ROS	Reactive oxygen species
RNS	Reactive nitrogen species
S. aureus	*Staphylococcus aureus*
SEM	Scanning electron microscopy
SF	Soft formulation
SOD	Superoxide dismutase
ssDNA	Single-stranded DNA
SuOx	Sulfite oxidase
TACN	1,4,7-Triazacyclononane
TCPP	Tetrakis(4-carboxyphenyl)porphyrin
TEM	Transmission electron microscopy
TMB	3,3′,5,5′-Tetramethylbenzidine
TOF	Turnover number
TPP	Triphenylphosphonium
TPP–nanoceria	Triphenylphosphonium-conjugated nanoceria
UiO	University of Oslo

Conflicts of interest

There are no conflicts to declare.

Acknowledgements

This work was supported by the National Natural Science Foundation of China (21722503 and 21874067), Natural Science Foundation of Jiangsu Province (BK20160615), 973 Program (2015CB659400), PAPD program, Shuangchuang Program of Jiangsu Province, Open Funds of the State Key Laboratory of Coordination Chemistry (SKLCC1819), Open Funds of the State Key Laboratory of Analytical Chemistry for Life Science (SKLACLS1704), Fundamental Research Funds for the Central Universities (021314380103) and Thousand Talents Program for Young Researchers. We thank Guopo Shen, Yifan Ni, and Yuchen Zhang for the help with the website for nanozyme timeline. We thank Junshu Lin, Anqi Lin, Yihong Zhang, Ying Wei, Liyun Wu, and Yibei Wu for proof-reading.

References

1 L. Z. Gao, J. Zhuang, L. Nie, J. B. Zhang, Y. Zhang, N. Gu, T. H. Wang, J. Feng, D. L. Yang, S. Perrett and X. Y. Yan, *Nat. Nanotechnol.*, 2007, **2**, 577–583.
2 H. Wei and E. K. Wang, *Chem. Soc. Rev.*, 2013, **42**, 6060–6093.
3 S. Das, J. M. Dowding, K. E. Klump, J. F. McGinnis, W. Self and S. Seal, *Nanomedicine*, 2013, **8**, 1483–1508.
4 L. Z. Gao and X. Y. Yan, *Prog. Biochem. Biophys.*, 2013, **40**, 892–902.
5 S. Hou, X. N. Hu, T. Wen, W. Q. Liu and X. C. Wu, *Adv. Mater.*, 2013, **25**, 3857–3862.
6 M. Iranifam, *TrAC-Trend Anal. Chem.*, 2013, **51**, 51–70.
7 L. M. Rossi, N. J. S. Costa, F. P. Silva and R. V. Goncalves, *Nanotechnol. Rev.*, 2013, **2**, 597–614.
8 Y. Zhang, Y. M. Guo, Y. L. Xianyu, W. W. Chen, Y. Y. Zhao and X. Y. Jiang, *Adv. Mater.*, 2013, **25**, 3802–3819.
9 W. W. He, W. Wamer, Q. S. Xia, J. J. Yin and P. P. Fu, *J. Environ. Sci. Health, Part C: Environ. Carcinog. Ecotoxicol. Rev.*, 2014, **32**, 186–211.
10 A. Kumar, S. Das, P. Munusamy, W. Self, D. R. Baer, D. C. Sayle and S. Seal, *Environ. Sci.-Nano*, 2014, **1**, 516–532.
11 Y. H. Lin, J. S. Ren and X. G. Qu, *Adv. Mater.*, 2014, **26**, 4200–4217.
12 Y. H. Lin, J. S. Ren and X. G. Qu, *Acc. Chem. Res.*, 2014, **47**, 1097–1105.
13 C. Xu and X. G. Qu, *NPG Asia Mater.*, 2014, **6**, e90.
14 C. Xu and X. G. Qu, *Sci. Sin.: Chim.*, 2014, **44**, 506–520.
15 Q. Yu, H. Liu and H. Chen, *J. Mater. Chem. B*, 2014, **2**, 7849–7860.
16 Y. Zhang, T. Tian, Y. H. Sun, Y. Zhu and Q. Huang, *Sci. Bull.*, 2014, 158–168.
17 B. Garg, T. Bisht and Y. C. Ling, *Molecules*, 2015, **20**, 14155–14190.

18 C. Luo, Y. Li and J. G. Long, *Sci. Bull.*, 2015, **60**, 3478–3488.
19 L. Zheng, J. H. Zhao, X. F. Niu and Y. H. Yang, *Mater. Rev*, 2015, **29**, 115–120.
20 L. Z. Gao and X. Y. Yan, *Sci. China: Life Sci.*, 2016, **59**, 400–402.
21 P. Jacquet, D. Daude, J. Bzdrenga, P. Masson, M. Elias and E. Chabriere, *Environ. Sci. Pollut. Res.*, 2016, **23**, 8200–8218.
22 E. Kuah, S. Toh, J. Yee, Q. Ma and Z. Gao, *Chem. – Eur. J.*, 2016, **22**, 8404–8430.
23 J. R. Li, A. G. Shen and J. M. Hu, *Chin. J. Appl. Chem.*, 2016, **33**, 1245–1252.
24 C. Luo, Y. Li, Q. W. Long and J. G. Long, *Chin. J. Biomed. Eng.*, 2016, **35**, 105–113.
25 F. Mancin, L. J. Prins, P. Pengo, L. Pasquato, P. Tecilla and P. Scrimin, *Molecules*, 2016, **21**, 1014.
26 T. Montini, M. Melchionna, M. Monai and P. Fornasiero, *Chem. Rev.*, 2016, **116**, 5987–6041.
27 R. Ragg, M. N. Tahir and W. Tremel, *Eur. J. Inorg. Chem.*, 2016, 1906–1915.
28 S. Singh, *Biointerphases*, 2016, **11**, 04B202.
29 X. Y. Wang, Y. H. Hu and H. Wei, *Inorg. Chem. Front.*, 2016, **3**, 41–60.
30 X. Y. Wang, W. J. Guo, Y. H. Hu, J. J. Wu and H. Wei, *Nanozymes: Next Wave of Artificial Enzymes*, Springer, 2016.
31 B. Yang, J. P. Li, H. Deng and L. M. Zhang, *Crit. Rev. Anal. Chem.*, 2016, **46**, 469–481.
32 W. S. Zheng and X. Y. Jiang, *Analyst*, 2016, **141**, 1196–1208.
33 H. J. Cheng, X. Y. Wang and H. Wei, *Encyclopedia of Physical Organic Chemistry*, 2017, pp. 3885–3948.
34 B. J. Du, D. Li, J. Wang and E. K. Wang, *Adv. Drug Delivery Rev.*, 2017, **118**, 78–93.
35 L. Z. Gao, K. L. Fan and X. Y. Yan, *Theranostics*, 2017, **7**, 3207–3227.
36 L. Z. Gao and H. Koo, *Nanomedicine*, 2017, **12**, 275–279.
37 J. Golchin, K. Golchin, N. Alidadian, S. Ghaderi, S. Eslamkhah, M. Eslamkhah and A. Akbarzadeh, *Artif. Cells, Nanomed., Biotechnol.*, 2017, **45**, 1069–1076.
38 S. B. He, Y. F. Zhang, H. N. Huang, Z. Q. Lin and W. Chen, *J. Anal. Sci.*, 2017, **33**, 567–572.
39 H. X. Ju, *J. Anal. Test.*, 2017, **1**, 7.
40 L. P. Kowsalya Vellingiri and K. Hyun Kim, *Coord. Chem. Rev.*, 2017, **353**, 159–179.
41 B. W. Liu and J. W. Liu, *Nano Res.*, 2017, **10**, 1125–1148.
42 J. Lu, H. C. Zhang, B. Zhang, W. C. Gao, X. Li, H. H. Chang and W. L. Wei, *Chem. Ind. Eng. Prog*, 2017, **36**, 20–28.
43 M. Nasir, M. H. Nawaz, U. Latif, M. Yaqub, A. Hayat and A. Rahim, *Microchim. Acta*, 2017, **184**, 323–342.
44 C. M. Sims, S. K. Hanna, D. A. Heller, C. P. Horoszko, M. E. Johnson, A. R. M. Bustos, V. Reipa, K. R. Riley and B. C. Nelson, *Nanoscale*, 2017, **9**, 15226–15251.
45 D. Pedone, M. Moglianetti, E. De Luca, G. Bardi and P. P. Pompa, *Chem. Soc. Rev.*, 2017, **46**, 4951–4975.
46 L. Syedmoradi, M. Daneshpour, M. Alvandipour, F. A. Gomez, H. Hajghassem and K. Omidfar, *Biosens. Bioelectron.*, 2017, **87**, 373–387.
47 T. Tangchaikeeree, D. Polpanich, A. Elaissari and K. Jangpatarapongsa, *Colloids Surf., B*, 2017, **158**, 1–8.
48 L. B. Wan, Z. L. Chen, C. X. Huang and X. T. Shen, *TrAC-Trend Anal. Chem.*, 2017, **95**, 110–121.
49 G. H. Wang, J. Z. Zhang, X. He, Z. Y. Zhang and Y. L. Zhao, *Chin. J. Chem.*, 2017, **35**, 791–800.
50 P. Weerathunge, T. K. Sharma, R. Ramanathan and V. Bansal, *Advanced Environmental Analysis: Applications of Nanomaterials, Volume 2*, ed. C. M. Hussain and B. Kharisov, 2017, vol. 10, pp. 108–132.
51 Y. B. Zhou, B. W. Liu, R. H. Yang and J. W. Liu, *Bioconjugate Chem.*, 2017, **28**, 2903–2909.
52 Y. Choi, J. H. Hwang and S. Y. Lee, *Small Methods*, 2018, **2**, 1700351.
53 D. P. Cormode, L. Z. Gao and H. Koo, *Trends Biotechnol.*, 2018, **36**, 15–29.
54 K. Herget, H. Frerichs, F. Pfitzner, M. N. Tahir and W. Tremel, *Adv. Mater.*, 2018, 1707073.
55 Y. Hu and T. L. Ma, *Modern Chem. Ind.*, 2018, **38**, 71–75.
56 H. X. Ju, *Appl. Mater. Today*, 2018, **10**, 51–71.
57 K. Korschelt, M. N. Tahir and W. Tremel, *Chem. – Eur. J.*, 2018, **24**, 9703–9713.
58 S. Lin, J. Wu, J. Yao, W. Cao, F. Muhammad and H. Wei, *Biomedical Applications of Functionalized Nanomaterials*, Elsevier, 2018, pp. 171–201.
59 Y. Y. Ma, W. Gao, Z. Y. Zhang, S. Zhang, Z. M. Tian, Y. X. Liu, J. C. Ho and Y. Q. Qu, *Surf. Sci. Rep.*, 2018, **73**, 1–36.
60 B. Sharma, A. K. Dangi and P. Shukla, *J. Environ. Manage.*, 2018, **210**, 10–22.
61 H. J. Sun, Y. Zhou, J. S. Ren and X. G. Qu, *Angew. Chem., Int. Ed.*, 2018, **57**, 9224–9237.
62 T. Van Tan, J. Kim, L. T. Tufa, S. Oh, J. Kwon and J. Lee, *Anal. Chem.*, 2018, **90**, 225–239.
63 L. Valgimigli, A. Baschieri and R. Amorati, *J. Mater. Chem. B*, 2018, **6**, 2036–2051.
64 Q. Wang, H. Wei, Z. Zhang, E. Wang and S. Dong, *TrAC-Trend Anal. Chem.*, 2018, **105**, 218–224.
65 L. Y. Wang, M. F. Huo, Y. Chen and J. L. Shi, *Adv. Healthcare Mater.*, 2018, **7**, 1701156.
66 Y. J. Wen, L. Y. Yan and Y. C. Ling, *Sci. China: Chem.*, 2018, **61**, 266–275.
67 J. Wu, S. Li and H. Wei, *Chem. Commun.*, 2018, **54**, 6520–6530.
68 J. Wu, S. Li and H. Wei, *Nanoscale Horiz.*, 2018, **3**, 367–382.
69 H. Y. Xu, M. M. Liang, Y. Zhang and Q. B. Wang, *Prog. Biochem. Biophys.*, 2018, **45**, 277–278.
70 X. Q. Meng and K. L. Fan, *Prog. Biochem. Biophys.*, 2018, **45**, 218–236.
71 S. R. Li, Y. C. Huang, J. R. Liu, E. K. Wang and H. Wei, *Prog. Biochem. Biophys.*, 2018, **45**, 129–147.

72 W. C. Mo, J. Zhao, Y. Liu and R. Q. He, *Prog. Biochem. Biophys.*, 2018, **45**, 268–271.
73 A. P. Li, Q. X. Yuchi and L. B. Zhang, *Prog. Biochem. Biophys.*, 2018, **45**, 193–203.
74 X. M. Shen, X. J. Gao and X. F. Gao, *Prog. Biochem. Biophys.*, 2018, **45**, 204–217.
75 Y. Y. Huang, Y. H. Lin, F. Pu, J. S. Ren and X. G. Qu, *Prog. Biochem. Biophys.*, 2018, **45**, 256–267.
76 H. J. Dong, C. Zhang, Y. Y. Fan, W. Zhang, N. Gu and Y. Zhang, *Prog. Biochem. Biophys.*, 2018, **45**, 105–117.
77 M. M. Liang and F. X. Meng, *Prog. Biochem. Biophys.*, 2018, **45**, 272–276.
78 L. Bixenmann, J. Y. He, M. M. Liang and W. Tremel, *Prog. Biochem. Biophys.*, 2018, **45**, 148–169.
79 Y. Tang, Z. Y. Qiu, Z. B. Xu and L. Z. Gao, *Prog. Biochem. Biophys.*, 2018, **45**, 118–128.
80 X. Y. Yan, *Prog. Biochem. Biophys.*, 2018, **45**, 101–104.
81 B. W. Yang, Y. Chen and J. L. Shi, *Prog. Biochem. Biophys.*, 2018, **45**, 237–255.
82 R. Yang, S. F. Cai and C. Wang, *Prog. Biochem. Biophys.*, 2018, **45**, 170–192.
83 Z. Z. Yang, C. Wang and X. F. Lu, *Sci. China Mater.*, 2018, **61**, 653–670.
84 H. Wei and E. K. Wang, *Anal. Chem.*, 2008, **80**, 2250–2254.
85 X. L. He, L. F. Tan, D. Chen, X. L. Wu, X. L. Ren, Y. Q. Zhang, X. W. Meng and F. Q. Tang, *Chem. Commun.*, 2013, **49**, 4643–4645.
86 M. M. Liang, K. L. Fan, Y. Pan, H. Jiang, F. Wang, D. L. Yang, D. Lu, J. Feng, J. J. Zhao, L. Yang and X. Y. Yan, *Anal. Chem.*, 2013, **85**, 308–312.
87 M. A. Woo, M. I. Kim, J. H. Jung, K. S. Park, T. S. Seo and H. G. Park, *Int. J. Mol. Sci.*, 2013, **14**, 9999–10014.
88 Z. Can, A. Uzer, K. Turkekul, E. Ercag and R. Apak, *Anal. Chem.*, 2015, **87**, 9589–9594.
89 M. Z. Yang, Y. P. Guan, Y. Yang, T. T. Xia, W. B. Xiong, N. Wang and C. Guo, *J. Colloid Interface Sci.*, 2013, **405**, 291–295.
90 X. Ai, L. Wu, M. N. Zhang, X. D. Hou, L. Yang and C. B. Zheng, *J. Agric. Food Chem.*, 2014, **62**, 8586–8593.
91 J. Z. Chen, Y. J. Liu, G. X. Zhu and A. H. Yuan, *Cryst. Res. Technol.*, 2014, **49**, 309–314.
92 X. L. Cheng, J. S. Jiang, D. M. Jiang and Z. J. Zhao, *J. Phys. Chem. C*, 2014, **118**, 12588–12598.
93 Y. Gao, Z. Wei, F. Li, Z. M. Yang, Y. M. Chen, M. Zrinyi and Y. Osada, *Green Chem.*, 2014, **16**, 1255–1261.
94 J. Y. Qu, Y. Dong, Y. Wang, T. F. Lou and X. P. Du, *Micro Nano Lett.*, 2014, **9**, 572–576.
95 R. V. Shutov, A. Guerreiro, E. Moczko, I. P. de Vargas-Sansalvador, I. Chianella, M. J. Whitcombe and S. A. Piletsky, *Small*, 2014, **10**, 1086–1089.
96 L. J. Wang, Y. Min, D. D. Xu, F. J. Yu, W. Z. Zhou and A. Cuschieri, *Chem. Commun.*, 2014, **50**, 11147–11150.
97 D. Bhuyan, S. S. Arbuj and L. Saikia, *New J. Chem.*, 2015, **39**, 7759–7762.
98 R. Cheng, G. Q. Li, C. Cheng, L. Shi, X. Zheng and Z. Ma, *RSC Adv.*, 2015, **5**, 66927–66933.
99 Y. Pan, N. Li, J. S. Mu, R. H. Zhou, Y. Xu, D. Z. Cui, Y. Wang and M. Zhao, *Appl. Microbiol. Biotechnol.*, 2015, **99**, 703–715.
100 J. L. Sang, R. L. Wu, P. P. Guo, J. Du, S. M. Xu and J. D. Wang, *J. Appl. Polym. Sci.*, 2016, **133**, 43065.
101 Y. H. Wu, L. Chu, W. Liu, L. Jiang, X. Y. Chen, Y. H. Wang and Y. L. Zhao, *RSC Adv.*, 2017, **7**, 47309–47315.
102 Y. H. Ling, M. C. Long, P. D. Hu, Y. Chen and J. W. Huang, *J. Hazard. Mater.*, 2014, **264**, 195–202.
103 K. Mitra, A. B. Ghosh, A. Sarkar, N. Saha and A. K. Dutta, *Biochem. Biophys. Res. Commun.*, 2014, **451**, 30–35.
104 Z. C. Xing, J. Q. Tian, A. M. Asiri, A. H. Qusti, A. O. Al-Youbi and X. P. Sun, *Biosens. Bioelectron.*, 2014, **52**, 452–457.
105 Q. Y. Liu, L. Y. Zhang, H. Li, Q. Y. Jia, Y. L. Jiang, Y. T. Yang and R. R. Zhu, *Mater. Sci. Eng., C*, 2015, **55**, 193–200.
106 C. Lu, X. J. Liu, Y. F. Li, F. Yu, L. H. Tang, Y. J. Hu and Y. B. Yine, *ACS Appl. Mater. Interfaces*, 2015, **7**, 15395–15402.
107 C. Hao, Y. R. Shen, Z. Y. Wang, X. H. Wang, F. Feng, C. W. Ge, Y. T. Zhao and K. Wang, *ACS Sustainable Chem. Eng.*, 2016, **4**, 1069–1077.
108 M. Klünker, M. Nawaz Tahir, R. Ragg, K. Korschelt, P. Simon, T. E. Gorelik, B. Barton, S. I. Shylin, M. Panthoefer, J. Herzberger, H. Frey, D. V. Ksenofontov, A. Möller, U. Kolb, Y. Grin and W. Tremel, *Chem. Mater.*, 2016, **29**, 1134–1146.
109 A. Roy, R. Sahoo, C. Ray, S. Dutta and T. Pal, *RSC Adv.*, 2016, **6**, 32308–32318.
110 L. N. Song, C. Huang, W. Zhang, M. Ma, Z. W. Chen, N. Gu and Y. Zhang, *Colloids Surf., A*, 2016, **506**, 747–755.
111 M. Kluenker, M. N. Tahir, R. Ragg, K. Korschelt, P. Simon, T. E. Gorelik, B. Barton, S. I. Shylin, M. Panthoefer, J. Herzberger, H. Frey, V. Ksenofontov, A. Moeller, U. Kolb, J. Grin and W. Tremel, *Chem. Mater.*, 2017, **29**, 1134–1146.
112 M. Hosseini, F. S. Sabet, H. Khabbaz, M. Aghazadeh, F. Mizani and M. R. Ganjali, *Anal. Methods*, 2017, **9**, 3519–3524.
113 L. Melnikova, K. Pospiskova, Z. Mitroova, P. Kopcansky and I. Safarik, *Microchim. Acta*, 2014, **181**, 295–301.
114 M. Kaur and N. Kaur, *ACS Symp. Ser.*, 2016, **1238**, 113–136.
115 P. Roonasi and A. Y. Nezhad, *Mater. Chem. Phys.*, 2016, **172**, 143–149.
116 S. Mumtaz, L. S. Wang, M. Abdullah, S. Z. Hussain, Z. Iqbal, V. M. Rotello and I. Hussain, *J. Phys. D: Appl. Phys.*, 2017, **50**, 11LT02.
117 T. Zhang, C. Cao, X. Tang, Y. Cai, C. Yang and Y. Pan, *Nanotechnology*, 2017, **28**, 045704.
118 X. Ai, Y. Wang, X. D. Hou, L. Yang, C. B. Zheng and L. Wu, *Analyst*, 2013, **138**, 3494–3501.
119 W. T. Yao, H. Z. Zhu, W. G. Li, H. B. Yao, Y. C. Wu and S. H. Yu, *ChemPlusChem*, 2013, **78**, 723–727.
120 C. P. Ding, Y. H. Yan, D. S. Xiang, C. L. Zhang and Y. Z. Xian, *Microchim. Acta*, 2016, **183**, 625–631.

121 L. L. Li, K. X. Liang, Z. T. Hua, M. Zou, K. Z. Chen and W. Wang, *Polym. Chem.*, 2015, **6**, 2290–2296.
122 T. B. Zhang, Y. C. Lu and G. S. Luo, *ACS Appl. Mater. Interfaces*, 2014, **6**, 14433–14438.
123 J. L. Guo, Y. Wang and M. Zhao, *Talanta*, 2018, **182**, 230–240.
124 Q. M. Yang, S. Y. Lu, B. L. Shen, S. J. Bao and Y. S. Liu, *New J. Chem.*, 2018, **42**, 6803–6809.
125 W. M. Zhang, D. Ma and J. X. Du, *Talanta*, 2014, **120**, 362–367.
126 V. Cunderlova, A. Hlavacek, V. Hornakova, M. Peterek, D. Nemecek, A. Hampl, L. Eyer and P. Skladal, *Microchim. Acta*, 2016, **183**, 651–658.
127 P. C. Pandey and D. Panday, *Electrochim. Acta*, 2016, **190**, 758–765.
128 P. J. Ni, Y. J. Sun, H. C. Dai, W. D. Lu, S. Jiang, Y. L. Wang, Z. Li and Z. Li, *Sens. Actuators, B*, 2017, **240**, 1314–1320.
129 M. Vazquez-Gonzalez, R. M. Torrente-Rodriguez, A. Kozell, W. C. Liao, A. Cecconello, S. Campuzano, J. M. Pingarron and I. Willner, *Nano Lett.*, 2017, **17**, 4958–4963.
130 A. A. Karyakin, O. V. Gitelmacher and E. E. Karyakina, *Anal. Chem.*, 1995, **67**, 2419–2423.
131 A. A. Karyakin, E. E. Karyakina and L. Gorton, *J. Electroanal. Chem.*, 1998, **456**, 97–104.
132 X. Q. Zhang, S. W. Gong, Y. Zhang, T. Yang, C. Y. Wang and N. Gu, *J. Mater. Chem.*, 2010, **20**, 5110–5116.
133 W. Zhang, S. Hu, J. J. Yin, W. He, W. Lu, M. Ma, N. Gu and Y. Zhang, *J. Am. Chem. Soc.*, 2016, **138**, 5860–5865.
134 R. Andre, F. Natalio, M. Humanes, J. Leppin, K. Heinze, R. Wever, H. C. Schroder, W. E. G. Muller and W. Tremel, *Adv. Funct. Mater.*, 2011, **21**, 501–509.
135 F. Natalio, R. Andre, A. F. Hartog, B. Stoll, K. P. Jochum, R. Wever and W. Tremel, *Nat. Nanotechnol.*, 2012, **7**, 530–535.
136 G. D. Nie, L. Zhang, J. Y. Lei, L. Yang, Z. Zhang, X. F. Lu and C. Wang, *J. Mater. Chem. A*, 2014, **2**, 2910–2914.
137 J. X. Xie, X. D. Zhang, H. Jiang, S. Wang, H. Liu and Y. M. Huang, *RSC Adv.*, 2014, **4**, 26046–26049.
138 X. H. Niu, Y. F. He, X. Li, H. W. Song, W. C. Zhang, Y. X. Peng, J. M. Pan and F. X. Qiu, *ChemistrySelect*, 2017, **2**, 10854–10859.
139 R. Tian, J. H. Sun, Y. F. Qi, B. Y. Zhang, S. L. Guo and M. M. Zhao, *Nanomaterials*, 2017, **7**, 347.
140 L. J. Huang, W. X. Zhu, W. T. Zhang, K. Chen, J. Wang, R. Wang, Q. F. Yang, N. Hu, Y. R. Suo and J. L. Wang, *Microchim. Acta*, 2018, **185**, 7.
141 A. A. Vernekar, D. Sinha, S. Srivastava, P. U. Paramasivam, P. D'Silva and G. Mugesh, *Nat. Commun.*, 2014, **5**, 5301.
142 S. Ghosh, P. Roy, N. Karmodak, E. D. Jemmis and G. Mugesh, *Angew. Chem., Int. Ed.*, 2018, **57**, 4510–4515.
143 Y. S. Wu, F. F. Huang and Y. W. Lin, *ACS Appl. Mater. Interfaces*, 2013, **5**, 1503–1509.
144 R. Zhu, Y. Zhou, X. L. Wang, L. P. Liang, Y. J. Long, Q. L. Wang, H. J. Zhang, X. X. Huang and H. Z. Zheng, *Talanta*, 2013, **117**, 127–132.
145 H. H. Deng, G. W. Li, L. Hong, A. L. Liu, W. Chen, X. H. Lin and X. H. Xia, *Food Chem.*, 2014, **147**, 257–261.
146 T. H. Han, M. M. Khan, J. Lee and M. H. Cho, *J. Ind. Eng. Chem.*, 2014, **20**, 2003–2009.
147 Y. P. Liu, C. W. Wang, N. Cai, S. H. Long and F. Q. Yu, *J. Mater. Sci.*, 2014, **49**, 7143–7150.
148 P. Weerathunge, R. Ramanathan, R. Shukla, T. K. Sharma and V. Bansal, *Anal. Chem.*, 2014, **86**, 11937–11941.
149 M. Drozd, M. Pietrzak, P. Parzuchowski, M. Mazurkiewicz-Pawlicka and E. Malinowska, *Nanotechnology*, 2015, **26**, 495101.
150 X. Jiang, C. J. Sun, Y. Guo, G. J. Nie and L. Xu, *Biosens. Bioelectron.*, 2015, **64**, 165–170.
151 M. Drozd, M. Pietrzak, P. G. Parzuchowski and E. Malinowska, *Anal. Bioanal. Chem.*, 2016, **408**, 8505–8513.
152 C. F. Jiang, J. Zhu, Z. Li, J. H. Luo, J. S. Wang and Y. Sun, *RSC Adv.*, 2017, **7**, 44463–44469.
153 X. L. Zhu, X. X. Mao, Z. H. Wang, C. Feng, G. F. Chen and G. X. Li, *Nano Res.*, 2017, **10**, 959–970.
154 R. Singh, R. Belgamwar, M. Dhiman and V. Polshettiwar, *J. Mater. Chem. B*, 2018, **6**, 1600–1604.
155 Z. Z. Sun, N. Zhang, Y. M. Si, S. Li, J. W. Wen, X. B. Zhu and H. Wang, *Chem. Commun.*, 2014, **50**, 9196–9199.
156 L. Chen, L. Sha, Y. W. Qiu, G. F. Wang, H. Jiang and X. J. Zhang, *Nanoscale*, 2015, **7**, 3300–3308.
157 J. T. Hu, P. J. Ni, H. C. Dai, Y. J. Sun, Y. L. Wang, S. Jiang and Z. Li, *Analyst*, 2015, **140**, 3581–3586.
158 S. Sloan-Dennison, S. Laing, N. C. Shand, D. Graham and K. Faulds, *Analyst*, 2017, **142**, 2484–2490.
159 M. N. Karim, S. R. Anderson, S. Singh, R. Ramanathan and V. Bansal, *Biosens. Bioelectron.*, 2018, **110**, 8–15.
160 Y. Fu, H. X. Zhang, S. D. Dai, X. Zhi, J. L. Zhang and W. Li, *Analyst*, 2015, **140**, 6676–6683.
161 W. Li, C. Bin, H. X. Zhang, Y. H. Sun, J. Wang, J. L. Zhang and Y. Fu, *Biosens. Bioelectron.*, 2015, **66**, 251–258.
162 W. Li, H. X. Zhang, J. L. Zhang and Y. Fu, *Anal. Methods*, 2015, **7**, 4464–4471.
163 G. W. Wu, S. B. He, H. P. Peng, H. H. Deng, A. L. Liu, X. H. Lin, X. H. Xia and W. Chen, *Anal. Chem.*, 2014, **86**, 10955–10960.
164 X. Q. Lin, H. H. Deng, G. W. Wu, H. P. Peng, A. L. Liu, X. H. Lin, X. H. Xia and W. Chen, *Analyst*, 2015, **140**, 5251–5256.
165 K. Cai, Z. C. Lv, K. Chen, L. Huang, J. Wang, F. Shao, Y. J. Wang and H. Y. Han, *Chem. Commun.*, 2013, **49**, 6024–6026.
166 Z. Q. Gao, M. D. Xu, L. Hou, G. N. Chen and D. P. Tang, *Anal. Chim. Acta*, 2013, **776**, 79–86.
167 S. B. He, H. H. Deng, A. L. Liu, G. W. Li, X. H. Lin, W. Chen and X. H. Xia, *ChemCatChem*, 2014, **6**, 1543–1548.
168 Y. Liu, H. H. Wu, M. Li, J. J. Yin and Z. H. Nie, *Nanoscale*, 2014, **6**, 11904–11910.
169 Z. F. Wang, X. Yang, J. Feng, Y. J. Tang, Y. Y. Jiang and N. Y. He, *Analyst*, 2014, **139**, 6088–6091.
170 Y. Ju and J. Kim, *Chem. Commun.*, 2015, **51**, 13752–13755.

171 M. Kim, M. S. Kim, S. H. Kweon, S. Jeong, M. H. Kang, M. I. Kim, J. Lee and J. Doh, *Adv. Healthcare Mater.*, 2015, **4**, 1311–1316.
172 Z. F. Wang, X. Yang, J. J. Yang, Y. Y. Jiang and N. Y. He, *Anal. Chim. Acta*, 2015, **862**, 53–63.
173 L. H. Jin, Z. Meng, Y. Q. Zhang, S. J. Cai, Z. H. Zhang, C. Li, L. Shang and Y. H. Shen, *ACS Appl. Mater. Interfaces*, 2017, **9**, 10027–10033.
174 H. H. Ye, Y. Z. Liu, A. Chhabra, E. Lilla and X. H. Xia, *ChemNanoMat*, 2017, **3**, 33–38.
175 J. M. Lan, W. M. Xu, Q. P. Wan, X. Zhang, J. Lin, J. H. Chen and J. Z. Chen, *Anal. Chim. Acta*, 2014, **825**, 63–68.
176 Y. Liu, D. L. Purich, C. C. Wu, Y. Wu, T. Chen, C. Cui, L. Q. Zhang, S. Cansiz, W. J. Hou, Y. Y. Wang, S. Y. Yang and W. H. Tan, *J. Am. Chem. Soc.*, 2015, **137**, 14952–14958.
177 J. P. Wei, X. L. Chen, S. G. Shi, S. G. Mo and N. F. Zheng, *Nanoscale*, 2015, **7**, 19018–19026.
178 X. Feng, X. Li, H. Y. Shi, H. Huang, X. C. Wu and W. B. Song, *Anal. Chim. Acta*, 2014, **852**, 37–44.
179 S. G. Ge, F. Liu, W. Y. Liu, M. Yan, X. R. Song and J. H. Yu, *Chem. Commun.*, 2014, **50**, 475–477.
180 X. N. Hu, A. Saran, S. Hou, T. Wen, Y. L. Ji, W. Q. Liu, H. Zhang and X. C. Wu, *Chin. Sci. Bull.*, 2014, **59**, 2588–2596.
181 C. Zheng, A. X. Zheng, B. Liu, X. L. Zhang, Y. He, J. Li, H. H. Yang and G. N. Chen, *Chem. Commun.*, 2014, **50**, 13103–13106.
182 Z. Q. Gao, M. D. Xu, M. H. Lu, G. N. Chen and D. P. Tang, *Biosens. Bioelectron.*, 2015, **70**, 194–201.
183 S. G. Ge, W. Y. Liu, H. Y. Liu, F. Liu, J. H. Yu, M. Yan and J. D. Huang, *Biosens. Bioelectron.*, 2015, **71**, 456–462.
184 L. Han, C. C. Li, T. Zhang, Q. L. Lang and A. H. Liu, *ACS Appl. Mater. Interfaces*, 2015, **7**, 14463–14470.
185 F. S. Kang, X. S. Hou and K. Xu, *Nanotechnology*, 2015, **26**, 405707.
186 J. R. Li, G. N. Zhang, L. H. Wang, A. G. Shen and J. M. Hu, *Talanta*, 2015, **140**, 204–211.
187 Y. H. Sun, J. Wang, W. Li, J. L. Zhang, Y. D. Zhang and Y. Fu, *Biosens. Bioelectron.*, 2015, **74**, 1038–1046.
188 X. M. Fu, Z. J. Liu, S. X. Cai, P. Li, Y. T. Li and J. H. Chen, *J. Instrum. Anal.*, 2016, **35**, 426–431.
189 X. M. Fu, Z. J. Liu, S. X. Cai, Y. P. Zhao, D. Z. Wu, C. Y. Li and J. H. Chen, *Chin. Chem. Lett.*, 2016, **27**, 920–926.
190 T. Jiang, Y. Song, T. X. Wei, H. Li, D. Du, M. J. Zhu and Y. H. Lin, *Biosens. Bioelectron.*, 2016, **77**, 687–694.
191 L. Q. Yang, X. Y. Liu, Q. J. Lu, N. Huang, M. L. Liu, Y. Y. Zhang and S. Z. Yao, *Anal. Chim. Acta*, 2016, **930**, 23–30.
192 L. L. Wu, Z. J. Qian, Z. J. Xie, Y. Y. Zhang and C. F. Peng, *Chin. J. Anal. Chem.*, 2017, **45**, 471–476.
193 S. L. Wan, Q. X. Wang, H. H. Ye, M. J. Kim and X. H. Xia, *Part. Part. Syst. Charact.*, 2018, **35**, 1700386.
194 H. Ye, K. Yang, J. Tao, Y. Liu, Q. Zhang, S. Habibi, Z. Nie and X. Xia, *ACS Nano*, 2017, **11**, 2052–2059.
195 J. N. Li, W. Q. Liu, X. C. Wu and X. F. Gao, *Biomaterials*, 2015, **48**, 37–44.
196 Y. J. Song, X. H. Wang, C. Zhao, K. G. Qu, J. S. Ren and X. G. Qu, *Chem. – Eur. J.*, 2010, **16**, 3617–3621.
197 Y. J. Song, K. G. Qu, C. Zhao, J. S. Ren and X. G. Qu, *Adv. Mater.*, 2010, **22**, 2206–2210.
198 D. Wu, X. Deng, X. M. Huang, K. Wang and Q. Y. Liu, *J. Nanosci. Nanotechnol.*, 2013, **13**, 6611–6616.
199 Z. Mohammadpour, A. Safavi and M. Shamsipur, *Chem. Eng. J.*, 2014, **255**, 1–7.
200 M. Shamsipur, A. Safavi and Z. Mohammadpour, *Sens. Actuators, B*, 2014, **199**, 463–469.
201 W. F. Zhu, J. Zhang, Z. C. Jiang, W. W. Wang and X. H. Liu, *RSC Adv.*, 2014, **4**, 17387–17392.
202 B. Garg and T. Bisht, *Molecules*, 2016, **21**, 1653.
203 D. S. Tang, J. J. Liu, X. M. Yan and L. T. Kang, *RSC Adv.*, 2016, **6**, 50609–50617.
204 N. R. Nirala, G. Khandelwal, B. Kumar, Vinita, R. Prakash and V. Kumar, *Talanta*, 2017, **173**, 36–43.
205 M. Vazquez-Gonzalez, W. C. Liao, R. Gazelles, S. Wang, X. Yu, V. Gutkin and I. Willner, *ACS Nano*, 2017, **11**, 3247–3253.
206 Y. Dong, J. Li, L. Shi and Z. G. Guo, *ACS Appl. Mater. Interfaces*, 2015, **7**, 15403–15413.
207 Y. Dong, J. Li, L. Shi, J. Xu, X. B. Wang, Z. G. Guo and W. M. Liu, *J. Mater. Chem. A*, 2013, **1**, 644–650.
208 P. Gayathri and A. S. Kumar, *Chem. – Eur. J.*, 2013, **19**, 17103–17112.
209 L. P. Lin, X. H. Song, Y. Y. Chen, M. C. Rong, T. T. Zhao, Y. R. Wang, Y. Q. Jiang and X. Chen, *Anal. Chim. Acta*, 2015, **869**, 89–95.
210 R. Z. Zhang, S. J. He, C. M. Zhang and W. Chen, *J. Mater. Chem. B*, 2015, **3**, 4146–4154.
211 W. Yang, T. Huang, M. Zhao, F. Luo, W. Weng, Q. Wei, Z. Lin and G. Chen, *Talanta*, 2017, **164**, 1–6.
212 J. Q. Tian, Q. Liu, A. M. Asiri, A. H. Qusti, A. O. Al-Youbi and X. P. Sun, *Nanoscale*, 2013, **5**, 11604–11609.
213 T. R. Lin, L. S. Zhong, J. Wang, L. Q. Guo, H. Y. Wu, Q. Q. Guo, F. F. Fu and G. N. Chen, *Biosens. Bioelectron.*, 2014, **59**, 89–93.
214 F. M. Qian, J. M. Wang, S. Y. Ai and L. F. Li, *Sens. Actuators, B*, 2015, **216**, 418–427.
215 Z. B. Wang, X. C. Lv and J. Weng, *Carbon*, 2013, **62**, 51–60.
216 A. X. Zheng, Z. X. Cong, J. R. Wang, J. Li, H. H. Yang and G. N. Chen, *Biosens. Bioelectron.*, 2013, **49**, 519–524.
217 W. Sun, X. M. Ju, Y. Y. Zhang, X. H. Sun, G. J. Li and Z. F. Sun, *Electrochem. Commun.*, 2013, **26**, 113–116.
218 Q. An, C. Y. Sun, D. Li, K. Xu, J. Guo and C. C. Wang, *ACS Appl. Mater. Interfaces*, 2013, **5**, 13248–13257.
219 S. Chen, X. Hai, X. W. Chen and J. H. Wang, *Anal. Chem.*, 2014, **86**, 6689–6694.
220 J. Chen, J. Ge, L. Zhang, Z. H. Li, S. S. Zhou and L. B. Qu, *RSC Adv.*, 2015, **5**, 90400–90407.
221 S. Wang, R. Cazelles, W. C. Liao, M. Vázquez-González, A. Zoabi, R. Abu-Reziq and I. Willner, *Nano Lett.*, 2017, **17**, 2043–2048.
222 H. J. Sun, N. Gao, K. Dong, J. S. Ren and X. G. Qu, *ACS Nano*, 2014, **8**, 6202–6210.

223 M. Huang, J. L. Gu, S. P. Elangovan, Y. S. Li, W. R. Zhao, T. Iijima, Y. Yamazaki and J. L. Shi, *Chem. Lett.*, 2013, **42**, 785–787.
224 W. Qi, W. Liu, B. S. Zhang, X. M. Gu, X. L. Guo and D. S. Su, *Angew. Chem., Int. Ed.*, 2013, **52**, 14224–14228.
225 R. S. Zhao, X. Zhao and X. F. Gao, *Chem. – Eur. J.*, 2015, **21**, 960–964.
226 H. J. Sun, A. D. Zhao, N. Gao, K. Li, J. S. Ren and X. G. Qu, *Angew. Chem., Int. Ed.*, 2015, **54**, 7176–7180.
227 H. Wang, C. Q. Liu, Z. Liu, J. S. Ren and X. G. Qu, *Small*, 2018, **14**, 1703710.
228 H. Wang, P. H. Li, D. Q. Yu, Y. Zhang, Z. Z. Wang, C. Q. Liu, H. Qiu, Z. Liu, J. S. Ren and X. G. Qu, *Nano Lett.*, 2018, **18**, 3344–3351.
229 J. H. Hao, Z. Zhang, W. S. Yang, B. P. Lu, X. Ke, B. L. Zhang and J. L. Tang, *J. Mater. Chem. A*, 2013, **1**, 4352–4357.
230 C. O. Song, J. W. Lee, H. S. Choi and J. K. Kang, *RSC Adv.*, 2013, **3**, 20179–20185.
231 Y. Tao, Y. H. Lin, Z. Z. Huang, J. S. Ren and X. G. Qu, *Adv. Mater.*, 2013, **25**, 2594–2599.
232 L. Wang, Y. J. Ye, X. P. Lu, Y. Wu, L. L. Sun, H. L. Tan, F. G. Xu and Y. H. Song, *Electrochim. Acta*, 2013, **114**, 223–232.
233 J. X. Xie, H. Y. Cao, H. Jiang, Y. J. Chen, W. B. Shi, H. Z. Zheng and Y. M. Huang, *Anal. Chim. Acta*, 2013, **796**, 92–100.
234 Y. F. Zhang, C. L. Xu and B. X. Li, *RSC Adv.*, 2013, **3**, 6044–6050.
235 Z. Zhang, J. H. Hao, W. S. Yang, B. P. Lu, X. Ke, B. L. Zhang and J. L. Tang, *ACS Appl. Mater. Interfaces*, 2013, **5**, 3809–3815.
236 X. M. Chen, B. Y. Su, Z. X. Cai, X. Chen and M. Oyama, *Sens. Actuators, B*, 2014, **201**, 286–292.
237 X. M. Chen, X. T. Tian, B. Y. Su, Z. Y. Huang, X. Chen and M. Oyama, *Dalton Trans.*, 2014, **43**, 7449–7454.
238 Y. Guo, W. W. Li, M. Y. Zheng and Y. Huang, *Acta Chim. Sin.*, 2014, **72**, 713–719.
239 J. Huang, Q. Chang, G. D. Jiang, Y. Qiu and H. Q. Tang, *Phys. Test. Chem. Anal., Part B*, 2014, **50**, 417–420.
240 R. L. Sun, Y. Wang, Y. N. Ni and S. Kokot, *J. Hazard. Mater.*, 2014, **266**, 60–67.
241 H. L. Tan, C. J. Ma, L. Gao, Q. Li, Y. H. Song, F. G. Xu, T. Wang and L. Wang, *Chem. – Eur. J.*, 2014, **20**, 16377–16383.
242 X. Chen, N. Zhai, J. H. Snyder, Q. S. Chen, P. P. Liu, L. F. Jin, Q. X. Zheng, F. C. Lin, J. M. Hu and H. N. Zhou, *Anal. Methods*, 2015, **7**, 1951–1957.
243 Y. M. Dong, J. J. Zhang, P. P. Jiang, G. L. Wang, X. M. Wu, H. Zhao and C. Zhang, *New J. Chem.*, 2015, **39**, 4141–4146.
244 A. Hayat, W. Haider, Y. Raza and J. L. Marty, *Talanta*, 2015, **143**, 157–161.
245 B. Reuillard, S. Gentil, M. Carriere, A. Le Goff and S. Cosnier, *Chem. Sci.*, 2015, **6**, 5139–5143.
246 W. J. Shi, H. Fan, S. Y. Ai and L. S. Zhu, *RSC Adv.*, 2015, **5**, 32183–32190.
247 J. Shu, Z. L. Qiu, Q. H. Wei, J. Y. Zhuang and D. P. Tang, *Sci. Rep.*, 2015, **5**, 15113.
248 N. Wang, Z. W. Han, H. Fan and S. Y. Ai, *RSC Adv.*, 2015, **5**, 91302–91307.
249 F. Yuan, H. M. Zhao, M. Liu and X. Quan, *Biosens. Bioelectron.*, 2015, **68**, 7–13.
250 M. C. Kim, D. Lee, S. H. Jeong, S. Y. Lee and E. Kang, *ACS Appl. Mater. Interfaces*, 2016, **8**, 34317–34326.
251 C. Socaci, F. Pogacean, A. R. Bins, M. Coros, M. C. Rosu, L. Magerusan, G. Katona and S. Pruneanu, *Talanta*, 2016, **148**, 511–517.
252 S. R. Ahmed, K. Takemeura, T.-C. Li, N. Kitamoto, T. Tanaka, T. Suzuki and E. Y. Park, *Biosens. Bioelectron.*, 2017, **87**, 558–565.
253 Z. Wang, K. Dong, Z. Liu, Y. Zhang, Z. Chen, H. Sun, J. Ren and X. Qu, *Biomaterials*, 2017, **113**, 145–157.
254 L. Zhang, X. Hai, C. Xia, X. W. Chen and J. H. Wang, *Sens. Actuators, B*, 2017, **248**, 374–384.
255 W. C. Zhang, X. H. Niu, X. Li, Y. F. He, H. W. Song, Y. X. Peng, J. M. Pan, F. X. Qiu, H. L. Zhao and M. B. Lan, *Sens. Actuators, B*, 2018, **265**, 412–420.
256 Y. L. Liu, X. J. Zhao, X. X. Yang and Y. F. Li, *Analyst*, 2013, **138**, 4526–4531.
257 Z. W. Jiang, Y. Liu, X. O. Hu and Y. F. Li, *Anal. Methods*, 2014, **6**, 5647–5651.
258 J. W. Zhang, H. T. Zhang, Z. Y. Du, X. Q. Wang, S. H. Yua and H. L. Jiang, *Chem. Commun.*, 2014, **50**, 1092–1094.
259 D. M. Chen, B. Li, L. Jiang, D. L. Duan, Y. Z. Li, J. Q. Wang, J. He and Y. B. Zeng, *RSC Adv.*, 2015, **5**, 97910–97917.
260 W. F. Dong, X. D. Liu, W. B. Shi and Y. M. Huang, *RSC Adv.*, 2015, **5**, 17451–17457.
261 J. Y. Lu, Y. H. Xiong, C. J. Liao and F. G. Ye, *Anal. Methods*, 2015, **7**, 9894–9899.
262 Y. Wang, Y. J. Zhu, A. Binyam, M. S. Liu, Y. N. Wu and F. T. Li, *Biosens. Bioelectron.*, 2016, **86**, 432–438.
263 F. F. Chen, Y. J. Zhu, Z. C. Xiong and T. W. Sun, *Chem. – Eur. J.*, 2017, **23**, 3328–3337.
264 C. J. Gao, H. M. Zhu, J. Chen and H. D. Qiu, *Chin. Chem. Lett.*, 2017, **28**, 1006–1012.
265 T. R. Lin, Y. M. Qin, Y. L. Huang, R. T. Yang, L. Hou, F. G. Ye and S. L. Zhao, *Chem. Commun.*, 2018, **54**, 1762–1765.
266 I. Ortiz Gomez, A. Salinas Castillo, A. Garcia Garcia, J. Antonio Alvarez-Bermejo, I. de Orbe Paya, A. Rodriguez Dieguez and L. Fermin Capitan Vallvey, *Microchim. Acta*, 2018, **185**, 47.
267 H. L. Tan, Q. Li, Z. C. Zhou, C. J. Ma, Y. H. Song, F. G. Xu and L. Wang, *Anal. Chim. Acta*, 2015, **856**, 90–95.
268 F. F. Liu, J. He, M. L. Zeng, J. Hao, Q. H. Guo, Y. H. Song and L. Wang, *J. Nanopart. Res.*, 2016, **18**, 106.
269 S. Q. Wang, W. F. Deng, L. Yang, Y. M. Tan, Q. J. Xie and S. Z. Yao, *ACS Appl. Mater. Interfaces*, 2017, **9**, 24440–24445.
270 H. G. Yang, R. Yang, P. Zhang, Y. M. Qin, T. Chen and F. G. Ye, *Microchim. Acta*, 2017, **184**, 4629–4635.

271 D. W. Feng, Z. Y. Gu, J. R. Li, H. L. Jiang, Z. W. Wei and H. C. Zhou, *Angew. Chem., Int. Ed.*, 2012, **51**, 10307–10310.
272 L. Cui, J. Wu, J. Li and H. X. Ju, *Anal. Chem.*, 2015, **87**, 10635–10641.
273 P. H. Ling, J. P. Lei, L. Zhang and H. X. Ju, *Anal. Chem.*, 2015, **87**, 3957–3963.
274 K. C. Wang, D. W. Feng, T. F. Liu, J. Su, S. Yuan, Y. P. Chen, M. Bosch, X. D. Zou and H. C. Zhou, *J. Am. Chem. Soc.*, 2014, **136**, 13983–13986.
275 H. J. Cheng, Y. F. Liu, Y. H. Hu, Y. B. Ding, S. C. Lin, W. Cao, Q. Wang, J. J. X. Wu, F. Muhammad, X. Z. Zhao, D. Zhao, Z. Li, H. Xing and H. Wei, *Anal. Chem.*, 2017, **89**, 11552–11559.
276 W. H. Chen, M. Vazquez Gonzalez, A. Kozell, A. Cecconello and I. Willner, *Small*, 2018, **14**, 1703149.
277 A. H. Valekar, B. S. Batule, M. I. Kim, K. H. Cho, D. Y. Hong, U. H. Lee, J. S. Chang, H. G. Park and Y. K. Hwang, *Biosens. Bioelectron.*, 2018, **100**, 161–168.
278 H. P. Li, H. F. Liu, J. D. Zhang, Y. X. Cheng, C. L. Zhang, X. Y. Fei and Y. Z. Xian, *ACS Appl. Mater. Interfaces*, 2017, **9**, 40716–40725.
279 C. Hou, Y. Wang, Q. H. Ding, L. Jiang, M. Li, W. W. Zhu, D. Pan, H. Zhu and M. Z. Liu, *Nanoscale*, 2015, **7**, 18770–18779.
280 L. J. Su, Y. H. Xiong, H. G. Yang, P. Zhang and F. G. Ye, *J. Mater. Chem. B*, 2016, **4**, 128–134.
281 Y. H. Hu, H. J. Cheng, X. Z. Zhao, J. J. Wu, F. Muhammad, S. C. Lin, J. He, L. Q. Zhou, C. P. Zhang, Y. Deng, P. Wang, Z. Y. Zhou, S. M. Nie and H. Wei, *ACS Nano*, 2017, **11**, 5558–5566.
282 X. Q. Tang, Y. D. Zhang, Z. W. Jiang, D. M. Wang, C. Z. Huang and Y. F. Li, *Talanta*, 2018, **179**, 43–50.
283 F. J. Cui, Q. F. Deng and L. Sun, *RSC Adv.*, 2015, **5**, 98215–98221.
284 Y. L. Liu, W. L. Fu, C. M. Li, C. Z. Huang and Y. F. Li, *Anal. Chim. Acta*, 2015, **861**, 55–61.
285 Y. Zhang, W. T. Zhang, K. Chen, Q. F. Yang, N. Hu, Y. R. Suo and J. L. Wang, *Sens. Actuators, B*, 2018, **262**, 95–101.
286 L. J. Chen, B. Sun, X. D. Wang, F. M. Qiao and S. Y. Ai, *J. Mater. Chem. B*, 2013, **1**, 2268–2274.
287 Y. J. Chen, H. Y. Cao, W. B. Shi, H. Liu and Y. M. Huang, *Chem. Commun.*, 2013, **49**, 5013–5015.
288 L. Hong, A. L. Liu, G. W. Li, W. Chen and X. H. Lin, *Biosens. Bioelectron.*, 2013, **43**, 1–5.
289 Y. J. Jiang, W. Wang, X. T. Li, X. C. Wang, J. W. Zhou and X. D. Mu, *ACS Appl. Mater. Interfaces*, 2013, **5**, 1913–1916.
290 Y. C. Lee, M. I. Kim, M. A. Woo, H. G. Park and J. I. Han, *Biosens. Bioelectron.*, 2013, **42**, 373–378.
291 D. Li, H. Y. Han, Y. H. Wang, X. Wang, Y. G. Li and E. B. Wang, *Eur. J. Inorg. Chem.*, 2013, 1926–1934.
292 P. C. Pandey and A. K. Pandey, *Analyst*, 2013, **138**, 2295–2301.
293 W. B. Shi, X. D. Zhang, S. H. He, J. Li and Y. M. Huang, *Sci. Sin.: Chim.*, 2013, **43**, 1591–1598.
294 Y. R. Tang, Y. Zhang, R. Liu, Y. Y. Su and Y. Lu, *Chin. J. Anal. Chem.*, 2013, **41**, 330–336.
295 J. Xu, J. Wu, C. Zong, H. X. Ju and F. Yan, *Anal. Chem.*, 2013, **85**, 3374–3379.
296 L. L. Zhang, L. Han, P. Hu, L. Wang and S. J. Dong, *Chem. Commun.*, 2013, **49**, 10480–10482.
297 M. G. Zhao, J. Y. Huang, Y. Zhou, X. H. Pan, H. P. He, Z. Z. Ye and X. Q. Pan, *Chem. Commun.*, 2013, **49**, 7656–7658.
298 L. Artiglia, S. Agnoli, M. C. Paganini, M. Cattelan and G. Granozzi, *ACS Appl. Mater. Interfaces*, 2014, **6**, 20130–20136.
299 Q. Chen, M. L. Liu, J. N. Zhao, X. Peng, X. J. Chen, N. X. Mi, B. D. Yin, H. T. Li, Y. Y. Zhang and S. Z. Yao, *Chem. Commun.*, 2014, **50**, 6771–6774.
300 L. L. Li, W. Wang and K. Z. Chen, *J. Phys. Chem. C*, 2014, **118**, 26351–26358.
301 N. Li, Y. Yan, B. Y. Xia, J. Y. Wang and X. Wang, *Biosens. Bioelectron.*, 2014, **54**, 521–527.
302 Y. J. Liu, G. X. Zhu, C. L. Bao, A. H. Yuan and X. P. Shen, *Chin. J. Chem.*, 2014, **32**, 151–156.
303 Y. J. Liu, G. X. Zhu, J. Yang, A. H. Yuan and X. P. Shen, *PLoS One*, 2014, **9**, e109158.
304 X. Y. Niu, Y. Y. Xu, Y. L. Dong, L. Y. Qi, S. D. Qi, H. L. Chen and X. G. Chen, *J. Alloys Compd.*, 2014, **587**, 74–81.
305 P. C. Pandey, D. Panday and G. Pandey, *RSC Adv.*, 2014, **4**, 60563–60572.
306 P. C. Pandey, A. Prakash and A. K. Pandey, *Electrochim. Acta*, 2014, **127**, 132–138.
307 C. Ray, S. Dutta, S. Sarkar, R. Sahoo, A. Roy and T. Pal, *J. Mater. Chem. B*, 2014, **2**, 6097–6105.
308 M. C. Kim and S. Y. Lee, *Nanoscale*, 2015, **7**, 17063–17070.
309 L. J. Wan, J. H. Liu and X. J. Huang, *Chem. Commun.*, 2014, **50**, 13589–13591.
310 A. K. Dutta, S. Das, S. Samanta, P. K. Samanta, B. Adhikary and P. Biswas, *Talanta*, 2013, **107**, 361–367.
311 Q. Y. Liu, Y. T. Yang, H. Li, R. R. Zhu, Q. Shao, S. G. Yang and J. J. Xu, *Biosens. Bioelectron.*, 2015, **64**, 147–153.
312 F. T. Zhang, X. Long, D. W. Zhang, Y. L. Sun, Y. L. Zhou, Y. R. Ma, L. M. Qi and X. X. Zhang, *Sens. Actuators, B*, 2014, **192**, 150–156.
313 F. M. Qiao, L. J. Chen, X. N. Li, L. F. Li and S. Y. Ai, *Sens. Actuators, B*, 2014, **193**, 255–262.
314 Y. Tao, E. G. Ju, J. S. Ren and X. G. Qu, *Chem. Commun.*, 2014, **50**, 3030–3032.
315 A. Dalui, B. Pradhan, U. Thupakula, A. H. Khan, G. S. Kumar, T. Ghosh, B. Satpati and S. Acharya, *Nanoscale*, 2015, **7**, 9062–9074.
316 H. Y. Liu, C. C. Gu, W. W. Xiong and M. Z. Zhang, *Sens. Actuators, B*, 2015, **209**, 670–676.
317 J. F. Guan, J. Peng and X. Y. Jin, *Anal. Methods*, 2015, **7**, 5454–5461.
318 Q. Wang, S. W. Liu, H. Y. Sun and Q. F. Lu, *Ind. Eng. Chem. Res.*, 2014, **53**, 7917–7922.
319 W. S. Yang, J. H. Hao, Z. Zhang, B. P. Lu, B. L. Zhang and J. L. Tang, *RSC Adv.*, 2014, **4**, 35500–35504.

320 Y. B. Feng, L. Hong, A. L. Liu, W. D. Chen, G. W. Li, W. Chen and X. H. Xia, *Int. J. Environ. Sci. Technol.*, 2015, **12**, 653–660.
321 D. F. Chai, Z. Ma, H. Yan, Y. F. Qiu, H. Liu, H. D. Guo and G. G. Gao, *RSC Adv.*, 2015, **5**, 78771–78779.
322 Y. Wang, D. Zhang and Z. B. Xiang, *Mater. Res. Bull.*, 2015, **67**, 152–157.
323 R. Cai, D. Yang, X. Chen, Y. Huang, Y. F. Lyv, J. L. He, M. L. Shi, I. T. Teng, S. Wan, W. J. Hou and W. H. Tan, *J. Mater. Chem. B*, 2016, **4**, 4657–4661.
324 T. M. Chen, J. Xiao and G. W. Yang, *RSC Adv.*, 2016, **6**, 70124–70132.
325 Y. Dogra, K. P. Arkill, C. Elgy, B. Stolpe, J. Lead, E. Valsami-Jones, C. R. Tyler and T. S. Galloway, *Nanotoxicology*, 2016, **10**, 480–487.
326 G. L. Li, P. Ma, Y. F. Zhang, X. L. Liu, H. Zhang, W. M. Xue, Y. Mi, Y. E. Luo and H. M. Fan, *J. Mater. Sci.*, 2016, **51**, 3979–3988.
327 A. G. Thawari and C. P. Rao, *ACS Appl. Mater. Interfaces*, 2016, **8**, 10392–10402.
328 Y. Wang, D. Zhang and Z. B. Xiang, *J. Taiwan Inst. Chem. Eng.*, 2016, **59**, 547–552.
329 Z. F. Wu, Z. Wang, Y. Zhang, Y. L. Ma, C. Y. He, H. Li, L. Chen, Q. S. Huo, L. Wang and Z. Q. Li, *Sci. Rep.*, 2016, **6**, 22412.
330 Z. B. Xiang, Y. Wang, P. Ju and D. Zhang, *Microchim. Acta*, 2016, **183**, 457–463.
331 Y. Z. Li, T. T. Li, W. Chen and Y. Y. Song, *ACS Appl. Mater. Interfaces*, 2017, **9**, 29881–29888.
332 Z. Moradi Shoeili, *React. Kinet., Mech. Catal.*, 2017, **120**, 323–332.
333 J. S. Mu, X. Zhao, J. Li, E. C. Yang and X. J. Zhao, *Mater. Sci. Eng., C*, 2017, **74**, 434–442.
334 C. Y. Park, J. M. Seo, H. Jo, J. Park, K. M. Ok and T. J. Park, *Sci. Rep.*, 2017, **7**, 40928.
335 H. P. Peng, D. W. Lin, P. Liu, Y. H. Wu, S. H. Li, Y. Lei, W. Chen, Y. Z. Chen, X. H. Lin, X. H. Xia and A. L. Liu, *Anal. Chim. Acta*, 2017, **992**, 128–134.
336 M. Rahimi Nasrabadi, F. Mizani, M. Hosseini, A. H. Keihan and M. R. Ganjali, *Spectrochim. Acta, Part A*, 2017, **186**, 82–88.
337 X. N. Ren, M. Xia, Q. Z. Yan and C. C. Ge, *Chin. Phys. B*, 2017, **26**, 048103.
338 N. Salarizadeh, M. Sadri, H. Hosseini and R. H. Sajedi, *Carbon Lett.*, 2017, **24**, 103–110.
339 K. Y. Wang, J. Z. Song, X. J. Duan, J. S. Mu and Y. Wang, *New J. Chem.*, 2017, **41**, 8554–8560.
340 K. Chen, A. Bayaguud, H. Li, Y. Chu, H. C. Zhang, H. L. Jia, B. F. Zhang, Z. C. Xiao, P. F. Wu, T. B. Liu and Y. G. Wei, *Nano Res.*, 2018, **11**, 1313–1321.
341 P. H. Ling, Q. Zhang, T. T. Cao and F. Gao, *Angew. Chem., Int. Ed.*, 2018, **57**, 6819–6824.
342 J. S. Mu, J. Li, X. Zhao, E. C. Yang and X. J. Zhao, *Sens. Actuators, B*, 2018, **258**, 32–41.
343 T. R. Zhan, J. X. Kang, X. J. Li, L. Pan, G. J. Li and W. G. Hou, *Sens. Actuators, B*, 2018, **255**, 2635–2642.
344 R. Cai, D. Yang, S. J. Peng, X. G. Chen, Y. Huang, Y. Liu, W. J. Hou, S. Y. Yang, Z. B. Liu and W. H. Tan, *J. Am. Chem. Soc.*, 2015, **137**, 13957–13963.
345 T. R. Lin, L. S. Zhong, L. Q. Guo, F. F. Fu and G. N. Chen, *Nanoscale*, 2014, **6**, 11856–11862.
346 T. R. Lin, L. S. Zhong, Z. P. Song, L. Q. Guo, H. Y. Wu, Q. Q. Guo, Y. Chen, F. F. Fu and G. N. Chen, *Biosens. Bioelectron.*, 2014, **62**, 302–307.
347 X. R. Guo, Y. Wang, F. Y. Wu, Y. N. Ni and S. Kokot, *Analyst*, 2015, **140**, 1119–1126.
348 J. Yu, X. Y. Ma, W. Y. Yin and Z. J. Gu, *RSC Adv.*, 2016, **6**, 81174–81183.
349 T. M. Chen, X. J. Wu, J. X. Wang and G. W. Yang, *Nanoscale*, 2017, **9**, 11806–11813.
350 X. W. Huang, J. J. Wei, T. Liu, X. L. Zhang, S. M. Bai and H. H. Yang, *Nanoscale*, 2017, **9**, 17193–17198.
351 X. J. Wu, T. M. Chen, J. X. Wang and G. W. Yang, *J. Mater. Chem. B*, 2018, **6**, 105–111.
352 B. L. Li, H. Q. Luo, J. L. Lei and N. B. Li, *RSC Adv.*, 2014, **4**, 24256–24262.
353 Q. Chen, J. Chen, C. J. Gao, M. L. Zhang, J. Y. Chen and H. D. Qiu, *Analyst*, 2015, **140**, 2857–2863.
354 J. Y. Lei, X. F. Lu, G. D. Nie, Z. Q. Jiang and C. Wang, *Part. Part. Syst. Charact.*, 2015, **32**, 886–892.
355 Z. Sun, Q. S. Zhao, G. H. Zhang, Y. Li, G. L. Zhang, F. B. Zhang and X. B. Fan, *RSC Adv.*, 2015, **5**, 10352–10357.
356 S. F. Cai, Q. S. Han, C. Qi, Z. Lian, X. H. Jia, R. Yang and C. Wang, *Nanoscale*, 2016, **8**, 3685–3693.
357 C. Qi, S. F. Cai, X. H. Wang, J. Y. Li, Z. Lian, S. S. Sun, R. Yang and C. Wang, *RSC Adv.*, 2016, **6**, 54949–54955.
358 J. Hassanzadeh, A. Khataee and H. Eskandari, *Sens. Actuators, B*, 2018, **259**, 402–410.
359 A. Khataee, M. H. Irani-nezhad, J. Hassanzadeh and S. W. Joo, *J. Colloid Interface Sci.*, 2018, **515**, 39–49.
360 S. F. Cai, Q. S. Han, C. Qi, X. H. Wang, T. Wang, X. H. Jia, R. Yang and C. Wang, *Chin. J. Chem.*, 2017, **35**, 605–612.
361 X. D. Zhang, S. H. He, Z. H. Chen and Y. M. Huang, *J. Agric. Food Chem.*, 2013, **61**, 840–847.
362 J. K. Zhao, Y. F. Xie, W. J. Yuan, D. X. Li, S. F. Liu, B. Zheng and W. G. Hou, *J. Mater. Chem. B*, 2013, **1**, 1263–1269.
363 Y. T. Zhou, W. W. He, W. G. Wamer, X. N. Hu, X. C. Wu, Y. M. Lo and J. J. Yin, *Nanoscale*, 2013, **5**, 1583–1591.
364 A. Hayat and S. Andreescu, *Anal. Chem.*, 2013, **85**, 10028–10032.
365 W. J. Qin, L. Su, C. Yang, Y. H. Ma, H. J. Zhang and X. G. Chen, *J. Agric. Food Chem.*, 2014, **62**, 5827–5834.
366 G. L. Wang, X. F. Xu, L. H. Cao, C. H. He, Z. J. Li and C. Zhang, *RSC Adv.*, 2014, **4**, 5867–5872.
367 C. J. Yu, T. H. Chen, J. Y. Jiang and W. L. Tseng, *Nanoscale*, 2014, **6**, 9618–9624.
368 Y. D. Zhu, J. Peng, L. P. Jiang and J. J. Zhu, *Analyst*, 2014, **139**, 649–655.
369 A. Hayat, J. Cunningham, G. Bulbul and S. Andreescu, *Anal. Chim. Acta*, 2015, **885**, 140–147.
370 Y. Ji, J. Xu, X. L. Chen, L. Han, X. H. Wang, F. Chai and M. S. Zhao, *Sens. Actuators, B*, 2015, **208**, 497–504.

371 W. Y. Lu, J. X. Shu, Z. H. Wang, N. Huang and W. J. Song, *Mater. Lett.*, 2015, **154**, 33–36.
372 L. H. Wang, Y. Zeng, A. G. Shen, X. D. Zhou and J. M. Hu, *Chem. Commun.*, 2015, **51**, 2052–2055.
373 Y. H. Xiong, S. H. Chen, F. G. Ye, L. J. Su, C. Zhang, S. F. Shen and S. L. Zhao, *Chem. Commun.*, 2015, **51**, 4635–4638.
374 H. G. Yang, Y. H. Xiong, P. Zhang, L. J. Su and F. G. Ye, *Anal. Methods*, 2015, **7**, 4596–4601.
375 X. D. Zhang and Y. M. Huang, *Anal. Methods*, 2015, **7**, 8640–8646.
376 S. F. Cai, C. Qi, Y. D. Li, Q. S. Han, R. Yang and C. Wang, *J. Mater. Chem. B*, 2016, **4**, 1869–1877.
377 D. F. Chai, Z. Ma, Y. F. Qiu, Y. G. Lv, H. Liu, C. Y. Song and G. G. Gao, *Dalton Trans.*, 2016, **45**, 3048–3054.
378 L. L. Guo, K. X. Huang and H. M. Liu, *J. Nanopart. Res.*, 2016, **18**, 74.
379 M. Chen, J. X. Shu, Z. H. Wang and C. G. Ren, *J. Porous Mater.*, 2017, **24**, 973–977.
380 D. Q. Fan, C. S. Shang, W. L. Gu, E. K. Wang and S. J. Dong, *ACS Appl. Mater. Interfaces*, 2017, **9**, 25870–25877.
381 M. Gao, X. F. Lu, G. D. Nie, M. Q. Chi and C. Wang, *Nanotechnology*, 2017, **28**, 485708.
382 J. N. Wang, P. Su, D. Li, T. Wang and Y. Yang, *Chem. Res. Chin. Univ.*, 2017, **33**, 540–545.
383 H. K. Yang, J. Y. Xiao, L. Su, T. Feng, Q. Y. Lv and X. J. Zhang, *Chem. Commun.*, 2017, **53**, 3882–3885.
384 S. G. Liu, L. Han, N. Li, N. Xiao, Y. J. Ju, N. B. Li and H. Q. Luo, *J. Mater. Chem. B*, 2018, **6**, 2843–2850.
385 H. H. Deng, X. L. Lin, Y. H. Liu, K. L. Li, Q. Q. Zhuang, H. P. Peng, A. L. Liu, X. H. Xia and W. Chen, *Nanoscale*, 2017, **9**, 10292–10300.
386 S. Biella, L. Prati and M. Rossi, *J. Catal.*, 2002, **206**, 242–247.
387 M. Comotti, C. Della Pina, R. Matarrese and M. Rossi, *Angew. Chem., Int. Ed.*, 2004, **43**, 5812–5815.
388 P. Beltrame, M. Comotti, C. Della Pina and M. Rossi, *Appl. Catal., A*, 2006, **297**, 1–7.
389 M. Comotti, C. Della Pina, E. Falletta and M. Rossi, *Adv. Synth. Catal.*, 2006, **348**, 313–316.
390 I. V. Delidovich, B. L. Moroz, O. P. Taran, N. V. Gromov, P. A. Pyrjaev, I. P. Prosvirin, V. I. Bukhtiyarov and V. N. Parmon, *Chem. Eng. J.*, 2013, **223**, 921–931.
391 C. Y. Ma, W. J. Xue, J. J. Li, W. Xing and Z. P. Hao, *Green Chem.*, 2013, **15**, 1035–1041.
392 P. J. Miedziak, H. Alshammari, S. A. Kondrat, T. J. Clarke, T. E. Davies, M. Morad, D. J. Morgan, D. J. Willock, D. W. Knight, S. H. Taylor and G. J. Hutchings, *Green Chem.*, 2014, **16**, 3132–3141.
393 K. Odrozek, K. Maresz, A. Koreniuk, K. Prusik and J. Mrowiec-Bialon, *Appl. Catal., A*, 2014, **475**, 203–210.
394 Y. Wang, S. Van de Vyver, K. K. Sharma and Y. Roman-Leshkov, *Green Chem.*, 2014, **16**, 719–726.
395 H. J. Zhang and N. Toshima, *Catal. Sci. Technol.*, 2013, **3**, 268–278.
396 H. J. Zhang, L. L. Lu, Y. N. Cao, S. Du, Z. Cheng and S. W. Zhang, *Mater. Res. Bull.*, 2014, **49**, 393–398.
397 H. Zhang, T. Watanabe, M. Okumura, M. Haruta and N. Toshima, *Nat. Mater.*, 2012, **11**, 49–52.
398 K. Li, K. Wang, W. W. Qin, S. H. Deng, D. Li, J. Y. Shi, Q. Huang and C. H. Fan, *J. Am. Chem. Soc.*, 2015, **137**, 4292–4295.
399 A. P. Periasamy, P. Roy, W. P. Wu, Y. H. Huang and H. T. Chang, *Electrochim. Acta*, 2016, **215**, 253–260.
400 X. L. Ren, J. Liu, J. Ren, F. Q. Tang and X. W. Meng, *Nanoscale*, 2015, **7**, 19641–19646.
401 H. Liang, F. F. Lin, Z. J. Zhang, B. W. Liu, S. H. Jiang, Q. P. Yuan and J. W. Liu, *ACS Appl. Mater. Interfaces*, 2017, **9**, 1352–1360.
402 H. J. Cheng, S. C. Lin, F. Muhammad, Y. W. Lin and H. Wei, *ACS Sens.*, 2016, **1**, 1336–1343.
403 M. Chen, Z. H. Wang, J. X. Shu, X. H. Jiang, W. Wang, Z. H. Shi and Y. W. Lin, *Inorg. Chem.*, 2017, **56**, 9400–9403.
404 R. Ragg, F. Natalio, M. N. Tahir, H. Janssen, A. Kashyap, D. Strand, S. Strand and W. Tremel, *ACS Nano*, 2014, **8**, 5182–5189.
405 L. Li, L. Zhang, U. Carmona and M. Knez, *Chem. Commun.*, 2014, **50**, 8021–8023.
406 J. B. Liu, X. M. Jiang, L. M. Wang, Z. J. Hu, T. Wen, W. Q. Liu, J. J. Yin, C. Y. Chen and X. C. Wu, *Nano Res.*, 2015, **8**, 4024–4037.
407 Y. Wang, C. He, W. Li, J. Zhang and Y. Fu, *Catal. Lett.*, 2017, **147**, 2144–2152.
408 J. W. Lee, S. Yoon, Y. M. Lo, H. H. Wu, S. Y. Lee and B. Moon, *RSC Adv.*, 2015, **5**, 63757–63764.
409 Y. Liu, H. H. Wu, Y. Chong, W. G. Wamer, Q. S. Xia, L. N. Cai, Z. H. Nie, P. P. Fu and J. J. Yin, *ACS Appl. Mater. Interfaces*, 2015, **7**, 19709–19717.
410 J. W. Hou, M. Vazquez Gonzalez, M. Fadeev, X. Liu, R. Lavi and I. Willner, *Nano Lett.*, 2018, **18**, 4015–4022.
411 J. S. Mu, L. Zhang, M. Zhao and Y. Wang, *J. Mol. Catal. A: Chem.*, 2013, **378**, 30–37.
412 X. Y. Wang, Y. C. Zhang, T. F. Li, W. D. Tian, Q. Zhang and Y. Y. Cheng, *Langmuir*, 2013, **29**, 5262–5270.
413 W. Zhang, Y. Zhang and N. Gu, *Key Eng. Mater.*, 2013, **562–565**, 1333–1339.
414 Z. Zhu, Z. C. Guan, S. S. Jia, Z. C. Lei, S. C. Lin, H. M. Zhang, Y. L. Ma, Z. Q. Tian and C. Y. J. Yang, *Angew. Chem., Int. Ed.*, 2014, **53**, 12503–12507.
415 V. Nicolini, E. Gambuzzi, G. Malavasi, L. Menabue, M. C. Menziani, G. Lusvardi, A. Pedone, F. Benedetti, P. Luches, S. D'Addato and S. Valeri, *J. Phys. Chem. B*, 2015, **119**, 4009–4019.
416 K. Aneesh, C. S. Vusa and S. Berchmans, *Analyst*, 2016, **141**, 4024–4028.
417 M. H. Hu, K. Korschelt, P. Daniel, K. Landfester, W. Tremel and M. B. Bannwarth, *ACS Appl. Mater. Interfaces*, 2017, **9**, 38024–38031.
418 M. Y. Kim and J. Kim, *ACS Biomater. Sci. Eng.*, 2017, **3**, 572–578.
419 W. Zhang, J. L. Dong, Y. Wu, P. Cao, L. N. Song, M. Ma, N. Gu and Y. Zhang, *Colloids Surf., B*, 2017, **154**, 55–62.

420 K. Sobanska, P. Pietrzyk and Z. Sojka, *ACS Catal.*, 2017, **7**, 2935–2947.
421 J. S. Mu, Y. Wang, M. Zhao and L. Zhang, *Chem. Commun.*, 2012, **48**, 2540–2542.
422 X. Q. Ma, W. H. Hu, C. X. Guo, L. Yu, L. X. Gao, J. L. Xie and C. M. Li, *Adv. Funct. Mater.*, 2014, **24**, 5897–5903.
423 L. Yuan, S. L. Liu, W. W. Tu, Z. S. Zhang, J. C. Bao and Z. H. Dai, *Anal. Chem.*, 2014, **86**, 4783–4790.
424 F. Dashtestani, H. Ghourchian, K. Eskandari and H.-A. Rafiee-Pour, *Microchim. Acta*, 2015, **182**, 1045–1053.
425 K. Kamada and N. Soh, *J. Phys. Chem. B*, 2015, **119**, 5309–5314.
426 T. T. Liu, X. H. Niu, L. B. Shi, X. Zhu, H. L. Zhao and M. B. Lana, *Electrochim. Acta*, 2015, **176**, 1280–1287.
427 X. M. Shen, W. Q. Liu, X. J. Gao, Z. H. Lu, X. C. Wu and X. F. Gao, *J. Am. Chem. Soc.*, 2015, **137**, 15882–15891.
428 J. S. Mu, X. Zhao, J. Li, E. C. Yang and X. J. Zhao, *J. Mater. Chem. B*, 2016, **4**, 5217–5221.
429 X. H. Shen, Q. Wang, Y. H. Liu, W. X. Xue, L. Ma, S. H. Feng, M. M. Wan, F. H. Wang and C. Mao, *Sci. Rep.*, 2016, **6**, 28989.
430 M. Q. Wang, C. Ye, S. J. Bao, M. W. Xu, Y. Zhang, L. Wang, X. Q. Ma, J. Guo and C. M. Li, *Biosens. Bioelectron.*, 2017, **87**, 998–1004.
431 L. L. Dugan, J. K. Gabrielsen, S. P. Yu, T. S. Lin and D. W. Choi, *Neurobiol. Dis.*, 1996, **3**, 129–135.
432 P. J. Krusic, E. Wasserman, P. N. Keizer, J. R. Morton and K. F. Preston, *Science*, 1991, **254**, 1183–1185.
433 Z. Z. Wang, S. K. Wang, Z. H. Lu and X. F. Gao, *J. Cluster Sci.*, 2015, **26**, 375–388.
434 L. L. Dugan, D. M. Turetsky, C. Du, D. Lobner, M. Wheeler, C. R. Almli, C. K. F. Shen, T. Y. Luh, D. W. Choi and T. S. Lin, *Proc. Natl. Acad. Sci. U. S. A.*, 1997, **94**, 9434–9439.
435 S. S. Ali, J. I. Hardt, K. L. Quick, J. S. Kim-Han, B. F. Erlanger, T. T. Huang, C. J. Epstein and L. L. Dugan, *Free Radical Biol. Med.*, 2004, **37**, 1191–1202.
436 G. F. Liu, M. Filipovic, I. Ivanovic-Burmazovic, F. Beuerle, P. Witte and A. Hirsch, *Angew. Chem., Int. Ed.*, 2008, **47**, 3991–3994.
437 E. L. G. Samuel, D. C. Marcano, V. Berka, B. R. Bitner, G. Wu, A. Potter, R. H. Fabian, R. G. Pautler, T. A. Kent, A.-L. Tsai and J. M. Tour, *Proc. Natl. Acad. Sci. U. S. A.*, 2015, **112**, 2343–2348.
438 E. L. G. Samuel, M. T. Duong, B. R. Bitner, D. C. Marcano, J. M. Tour and T. A. Kent, *Trends Biotechnol.*, 2014, **32**, 501–505.
439 L. G. Nilewski, W. K. A. Sikkema, T. A. Kent and J. M. Tour, *Nanomedicine*, 2015, **10**, 1677–1679.
440 A. S. Jalilov, L. G. Nilewski, V. Berka, C. Zhang, A. A. Yakovenko, G. Wu, T. A. Kent, A. L. Tsai and J. M. Tour, *ACS Nano*, 2017, **11**, 2024–2032.
441 X. L. Ren, X. W. Meng, J. Ren and F. Q. Tang, *RSC Adv.*, 2016, **6**, 92839–92844.
442 K. L. Fan, J. Q. Xi, L. Fan, P. X. Wang, C. H. Zhu, Y. Tang, X. D. Xu, M. M. Liang, B. Jiang, X. Y. Yan and L. Z. Gao, *Nat. Commun.*, 2018, **9**, 1440.
443 Z. Q. Xu, J. Y. Lan, J. C. Jin, P. Dong, F. L. Jiang and Y. Liu, *ACS Appl. Mater. Interfaces*, 2015, **7**, 28346–28352.
444 A. A. Vernekar and G. Mugesh, *Chem. – Eur. J.*, 2012, **18**, 15122–15132.
445 R. W. Tarnuzzer, J. Colon, S. Patil and S. Seal, *Nano Lett.*, 2005, **5**, 2573–2577.
446 C. Korsvik, S. Patil, S. Seal and W. T. Self, *Chem. Commun.*, 2007, 1056–1058.
447 E. G. Heckert, A. S. Karakoti, S. Seal and W. T. Self, *Biomaterials*, 2008, **29**, 2705–2709.
448 Z. Y. Yang, S. L. Luo, H. Li, S. W. Dong, J. He, H. Jiang, R. Li and X. C. Yang, *RSC Adv.*, 2014, **4**, 59965–59969.
449 G. Pulido-Reyes, I. Rodea-Palomares, S. Das, T. S. Sakthivel, F. Leganes, R. Rosal, S. Seal and F. Fernandez-Pinas, *Sci. Rep.*, 2015, **5**, 15613.
450 V. Baldim, F. Bedioui, N. Mignet, I. Margaill and J. F. Berret, *Nanoscale*, 2018, **10**, 6971–6980.
451 M. Soh, D. W. Kang, H. G. Jeong, D. Kim, D. Y. Kim, W. Yang, C. Song, S. Baik, I. Y. Choi, S. K. Ki, H. J. Kwon, T. Kim, C. K. Kim, S. H. Lee and T. Hyeon, *Angew. Chem., Int. Ed.*, 2017, **56**, 11399–11403.
452 S. Fernandez-Garcia, L. Jiang, M. Tinoco, A. B. Hungria, J. Han, G. Blanco, J. J. Calvino and X. Chen, *J. Phys. Chem. C*, 2016, **120**, 1891–1901.
453 L. Alili, M. Sack, C. von Montfort, S. Giri, S. Das, K. S. Carroll, K. Zanger, S. Seal and P. Brenneisen, *Antioxid. Redox Signaling*, 2013, **19**, 765–778.
454 K. Chaudhury, K. N. Babu, A. K. Singh, S. Das, A. Kumar and S. Seal, *Nanomedicine*, 2013, **9**, 439–448.
455 S. M. Hirst, A. Karakoti, S. Singh, W. Self, R. Tyler, S. Seal and C. M. Reilly, *Environ. Toxicol.*, 2013, **28**, 107–118.
456 N. P. Sardesai, D. Andreescu and S. Andreescu, *J. Am. Chem. Soc.*, 2013, **135**, 16770–16773.
457 B. Bhushan and P. Gopinath, *J. Mater. Chem. B*, 2015, **3**, 4843–4852.
458 C. J. Szymanski, P. Munusamy, C. Mihai, Y. Xie, D. Hu, M. K. Gilles, T. Tyliszczak, S. Thevuthasan, D. R. Baer and G. Orr, *Biomaterials*, 2015, **62**, 147–154.
459 J. M. Dowding, T. Dosani, A. Kumar, S. Seal and W. T. Self, *Chem. Commun.*, 2012, **48**, 4896–4898.
460 A. Y. Estevez, S. Pritchard, K. Harper, J. W. Aston, A. Lynch, J. J. Lucky, J. S. Ludington, P. Chatani, W. P. Mosenthal, J. C. Leiter, S. Andreescu and J. S. Erlichman, *Free Radical Biol. Med.*, 2011, **51**, 1155–1163.
461 Y. Xue, Q. F. Luan, D. Yang, X. Yao and K. B. Zhou, *J. Phys. Chem. C*, 2011, **115**, 4433–4438.
462 E. Ozel, R. Alkasir, K. Ray, K. N. Wallace and S. Andreescu, *Small*, 2013, **9**, 4250–4261.
463 C. K. Kim, T. Kim, I. Y. Choi, M. Soh, D. Kim, Y. J. Kim, H. Jang, H. S. Yang, J. Y. Kim, H. K. Park, S. P. Park, S. Park, T. Yu, B. W. Yoon, S. H. Lee and T. Hyeon, *Angew. Chem., Int. Ed.*, 2012, **51**, 11039–11043.
464 S. Saraf, C. J. Neal, S. Das, S. Barkam, R. McCormack and S. Seal, *ACS Appl. Mater. Interfaces*, 2014, **6**, 5472–5482.

465 M. Hijaz, S. Das, I. Mert, A. Gupta, Z. Al-Wahab, C. Tebbe, S. Dar, J. Chhina, S. Giri, A. Munkarah, S. Seal and R. Rattan, *BMC Cancer*, 2016, **16**, 220.
466 R. N. McCormack, P. Mendez, S. Barkam, C. J. Neal, S. Das and S. Seal, *J. Phys. Chem. C*, 2014, **118**, 18992–19006.
467 Y. Y. Li, X. He, J. J. Yin, Y. H. Ma, P. Zhang, J. Y. Li, Y. Y. Ding, J. Zhang, Y. L. Zhao, Z. F. Chai and Z. Y. Zhang, *Angew. Chem., Int. Ed.*, 2015, **54**, 1832–1835.
468 Y. L. Liu, K. L. Ai, X. Y. Ji, D. Askhatova, R. Du, L. H. Lu and J. J. Shi, *J. Am. Chem. Soc.*, 2017, **139**, 856–862.
469 S. Kishi, T. Hirakawa, K. Sato, A. Komano, C. K. Nishimoto, N. Mera, M. Kugishima, T. Sano, N. Negishi, H. Ichinose, Y. Seto and K. Takeuchi, *Chem. Lett.*, 2013, **42**, 518–520.
470 A. Komano, T. Hirakawa, K. Sato, S. Kishi, C. K. Nishimoto, N. Mera, M. Kugishima, T. Sano, N. Negishi, H. Ichinose, Y. Seto and K. Takeuchi, *Appl. Catal., B*, 2013, **134**, 19–25.
471 M. T. Naseri, M. Sarabadani, D. Ashrafi, H. Saeidian and M. Babri, *Environ. Sci. Pollut. Res.*, 2013, **20**, 907–916.
472 S. Y. Lee, S. Lee, J. Lee, H. S. Lee and J. H. Chang, *Mater. Lett.*, 2013, **110**, 229–232.
473 J. Praveen Kumar, G. K. Prasad, P. V. R. K. Ramacharyulu, P. Garg and K. Ganesan, *Mater. Chem. Phys.*, 2013, **142**, 484–490.
474 P. K. Sharma, G. Gupta, A. K. Nigam, P. Pandey, M. Boopathi, K. Ganesan and B. Singh, *J. Mol. Catal. A: Chem.*, 2013, **366**, 368–374.
475 V. Stengl, T. M. Grygar, F. Oplustil and M. Olsanska, *Ind. Eng. Chem. Res.*, 2013, **52**, 3436–3440.
476 A. K. Verma, A. K. Srivastava, B. Singh, D. Shah, S. Shrivastava and C. K. P. Shinde, *Chemosphere*, 2013, **90**, 2254–2260.
477 L. M. Zimmermann, G. I. Almerindo, J. R. Mora, I. H. Bechtold, H. D. Fiedler and F. Nome, *J. Phys. Chem. C*, 2013, **117**, 26097–26105.
478 M. K. Kinnan, W. R. Creasy, L. B. Fullmer, H. L. Schreuder-Gibson and M. Nyman, *Eur. J. Inorg. Chem.*, 2014, 2361–2367.
479 P. Janos, P. Kuran, V. Pilarova, J. Trogl, M. Stastny, O. Pelant, J. Henych, S. Bakardjieva, O. Zivotsky, M. Kormunda, K. Mazanec and M. Skoumal, *Chem. Eng. J.*, 2015, **262**, 747–755.
480 C. Savelli and R. Salvio, *Chem. – Eur. J.*, 2015, **21**, 5856–5863.
481 V. V. Singh, B. Jurado-Sanchez, S. Sattayasamitsathit, J. Orozco, J. Li, M. Galarnyk, Y. Fedorak and J. Wang, *Adv. Funct. Mater.*, 2015, **25**, 2147–2155.
482 Y.-M. Wong, Y. Hoshino, K. Sudesh, Y. Miura and K. Numata, *Biomacromolecules*, 2015, **16**, 411–421.
483 W. Guo, H. Lv, K. P. Sullivan, W. O. Gordon, A. Balboa, G. W. Wagner, D. G. Musaev, J. Bacsa and C. L. Hill, *Angew. Chem., Int. Ed.*, 2016, **55**, 7403–7407.
484 R. B. Balow, J. G. Lundin, G. C. Daniels, W. O. Gordon, M. McEntee, G. W. Peterson, J. H. Wynne and P. E. Pehrsson, *ACS Appl. Mater. Interfaces*, 2017, **9**, 39747–39757.
485 J. Dong, J. F. Hu, Y. N. Chi, Z. G. Lin, B. Zou, S. Yang, C. L. Hill and C. W. Hu, *Angew. Chem., Int. Ed.*, 2017, **56**, 4473–4477.
486 M. Florent, D. A. Giannakoudakis, R. Wallace and T. J. Bandosz, *J. Hazard. Mater.*, 2017, **329**, 141–149.
487 S. Kim, W. B. Ying, H. Jung, S. G. Ryu, B. Lee and K. J. Lee, *Chem. – Asian J.*, 2017, **12**, 698–705.
488 V. B. Silva, T. S. Rodrigues, P. H. C. Camargo and E. S. Orth, *RSC Adv.*, 2017, **7**, 40711–40719.
489 Q. Wang, R. C. Chapleski, Jr., A. M. Plonka, W. O. Gordon, W. Guo, N. P. Thuy-Duong, C. H. Sharp, N. S. Marinkovic, S. D. Senanayake, J. R. Morris, C. L. Hill, D. Troya and A. I. Frenkel, *Sci. Rep.*, 2017, **7**, 773.
490 X. L. Huang, *Astrobiology*, 2018, **18**, 294–310.
491 H. Tokuyama, S. Yamago, E. Nakamura, T. Shiraki and Y. Sugiura, *J. Am. Chem. Soc.*, 1993, **115**, 7918–7919.
492 A. S. Boutorine, H. Tokuyama, M. Takasugi, H. Isobe, E. Nakamura and C. Helene, *Angew. Chem., Int. Ed.*, 1995, **33**, 2462–2465.
493 Y. N. Yamakoshi, T. Yagami, S. Sueyoshi and N. Miyata, *J. Org. Chem.*, 1996, **61**, 7236–7237.
494 L. Hostert, S. F. Blaskievicz, J. E. S. Fonsaca, S. H. Domingues, A. J. G. Zarbin and E. S. Orth, *J. Catal.*, 2017, **356**, 75–84.
495 X. J. Ma, L. Zhang, M. F. Xia, S. Q. Li, X. H. Zhang and Y. D. Zhang, *ACS Appl. Mater. Interfaces*, 2017, **9**, 21089–21093.
496 T. Wang, J. N. Wang, Y. Yang, P. Su and Y. Yang, *Ind. Eng. Chem. Res.*, 2017, **56**, 9762–9769.
497 X. He, F. Zhang, J. Liu, G. Fang and S. Wang, *Nanoscale*, 2017, **9**, 18066–18074.
498 Q. Zhang, X. X. He, A. L. Han, Q. X. Tu, G. Z. Fang, J. F. Liu, S. Wang and H. B. Li, *Nanoscale*, 2016, **8**, 16851–16856.
499 F. Manea, F. B. Houillon, L. Pasquato and P. Scrimin, *Angew. Chem., Int. Ed.*, 2004, **43**, 6165–6169.
500 L. J. Prins, *Acc. Chem. Res.*, 2015, **48**, 1920–1928.
501 G. Zaupa, C. Mora, R. Bonomi, L. J. Prins and P. Scrimin, *Chem. – Eur. J.*, 2011, **17**, 4879–4889.
502 R. Bonomi, A. Cazzolaro, A. Sansone, P. Scrimin and L. J. Prins, *Angew. Chem., Int. Ed.*, 2011, **50**, 2307–2312.
503 S. Maiti, C. Pezzato, S. Garcia Martin and L. J. Prins, *J. Am. Chem. Soc.*, 2014, **136**, 11288–11291.
504 C. Pezzato and L. J. Prins, *Nat. Commun.*, 2015, **6**, 7790.
505 M. Diez-Castellnou, F. Mancin and P. Scrimin, *J. Am. Chem. Soc.*, 2014, **136**, 1158–1161.
506 J. L. Chen, C. Pezzato, P. Scrimin and L. J. Prins, *Chem. – Eur. J.*, 2016, **22**, 7028–7032.
507 D. Zaramella, P. Scrimin and L. J. Prins, *J. Am. Chem. Soc.*, 2012, **134**, 8396–8399.
508 R. Levy, *ChemBioChem*, 2006, **7**, 1141–1145.
509 R. Bonomi, P. Scrimin and F. Mancin, *Org. Biomol. Chem.*, 2010, **8**, 2622–2626.
510 R. Salvio and A. Cincotti, *RSC Adv.*, 2014, **4**, 28678–28682.

511 F. Mancin, L. J. Prins and P. Scrimin, *Curr. Opin. Colloid Interface Sci.*, 2013, **18**, 61–69.
512 D. Sheet, P. Halder and T. K. Paine, *Angew. Chem., Int. Ed.*, 2013, **52**, 13314–13318.
513 S. Yapar, M. Oikonomou, A. H. Velders and S. Kubik, *Chem. Commun.*, 2015, **51**, 14247–14250.
514 R. Bonomi, F. Selvestrel, V. Lombardo, C. Sissi, S. Polizzi, F. Mancin, U. Tonellato and P. Scrimin, *J. Am. Chem. Soc.*, 2008, **130**, 15744–15745.
515 G. Y. Tonga, Y. D. Jeong, B. Duncan, T. Mizuhara, R. Mout, R. Das, S. T. Kim, Y. C. Yeh, B. Yan, S. Hou and V. M. Rotello, *Nat. Chem.*, 2015, **7**, 597–603.
516 P. Li, R. C. Klet, S. Y. Moon, T. C. Wang, P. Deria, A. W. Peters, B. M. Klahr, H. J. Park, S. S. Al-Juaid, J. T. Hupp and O. K. Farha, *Chem. Commun.*, 2015, **51**, 10925–10928.
517 J. E. Mondloch, M. J. Katz, W. C. Isley Iii, P. Ghosh, P. Liao, W. Bury, G. W. Wagner, M. G. Hall, J. B. DeCoste, G. W. Peterson, R. Q. Snurr, C. J. Cramer, J. T. Hupp and O. K. Farha, *Nat. Mater.*, 2015, **14**, 512–516.
518 S. Y. Moon, G. W. Wagner, J. E. Mondloch, G. W. Peterson, J. B. DeCoste, J. T. Hupp and O. K. Farha, *Inorg. Chem.*, 2015, **54**, 10829–10833.
519 P. Nunes, A. C. Gomes, M. Pillinger, I. S. Goncalves and M. Abrantes, *Microporous Mesoporous Mater.*, 2015, **208**, 21–29.
520 E. López-Maya, C. Montoro, L. M. Rodríguez-Albelo, S. D. Aznar Cervantes, A. A. Lozano-Pérez, J. L. Cenís, E. Barea and J. A. R. Navarro, *Angew. Chem., Int. Ed.*, 2015, **54**, 6790–6794.
521 I. Nath, J. Chakraborty and F. Verpoort, *Chem. Soc. Rev.*, 2016, **45**, 4127–4170.
522 D. T. Lee, J. Zhao, G. W. Peterson and G. N. Parsons, *Chem. Mater.*, 2017, **29**, 4894–4903.
523 D. L. McCarthy, J. Liu, D. B. Dwyer, J. L. Troiano, S. M. Boyer, J. B. DeCoste, W. E. Bernier and J. W. E. Jones, *New J. Chem.*, 2017, **41**, 8748–8753.
524 H. J. Park, J. K. Jang, S. Y. Kim, J. W. Ha, D. Moon, I. N. Kang, Y. S. Bae, S. Kim and D. H. Hwang, *Inorg. Chem.*, 2017, **56**, 12098–12101.
525 M. J. Katz, J. E. Mondloch, R. K. Totten, J. K. Park, S. T. Nguyen, O. K. Farha and J. T. Hupp, *Angew. Chem., Int. Ed.*, 2014, **53**, 497–501.
526 M. J. Katz, S.-Y. Moon, J. E. Mondloch, M. H. Beyzavi, C. J. Stephenson, J. T. Hupp and O. K. Farha, *Chem. Sci.*, 2015, **6**, 2286–2291.
527 S.-Y. Moon, Y. Liu, J. T. Hupp and O. K. Farha, *Angew. Chem., Int. Ed.*, 2015, **54**, 6795–6799.
528 M. C. de Koning, M. van Grol and T. Breijaert, *Inorg. Chem.*, 2017, **56**, 11804–11809.
529 G. Wang, C. Sharp, A. M. Plonka, Q. Wang, A. I. Frenkel, W. Guo, C. Hill, C. Smith, J. Kollar, D. Troya and J. R. Morris, *J. Phys. Chem. C*, 2017, **121**, 11261–11272.
530 H. Y. Chen, P. L. Liao, M. L. Mendonca and R. Q. Snurr, *J. Phys. Chem. C*, 2018, **122**, 12362–12368.
531 A. M. Plonka, Q. Wang, W. O. Gordon, A. Balboa, D. Troya, W. Guo, C. H. Sharp, S. D. Senanayake, J. R. Morris, C. L. Hill and A. I. Frenkel, *J. Am. Chem. Soc.*, 2017, **139**, 599–602.
532 S. S. Mondal and H.-J. Holdt, *Angew. Chem., Int. Ed.*, 2016, **55**, 42–44.
533 N. S. Bobbitt, M. L. Mendonca, A. J. Howarth, T. Islamoglu, J. T. Hupp, O. K. Farha and R. Q. Snurr, *Chem. Soc. Rev.*, 2017, **46**, 3357–3385.
534 G. W. Peterson and G. W. Wagner, *J. Porous Mater.*, 2014, **21**, 121–126.
535 S. Y. Moon, E. Proussaloglou, G. W. Peterson, J. B. DeCoste, M. G. Hall, A. J. Howarth, J. T. Hupp and O. K. Farha, *Chem. – Eur. J.*, 2016, **22**, 14864–14868.
536 J. Zhao, D. T. Lee, R. W. Yaga, M. G. Hall, H. F. Barton, I. R. Woodward, C. J. Oldham, H. J. Walls, G. W. Peterson and G. N. Parsons, *Angew. Chem., Int. Ed.*, 2016, **55**, 13224–13228.
537 P. Asha, M. Sinha and S. Mandal, *RSC Adv.*, 2017, **7**, 6691–6696.
538 Y. Kalinovskyy, N. J. Cooper, M. J. Main, S. J. Holder and B. A. Blight, *Dalton Trans.*, 2017, **46**, 15704–15709.
539 D. A. Giannakoudakis, Y. Hu, M. Florent and T. J. Bandosz, *Nanoscale Horiz.*, 2017, **2**, 356–364.
540 T. Islamoglu, A. Atilgan, S.-Y. Moon, G. W. Peterson, J. B. DeCoste, M. Hall, J. T. Hupp and O. K. Farha, *Chem. Mater.*, 2017, **29**, 2672–2675.
541 B. Li, D. M. Chen, J. Q. Wang, Z. Y. Yan, L. Jiang, D. L. Duan, J. He, Z. R. Luo, J. P. Zhang and F. G. Yuan, *Sci. Rep.*, 2014, **4**, 6759.
542 M. M. Najafpour, S. Madadkhani, Z. Zand, M. Hołyńska and S. I. Allakhverdiev, *Int. J. Hydrogen Energy*, 2016, **41**, 17826–17836.
543 M. Saeed and L. Y. Deng, *Int. J. Greenhouse Gas Control*, 2016, **53**, 254–262.
544 P. Nandhakumar, B. Kim, N. S. Lee, Y. H. Yoon, K. Lee and H. Yang, *Anal. Chem.*, 2018, **90**, 807–813.
545 K. R. Xu, Z. M. Zhong, H. D. Xu, X. Wang, M. Zhao and C. D. Wu, *Chin. J. Appl. Chem.*, 2017, **34**, 1079–1085.
546 J. J. Xu, M. M. Wang, L. Z. Liu, F. Li and J. S. Tian, *J. China Agric. Univ.*, 2018, **23**, 8–13.
547 W. L. Wan, Y. J. Lin, H. L. Chen, C. C. Huang, P. C. Shih, Y. R. Bow, W. T. Chia and H. W. Sung, *J. Am. Chem. Soc.*, 2017, **139**, 12923–12926.
548 T. Xue, B. Peng, M. Xue, X. Zhong, C. Y. Chiu, S. Yang, Y. Q. Qu, L. Y. Ruan, S. Jiang, S. Dubin, R. B. Kaner, J. I. Zink, M. E. Meyerhoff, X. F. Duan and Y. Huang, *Nat. Commun.*, 2014, **5**, 3200.
549 A. Fateeva, P. A. Chater, C. P. Ireland, A. A. Tahir, Y. Z. Khimyak, P. V. Wiper, J. R. Darwent and M. J. Rosseinsky, *Angew. Chem., Int. Ed.*, 2012, **51**, 7440–7444.
550 K. Sasan, Q. Lin, C. Mao and P. Feng, *Chem. Commun.*, 2014, **50**, 10390–10393.
551 S. Pullen, H. Fei, A. Orthaber, S. M. Cohen and S. Ott, *J. Am. Chem. Soc.*, 2013, **135**, 16997–17003.
552 P. C. Sahoo, Y. N. Jang and S. W. Lee, *J. Cryst. Growth*, 2013, **373**, 96–101.

553 Y. Fillon, A. Verma, P. Ghosh, D. Ernenwein, V. M. Rotello and J. Chmielewski, *J. Am. Chem. Soc.*, 2007, **129**, 6676–6677.
554 B. E. R. Snyder, P. Vanelderen, M. L. Bols, S. D. Hallaert, L. H. Bottger, L. Ungur, K. Pierloot, R. A. Schoonheydt, B. F. Sels and E. I. Solomon, *Nature*, 2016, **536**, 317–321.
555 D. Kisailus, M. Najarian, J. C. Weaver and D. E. Morse, *Adv. Mater.*, 2005, **17**, 1234–1239.
556 S. Grundner, M. A. C. Markovits, G. Li, M. Tromp, E. A. Pidko, E. J. M. Hensen, A. Jentys, M. Sanchez-Sanchez and J. A. Lercher, *Nat. Commun.*, 2015, **6**, 7546.
557 W. W. He, Y. T. Zhou, W. G. Warner, X. N. Hu, X. C. Wu, Z. Zheng, M. D. Boudreau and J. J. Yin, *Biomaterials*, 2013, **34**, 765–773.
558 Y. H. Lin, Z. H. Li, Z. W. Chen, J. S. Ren and X. G. Qu, *Biomaterials*, 2013, **34**, 2600–2610.
559 J. L. Dong, L. N. Song, J. J. Yin, W. W. He, Y. H. Wu, N. Gu and Y. Zhang, *ACS Appl. Mater. Interfaces*, 2014, **6**, 1959–1970.
560 H. Wang, W. Jiang, Y. Wang, X. Liu, J. Yao, L. Yuan, Z. Wu, D. Li, B. Song and H. Chen, *Langmuir*, 2013, **29**, 3–7.
561 H. Su, D. D. Liu, M. Zhao, W. L. Hu, S. S. Xue, Q. Cao, X. Y. Le, L. N. Ji and Z. W. Mao, *ACS Appl. Mater. Interfaces*, 2015, **7**, 8233–8242.
562 L. Su, W. J. Qin, H. G. Zhang, Z. U. Rahman, C. L. Ren, S. D. Ma and X. G. Chen, *Biosens. Bioelectron.*, 2015, **63**, 384–391.
563 P. Jawaid, M. U. Rehman, Q. L. Zhao, K. Takeda, K. Ishikawa, M. Hori, T. Shimizu and T. Kondo, *J. Cell. Mol. Med.*, 2016, **20**, 1737–1748.
564 Q. Q. Wang, L. L. Zhang, C. S. Shang, Z. Q. Zhang and S. J. Dong, *Chem. Commun.*, 2016, **52**, 5410–5413.
565 G. J. Cao, X. M. Jiang, H. Zhang, T. R. Croley and J. J. Yin, *RSC Adv.*, 2017, **7**, 52210–52217.
566 J. He, F. J. Xu, J. Hu, S. L. Wang, X. D. Hou and Z. Long, *Microchem. J.*, 2017, **135**, 91–99.
567 A. L. Hu, H. H. Deng, X. Q. Zheng, Y. Y. Wu, X. L. Lin, A. L. Liu, X. H. Xia, H. P. Peng, W. Chen and G. L. Hong, *Biosens. Bioelectron.*, 2017, **97**, 21–25.
568 H. G. Yang, J. Q. Zha, P. Zhang, Y. M. Qin, T. Chen and F. G. Ye, *Sens. Actuators, B*, 2017, **247**, 469–478.
569 L. Han, H. J. Zhang, D. Y. Chen and F. Li, *Adv. Funct. Mater.*, 2018, **28**, 1800018.
570 H. Li, T. Wang, Y. Wang, S. Wang, P. Su and Y. Yang, *Ind. Eng. Chem. Res.*, 2018, **57**, 2416–2425.
571 W. Zhang, Y. Wu, H. J. Dong, J. J. Yin, H. Zhang, H. A. Wu, L. N. Song, Y. Chong, Z. X. Li, N. Gu and Y. Zhang, *Colloids Surf., B*, 2018, **163**, 379–384.
572 C. Xu, Y. H. Lin, J. S. Wang, L. Wu, W. L. Wei, J. S. Ren and X. G. Qu, *Adv. Healthcare Mater.*, 2013, **2**, 1591–1599.
573 N. Singh, M. A. Savanur, S. Srivastava, P. D'Silva and G. Mugesh, *Angew. Chem., Int. Ed.*, 2017, **56**, 14267–14271.
574 N. Gao, K. Dong, A. D. Zhao, H. J. Sun, Y. Wang, J. S. Ren and X. G. Qu, *Nano Res.*, 2016, **9**, 1079–1090.
575 J. Liu, W. Zhang, H. L. Zhang, Z. Y. Yang, T. R. Li, B. D. Wang, X. Huo, R. Wang and H. T. Chen, *Chem. Commun.*, 2013, **49**, 4938–4940.
576 K. S. McKeating, S. Sloan Dennison, D. Graham and K. Faulds, *Analyst*, 2013, **138**, 6347–6353.
577 W. Shen, C. L. Lim and Z. Q. Gao, *Chem. Commun.*, 2013, **49**, 8114–8116.
578 Y. Tao, Y. H. Lin, J. S. Ren and X. G. Qu, *Biosens. Bioelectron.*, 2013, **42**, 41–46.
579 Q. Cai, S. K. Lu, F. Liao, Y. Q. Li, S. Z. Ma and M. W. Shao, *Nanoscale*, 2014, **6**, 8117–8123.
580 J. A. R. Guivar, E. G. R. Fernandes and V. Zucolotto, *Talanta*, 2015, **141**, 307–314.
581 Y. Jia, H. M. Yu, L. Wu, X. D. Hou, L. Yang and C. B. Zheng, *Anal. Chem.*, 2015, **87**, 5866–5871.
582 Y. Shi, J. Huang, J. N. Wang, P. Su and Y. Yang, *Talanta*, 2015, **143**, 457–463.
583 Y. H. Wang, B. Zhou, S. Wu, K. M. Wang and X. X. He, *Talanta*, 2015, **134**, 712–717.
584 Z. Yu, Y. Park, L. Chen, B. Zhao, Y. M. Jung and Q. Cong, *ACS Appl. Mater. Interfaces*, 2015, **7**, 23472–23480.
585 B. W. Liu, X. Han and J. W. Liu, *Nanoscale*, 2016, **8**, 13620–13626.
586 A. Muthurasu and V. Ganesh, *RSC Adv.*, 2016, **6**, 7212–7223.
587 W. Song, G. D. Nie, W. Ji, Y. Z. Jiang, X. F. Lu, B. Zhao and Y. Ozaki, *RSC Adv.*, 2016, **6**, 54456–54462.
588 C. Q. Wang, J. Qian, K. Wang, X. W. Yang, Q. Liu, N. Hao, C. K. Wang, X. Y. Dong and X. Y. Huang, *Biosens. Bioelectron.*, 2016, **77**, 1183–1191.
589 Y. Guo, H. Wang, X. W. Ma, J. Jin, W. Ji, X. Wang, W. Song, B. Zhao and C. Y. He, *ACS Appl. Mater. Interfaces*, 2017, **9**, 19074–19081.
590 M. S. Kim, S. H. Kweon, S. Cho, S. S. A. An, M. I. Kim, J. Doh and J. Lee, *ACS Appl. Mater. Interfaces*, 2017, **9**, 35133–35140.
591 S. Li, L. Y. Zhang, Y. Jiang, S. Y. Zhu, X. X. Lv, Z. Q. Duan and H. Wang, *Nanoscale*, 2017, **9**, 16005–16011.
592 J. Zhang, J. W. Ma, X. B. Fan, W. C. Peng, G. L. Zhang, F. B. Zhang and Y. Li, *Catal. Commun.*, 2017, **89**, 148–151.
593 T. Gao, C. L. Mu, H. Shi, L. Shi, X. X. Mao and G. X. Li, *ACS Appl. Mater. Interfaces*, 2018, **10**, 59–65.
594 M. V. Gorbachevskii, D. S. Kopitsyn, M. S. Kotelev, E. V. Ivanov, V. A. Vinokurov and A. A. Novikov, *RSC Adv.*, 2018, **8**, 19051–19057.
595 J. J. Wu, K. Qin, D. Yuan, J. Tan, L. Qin, X. J. Zhang and H. Wei, *ACS Appl. Mater. Interfaces*, 2018, **10**, 12954–12959.
596 M. Konczol, A. Weiss, E. Stangenberg, R. Gminski, M. Garcia-Kaufer, R. Giere, I. Merfort and V. Mersch-Sundermann, *Chem. Res. Toxicol.*, 2013, **26**, 693–702.
597 S. S. Lee, W. Song, M. Cho, H. L. Puppala, N. Phuc, H. Zhu, L. Segatori and V. L. Colvin, *ACS Nano*, 2013, **7**, 9693–9703.
598 N. J. Lang, B. W. Liu and J. W. Liu, *J. Colloid Interface Sci.*, 2014, **428**, 78–83.
599 Y. H. Peng, Z. Y. Wang, W. S. Liu, H. L. Zhang, W. Zuo, H. A. Tang, F. J. Chen and B. D. Wang, *Dalton Trans.*, 2015, **44**, 12871–12877.

600 Y. Fu, X. Y. Zhao, J. L. Zhang and W. Li, *J. Phys. Chem. C*, 2014, **118**, 18116–18125.
601 J. M. Dowding, S. Das, A. Kumar, T. Dosani, R. McCormack, A. Gupta, T. X. T. Sayle, D. C. Sayle, L. von Kalm, S. Seal and W. T. Self, *ACS Nano*, 2013, **7**, 4855–4868.
602 E. Grulke, K. Reed, M. Beck, X. Huang, A. Cormack and S. Seal, *Environ. Sci.: Nano*, 2014, **1**, 429–444.
603 J. S. Mu, L. Zhang, G. Y. Zhao and Y. Wang, *Phys. Chem. Chem. Phys.*, 2014, **16**, 15709–15716.
604 J. S. Mu, L. Zhang, M. Zhao and Y. Wang, *ACS Appl. Mater. Interfaces*, 2014, **6**, 7090–7098.
605 J. Qian, X. W. Yang, L. Jiang, C. D. Zhu, H. P. Mao and K. Wang, *Sens. Actuators, B*, 2014, **201**, 160–166.
606 K. Zhang, W. Zuo, Z. Y. Wang, J. Liu, T. R. Li, B. D. Wang and Z. Y. Yang, *RSC Adv.*, 2015, **5**, 10632–10640.
607 A. B. Ghosh, N. Saha, A. Sarkar, A. K. Dutta, P. Biswas, K. Nag and B. Adhikary, *New J. Chem.*, 2016, **40**, 1595–1604.
608 D. Wan, W. B. Li, G. H. Wang and X. B. Wei, *J. Mater. Eng. Perform.*, 2016, **25**, 4333–4340.
609 Y. S. Yang, Z. Mao, W. J. Huang, L. H. Liu, J. L. Li, J. L. Li and Q. Z. Wu, *Sci. Rep.*, 2016, **6**, 35344.
610 G. W. Peterson, A. X. Lu and T. H. Epps, *ACS Appl. Mater. Interfaces*, 2017, **9**, 32248–32254.
611 Z. L. Wu, J. J. Wu, X. Y. Sun, B. Liu and J. S. Shen, *Sci. Sin.: Chim.*, 2017, **47**, 1226–1232.
612 N. Singh, M. Geethika, S. M. Eswarappa and G. Mugesh, *Chem. – Eur. J.*, 2018, **24**, 8393–8403.
613 X. D. Zhang, X. X. Mao, S. Q. Li, W. F. Dong and Y. M. Huang, *Sens. Actuators, B*, 2018, **258**, 80–87.
614 A. A. Vernekar, T. Das, S. Ghosh and G. Mugesh, *Chem. – Asian. J.*, 2016, **11**, 72–76.
615 C. Ge, G. Fang, X. M. Shen, Y. Chong, W. G. Wamer, X. F. Gao, Z. F. Chai, C. Y. Chen and J. J. Yin, *ACS Nano*, 2016, **10**, 10436–10445.
616 G. Fang, W. F. Li, X. M. Shen, J. M. Perez Aguilar, Y. Chong, X. F. Gao, Z. F. Chai, C. Y. Chen, C. C. Ge and R. H. Zhou, *Nat. Commun.*, 2018, **9**, 129.
617 X. N. Hu, A. Saran, S. Hou, T. Wen, Y. L. Ji, W. Q. Liu, H. Zhang, W. W. He, J. J. Yin and X. C. Wu, *RSC Adv.*, 2013, **3**, 6095–6105.
618 A. Boujakhrout, P. Díez, P. Martínez-Ruíz, A. Sánchez, C. Parrado, E. Povedano, P. Soto, J. M. Pingarrón and R. Villalonga, *RSC Adv.*, 2016, **6**, 74957–74960.
619 J. R. Li, L. Lv, G. N. Zhang, X. D. Zhou, A. G. Shen and J. M. Hu, *Anal. Methods*, 2016, **8**, 2097–2105.
620 Z. Q. Gao, H. H. Ye, D. Y. Tang, J. Tao, S. Habibi, A. Minerick, D. P. Tang and X. H. Xia, *Nano Lett.*, 2017, **17**, 5572–5579.
621 L. Long, J. B. Liu, K. S. Lu, T. Zhang, Y. Q. Xie, Y. L. Ji and X. C. Wu, *J. Nanobiotechnol.*, 2018, **16**, 46.
622 X. H. Xia, J. T. Zhang, N. Lu, M. J. Kim, K. S. Ghale, Y. Xu, E. McKenzie, J. B. Liu and H. H. Yet, *ACS Nano*, 2015, **9**, 9994–10004.
623 R. F. Wu, Y. Chong, G. Fang, X. M. Jiang, Y. Pan, C. Y. Chen, J. J. Yin and C. C. Ge, *Adv. Funct. Mater.*, 2018, **28**, 1801484.
624 H. Y. Zhang, S. Pokhrel, Z. X. Ji, H. Meng, X. Wang, S. J. Lin, C. H. Chang, L. J. Li, R. B. Li, B. B. Sun, M. Y. Wang, Y. P. Liao, R. Liu, T. Xia, L. Maedler and A. E. Nel, *J. Am. Chem. Soc.*, 2014, **136**, 6406–6420.
625 F. Pogacean, C. Socaci, S. Pruneanu, A. R. Biris, M. Coros, L. Magerusan, G. Katona, R. Turcu and G. Borodi, *Sens. Actuators, B*, 2015, **213**, 474–483.
626 A. L. Tiano, G. C. Papaefthymiou, C. S. Lewis, J. Han, C. Zhang, Q. Li, C. Y. Shi, A. M. M. Abeykoon, S. J. L. Billinge, E. Stach, J. Thomas, K. Guerrero, P. Munayco, J. Munayco, R. B. Scorzelli, P. Burnham, A. J. Viescas and S. S. Wong, *Chem. Mater.*, 2015, **27**, 3572–3592.
627 D. Jampaiah, T. Srinivasa Reddy, A. E. Kandjani, P. R. Selvakannan, Y. M. Sabri, V. E. Coyle, R. Shukla and S. K. Bhargava, *J. Mater. Chem. B*, 2016, **4**, 3874–3885.
628 C. L. Hsu, C. W. Lien, S. G. Harroun, R. Ravindranath, H. T. Chang, J. Y. Mao and C. C. Huang, *Mater. Chem. Front.*, 2017, **1**, 893–899.
629 L. Jiang, S. Fernandez-Garcia, M. Tinoco, Z. Yan, Q. Xue, G. Blanco, J. J. Calvino, A. B. Hungria and X. Chen, *ACS Appl. Mater. Interfaces*, 2017, **9**, 18595–18608.
630 X. L. Huang, C. Xu, J. P. Ma and F. X. Chen, *Adv. Powder Technol.*, 2018, **29**, 796–803.
631 X. Jiao, W. Y. Liu, D. Wu, W. H. Liu and H. J. Song, *Anal. Methods*, 2018, **10**, 76–83.
632 B. Wang, F. Liu, Y. Y. Wu, Y. F. Chen, B. Weng and C. M. Li, *Sens. Actuators, B*, 2018, **255**, 2601–2607.
633 Y. J. Sang, Y. Y. Huang, W. Li, J. S. Ren and X. G. Qu, *Chem. – Eur. J.*, 2018, **24**, 7259–7263.
634 X. F. Lu, X. J. Bian, Z. C. Li, D. M. Chao and C. Wang, *Sci. Rep.*, 2013, **3**, 2955.
635 X. C. Lv and J. Weng, *Sci. Rep.*, 2013, **3**, 3285.
636 M. Ma, J. Xie, Y. Zhang, Z. P. Chen and N. Gu, *Mater. Lett.*, 2013, **105**, 36–39.
637 H. Y. Sun, X. L. Jiao, Y. Y. Han, Z. Jiang and D. R. Chen, *Eur. J. Inorg. Chem.*, 2013, 109–114.
638 Y. X. Wang, X. Zhang, Z. M. Luo, X. Huang, C. L. Tan, H. Li, B. Zheng, B. Li, Y. Huang, J. Yang, Y. Zong, Y. B. Ying and H. Zhang, *Nanoscale*, 2014, **6**, 12340–12344.
639 Y. L. Guo, X. Y. Liu, X. D. Wang, A. Iqbal, C. D. Yang, W. S. Liu and W. W. Qin, *RSC Adv.*, 2015, **5**, 95495–95503.
640 Y. L. Guo, X. Y. Liu, C. D. Yang, X. D. Wang, D. Wang, A. Iqbal, W. S. Liu and W. W. Qin, *ChemCatChem*, 2015, **7**, 2467–2474.
641 S. Kandula and P. Jeevanandam, *RSC Adv.*, 2015, **5**, 5295–5306.
642 Q. Li, G. E. Tang, X. W. Xiong, Y. L. Cao, L. L. Chen, F. G. Xu and H. L. Tan, *Sens. Actuators, B*, 2015, **215**, 86–92.
643 X. Wang, D. P. Liu, J. Q. Li, J. M. Zhen and H. J. Zhang, *NPG Asia Mater.*, 2015, **7**, e158.
644 H. Zhao, Y. M. Dong, P. P. Jiang, G. L. Wang and J. J. Zhang, *ACS Appl. Mater. Interfaces*, 2015, **7**, 6451–6461.
645 J. B. Essner, R. N. McCay, C. J. Smith II, S. M. Cobb, C. H. Laber and G. A. Baker, *J. Mater. Chem. B*, 2016, **4**, 2163–2170.

646 C. L. Hsu, C. W. Lien, C. W. Wang, S. G. Harroun, C. C. Huang and H. T. Chang, *Biosens. Bioelectron.*, 2016, **75**, 181–187.
647 Y. Z. Jiang, G. D. Nie, M. Q. Chi, Z. Z. Yang, Z. Zhang, C. Wang and X. F. Lu, *RSC Adv.*, 2016, **6**, 31107–31113.
648 L. Magerusan, C. Socaci, F. Pogacean, M. C. Rosu, A. R. Biris, M. Coros, A. Turza, V. Floare-Avram, G. Katona and S. Pruneanu, *RSC Adv.*, 2016, **6**, 79497–79506.
649 F. M. Qiao, Q. Q. Qi, Z. Z. Wang, K. Xu and S. Y. Ai, *Sens. Actuators, B*, 2016, **229**, 379–386.
650 Z. Z. Yang, Z. Zhang, Y. Z. Jiang, M. Q. Chi, G. D. Nie, X. F. Lu and C. Wang, *RSC Adv.*, 2016, **6**, 33636–33642.
651 C. Zheng, W. J. Ke, T. X. Yin and X. Q. An, *RSC Adv.*, 2016, **6**, 35280–35286.
652 M. M. Chen, Y. N. Ding, Y. Gao, X. X. Zhu, P. Wang, Z. Q. Shi and Q. Y. Liu, *RSC Adv.*, 2017, **7**, 25220–25228.
653 M. M. Chen, L. F. Sun, Y. N. Ding, Z. Q. Shi and Q. Y. Liu, *New J. Chem.*, 2017, **41**, 5853–5862.
654 M. Q. Chi, Y. Zhu, Z. Z. Yang, M. Gao, S. H. Chen, N. Song, C. Wang and X. F. Lu, *Nanotechnology*, 2017, **28**, 295704.
655 Y. Ding, M. M. Chen, K. Wu, M. X. Chen, L. F. Sun, Z. X. Liu, Z. Q. Shi and Q. Y. Liu, *Mater. Sci. Eng., C*, 2017, **80**, 558–565.
656 D. Jampaiah, T. Srinivasa Reddy, V. E. Coyle, A. Nafady and S. K. Bhargava, *J. Mater. Chem. B*, 2017, **5**, 720–730.
657 Q. Y. Liu, P. P. Chen, Z. Xu, M. M. Chen, Y. N. Ding, K. Yue and J. Xu, *Sens. Actuators, B*, 2017, **251**, 339–348.
658 Q. Y. Liu, Y. T. Yang, X. T. Lv, Y. N. Ding, Y. Z. Zhang, J. J. Jing and C. X. Xu, *Sens. Actuators, B*, 2017, **240**, 726–734.
659 S. F. Cai, X. L. Liu, Q. S. Han, C. Qi, R. Yang and C. Wang, *Nano Res.*, 2018, **11**, 3272–3281.
660 M. Q. Chi, S. H. Chen, M. X. Zhong, C. Wang and X. F. Lu, *Chem. Commun.*, 2018, **54**, 5827–5830.
661 F. Huang, J. Z. Wang, W. M. Chen, Y. J. Wan, X. M. Wang, N. Cai, J. Liu and F. Q. Yu, *J. Taiwan Inst. Chem. Eng.*, 2018, **83**, 40–49.
662 S. R. Kim, S. Cho and M. I. Kim, *J. Nanosci. Nanotechnol.*, 2018, **18**, 1246–1250.
663 Z. H. Li, X. D. Yang, Y. B. Yang, Y. N. Tan, Y. He, M. Liu, X. W. Liu and Q. Yuan, *Chem. – Eur. J.*, 2018, **24**, 409–415.
664 L. Liu, B. J. Du, C. S. Shang, J. Wang and E. K. Wang, *Anal. Chim. Acta*, 2018, **1014**, 77–84.
665 Z. Z. Yang, Y. Zhu, M. Q. Chi, C. Wang, Y. Wei and X. F. Lu, *J. Colloid Interface Sci.*, 2018, **511**, 383–391.
666 X. X. Zhou, S. J. Guo, J. X. Gao, J. M. Zhao, S. Y. Xue and W. J. Xu, *Biosens. Bioelectron.*, 2017, **98**, 83–90.
667 X. L. Sun, S. J. Guo, C. S. Chung, W. L. Zhu and S. H. Sun, *Adv. Mater.*, 2013, **25**, 132–136.
668 H. Wang, S. Li, Y. M. Si, Z. Z. Sun, S. Y. Li and Y. H. Lin, *J. Mater. Chem. B*, 2014, **2**, 4442–4448.
669 H. Wang, S. Li, Y. M. Si, N. Zhang, Z. Z. Sun, H. Wu and Y. H. Lin, *Nanoscale*, 2014, **6**, 8107–8116.
670 X. C. Wu, Y. Zhang, T. Han, H. X. Wu, S. W. Guo and J. Y. Zhang, *RSC Adv.*, 2014, **4**, 3299–3305.
671 N. A. Zubir, C. Yacou, J. Motuzas, X. W. Zhang and J. C. D. da Costa, *Sci. Rep.*, 2014, **4**, 4594.
672 S. Dutta, C. Ray, S. Mallick, S. Sarkar, R. Sahoo, Y. Negishi and T. Pal, *J. Phys. Chem. C*, 2015, **119**, 23790–23800.
673 W. Haider, A. Hayat, Y. Raza, A. A. Chaudhry, R. Ihtesham Ur and J. L. Marty, *RSC Adv.*, 2015, **5**, 24853–24858.
674 L. L. Li, C. M. Zeng, L. H. Ai and J. Jiang, *J. Alloys Compd.*, 2015, **639**, 470–477.
675 J. Liu, X. Y. Xin, H. Zhou and S. S. Zhang, *Chem. – Eur. J.*, 2015, **21**, 1908–1914.
676 Z. Ma, Y. F. Qiu, H. H. Yang, Y. M. Huang, J. J. Liu, Y. Lu, C. Zhang and P. A. Hu, *ACS Appl. Mater. Interfaces*, 2015, **7**, 22036–22045.
677 S. T. Zhang, H. Li, Z. Y. Wang, J. Liu, H. L. Zhang, B. D. Wang and Z. Y. Yang, *Nanoscale*, 2015, **7**, 8495–8502.
678 X. H. Zhang, G. H. Wu, Z. X. Cai and X. Chen, *Talanta*, 2015, **134**, 132–135.
679 D. A. Giannakoudakis, J. A. Arcibar-Orozco and T. J. Bandosz, *Appl. Catal., B*, 2016, **183**, 37–46.
680 S. L. Li, H. Li, F. J. Chen, J. Liu, H. L. Zhang, Z. Y. Yang and B. D. Wang, *Dyes Pigm.*, 2016, **125**, 64–71.
681 K. V. Ragavan and N. K. Rastogi, *Sens. Actuators, B*, 2016, **229**, 570–580.
682 Y. Z. Jiang, Y. Gu, G. D. Nie, M. Q. Chi, Z. Z. Yang, C. Wang, Y. Wei and X. F. Lu, *Part. Part. Syst. Charact.*, 2017, **34**, 1600233.
683 W. Zhang, Y. Sun, Z. Lou, L. Song, Y. Wu, N. Gu and Y. Zhang, *Colloids Surf., B*, 2017, **151**, 215–223.
684 X. Jin, Y. Y. Zhong, L. Chen, L. J. Xu, Y. N. Wu and F. F. Fu, *Part. Part. Syst. Charact.*, 2018, **35**, 1700359.
685 T. Wang, Y. C. Fu, L. Y. Chai, L. Chao, L. J. Bu, Y. Meng, C. Chen, M. Ma, Q. J. Xie and S. Z. Yao, *Chem. – Eur. J.*, 2014, **20**, 2623–2630.
686 F. M. Qiao, Z. Z. Wang, K. Xu and S. Y. Ai, *Analyst*, 2015, **140**, 6684–6691.
687 B. B. Kou, Y. Q. Chai, Y. L. Yuan and R. Yuan, *Anal. Chem.*, 2017, **89**, 9383–9387.
688 H. Y. Shin, S. Cho and M. I. Kim, *J. Nanosci. Nanotechnol.*, 2017, **17**, 7971–7977.
689 Q. Zhang, S. Chen, H. Wang and H. T. Yu, *ACS Appl. Mater. Interfaces*, 2018, **10**, 8666–8675.
690 H. J. Cheng, L. Zhang, J. He, W. J. Guo, Z. Y. Zhou, X. J. Zhang, S. M. Nie and H. Wei, *Anal. Chem.*, 2016, **88**, 5489–5497.
691 Q. Q. Wang, X. P. Zhang, L. Huang, Z. Q. Zhang and S. J. Dong, *Angew. Chem., Int. Ed.*, 2017, **56**, 16082–16085.
692 M. I. Kim, Y. Ye, M. A. Woo, J. Lee and H. G. Park, *Adv. Healthcare Mater.*, 2014, **3**, 36–41.
693 Y. H. Lin, L. Wu, Y. Y. Huang, J. S. Ren and X. G. Qu, *Chem. Sci.*, 2015, **6**, 1272–1276.
694 Y. Y. Huang, Y. H. Lin, X. Ran, J. S. Ren and X. G. Qu, *Chem. – Eur. J.*, 2016, **22**, 5705–5711.
695 K. G. Qu, P. Shi, J. S. Ren and X. G. Qu, *Chem. – Eur. J.*, 2014, **20**, 7501–7506.
696 Y. Huang, M. T. Zhao, S. K. Han, Z. C. Lai, J. Yang, C. L. Tan, Q. L. Ma, Q. P. Lu, J. Z. Chen, X. Zhang,

Z. C. Zhang, B. Li, B. Chen, Y. Zong and H. Zhang, *Adv. Mater.*, 2017, **29**, 1700102.
697 R. Pautler, E. Y. Kelly, P. J. J. Huang, J. Cao, B. W. Liu and J. W. Liu, *ACS Appl. Mater. Interfaces*, 2013, **5**, 6820–6825.
698 L. Zhan, Y. Zhang, Q. L. Zeng, Z. D. Liu and C. Z. Huang, *J. Colloid Interface Sci.*, 2014, **426**, 293–299.
699 S. M. Taghdisi, N. M. Danesh, P. Lavaee, A. S. Emrani, M. Ramezani and K. Abnous, *RSC Adv.*, 2015, **5**, 43508–43514.
700 P. P. Zhou, S. S. Jia, D. Pan, L. H. Wang, J. M. Gao, J. X. Lu, J. Y. Shi, Z. S. Tang and H. J. Liu, *Sci. Rep.*, 2015, **5**, 14402.
701 F. Yuan, H. M. Zhao, H. M. Zang, F. Ye and X. Quan, *ACS Appl. Mater. Interfaces*, 2016, **8**, 9855–9864.
702 Y. Liu, M. Yuan, L. J. Qiao and R. Guo, *Biosens. Bioelectron.*, 2014, **52**, 391–396.
703 K. Zhao, W. Gu, S. S. Zheng, C. L. Zhang and Y. Z. Xian, *Talanta*, 2015, **141**, 47–52.
704 Y. Lu, J. Yu, W. C. Ye, X. Yao, P. P. Zhou, H. X. Zhang, S. Q. Zhao and L. P. Jia, *Microchim. Acta*, 2016, **183**, 2481–2489.
705 G. Bülbül, A. Hayat and S. Andreescu, *Adv. Healthcare Mater.*, 2016, **5**, 822–828.
706 M. Y. Wang, G. Siddiqui, O. J. R. Gustafsson, A. Kakinen, I. Javed, N. H. Voelcker, D. J. Creek, P. C. Ke and T. P. Davis, *Small*, 2017, **13**, 1701528.
707 L. Han, Y. Li and A. P. Fan, *Luminescence*, 2018, **33**, 751–758.
708 J. Yu, D. Q. Ma, L. Q. Mei, Q. Gao, W. Y. Yin, X. Zhang, L. Yan, Z. J. Gu, X. Y. Ma and Y. L. Zhao, *J. Mater. Chem. B*, 2018, **6**, 487–498.
709 L. J. Chen, K. F. Sun, P. P. Li, X. Z. Fan, J. C. Sun and S. Y. Ai, *Nanoscale*, 2013, **5**, 10982–10988.
710 J. T. Hu, P. J. Ni, H. C. Dai, Y. J. Sun, Y. L. Wang, S. Jiang and Z. Li, *RSC Adv.*, 2015, **5**, 16036–16041.
711 B. W. Liu and J. W. Liu, *Nanoscale*, 2015, **7**, 13831–13835.
712 M. S. Hizir, M. Top, M. Balcioglu, M. Rana, N. M. Robertson, F. S. Shen, J. Sheng and M. V. Yigit, *Anal. Chem.*, 2016, **88**, 600–605.
713 L. Z. Hu, H. Liao, L. Y. Feng, M. Wang and W. S. Fu, *Anal. Chem.*, 2018, **90**, 6247–6252.
714 D. Garg, M. Kaur, S. Sharma and V. Verma, *Bull. Mater. Sci.*, 2018, **41**, 134.
715 D. Antuna-Jimenez, M. C. Blanco-Lopez, A. J. Miranda-Ordieres and M. J. Lobo-Castanon, *Polymer*, 2014, **55**, 1113–1119.
716 E. d. S. Moretti, J. de Fátima Giarola, M. Kuceki, M. C. Prete, A. C. Pereira and C. R. Teixeira Tarley, *RSC Adv.*, 2016, **6**, 28751–28760.
717 L. Wang, L. F. Miao, H. Yang, J. Yu, Y. Z. Xie, L. J. Xu and Y. H. Song, *Sens. Actuators, B*, 2017, **253**, 108–114.
718 N. Bagheri, A. Khataee, B. Habibi and J. Hassanzadeh, *Talanta*, 2018, **179**, 710–718.
719 Z. J. Zhang, X. H. Zhang, B. W. Liu and J. W. Liu, *J. Am. Chem. Soc.*, 2017, **139**, 5412–5419.
720 C. Xu, C. Q. Zhao, M. Li, L. Wu, J. S. Ren and X. G. Qu, *Small*, 2014, **10**, 1841–1847.
721 P. F. Zhan, Z. G. Wang, N. Li and B. Q. Ding, *ACS Catal.*, 2015, **5**, 1489–1498.
722 R. Qu, H. Shi, R. Wang, T. Cheng, R. Ma, Y. An and L. Shi, *Biomater. Sci.*, 2017, **5**, 570–577.
723 Y. H. Sun, C. Q. Zhao, N. Gao, J. S. Ren and X. G. Qu, *Chem. – Eur. J.*, 2017, **23**, 18146–18150.
724 K. L. Fan, H. Wang, J. Q. Xi, Q. Liu, X. Q. Meng, D. M. Duan, L. Z. Gao and X. Y. Yan, *Chem. Commun.*, 2017, **53**, 424–427.
725 C. P. Liu, T. H. Wu, Y. L. Lin, C. Y. Liu, S. Wang and S. Y. Lin, *Small*, 2016, **12**, 4127–4135.
726 C. P. Liu, T. H. Wu, C. Y. Liu, K. C. Chen, Y. X. Chen, G. S. Chen and S. Y. Lin, *Small*, 2017, **13**, 1700278.
727 C. Xu, Z. Liu, L. Wu, J. S. Ren and X. G. Qu, *Adv. Funct. Mater.*, 2014, **24**, 1624–1630.
728 C. F. Peng, Q. L. Pan, Z. J. Xie and F. M. Wan, *J. Instrum. Anal.*, 2014, **33**, 1312–1316.
729 L. Zhan, C. M. Li, W. B. Wu and C. Z. Huang, *Chem. Commun.*, 2014, **50**, 11526–11528.
730 J. Shah, R. Purohit, R. Singh, A. S. Karakoti and S. Singh, *J. Colloid Interface Sci.*, 2015, **456**, 100–107.
731 G. L. Wang, L. Y. Jin, X. M. Wu, Y. M. Dong and Z. J. Li, *Anal. Chim. Acta*, 2015, **871**, 1–8.
732 X. J. Li, Y. S. Wang, S. Y. Yang, X. Tang, L. Liu, B. Zhou, X. F. Wang, Y. F. Zhu, Y. Q. Huang and S. Z. He, *Microchim. Acta*, 2016, **183**, 2123–2129.
733 K. N. Han, J. S. Choi and J. Kwon, *Sci. Rep.*, 2017, **7**, 2806.
734 L. J. Huang, W. T. Zhang, K. Chen, W. X. Zhu, X. N. Liu, R. Wang, X. Zhang, N. Hu, Y. R. Suo and J. L. Wang, *Chem. Eng. J.*, 2017, **330**, 746–752.
735 N. V. S. Vallabani, A. S. Karakoti and S. Singh, *Colloids Surf., B*, 2017, **153**, 52–60.
736 Y. C. Yang, Y. T. Wang and W. L. Tseng, *ACS Appl. Mater. Interfaces*, 2017, **9**, 10069–10077.
737 J. Shah and S. Singh, *3 Biotech.*, 2018, **8**, 67.
738 S. T. Zhang, D. X. Zhang, X. H. Zhang, D. H. Shang, Z. H. Xue, D. L. Shan and X. Q. Lu, *Anal. Chem.*, 2017, **89**, 3538–3544.
739 B. W. Liu, Z. C. Huang and J. W. Liu, *Nanoscale*, 2016, **8**, 13562–13567.
740 H. Abdolmohammad-Zadeh and E. Rahimpour, *Sens. Actuators, B*, 2015, **209**, 496–504.
741 C. X. Chen, L. X. Lu, Y. Zheng, D. Zhao, F. Yang and X. R. Yang, *Anal. Methods*, 2015, **7**, 161–167.
742 G. W. Li, L. Hong, M. S. Tong, H. H. Deng, X. H. Xia and W. Chen, *Anal. Methods*, 2015, **7**, 1924–1928.
743 R. Singh and S. Singh, *Colloids Surf., B*, 2015, **132**, 78–84.
744 D. Zhao, C. X. Chen, L. X. Lu, F. Yang and X. R. Yang, *Sens. Actuators, B*, 2015, **215**, 437–444.
745 Y. Liu, Y. p. Xiang, D. Ding and R. Guo, *RSC Adv.*, 2016, **6**, 112435.
746 S. N. Wang, P. C. Liu, Y. M. Qin, Z. J. Chen and J. C. Shen, *Sens. Actuators, B*, 2016, **223**, 178–185.
747 H. H. Deng, X. Q. Zheng, Y. Y. Wu, X. Q. Shi, X. L. Lin, X. H. Xia, H. P. Peng, W. Chen and G. L. Hong, *Analyst*, 2017, **142**, 3986–3992.

748 C. W. Hsu, Z. Y. Lin, T. Y. Chan, T. C. Chiu and C. C. Hu, *Food Chem.*, 2017, **224**, 353–358.
749 D. l. Li, K. Dai, X. Zhang, K. L. Zhang, R. Y. Bai, R. Hu and Y. H. Yang, *J. Yunnan Univ.*, 2017, **39**, 447–453.
750 U. Carmona, L. B. Zhang, L. Li, W. Munchgesang, E. Pippel and M. Knez, *Chem. Commun.*, 2014, **50**, 701–703.
751 Y. W. Fan, W. B. Shi, X. D. Zhang and Y. M. Huang, *J. Mater. Chem. A*, 2014, **2**, 2482–2486.
752 Y. Y. Ding, L. F. Sun, Y. L. Jiang, S. X. Liu, M. X. Chen, M. M. Chen, Y. N. Ding and Q. Y. Liu, *Mater. Sci. Eng., C*, 2016, **67**, 188–194.
753 M. M. Dong, L. Y. Zhang, R. Li, S. Y. Li, Y. Jiang, Y. C. Qiao, Z. Q. Duan, R. Li, Q. F. Wang and H. Wang, *RSC Adv.*, 2016, **6**, 47595–47599.
754 H. Y. Sun and W. Y. Zhu, *Appl. Surf. Sci.*, 2016, **399**, 298–304.
755 H. H. Ye, J. Mohar, Q. X. Wang, M. Catalano, M. J. Kim and X. H. Xia, *Sci. Bull.*, 2016, **61**, 1739–1745.
756 W. Na, Y. Y. Li, Y. Yuan and W. G. Gao, *J. Nano Res.*, 2017, **46**, 12–19.
757 T. M. Chen, X. M. Tian, L. Huang, J. Xiao and G. W. Yang, *Nanoscale*, 2017, **9**, 15673–15684.
758 X. Y. Wang, W. Cao, L. Qin, T. S. Lin, W. Chen, S. C. Lin, J. Yao, X. Z. Zhao, M. Zhou, C. Hang and H. Wei, *Theranostics*, 2017, **7**, 2277–2286.
759 Y. H. Lin, A. D. Zhao, Y. Tao, J. S. Ren and X. G. Qu, *J. Am. Chem. Soc.*, 2013, **135**, 4207–4210.
760 Y. H. Lin, Y. Y. Huang, J. S. Ren and X. G. Qu, *NPG Asia Mater.*, 2014, **6**, e114.
761 C. Xu, W. Bing, F. M. Wang, J. S. Ren and X. G. Qu, *ACS Nano*, 2017, **11**, 7770–7780.
762 L. L. Li, L. H. Ai, C. H. Zhang and J. Jiang, *Nanoscale*, 2014, **6**, 4627–4634.
763 G. L. Wang, X. F. Xu, X. M. Wu, G. X. Cao, Y. M. Dong and Z. J. Li, *J. Phys. Chem. C*, 2014, **118**, 28109–28117.
764 S. Barkam, S. Das, S. Saraf, R. McCormack, D. Richardson, L. Atencio, V. Moosavifazel and S. Seal, *Chem. – Eur. J.*, 2015, **21**, 12646–12656.
765 K. F. Li, C. F. Chen, C. Y. Chen, Y. Z. Wang, Z. Wei, W. D. Pan and T. Song, *Enzyme Microb. Technol.*, 2015, **72**, 72–78.
766 J. Peng and J. Weng, *Biosens. Bioelectron.*, 2017, **89**, 652–658.
767 F. Wang, E. Ju, Y. Guan, J. Ren and X. Qu, *Small*, 2017, **13**, 1603051.
768 S. Neri, S. G. Martin, C. Pezzato and L. J. Prins, *J. Am. Chem. Soc.*, 2017, **139**, 1794–1797.
769 F. M. Wang, Y. Zhang, Z. Du, J. S. Ren and X. G. Qu, *Nat. Commun.*, 2018, **9**, 1209.
770 Y. Chong, C. C. Ge, G. Fang, X. Tian, X. C. Ma, T. Wen, W. G. Wamer, C. Y. Chen, Z. F. Chai and J. J. Yin, *ACS Nano*, 2016, **10**, 8690–8699.
771 G. L. Wang, L. Y. Jin, Y. M. Dong, X. M. Wu and Z. J. Li, *Biosens. Bioelectron.*, 2015, **64**, 523–529.
772 C. Wang, Y. Shi, Y. Y. Dan, X. G. Nie, J. Li and X. H. Xia, *Chem. – Eur. J.*, 2017, **23**, 6717–6723.
773 A. A. Vernekar, T. Das and G. Mugesh, *Angew. Chem., Int. Ed.*, 2016, **55**, 1412–1416.
774 M. F. Xia, C. X. Zhuo, X. J. Ma, X. H. Zhang, H. M. Sun, Q. G. Zhai and Y. D. Zhang, *Chem. Commun.*, 2017, **53**, 11302–11305.
775 R. Gil-San Millan, E. Lopez Maya, M. Hall, N. M. Padial, G. W. Peterson, J. B. DeCoste, L. M. Rodriguez Albelo, J. E. Oltra, E. Barea and J. A. R. Navarro, *ACS Appl. Mater. Interfaces*, 2017, **9**, 23967–23973.
776 Z. W. Chen, C. Q. Zhao, E. G. Ju, H. W. Ji, J. S. Ren, B. P. Binks and X. G. Qu, *Adv. Mater.*, 2016, **28**, 1682–1688.
777 Y. Zhang, C. Y. Wu, X. J. Zhou, X. C. Wu, Y. Q. Yang, H. X. Wu, S. W. Guo and J. Y. Zhang, *Nanoscale*, 2013, **5**, 1816–1819.
778 Q. Chang and H. Q. Tang, *Microchim. Acta*, 2014, **181**, 527–534.
779 Q. Y. Liu, R. R. Zhu, H. Du, H. Li, Y. T. Yang, Q. Y. Jia and B. Bian, *Mater. Sci. Eng., C*, 2014, **43**, 321–329.
780 S. Y. Deng, P. X. Yuan, X. B. Ji, D. Shan and X. J. Zhang, *ACS Appl. Mater. Interfaces*, 2015, **7**, 543–552.
781 J. M. Kong, X. H. Yu, W. W. Hu, Q. Hu, S. L. Shui, L. Z. Li, X. J. Han, H. F. Xie, X. J. Zhang and T. H. Wang, *Analyst*, 2015, **140**, 7792–7798.
782 J. Li, Y. Li, J. N. Peng and S. L. Feng, *Chem. Res. Appl.*, 2015, 388–392.
783 P. Martinkova and M. Pohanka, *Int. J. Electrochem. Sci.*, 2015, **10**, 7033–7048.
784 W. S. Yang, J. H. Hao, Z. Zhang and B. L. Zhang, *J. Colloid Interface Sci.*, 2015, **460**, 55–60.
785 X. Yang, L. N. Wang, G. Z. Zhou, N. Sui, Y. X. Gu and J. Wan, *J. Cluster Sci.*, 2015, **26**, 789–798.
786 E. L. Zhou, C. Qin, P. Huang, X. L. Wang, W. C. Chen, K. Z. Shao and Z. M. Su, *Chem. – Eur. J.*, 2015, **21**, 11894–11898.
787 P. Ju, Y. H. Xiang, Z. B. Xiang, M. Wang, Y. Zhao, D. Zhang, J. Q. Yu and X. X. Han, *RSC Adv.*, 2016, **6**, 17483–17493.
788 P. Ju, Y. Z. Yu, M. Wang, Y. Zhao, D. Zhang, C. J. Sun and X. X. Han, *J. Mater. Chem. B*, 2016, **4**, 6316–6325.
789 Q. Y. Liu, Y. L. Jiang, L. Y. Zhang, X. P. Zhou, X. T. Lv, Y. Y. Ding, L. F. Sun, P. P. Chen and H. L. Yin, *Mater. Sci. Eng., C*, 2016, **65**, 109–115.
790 Y. Lu, W. C. Ye, Q. Yang, J. Yu, Q. Wang, P. P. Zhou, C. M. Wang, D. S. Xue and S. Q. Zhao, *Sens. Actuators, B*, 2016, **230**, 721–730.
791 C. M. Maroneze, G. P. dos Santos, V. B. de Moraes, L. P. da Costa and L. T. Kubota, *Biosens. Bioelectron.*, 2016, **77**, 746–751.
792 B. Wang, P. Ju, D. Zhang, X. X. Han, L. Zheng, X. F. Yin and C. J. Sun, *Microchim. Acta*, 2016, **183**, 3025–3033.
793 L. Wang, H. Yang, J. He, Y. Y. Zhang, J. Yu and Y. H. Song, *Electrochim. Acta*, 2016, **213**, 691–697.
794 H. G. Yang, J. Q. Zha, P. Zhang, Y. H. Xiong, L. J. Su and F. G. Ye, *RSC Adv.*, 2016, **6**, 66963–66970.
795 H. H. Zeng, W. B. Qiu, L. Zhang, R. P. Liang and J. D. Qiu, *Anal. Chem.*, 2016, **88**, 6342–6348.

796 S. Chen, M. Chi, Z. Yang, M. Gao, C. Wang and X. Lu, *Inorg. Chem. Front.*, 2017, **4**, 1621–1627.
797 M. L. Cui, J. D. Zhou, Y. Zhao and Q. J. Song, *Sens. Actuators, B*, 2017, **243**, 203–210.
798 S. Kumar, P. Bhushan and S. Bhattacharya, *RSC Adv.*, 2017, **7**, 37568–37577.
799 K. Y. Luo and Z. Z. Shao, *Chin. J. Polym. Sci.*, 2017, **35**, 515–523.
800 W. W. Mao, B. Cai, Z. Z. Ye and J. Y. Huang, *J. Electroanal. Chem.*, 2017, **807**, 76–81.
801 Y. Qin, Q. Zhang, Y. D. Li, X. L. Liu, Z. X. Lu, L. Y. Zheng, S. X. Liu, Q. E. Cao and Z. T. Ding, *J. Mater. Chem. B*, 2017, **5**, 9365–9370.
802 Z. J. Qin, Y. Zhao, L. Lin, P. Zou, L. Zhang, H. Chen, Y. Wang, G. T. Wang and Y. S. Zhang, *Microchim. Acta*, 2017, **184**, 4513–4520.
803 H. Y. Shin, B. G. Kim, S. Cho, J. Lee, H. B. Na and M. I. Kim, *Microchim. Acta*, 2017, **184**, 2115–2122.
804 N. Sui, F. Y. Liu, K. Wang, F. X. Xie, L. N. Wang, J. J. Tang, M. H. Liu and W. W. Yu, *Sens. Actuators, B*, 2017, **252**, 1010–1015.
805 L. F. Sun, Y. Y. Ding, Y. L. Jiang and Q. Y. Liu, *Sens. Actuators, B*, 2017, **239**, 848–856.
806 L. Wu, W. M. Yin, X. C. Tan, P. Wang, F. Ding, H. Zhang, B. R. Wang, W. Y. Zhang and H. Y. Han, *Sens. Actuators, B*, 2017, **248**, 367–373.
807 S. Y. Wu, H. Huang, X. Feng, C. C. Du and W. B. Song, *Talanta*, 2017, **167**, 385–391.
808 Z. Z. Yang, F. Q. Ma, Y. Zhu, S. H. Chen, C. Wang and X. F. Lu, *Dalton Trans.*, 2017, **46**, 11171–11179.
809 S. Yousefinejad, H. Rasti, M. Hajebi, M. Kowsari, S. Sadravi and F. Honarasa, *Sens. Actuators, B*, 2017, **247**, 691–696.
810 Y. Zeng, F. F. Miao, Z. Y. Zhao, Y. T. Zhu, T. Liu, R. S. Chen, S. M. Liu, Z. S. Lv and F. Liang, *Appl. Sci.*, 2017, **7**, 924.
811 L. Y. Zhang, M. X. Chen, Y. L. Jiang, M. M. Chen, Y. N. Ding and Q. Y. Liu, *Sens. Actuators, B*, 2017, **239**, 28–35.
812 L. Y. Zhang, S. Li, M. M. Dong, Y. Jiang, R. Li, S. Zhang, X. X. Lv, L. J. Chen and H. Wang, *Biosens. Bioelectron.*, 2017, **87**, 1036–1043.
813 H. M. Zhao, Y. Li, B. Tan, Y. B. Zhang, X. C. Chen and X. Quan, *New J. Chem.*, 2017, **41**, 6700–6708.
814 X. L. Zhao, Z. H. Li, C. Chen, Y. H. Wu, Z. G. Zhu, H. L. Zhao and M. B. Lan, *Electroanalysis*, 2017, **29**, 1518–1523.
815 X. L. Zhao, Z. H. Li, C. Chen and Z. G. Zhu, *Mater. Sci. Technol.*, 2017, **25**, 56–60.
816 Y. N. Zhao, D. Q. Huo, J. Bao, M. Yang, M. Chen, J. Z. Hou, H. B. Fa and C. J. Hou, *Sens. Actuators, B*, 2017, **244**, 1037–1044.
817 T. G. Choleva, V. A. Gatselou, G. Z. Tsogas and D. L. Giokas, *Microchim. Acta*, 2018, **185**, 22.
818 Y. N. Ding, B. C. Yang, H. Liu, Z. X. Liu, X. Zhang, X. W. Zheng and Q. Y. Liu, *Sens. Actuators, B*, 2018, **259**, 775–783.
819 X. L. Ke, G. D. Zhu, Y. Dai, Y. Q. Shen, J. M. Yang and J. Y. Liu, *J. Electroanal. Chem.*, 2018, **817**, 176–183.
820 H. Y. Liu, M. R. Jiao, C. C. Gu and M. Z. Zhang, *J. Alloys Compd.*, 2018, **741**, 197–204.
821 X. G. Peng, G. P. Wan, L. H. Wu, M. Zeng, S. W. Lin and G. Z. Wang, *Sens. Actuators, B*, 2018, **257**, 166–177.
822 H. J. Ren, T. G. Ma, J. Zhao and R. Zhou, *Chem. Res. Chin. Univ.*, 2018, **34**, 260–268.
823 Y. Wang, D. Zhang and J. Wang, *Microchim. Acta*, 2018, **185**, 1.
824 Q. Xu, H. Yuan, X. L. Dong, Y. Zhang, M. Asif, Z. H. Dong, W. S. He, J. H. Ren, Y. M. Sun and F. Xiao, *Biosens. Bioelectron.*, 2018, **107**, 153–162.
825 F. Zarif, S. Rauf, M. Z. Qureshi, N. S. Shah, A. Hayat, N. Muhammad, A. Rahim, M. H. Nawaz and M. Nasir, *Microchim. Acta*, 2018, **185**, 302.
826 L. Zhang, Y. C. Zhu, Y. Y. Liang, W. W. Zhao, J. J. Xu and H. Y. Chen, *Anal. Chem.*, 2018, **90**, 5439–5444.
827 Y. H. Zhao, Y. Huang, J. L. Wu, X. L. Zhan, Y. Y. Xie, D. Y. Tang, H. Y. Cao and W. Yun, *RSC Adv.*, 2018, **8**, 7252–7259.
828 J. L. Zhu, W. Nie, Q. Wang, J. W. Li, H. Li, W. Wen, T. Bao, H. Y. Xiong, X. H. Zhang and S. F. Wang, *Carbon*, 2018, **129**, 29–37.
829 X. X. Zhu, W. Chen, K. L. Wu, H. Y. Li, M. Fu, Q. Y. Liu and X. Zhang, *New J. Chem.*, 2018, **42**, 1501–1509.
830 Z. W. Qi, L. Wang, Q. You and Y. Chen, *Biosens. Bioelectron.*, 2017, **96**, 227–232.
831 B. W. Liu, Z. Y. Sun, P.-J. J. Huang and J. W. Liu, *J. Am. Chem. Soc.*, 2015, **137**, 1290–1295.
832 A. Pratsinis, G. A. Kelesidis, S. Zuercher, F. Krumeich, S. Bolisetty, R. Mezzenga, J. C. Leroux and G. A. Sotiriou, *ACS Nano*, 2017, **11**, 12210–12218.
833 L. Z. Hu, Y. L. Yuan, L. Zhang, J. M. Zhao, S. Majeed and G. B. Xu, *Anal. Chim. Acta*, 2013, **762**, 83–86.
834 A. K. Dutta, S. K. Maji, P. Biswas and B. Adhikary, *Sens. Actuators, B*, 2013, **177**, 676–683.
835 R. M. Li, M. M. Zhen, M. R. Guan, D. Q. Chen, G. Q. Zhang, J. C. Ge, P. Gong, C. R. Wang and C. Y. Shu, *Biosens. Bioelectron.*, 2013, **47**, 502–507.
836 F. X. Qin, S. Y. Jia, F. F. Wang, S. H. Wu, J. Song and Y. Liu, *Catal. Sci. Technol.*, 2013, **3**, 2761–2768.
837 W. Zhang, Y. Zhang, Y. H. Chen, S. Y. Li, N. Gu, S. L. Hu, Y. Sun, X. Chen and Q. Li, *J. Nanosci. Nanotechnol.*, 2013, **13**, 60–67.
838 P. Hu, L. Han and S. J. Dong, *ACS Appl. Mater. Interfaces*, 2014, **6**, 500–506.
839 Q. Y. Liu, Q. Y. Jia, R. R. Zhu, Q. Shao, D. M. Wang, P. Cui and J. C. Ge, *Mater. Sci. Eng., C*, 2014, **42**, 177–184.
840 Q. Y. Liu, H. Li, Q. R. Zhao, R. R. Zhu, Y. T. Yang, Q. Y. Jia, B. Bian and L. H. Zhuo, *Mater. Sci. Eng., C*, 2014, **41**, 142–151.
841 L. Han, L. X. Zeng, M. D. Wei, C. M. Li and A. H. Liu, *Nanoscale*, 2015, **7**, 11678–11685.
842 R. Qu, L. L. Shen, A. T. Qu, R. L. Wang, Y. L. An and L. Q. Shi, *ACS Appl. Mater. Interfaces*, 2015, **7**, 16694–16705.

843 T. Tian, L. H. Ai, X. M. Liu, L. L. Li, J. Li and J. Jiang, *Ind. Eng. Chem. Res.*, 2015, **54**, 1171–1178.
844 N. Wang, B. C. Li, F. M. Qiao, J. C. Sun, H. Fan and S. Y. Ai, *J. Mater. Chem. B*, 2015, **3**, 7718–7723.
845 M. Y. Wu, S. J. Meng, Q. Wang, W. L. Si, W. Huang and X. C. Dong, *ACS Appl. Mater. Interfaces*, 2015, **7**, 21089–21094.
846 X. J. Zheng, Q. Zhu, H. Q. Song, X. R. Zhao, T. Yi, H. L. Chen and X. G. Chen, *ACS Appl. Mater. Interfaces*, 2015, **7**, 3480–3491.
847 S. Y. Zhu, X. E. Zhao, J. M. You, G. B. Xu and H. Wang, *Analyst*, 2015, **140**, 6398–6403.
848 H. M. Jia, D. F. Yang, X. N. Han, J. H. Cai, H. Y. Liu and W. W. He, *Nanoscale*, 2016, **8**, 5938–5945.
849 Q. Y. Liu, Y. Y. Ding, Y. T. Yang, L. Y. Zhang, L. F. Sun, P. P. Chen and C. Gao, *Mater. Sci. Eng., C*, 2016, **59**, 445–453.
850 Y. J. Long, X. L. Wang, D. J. Shen and H. Z. Zheng, *Talanta*, 2016, **159**, 122–126.
851 J. S. Mu, Y. He and Y. Wang, *Talanta*, 2016, **148**, 22–28.
852 X. H. Niu, Y. F. He, J. M. Pan, X. Li, F. X. Qiu, Y. S. Yan, L. B. Shi, H. L. Zhao and M. B. Lan, *Anal. Chim. Acta*, 2016, **947**, 42–49.
853 W. J. Zhang, C. P. Chen, D. X. Yang, G. X. Dong, S. J. Jia, B. X. Zhao, L. Yan, Q. Q. Yao, A. Sunna and Y. Liu, *Adv. Mater. Interfaces*, 2016, 1600590.
854 X. Z. Zhang, Y. Zhou, W. Zhang, Y. Zhang and N. Gu, *Colloids Surf., A*, 2016, **490**, 291–299.
855 Y. P. Zhong, C. Deng, Y. He, Y. L. Ge and G. W. Song, *Microchim. Acta*, 2016, **183**, 2823–2830.
856 G. Darabdhara, B. Sharma, M. R. Das, R. Boukherroub and S. Szunerits, *Sens. Actuators, B*, 2017, **238**, 842–851.
857 L. Han, P. Liu, H. J. Zhang, F. Li and A. H. Liu, *Chem. Commun.*, 2017, **53**, 5216–5219.
858 L. Han, J. G. Shi and A. H. Liu, *Sens. Actuators, B*, 2017, **252**, 919–926.
859 W. Huang, T. Y. Lin, Y. Cao, X. Y. Lai, J. Peng and J. C. Tu, *Sensors*, 2017, **17**, 217.
860 R. M. Li, Y. Zhou, L. Zou, S. M. Li, J. Wang, C. Y. Shu, C. R. Wang, J. C. Ge and L. S. Ling, *Sens. Actuators, B*, 2017, **245**, 656–664.
861 J. Y. Lu, L. Q. Wei, D. M. Yao, X. J. Yin, H. F. Lai and X. X. Huang, *J. Chin. Chem. Soc.*, 2017, **64**, 795–803.
862 N. Lu, M. Zhang, L. Ding, J. Zheng, C. X. Zeng, Y. L. Wen, G. Liu, A. Aldalbahi, J. Y. Shi, S. P. Song, X. L. Zuo and L. H. Wang, *Nanoscale*, 2017, **9**, 4508–4515.
863 S. J. Luo, Y. Q. Liu, H. B. Rao, Y. Y. Wang and X. X. Wang, *Anal. Biochem.*, 2017, **538**, 26–33.
864 L. Rastogi, D. Karunasagar, R. B. Sashidhar and A. Giri, *Sens. Actuators, B*, 2017, **240**, 1182–1188.
865 S. Rauf, M. A. H. Nawaz, N. Muhammad, R. Raza, S. A. Shahid, J. L. Marty and A. Hayat, *J. Mol. Liq.*, 2017, **243**, 333–340.
866 S. S. Song, Y. Liu, A. X. Song, Z. D. Zhao, H. S. Lu and J. C. Hao, *J. Colloid Interface Sci.*, 2017, **506**, 46–57.
867 C. K. Su and J. C. Chen, *Sens. Actuators, B*, 2017, **247**, 641–647.
868 L. Su, W. P. Dong, C. K. Wu, Y. J. Gong, Y. Zhang, L. Li, G. J. Mao and S. L. Feng, *Anal. Chim. Acta*, 2017, **951**, 124–132.
869 L. Su, X. A. Yu, Y. X. Cai, P. H. Kang, W. J. Qin, W. P. Dong, G. J. Mao and S. L. Feng, *Anal. Chim. Acta*, 2017, **987**, 98–104.
870 L. Su, X. A. Yu, W. J. Qin, W. P. Dong, C. K. Wu, Y. Zhang, G. J. Mao and S. L. Feng, *J. Mater. Chem. B*, 2017, **5**, 116–122.
871 N. S. Surgutskaya, M. E. Trusova, G. B. Slepchenko, A. S. Minin, A. G. Pershina, M. A. Uimin, A. E. Yermakov and P. S. Postnikov, *Anal. Methods*, 2017, **9**, 2433–2439.
872 X. K. Tian, X. Wang, C. Dai, Y. Li, C. Yang, Z. X. Zhou and Y. X. Wang, *Sens. Actuators, B*, 2017, **245**, 221–229.
873 Q. Q. Wang, X. P. Zhang, L. Huang, Z. Q. Zhang and S. J. Dong, *ACS Appl. Mater. Interfaces*, 2017, **9**, 7465–7471.
874 Y. M. Wang, J. W. Liu, J. H. Jiang and W. Zhong, *Anal. Bioanal. Chem.*, 2017, **409**, 4225–4232.
875 S. Bhagat, N. V. S. Vallabani, V. Shutthanandan, M. Bowden, A. S. Karakoti and S. Singh, *J. Colloid Interface Sci.*, 2018, **513**, 831–842.
876 W. Dong, Y. Zhuang, S. Li, X. Zhang, H. Chai and Y. Huang, *Sens. Actuators, B*, 2018, **255**, 2050–2057.
877 A. Khataee, M. H. Irani-nezhad and J. Hassanzadeh, *Microchim. Acta*, 2018, **185**, 190.
878 N. Salarizadeh, M. Sadri and R. H. Sajedi, *Appl. Organomet. Chem.*, 2018, **32**, e4018.
879 H. P. Song, Y. Lee, B. Vu Khac Hoang, Y. K. Oh, H. G. Park, M. I. Kim and Y. C. Lee, *Sensors*, 2018, **18**, 457.
880 S. Tanaka, Y. V. Kaneti, R. Bhattacharjee, M. N. Islam, R. Nakahata, N. Abdullah, S.-i. Yusa, N. Nam-Trung, M. J. A. Shiddiky, Y. Yamauchi and M. S. A. Hossain, *ACS Appl. Mater. Interfaces*, 2018, **10**, 1039–1049.
881 Vinita, N. R. Nirala and R. Prakash, *Sens. Actuators, B*, 2018, **263**, 109–119.
882 S. D. Xu, W. D. Li, X. Xu and H. D. Wang, *Phys. Test. Chem. Anal., Part B*, 2018, **54**, 18–23.
883 J. Zhao, W. F. Dong, X. D. Zhang, H. X. Chai and Y. M. Huang, *Sens. Actuators, B*, 2018, **263**, 575–584.
884 L. Deng, C. G. Chen, C. Z. Zhu, S. J. Dong and H. M. Lu, *Biosens. Bioelectron.*, 2014, **52**, 324–329.
885 A. L. Hu, Y. H. Liu, H. H. Deng, G. L. Hong, A. L. Liu, X. H. Lin, X. H. Xia and W. Chen, *Biosens. Bioelectron.*, 2014, **61**, 374–378.
886 D. Feng, Q. S. Li, F. Liu, H. J. Li, D. H. Li and J. G. Shi, *Transd. Microsys. Technol.*, 2015, **34**, 5–8.
887 M. I. Kim, D. Cho and H. G. Park, *J. Nanosci. Nanotechnol.*, 2015, **15**, 7955–7961.
888 N. R. Nirala, S. Abraham, V. Kumar, A. Bansal, A. Srivastava and P. S. Saxena, *Sens. Actuators, B*, 2015, **218**, 42–50.
889 N. R. Nirala, S. Pandey, A. Bansal, V. K. Singh, B. Mukherjee, P. S. Saxena and A. Srivastava, *Biosens. Bioelectron.*, 2015, **74**, 207–213.

890 J. Qian, X. W. Yang, Z. T. Yang, G. B. Zhu, H. P. Mao and K. Wang, *J. Mater. Chem. B*, 2015, **3**, 1624–1632.
891 W. J. Shi, H. Fan, S. Y. Ai and L. S. Zhu, *Sens. Actuators, B*, 2015, **221**, 1515–1522.
892 S. J. Xu, Y. Q. Wang, D. Y. Zhou, M. Kuang, D. Fang, W. H. Yang, S. J. Wei and L. Ma, *Sci. Rep.*, 2016, **6**, 39157.
893 Y. F. He, X. H. Niu, L. B. Shi, H. L. Zhao, X. Li, W. C. Zhang, J. M. Pan, X. F. Zhang, Y. S. Yan and M. B. Lan, *Microchim. Acta*, 2017, **184**, 2181–2189.
894 X. T. Sun, Y. Zhang, D. H. Zheng, S. Yue, C. G. Yang and Z. R. Xu, *Biosens. Bioelectron.*, 2017, **92**, 81–86.
895 Y. Z. Wu, Y. J. Ma, G. H. Xu, F. D. Wei, Y. S. Ma, Q. Song, X. Wang, T. Tang, Y. Y. Song, M. L. Shi, X. M. Xu and Q. Hu, *Sens. Actuators, B*, 2017, **249**, 195–202.
896 Y. Zhang, Y. N. Wang, X. T. Sun, L. Chen and Z. R. Xu, *Sens. Actuators, B*, 2017, **246**, 118–126.
897 J. Hassanzadeh and A. Khataee, *Talanta*, 2018, **178**, 992–1000.
898 S. B. He, G. W. Wu, H. H. Deng, A. L. Liu, X. H. Lin, X. H. Xia and W. Chen, *Biosens. Bioelectron.*, 2014, **62**, 331–336.
899 N. R. Nirala, Vinita and R. Prakash, *Microchim. Acta*, 2018, **185**, 224.
900 Z. Y. Yan, Q. Q. Niu, M. Y. Mou, Y. Wu, X. X. Liu and S. H. Liao, *J. Nanopart. Res.*, 2017, **19**, 235.
901 Y. Zhao, Y. C. Huang, H. Zhu, Q. Q. Zhu and Y. S. Xia, *J. Am. Chem. Soc.*, 2016, **138**, 16645–16654.
902 G. L. Wang, K. L. Liu, J. X. Shu, T. T. Gu, X. M. Wu, Y. M. Dong and Z. J. Li, *Biosens. Bioelectron.*, 2015, **69**, 106–112.
903 G. Y. Zhang, S. Y. Deng, W. R. Cai, S. Cosnier, X. J. Zhang and D. Shan, *Anal. Chem.*, 2015, **87**, 9093–9100.
904 H. Zhou, T. Q. Han, Q. Wei and S. S. Zhang, *Anal. Chem.*, 2016, **88**, 2976–2983.
905 Q. B. Wang, J. P. Lei, S. Y. Deng, L. Zhang and H. X. Ju, *Chem. Commun.*, 2013, **49**, 916–918.
906 R. Bhattacharjee, S. Tanaka, S. Moriam, M. K. Masud, J. Lin, S. M. Alshehri, T. Ahamad, R. R. Salunkhe, N. T. Nguyen, Y. Yamauchi, M. S. Hossain and M. J. A. Shiddiky, *J. Mater. Chem. B*, 2018, **6**, 4783–4791.
907 L. Tian, J. X. Qi, O. Oderinde, C. Yao, W. Song and Y. H. Wang, *Biosens. Bioelectron.*, 2018, **110**, 110–117.
908 L. Y. Chau, Q. J. He, A. L. Qin, S. P. Yip and T. M. H. Lee, *J. Mater. Chem. B*, 2016, **4**, 4076–4083.
909 C. H. Chen, N. X. Li, J. W. Lan, X. H. Ji and Z. K. He, *Anal. Chim. Acta*, 2016, **902**, 154–159.
910 B. Tan, H. M. Zhao, W. H. Wu, X. Liu, Y. B. Zhang and X. Quan, *Nanoscale*, 2017, **9**, 18699–18710.
911 M. I. Kim, K. S. Park and H. G. Park, *Chem. Commun.*, 2014, **50**, 9577–9580.
912 Y. J. Song, Y. C. Wang and L. D. Qin, *J. Am. Chem. Soc.*, 2013, **135**, 16785–16788.
913 Z. Q. Gao, M. D. Xu, L. Hou, G. N. Chen and D. P. Tang, *Anal. Chem.*, 2013, **85**, 6945–6952.
914 Z. Q. Gao, L. Hou, M. D. Xu and D. P. Tang, *Sci. Rep.*, 2014, **4**, 3966.
915 S. G. Ge, M. W. Sun, W. Y. Liu, S. Li, X. Wang, C. C. Chu, M. Yan and J. H. Yu, *Sens. Actuators, B*, 2014, **192**, 317–326.
916 S. Kumari, B. B. Dhar, C. Panda, A. Meena and S. Sen Gupta, *ACS Appl. Mater. Interfaces*, 2014, **6**, 13866–13873.
917 W. Q. Lai, J. Y. Zhuang, X. H. Que, L. B. Fu and D. P. Tang, *Biomater. Sci.*, 2014, **2**, 1073–1079.
918 W. Y. Liu, H. M. Yang, Y. A. Ding, S. G. Ge, J. H. Yu, M. Yan and X. R. Song, *Analyst*, 2014, **139**, 251–258.
919 Y. J. Song, X. F. Xia, X. F. Wu, P. Wang and L. D. Qin, *Angew. Chem., Int. Ed.*, 2014, **53**, 12451–12455.
920 Z. H. Yang, Y. Q. Chai, R. Yuan, Y. Zhuo, Y. Li, J. Han and N. Liao, *Sens. Actuators, B*, 2014, **193**, 461–466.
921 L. Y. Jin, Y. M. Dong, X. M. Wu, G. X. Cao and G. L. Wang, *Anal. Chem.*, 2015, **87**, 10429–10436.
922 Y. Li, J. Xuan, Y. J. Song, P. Wang and L. D. Qin, *Lab Chip*, 2015, **15**, 3300–3306.
923 L. L. Liang, S. G. Ge, L. Li, F. Liu and J. H. Yu, *Anal. Chim. Acta*, 2015, **862**, 70–76.
924 J. M. Park, H. W. Jung, Y. W. Chang, H. S. Kim, M. J. Kang and J. C. Pyun, *Anal. Chim. Acta*, 2015, **853**, 360–367.
925 Z. M. Tian, J. Li, Z. Y. Zhang, W. Gao, X. M. Zhou and Y. Q. Qu, *Biomaterials*, 2015, **59**, 116–124.
926 J. X. Wang, Y. Zhuo, Y. Zhou, R. Yuan and Y. Q. Chai, *Biosens. Bioelectron.*, 2015, **71**, 407–413.
927 Y. L. Wang, Y. G. Wang, X. H. Pang, B. Du, H. Li, D. Wu and Q. Wei, *Sens. Actuators, B*, 2015, **214**, 124–131.
928 S. R. Ahmed, J. Kim, T. Suzuki, J. Lee and E. Y. Park, *Biotechnol. Bioeng.*, 2016, **113**, 2298–2303.
929 T. Jiang, Y. Song, D. Du, X. T. Liu and Y. H. Lin, *ACS Sens.*, 2016, **1**, 717–724.
930 S. S. Wang, Z. P. Chen, J. Choo and L. X. Chen, *Anal. Bioanal. Chem.*, 2016, **408**, 1015–1022.
931 Q. Zhao, H. W. Huang, L. Y. Zhang, L. Q. Wang, Y. L. Zeng, X. D. Xia, F. P. Liu and Y. Chen, *Anal. Chem.*, 2016, **88**, 1412–1418.
932 Y. L. Zhao, H. Zhang, X. C. Wang and X. M. Xie, *Acad. J. Second Mil. Med. Univ.*, 2016, **37**, 1533–1537.
933 Z. Q. Gao, S. Z. Lv, M. D. Xu and D. P. Tang, *Analyst*, 2017, **142**, 911–917.
934 L. Y. Guo, P. Qian and M. H. Yang, *Anal. Lett.*, 2017, **50**, 1803–1811.
935 L. Jiao, L. H. Zhang, W. W. Du, S. Q. Liu, Q. Wei and H. Li, *Electrochim. Acta*, 2017, **252**, 374–380.
936 J. X. Li, Z. Q. Gao, H. H. Ye, S. L. Wan, M. Pierce, D. P. Tang and X. H. Xia, *Chem. Commun.*, 2017, **53**, 9055–9058.
937 J. H. T. Luong and S. K. Vashist, *Biosens. Bioelectron.*, 2017, **89**, 293–304.
938 M. K. Masud, S. Yadav, M. N. Isam, N. Nam-Trung, C. Salomon, R. Kline, H. R. Alamri, Z. A. Alothman, Y. Yamauchi, M. S. A. Hossain and M. J. A. Shiddiky, *Anal. Chem.*, 2017, **89**, 11005–11013.
939 S. Cho, S. M. Lee, H. Y. Shin, M. S. Kim, Y. H. Seo, Y. K. Cho, J. Lee, S. P. Lee and M. Il Kim, *Analyst*, 2018, **143**, 1182–1187.

940 Z. Farka, V. Cunderlova, V. Horackova, M. Pastucha, Z. Mikusova, A. Hlavacek and P. Skladal, *Anal. Chem.*, 2018, **90**, 2348–2354.
941 Z. Q. Gao, Y. Y. Li, X. B. Zhang, J. H. Feng, L. Kong, P. Wang, Z. W. Chen, Y. H. Dong and Q. Wei, *Biosens. Bioelectron.*, 2018, **102**, 189–195.
942 J. Li, Y. Cao, S. S. Hinman, K. S. McKeating, Y. Guan, X. Hu, Q. Cheng and Z. Yang, *Biosens. Bioelectron.*, 2018, **100**, 304–311.
943 D. D. Lou, Y. Y. Tian, Y. Zhang, J. J. Yin, T. Yang, C. He, M. Ma, W. Yu and N. Gu, *J. Nanosci. Nanotechnol.*, 2018, **18**, 951–958.
944 C. N. Loynachan, M. R. Thomas, E. R. Gray, D. A. Richards, J. Kim, B. S. Miller, J. C. Brookes, S. Agarwal, V. Chudasama, R. A. McKendry and M. M. Stevens, *ACS Nano*, 2018, **12**, 279–288.
945 Y. C. Ma, M. Y. Lu, Y. Deng, R. Y. Bai, X. Zhang, D. L. Li, K. L. Zhang, R. Hu and Y. H. Yang, *J. Biomed. Nanotechnol.*, 2018, **14**, 1169–1177.
946 S. Oh, J. Kim, T. Van Tan, D. K. Lee, S. R. Ahmed, J. C. Hong, J. Lee, E. Y. Park and J. Lee, *ACS Appl. Mater. Interfaces*, 2018, **10**, 12534–12543.
947 L. Y. Zhang, C. Fan, M. Liu, F. J. Liu, S. S. Bian, S. Y. Du, S. Y. Zhu and H. Wang, *Sens. Actuators, B*, 2018, **266**, 543–552.
948 Y. Zhao, M. Yang, Q. Fu, H. Ouyang, W. Wen, Y. Song, C. Zhu, Y. Lin and D. Du, *Anal. Chem.*, 2018, **90**, 7391–7398.
949 D. M. Duan, K. L. Fan, D. X. Zhang, S. G. Tan, M. F. Liang, Y. Liu, J. L. Zhang, P. H. Zhang, W. Liu, X. G. Qiu, G. P. Kobinger, G. F. Gao and X. Y. Yan, *Biosens. Bioelectron.*, 2015, **74**, 134–141.
950 W. J. Xu, S. Y. Xue, H. Y. Yi, P. Jing, Y. Q. Chai and R. Yuan, *Chem. Commun.*, 2015, **51**, 1472–1474.
951 C. W. Wu, S. G. Harroun, C. W. Lien, H. T. Chang, B. Unnikrishnan, I. P. J. Lai, J. Y. Chang and C. C. Huang, *Sens. Actuators, B*, 2016, **227**, 100–107.
952 Y. Zhang, W. Ren, H. Q. Luo and N. B. Li, *Biosens. Bioelectron.*, 2016, **80**, 463–470.
953 L. Wang, W. Yang, T. F. Li, D. Li, Z. M. Cui, Y. Wang, S. L. Ji, Q. X. Song, C. Shu and L. Ding, *Microchim. Acta*, 2017, **184**, 3145–3151.
954 J. J. Yang, J. T. Cao, Y. L. Wang, H. Wang, Y. M. Liu and S. H. Ma, *J. Electroanal. Chem.*, 2017, **787**, 88–94.
955 H. P. Song, J. Y. Jang, S. H. Bae, S. B. Choi, B. J. Yu and M. I. Kim, *J. Nanosci. Nanotechnol.*, 2018, **18**, 6570–6574.
956 C. C. Chang, C. P. Chen, C. H. Lee, C. Y. Chen and C. W. Lin, *Chem. Commun.*, 2014, **50**, 14443–14446.
957 Y. Z. Wang, W. J. Qi and Y. J. Song, *Chem. Commun.*, 2016, **52**, 7994–7997.
958 X. N. Li, F. Wen, B. Creran, Y. Jeong, X. R. Zhang and V. M. Rotello, *Small*, 2012, **8**, 3589–3592.
959 J. E. Yang, Y. X. Lu, L. Ao, F. Y. Wang, W. J. Jing, S. C. Zhang and Y. Y. Liu, *Sens. Actuators, B*, 2017, **245**, 66–73.
960 C. L. Sun, X. L. Chen, J. Xu, M. J. Wei, J. J. Wang, X. G. Mi, X. H. Wang, Y. Wu and Y. Liu, *J. Mater. Chem. A*, 2013, **1**, 4699–4705.
961 Z. F. Wang, S. Zheng, J. Cai, P. Wang, J. Feng, X. Yang, L. M. Zhang, M. Ji, F. G. Wu, N. Y. He and N. Wan, *Anal. Chem.*, 2013, **85**, 11602–11609.
962 M. I. Kim, M. S. Kim, M. A. Woo, Y. Ye, K. S. Kang, J. Lee and H. G. Park, *Nanoscale*, 2014, **6**, 1529–1536.
963 G. L. Wang, X. F. Xu, L. Qiu, Y. M. Dong, Z. J. Li and C. Zhang, *ACS Appl. Mater. Interfaces*, 2014, **6**, 6434–6442.
964 J. Liu, M. R. Cui, L. Niu, H. Zhou and S. S. Zhang, *Chem. – Eur. J.*, 2016, **22**, 18001–18008.
965 Y. Tao, M. Li, B. Kim and D. T. Auguste, *Theranostics*, 2017, **7**, 899–911.
966 G. W. Wu, Y. M. Shen, X. Q. Shi, H. H. Deng, X. Q. Zheng, H. P. Peng, A. L. Liu, X. H. Xia and W. Chen, *Anal. Chim. Acta*, 2017, **971**, 88–96.
967 L. Gao, M. Q. Liu, G. F. Ma, Y. L. Wang, L. N. Zhao, Q. Yuan, F. P. Gao, R. Liu, J. Zhai, Z. F. Chai, Y. L. Zhao and X. Y. Gao, *ACS Nano*, 2015, **9**, 10979–10990.
968 J. R. Li, J. Wang, Y. L. Wang and M. Trau, *Analyst*, 2017, **142**, 4788–4793.
969 L. Tian, J. X. Qi, K. Qian, O. Oderinde, Q. Y. Liu, C. Yao, W. Song and Y. H. Wang, *J. Electroanal. Chem.*, 2018, **812**, 1–9.
970 L. Tian, J. X. Qi, K. Qian, O. Oderinde, Y. Y. Cai, C. Yao, W. Song and Y. H. Wang, *Sens. Actuators, B*, 2018, **260**, 676–684.
971 L. N. Zhang, H. H. Deng, F. L. Lin, X. W. Xu, S. H. Weng, A. L. Liu, X. H. Lin, X. H. Xia and W. Chen, *Anal. Chem.*, 2014, **86**, 2711–2718.
972 T. T. Zheng, Q. F. Zhang, S. Feng, J. J. Zhu, Q. Wang and H. Wang, *J. Am. Chem. Soc.*, 2014, **136**, 2288–2291.
973 Y. S. Kim and J. Jurng, *Sens. Actuators, B*, 2013, **176**, 253–257.
974 B. Z. Zou, Y. Liu, J. Wang and C. Z. Huang, *Sci. Sin.: Chim.*, 2014, **44**, 1641–1646.
975 J. J. Zhang, P. Q. Dai, C. Li, N. W. Li, G. F. Cheng, P. G. He and Y. Z. Fang, *Acta Chim. Sin.*, 2014, **72**, 1029–1035.
976 Y. Q. Chang, Z. Zhang, J. H. Hao, W. S. Yang and J. L. Tang, *Sens. Actuators, B*, 2016, **232**, 692–697.
977 L. L. Guo, L. Mao, K. X. Huang and H. M. Liu, *J. Mater. Sci.*, 2017, **52**, 10738–10750.
978 Y. Liu, D. Ding, Y. L. Zhen and R. Guo, *Biosens. Bioelectron.*, 2017, **92**, 140–146.
979 Y. W. Wang, M. L. Wang, L. X. Wang, H. Xu, S. R. Tang, H. H. Yang, L. Zhang and H. B. Song, *Sensors*, 2017, **17**, 2521.
980 C. F. Jiang, Z. J. Li, Y. X. Wu, W. Guo, J. S. Wang and Q. Jiang, *Bull. Korean Chem. Soc.*, 2018, **39**, 625–630.
981 Z. Q. Gao, G. G. Liu, H. H. Ye, R. Rauschendorfer, D. P. Tang and X. H. Xia, *Anal. Chem.*, 2017, **89**, 3622–3629.
982 T. Aditya, J. Jana, R. Sahoo, A. Roy, A. Pal and T. Pal, *Cryst. Growth Des.*, 2017, **17**, 295–307.

983 X. Q. Li, F. Yuan, G. X. Cao and G. L. Wang, *J. Instrum. Anal.*, 2017, **36**, 794–799.
984 Y. Liu, Y. P. Xiang, Y. L. Zhen and R. Guo, *Langmuir*, 2017, **33**, 6372–6381.
985 Y. Liu, Y. L. Zheng, D. Ding and R. Guo, *Langmuir*, 2017, **33**, 13811–13820.
986 S. Singh, K. Mitra, A. Shukla, R. Singh, R. K. Gundampati, N. Misra, P. Maiti and B. Ray, *Anal. Chem.*, 2017, **89**, 783–791.
987 H. Liao, L. Z. Hu, Y. Zhang, X. R. Yu, Y. L. Liu and R. Li, *Microchim. Acta*, 2018, **185**, 143.
988 L. X. Lu, Y. Wang, X. X. Lin, X. Y. Li and M. N. Xin, *Chin. J. Anal. Chem.*, 2018, **46**, 94–99.
989 C. W. Lien, B. Unnikrishnan, S. G. Harroun, C. M. Wang, J. Y. Chang, H. T. Chang and C. C. Huang, *Biosens. Bioelectron.*, 2018, **102**, 510–517.
990 Z. B. Chen, L. L. Tan, S. X. Wang, Y. M. Zhang and Y. H. Li, *Biosens. Bioelectron.*, 2016, **79**, 749–757.
991 L. Qin, X. Y. Wang, Y. F. Liu and H. Wei, *Anal. Chem.*, 2018, **90**, 9983–9989.
992 X. Liu, Q. Wang, Y. Zhang, L. C. Zhang, Y. Y. Su and Y. Lv, *New J. Chem.*, 2013, **37**, 2174–2178.
993 R. Thiramanas, K. Jangpatarapongsa, P. Tangboriboonrat and D. Polpanich, *Anal. Chem.*, 2013, **85**, 5996–6002.
994 A. Hayat, G. Bulbul and S. Andreescu, *Biosens. Bioelectron.*, 2014, **56**, 334–339.
995 P. Jing, W. J. Xu, H. Y. Yi, Y. M. Wu, L. J. Bai and R. Yuan, *Analyst*, 2014, **139**, 1756–1761.
996 Y. H. Ma, C. F. Yu and X. G. Chen, *J. Anal. Sci.*, 2014, **30**, 709–712.
997 Y. Shi, P. Su, Y. Y. Wang and Y. Yang, *Talanta*, 2014, **130**, 259–264.
998 S. Chinthakindi, A. Purohit, V. Singh, V. Tak, D. R. Goud, D. K. Dubey and D. Pardasani, *J. Chromatogr. A*, 2015, **1394**, 9–17.
999 W. Y. Liu, H. M. Yang, S. G. Ge, L. Shen, J. H. Yu, M. Yan and J. D. Huang, *Sens. Actuators, B*, 2015, **209**, 32–39.
1000 P. C. Pandey, R. Singh and Y. Pandey, *RSC Adv.*, 2015, **5**, 49671–49679.
1001 S. Sadeghi, E. Fooladi and M. Malekaneh, *Appl. Biochem. Biotechnol.*, 2015, **175**, 1603–1616.
1002 N. P. Sardesai, M. Ganesana, A. Karimi, J. C. Leiter and S. Andreescu, *Anal. Chem.*, 2015, **87**, 2996–3003.
1003 S. L. Wei, J. W. Li and Y. Liu, *RSC Adv.*, 2015, **5**, 107670.
1004 D. Y. Zhang, Z. Chen, H. Omar, L. Deng and N. M. Khashab, *ACS Appl. Mater. Interfaces*, 2015, **7**, 4589–4594.
1005 Z. J. Zhang, Y. J. Guan, M. Li, A. D. Zhao, J. S. Ren and X. G. Qu, *Chem. Sci.*, 2015, **6**, 2822–2826.
1006 G. Bulbul, A. Hayat and S. Andreescu, *Nanoscale*, 2015, **7**, 13230–13238.
1007 G. X. Cao, X. M. Wu, Y. M. Dong, Z. J. Li and G. L. Wang, *Microchim. Acta*, 2016, **183**, 441–448.
1008 Y. C. Chang, Y. S. Lin, G. T. Xiao, T. C. Chiu and C. C. Hu, *Talanta*, 2016, **161**, 94–98.
1009 J. Chen, J. Ge, L. Zhang, Z. H. Li, J. J. Li, Y. J. Sun and L. B. Qu, *Microchim. Acta*, 2016, **183**, 1847–1853.
1010 H. H. Deng, G. L. Hong, F. L. Lin, A. L. Liu, X. H. Xia and W. Chen, *Anal. Chim. Acta*, 2016, **915**, 74–80.
1011 S. Q. Deng, H. Y. Zou, J. Lan and C. Z. Huang, *Anal. Methods*, 2016, **8**, 7516–7521.
1012 F. P. Liu, J. Q. Tang, J. Xu, Y. Shu, Q. Xu, H. M. Wang and X. Y. Hu, *Biosens. Bioelectron.*, 2016, **86**, 871–878.
1013 K. F. Peng, H. W. Zhao, P. Xie, S. Hu, Y. L. Yuan, R. Yuan and X. F. Wu, *Biosens. Bioelectron.*, 2016, **81**, 1–7.
1014 X. Y. Yan, Y. Gu, C. Li, L. Tang, B. Zheng, Y. R. Li, Z. Q. Zhang and M. Yang, *Biosens. Bioelectron.*, 2016, **77**, 1032–1038.
1015 P. C. Zhang, Y. H. Li, J. Zhen, J. Y. Chen, D. D. Chen, Y. Quan and R. J. Cui, *J. Anal. Sci.*, 2016, **32**, 769–773.
1016 S. S. Fan, M. G. Zhao, L. J. Ding, H. Li and S. G. Chen, *Biosens. Bioelectron.*, 2017, **89**, 846–852.
1017 M. Hosseini, M. Aghazadeh and M. R. Ganjali, *New J. Chem.*, 2017, **41**, 12678–12684.
1018 Y. Z. Jiang, N. Song, C. Wang, N. Pinna and X. F. Lu, *J. Mater. Chem. B*, 2017, **5**, 5499–5505.
1019 W. Lai, Q. Wei, M. Xu, J. Zhuang and D. Tang, *Biosens. Bioelectron.*, 2017, **89**, 645–651.
1020 S. Mumtaz, S. Wang, S. Z. Hussain, M. Abdullah, Z. Huma, Z. Iqbal, B. Creran, V. M. Rotello and I. Hussain, *Chem. Commun.*, 2017, **53**, 12306–12308.
1021 S. Sloan Dennison, N. C. Shand, D. Graham and K. Faulds, *Analyst*, 2017, **142**, 4715–4720.
1022 X. H. Wang, Q. S. Han, S. F. Cai, T. Wang, C. Qi, R. Yang and C. Wang, *Analyst*, 2017, **142**, 2500–2506.
1023 J. G. You, Y. W. Liu, C. Y. Lu, W. L. Tseng and C. J. Yu, *Biosens. Bioelectron.*, 2017, **92**, 442–448.
1024 Y. F. He, F. Qi, X. H. Niu, W. C. Zhang, X. F. Zhang and J. M. Pan, *Anal. Chim. Acta*, 2018, **1021**, 113–120.
1025 P. C. Kuo, C. W. Lien, J. Y. Mao, B. Unnikrishnan, H. T. Chang, H. J. Lin and C. C. Huang, *Anal. Chim. Acta*, 2018, **1009**, 89–97.
1026 P. Liu, L. Han, F. Wang, X. Q. Li, V. A. Petrenko and A. H. Liu, *Nanoscale*, 2018, **10**, 2825–2833.
1027 X. H. Niu, Y. F. He, W. C. Zhang, X. Li, F. X. Qiu and J. M. Pan, *Sens. Actuators, B*, 2018, **256**, 151–159.
1028 H. Ouyang, X. M. Tu, Z. F. Fu, W. W. Wang, S. F. Fu, C. Z. Zhu, D. Du and Y. H. Lin, *Biosens. Bioelectron.*, 2018, **106**, 43–49.
1029 N. Qiu, Y. Liu, M. Xiang, X. M. Lu, Q. Yang and R. Guo, *Sens. Actuators, B*, 2018, **266**, 86–94.
1030 Y. W. Song, M. G. Zhao, H. Li, X. T. Wang, Y. F. Cheng, L. J. Ding, S. S. Fan and S. G. Chen, *Sens. Actuators, B*, 2018, **255**, 1927–1936.
1031 Y. L. Wang, P. J. Ni, S. Jiang, W. D. Lu, Z. Li, H. M. Liu, J. Lin, Y. J. Sun and Z. Li, *Sens. Actuators, B*, 2018, **254**, 1118–1124.
1032 Z. W. Xiong, H. X. Zhong, S. Zheng, P. X. Deng, N. Li, W. Yun and L. Z. Yang, *Anal. Methods*, 2018, **10**, 2450–2455.

1033 Z. Zhang, N. F. Zhu, Y. M. Zou, X. Y. Wu, G. B. Qu and J. B. Shi, *Talanta*, 2018, **179**, 64–69.
1034 Y. Zhu, Z. Z. Yang, M. Q. Chi, M. X. Li, C. Wang and X. F. Lu, *Talanta*, 2018, **181**, 431–439.
1035 X. Wang, L. Qin, M. Zhou, Z. Lou and H. Wei, *Anal. Chem.*, 2018, **90**, 11696–11702.
1036 P. J. Ni, H. C. Dai, Y. L. Wang, Y. J. Sun, Y. Shi, J. T. Hu and Z. Li, *Biosens. Bioelectron.*, 2014, **60**, 286–291.
1037 J. Ju, R. Z. Zhang and W. Chen, *Sens. Actuators, B*, 2016, **228**, 66–73.
1038 L. L. Wu, L. Y. Wang, Z. J. Xie, N. Pan and C. F. Peng, *Sens. Actuators, B*, 2016, **235**, 110–116.
1039 J. Liu, L. J. Meng, Z. F. Fei, P. J. Dyson, X. N. Jing and X. Liu, *Biosens. Bioelectron.*, 2017, **90**, 69–74.
1040 N. Pan, L. Y. Wang, L. L. Wu, C. F. Peng and Z. J. Xie, *Microchim. Acta*, 2017, **184**, 65–72.
1041 M. Singh, P. Weerathunge, P. D. Liyanage, E. Mayes, R. Ramanathan and V. Bansal, *Langmuir*, 2017, **33**, 10006–10015.
1042 H. H. Xu, H. H. Deng, X. Q. Lin, Y. Y. Wu, X. L. Lin, H. P. Peng, A. L. Liu, X. H. Xia and W. Chen, *Microchim. Acta*, 2017, **184**, 3945–3951.
1043 Z. Z. Yang, Y. Zhu, G. D. Nie, M. X. Li, C. Wang and X. F. Lu, *Dalton Trans.*, 2017, **46**, 8942–8949.
1044 H. Y. Zou, T. Yang, J. Lan and C. Z. Huang, *Anal. Methods*, 2017, **9**, 841–846.
1045 S. H. Chen, M. Q. Chi, Y. Zhu, M. Gao, C. Wang and X. F. Lu, *Appl. Surf. Sci.*, 2018, **440**, 237–244.
1046 S. Q. Li, L. T. Wang, X. D. Zhang, H. X. Chai and Y. M. Huang, *Sens. Actuators, B*, 2018, **264**, 312–319.
1047 T. Wang, P. Su, F. Y. Lin, Y. Yang and Y. Yang, *Sens. Actuators, B*, 2018, **254**, 329–336.
1048 Y. M. Wang, J. W. Liu, G. B. Adkins, W. Shen, M. P. Trinh, L. Y. Duan, J. H. Jiang and W. Zhong, *Anal. Chem.*, 2017, **89**, 12327–12333.
1049 S. J. Wu, N. Duan, Y. T. Qiu, J. H. Li and Z. P. Wang, *Int. J. Food Microbiol.*, 2017, **261**, 42–48.
1050 Z. T. Yang, J. Qian, X. W. Yang, D. Jiang, X. J. Du, K. Wang, H. P. Mao and K. Wang, *Biosens. Bioelectron.*, 2015, **65**, 39–46.
1051 T. K. Sharma, R. Ramanathan, P. Weerathunge, M. Mohammadtaheri, H. K. Daima, R. Shukla and V. Bansal, *Chem. Commun.*, 2014, **50**, 15856–15859.
1052 C. S. Wang, C. Liu, J. B. Luo, Y. P. Tian and N. D. Zhou, *Anal. Chim. Acta*, 2016, **936**, 75–82.
1053 J. Yan, Y. F. Huang, C. H. Zhang, Z. Z. Fang, W. H. Bai, M. M. Yan, C. Zhu and A. L. Chen, *Microchim. Acta*, 2017, **184**, 59–63.
1054 J. Zhao, Y. G. Wu, H. Tao, H. Y. Chen, W. P. Yang and S. Y. Qiu, *RSC Adv.*, 2017, **7**, 38471–38478.
1055 Y. K. Xia, M. M. Liu, L. L. Wang, A. Yan, W. H. He, M. Chen, J. M. Lan, J. X. Xu, L. H. Guan and J. H. Chen, *Biosens. Bioelectron.*, 2017, **92**, 8–15.
1056 Y. X. Fang, S. J. Wang, Y. Y. Liu, Z. F. Xu, K. Zhang and Y. Guo, *Biosens. Bioelectron.*, 2018, **110**, 44–51.
1057 D. H. Hu, Z. H. Sheng, S. T. Fang, Y. N. Wang, D. Y. Gao, P. F. Zhang, P. Gong, Y. F. Ma and L. T. Cai, *Theranostics*, 2014, **4**, 142–153.
1058 S. L. Hu, X. Q. Zhang, F. C. Zang, Y. Zhang, W. Zhang, Y. H. Wu, M. J. Song, Y. H. Wang and N. Gu, *J. Nanosci. Nanotechnol.*, 2016, **16**, 1967–1974.
1059 W. Y. Zhen, Y. Liu, L. Lin, J. Bai, X. D. Jia, H. Y. Tian and X. Jiang, *Angew. Chem., Int. Ed.*, 2018, **57**, 10309–10313.
1060 K. L. Fan, C. Q. Cao, Y. X. Pan, D. Lu, D. L. Yang, J. Feng, L. N. Song, M. M. Liang and X. Y. Yan, *Nat. Nanotechnol.*, 2012, **7**, 459–464.
1061 A. Gupta, R. Das, G. Yesilbag Tonga, T. Mizuhara and V. M. Rotello, *ACS Nano*, 2018, **12**, 89–94.
1062 R. Ragg, A. M. Schilmann, K. Korschelt, C. Wieseotte, M. Kluenker, M. Viel, L. Voelker, S. Preiss, J. Herzberger, H. Frey, K. Heinze, P. Bluemler, M. N. Tahir, F. Natalio and W. Tremel, *J. Mater. Chem. B*, 2016, **4**, 7423–7428.
1063 W. Gao, X. P. Wei, X. J. Wang, G. W. Cui, Z. H. Liu and B. Tang, *Chem. Commun.*, 2016, **52**, 3643–3646.
1064 L. L. Dugan, E. G. Lovett, K. L. Quick, J. Lotharius, T. T. Lin and K. L. O'Malley, *Parkinsonism Relat. Disord.*, 2001, **7**, 243–246.
1065 L. L. Dugan, L. L. Tian, K. L. Quick, J. I. Hardt, M. Karimi, C. Brown, S. Loftin, H. Flores, S. M. Moerlein, J. Polich, S. D. Tabbal, J. W. Mink and J. S. Perlmutter, *Ann. Neurol.*, 2014, **76**, 393–402.
1066 K. L. Heckman, W. DeCoteau, A. Estevez, K. J. Reed, W. Costanzo, D. Sanford, J. C. Leiter, J. Clauss, K. Knapp, C. Gomez, P. Mullen, E. Rathbun, K. Prime, J. Marini, J. Patchefsky, A. S. Patchefsky, R. K. Hailstone and J. S. Erlichman, *ACS Nano*, 2013, **7**, 10582–10596.
1067 J. M. Dowding, W. Song, K. Bossy, A. Karakoti, A. Kumar, A. Kim, B. Bossy, S. Seal, M. H. Ellisman, G. Perkins, W. T. Self and E. Bossy-Wetzel, *Cell Death Differ.*, 2014, **21**, 1622–1632.
1068 L. L. Wong, Q. N. Pye, L. Chen, S. Seal and J. F. McGinnis, *PLoS One*, 2015, **10**, e0121977.
1069 Z. S. Bailey, E. Nilson, J. A. Bates, A. Oyalowo, K. S. Hockey, V. S. Sajja, C. Thorpe, H. Rogers, B. Dunn, A. S. Frey, M. J. Billings, C. A. Sholar, A. Hermundstad, C. Kumar, P. J. VandeVord and B. A. Rzigalinski, *J. Neurotrauma*, 2016, **33**, 1–11.
1070 H. J. Kwon, M.-Y. Cha, D. Kim, D. K. Kim, M. Soh, K. Shin, T. Hyeon and I. Mook-Jung, *ACS Nano*, 2016, **10**, 2860–2870.
1071 H. J. Kwon, D. Kim, K. Seo, Y. G. kIm, S. I. Han, T. Kang, M. Soh and T. Hyeon, *Angew. Chem., Int. Ed.*, 2018, **57**, 9408–9412.
1072 Y. J. Guan, M. Li, K. Dong, N. Gao, J. S. Ren, Y. C. Zheng and X. G. Qu, *Biomaterials*, 2016, **98**, 92–102.
1073 Q. Q. Bao, P. Hu, Y. Y. Xu, T. S. Cheng, C. Y. Wei, L. M. Pan and J. L. Shi, *ACS Nano*, 2018, **12**, 6794–6805.
1074 F. Zeng, Y. Wu, X. Li, X. Ge, Q. Guo, X. Lou, Z. Cao, B. Hu, N. J. Long, Y. Mao and C. Li, *Angew. Chem., Int. Ed.*, 2018, **57**, 5808–5812.

1075 J. Shin, S. Lee and M. Cha, *Med. Chem. Commun.*, 2017, **8**, 625–632.
1076 C. X. Ren, X. G. Hu and Q. X. Zhou, *Adv. Sci.*, 2018, **5**, 1700595.
1077 A. Clark, A. P. Zhu and H. R. Petty, *J. Nanopart. Res.*, 2013, **15**, 2126.
1078 M. Li, P. Shi, C. Xu, J. S. Ren and X. G. Qu, *Chem. Sci.*, 2013, **4**, 2536–2542.
1079 D. C. Marcano, B. R. Bitner, J. M. Berlin, J. Jarjour, J. M. Lee, A. Jacob, R. H. Fabian, T. A. Kent and J. M. Tour, *J. Neurotrauma*, 2013, **30**, 789–796.
1080 B. Xiong, R. L. Xu, R. Zhou, Y. He and E. S. Yeung, *Talanta*, 2014, **120**, 262–267.
1081 M. J. Akhtar, M. Ahamed, H. A. Alhadlaq, A. Alshamsan, M. A. M. Khan and S. A. Alrokayan, *J. Colloid Interface Sci.*, 2015, **457**, 370–377.
1082 M. J. Akhtar, M. Ahamed, H. A. Alhadlaq, M. A. M. Khan and S. A. Alrokayan, *J. Colloid Interface Sci.*, 2015, **453**, 21–27.
1083 H. Li, Z. Y. Yang, C. Liu, Y. P. Zeng, Y. H. Hao, Y. Gu, W. D. Wang and R. Li, *Free Radical Biol. Med.*, 2015, **87**, 26–35.
1084 A. B. Shcherbakov, N. M. Zholobak, A. E. Baranchikov, A. V. Ryabova and V. K. Ivanov, *Mater. Sci. Eng., C*, 2015, **50**, 151–159.
1085 J. D. Weaver and C. L. Stabler, *Acta Biomater.*, 2015, **16**, 136–144.
1086 C. Chen, S. H. Fan, C. Li, Y. Chong, X. Tian, J. W. Zheng, P. P. Fu, X. M. Jiang, W. G. Wamer and J. J. Yin, *J. Mater. Chem. B*, 2016, **4**, 7895–7901.
1087 M. Moglianetti, E. De Luca, D. Pedone, R. Marotta, T. Catelani, B. Sartori, H. Amenitsch, S. F. Retta and P. P. Pompa, *Nanoscale*, 2016, **8**, 3739–3752.
1088 E. Ju, K. Dong, Z. Wang, Y. Zhang, F. Cao, Z. Chen, F. Pu, J. Ren and X. Qu, *Chem. – Eur. J.*, 2017, **23**, 13518–13524.
1089 M. R. Khaksar, M. Rahimifard, M. Baeeri, F. Maqbool, M. Navaei-Nigjeh, S. Hassani, S. Moeini-Nodeh, A. Kebriaeezadeh and M. Abdollahi, *J. Trace Elem. Med. Biol.*, 2017, **41**, 79–90.
1090 T. M. Chen, H. Zou, X. J. Wu, C. C. Liu, B. Situ, L. Zheng and G. W. Yang, *ACS Appl. Mater. Interfaces*, 2018, **10**, 12453–12462.
1091 L. Wang, Z. J. Wang, X. M. Li, Y. Zhang, M. Yin, J. Li, H. Y. Song, J. Y. Shi, D. S. Ling, L. H. Wang, N. Chen and C. H. Fan, *Nano Res.*, 2018, **11**, 2746–2755.
1092 W. Li, Z. Liu, C. Liu, Y. Guan, J. Ren and X. Qu, *Angew. Chem., Int. Ed.*, 2017, **56**, 13661–13665.
1093 Y. Y. Huang, C. Q. Liu, F. Pu, Z. Liu, J. S. Ren and X. G. Qu, *Chem. Commun.*, 2017, **53**, 3082–3085.
1094 Y. Y. Huang, Z. Liu, C. Q. Liu, Y. Zhang, J. S. Ren and X. G. Qu, *Chem. – Eur. J.*, 2018, **24**, 10224–10230.
1095 F. Li, T. Y. Li, C. X. Sun, J. H. Xia, Y. Jiao and H. P. Xu, *Angew. Chem., Int. Ed.*, 2017, **56**, 9910–9914.
1096 D. Son, J. Lee, D. J. Lee, R. Ghaffari, S. Yun, S. J. Kim, J. E. Lee, H. R. Cho, S. Yoon, S. Yang, S. Lee, S. Qiao, D. Ling, S. Shin, J.-K. Song, J. Kim, T. Kim, H. Lee, J. Kim, M. Soh, N. Lee, C. S. Hwang, S. Nam, N. Lu, T. Hyeon, S. H. Choi and D.-H. Kim, *ACS Nano*, 2015, **9**, 5937–5946.
1097 D. Oro, T. Yudina, G. Fernandez-Varo, E. Casals, V. Reichenbach, G. Casals, B. Gonzalez de la Presa, S. Sandalinas, S. Carvajal, V. Puntes and W. Jimenez, *J. Hepatol.*, 2016, **64**, 691–698.
1098 S. Onizawa, K. Aoshiba, M. Kajita, Y. Miyamoto and A. Nagai, *Pulm. Pharmacol. Ther.*, 2009, **22**, 340–349.
1099 K. Korschelt, R. Ragg, C. S. Metzger, M. Kluenker, M. Oster, B. Barton, M. Panthofer, D. Strand, U. Kolb, M. Mondeshki, S. Strand, J. Brieger, M. Nawaz Tahir and W. Tremel, *Nanoscale*, 2017, **9**, 3952–3960.
1100 J. Yao, Y. Cheng, M. Zhou, S. Zhao, S. C. Lin, X. Y. Wang, J. J. Wu, S. R. Li and H. Wei, *Chem. Sci.*, 2018, **9**, 2927–2933.
1101 Y. Y. Huang, Z. Liu, C. Q. Liu, E. G. Ju, Y. Zhang, J. S. Ren and X. G. Qu, *Angew. Chem., Int. Ed.*, 2016, **55**, 6646–6650.
1102 D. Zhang, Y. X. Zhao, Y. J. Gao, F. P. Gao, Y. S. Fan, X. J. Li, Z. Y. Duan and H. Wang, *J. Mater. Chem. B*, 2013, **1**, 5100–5107.
1103 H. Y. Chang, J. S. Cang, P. Roy, H. T. Chang, Y. C. Huang and C. C. Huang, *ACS Appl. Mater. Interfaces*, 2014, **6**, 8305–8312.
1104 S. F. Cai, X. H. Jia, Q. S. Han, X. Y. Yan, R. Yang and C. Wang, *Nano Res.*, 2017, **10**, 2056–2069.
1105 Y. M. Ye, L. L. Xiao, B. He, Q. Zhang, T. Nie, X. R. Yang, D. B. Wu, H. L. Cheng, P. Li and Q. G. Wang, *J. Mater. Chem. B*, 2017, **5**, 1518–1524.
1106 X. Zhang, L. Liu, R. Liu, J. Wang, X. Hu, Q. Yuan, J. Guo, G. Xing, Y. Zhao and X. Gao, *Sci. China: Chem.*, 2018, **61**, 627–634.
1107 S. Bukhari, D. Kim, Y. Liu, B. Karabucak and H. Koo, *J. Endod.*, 2018, **44**, 806–812.
1108 H. S. Tuli, D. Kashyap, S. K. Bedi, P. Kumar, G. Kumar and S. S. Sandhu, *Life Sci.*, 2015, **143**, 71–79.
1109 Y. Tao, E. G. Ju, J. S. Ren and X. G. Qu, *Adv. Mater.*, 2015, **27**, 1097–1104.
1110 W. Y. Pan, C. C. Huang, T. T. Lin, H. Y. Hu, W. C. Lin, M. J. Li and H. W. Sung, *Nanomedicine*, 2016, **12**, 431–438.
1111 C. J. Pandian, R. Palanivel and U. Balasundaram, *J. Photochem. Photobiol., B*, 2017, **174**, 58–69.
1112 Q. W. Wu, G. Wei, Z. B. Xu, J. Han, J. Q. Xi, L. Fan and L. Z. Gao, *ACS Appl. Mater. Interfaces*, 2018, **10**, 25026–25036.
1113 W. Y. Yin, J. Yu, F. T. Lv, L. Yan, L. R. Zheng, Z. J. Gu and Y. L. Zhao, *ACS Nano*, 2016, **10**, 11000–11011.
1114 E. Alpaslan, H. Yazici, N. H. Golshan, K. S. Ziemer and T. J. Webster, *ACS Biomater. Sci. Eng.*, 2015, **1**, 1096–1103.
1115 J. K. Fu, Y. R. Shao, L. Y. Wang and Y. C. Zhu, *Nanoscale*, 2015, **7**, 7275–7283.
1116 S. K. Maji, A. K. Mandal, K. T. Nguyen, P. Borah and Y. L. Zhao, *ACS Appl. Mater. Interfaces*, 2015, **7**, 9807–9816.
1117 C. Zhang, W. B. Bu, D. L. Ni, S. J. Zhang, Q. Li, Z. W. Yao, J. W. Zhang, H. L. Yao, Z. Wang and J. L. Shi, *Angew. Chem., Int. Ed.*, 2016, **55**, 2101–2106.

1118 S. Y. Fu, S. Wang, X. D. Zhang, A. H. Qi, Z. R. Liu, X. Yu, C. F. Chen and L. L. Li, *Colloids Surf., B*, 2017, **154**, 239–245.
1119 P. Brenneisen and A. S. Reichert, *Antioxidants*, 2018, **7**, 31.
1120 L. Y. Wang, M. F. Huo, Y. Chen and J. L. Shi, *Biomaterials*, 2018, **163**, 1–13.
1121 M. F. Huo, L. Y. Wang, Y. Chen and J. L. Shi, *Nat. Commun.*, 2017, **8**, 357.
1122 J. Kim, H. R. Cho, H. Jeon, D. Kim, C. Song, N. Lee, S. H. Choi and T. Hyeon, *J. Am. Chem. Soc.*, 2017, **139**, 10992–10995.
1123 Y. Zhang, F. Wang, C. Liu, Z. Wang, L. Kang, Y. Huang, K. Dong, J. Ren and X. Qu, *ACS Nano*, 2018, **12**, 651–661.
1124 M. S. Wason, J. Colon, S. Das, S. Seal, J. Turkson, J. Zhao and C. H. Baker, *Nanomedicine*, 2013, **9**, 558–569.
1125 K. Zhang, Z. Yang, X. D. Meng, Y. Cao, Y. D. Zhang, W. H. Dai, H. T. Lu, Z. F. Yu, H. F. Dong and X. J. Zhang, *Mater. Chem. Front.*, 2018, **2**, 1184–1194.
1126 S. Prylutska, I. Grynyuk, O. Matyshevska, Y. Prylutskyy, M. Evstigneev, P. Scharff and U. Ritter, *Drugs R&D.*, 2014, **14**, 333–340.
1127 L. Fan, X. D. Xu, C. H. Zhu, J. Han, L. Z. Gao, J. Q. Xi and R. Guo, *ACS Appl. Mater. Interfaces*, 2018, **10**, 4502–4511.
1128 Y. Liu, W. Zhen, L. Jin, S. Zhang, G. Sun, T. Zhang, X. Xu, S. Song, Y. Wang, J. Liu and H. Zhang, *ACS Nano*, 2018, **12**, 4886–4893.
1129 L. Tan, J. Wan, W. Guo, C. Ou, T. Liu, C. Fu, Q. Zhang, X. Ren, X. J. Liang, J. Ren, L. Li and X. Meng, *Biomaterials*, 2018, **159**, 108–118.
1130 S. Chigurupati, M. R. Mughal, E. Okun, S. Das, A. Kumar, M. McCaffery, S. Seal and M. P. Mattson, *Biomaterials*, 2013, **34**, 2194–2201.
1131 S. Giri, A. Karakoti, R. P. Graham, J. L. Maguire, C. M. Reilly, S. Seal, R. Rattan and V. Shridhar, *PLoS One*, 2013, **8**, e54578.
1132 Q. Y. Li, G. H. Tang, S. H. Xue, X. S. He, P. Miao, Y. N. Li, J. X. Wang, L. Q. Xiong, Y. T. Wang, C. F. Zhang and G. Y. Yang, *Biomaterials*, 2013, **34**, 4982–4992.
1133 X. Q. Wang, Q. Tu, B. Zhao, Y. F. An, J. C. Wang, W. M. Liu, M. S. Yuan, S. M. Ahmed, J. Xu, R. Liu, Y. R. Zhang and J. Y. Wang, *Biomaterials*, 2013, **34**, 1155–1169.
1134 X. Cai, S. Seal and J. F. McGinnis, *Biomaterials*, 2014, **35**, 249–258.
1135 M. B. Kolli, N. D. P. K. Manne, R. Para, S. K. Nalabotu, G. Nandyala, T. Shokuhfar, K. He, A. Hamlekhan, J. Y. Ma, P. S. Wehner, L. Dornon, R. Arvapalli, K. M. Rice and E. R. Blough, *Biomaterials*, 2014, **35**, 9951–9962.
1136 S. Ponnurangam, G. D. O'Connell, I. V. Chernyshova, K. Wood, C. T. H. Hung and P. Somasundaran, *Tissue Eng., Part A*, 2014, **20**, 2908–2919.
1137 Z. Liu, X. J. Liu, Y. D. Du, J. S. Ren and X. G. Qu, *ACS Nano*, 2015, **9**, 10335–10346.
1138 M. Moriyama, S. Metzger, A. J. van der Vlies, H. Uyama, M. Ehrbar and U. Hasegawa, *Adv. Healthcare Mater.*, 2015, **4**, 569–575.
1139 V. Selvaraj, N. Nepal, S. Rogers, N. D. P. K. Manne, R. Arvapalli, K. M. Rice, S. Asano, E. Fankhanel, J. J. Ma, T. Shokuhfar, M. Maheshwari and E. R. Blough, *Biomaterials*, 2015, **59**, 160–171.
1140 F. Xiong, H. Wang, Y. D. Feng, Y. M. Li, X. Q. Hua, X. Y. Pang, S. Zhang, L. Song, Y. Zhang and N. Gu, *Sci. Rep.*, 2015, **5**, 8579.
1141 Q. W. Wang, B. Chen, M. Cao, J. F. Sun, H. Wu, P. Zhao, J. Xing, Y. Yang, X. Q. Zhang, M. Ji and N. Gu, *Biomaterials*, 2016, **86**, 11–20.
1142 Y. Zhang, Z. Y. Wang, X. J. Li, L. Wang, M. Yin, L. H. Wang, N. Chen, C. H. Fan and H. Y. Song, *Adv. Mater.*, 2016, **28**, 1387–1393.
1143 S. Shibuya, Y. Ozawa, K. Watanabe, N. Izuo, T. Toda, K. Yokote and T. Shimizu, *PLoS One*, 2014, **9**, e109288.
1144 T. K. Sharma, R. Ramanathan, R. Rakwal, G. K. Agrawal and V. Bansal, *Proteomics*, 2015, **15**, 1680–1692.
1145 N. Pan, Y. Zhu, L. L. Wu, Z. J. Xie, F. Xue and C. F. Peng, *Anal. Methods*, 2016, **8**, 7531–7536.
1146 Y. W. Wang, S. Tang, H. H. Yang and H. Song, *Talanta*, 2016, **146**, 71–74.
1147 L. L. Wu, L. Y. Wang, Z. J. Xie, F. Xue and C. F. Peng, *RSC Adv.*, 2016, **6**, 75384–75389.
1148 Y. Zhao, H. Qiang and Z. B. Chen, *Microchim. Acta*, 2016, **184**, 107–115.
1149 A. J. Kora and L. Rastogi, *Sens. Actuators, B*, 2018, **254**, 690–700.
1150 C. Chen, I. Ahmed and L. Fruk, *Nanoscale*, 2013, **5**, 11610–11614.
1151 Y. Y. Liu, Z. W. Chen, C. H. Shek, C. M. L. Wu and J. K. L. Lai, *ACS Appl. Mater. Interfaces*, 2014, **6**, 9776–9784.
1152 R. Qu, L. L. Shen, Z. H. Chai, C. Jing, Y. F. Zhang, Y. L. An and L. Q. Shi, *ACS Appl. Mater. Interfaces*, 2014, **6**, 19207–19216.
1153 P. V. R. K. Ramacharyulu, J. Praveen Kumar, G. K. Prasad, B. Singh, B. Sreedhar and K. Dwivedi, *J. Mol. Catal. A: Chem.*, 2014, **387**, 38–44.
1154 Y. Y. Huang, X. Ran, Y. H. Lin, J. S. Ren and X. G. Qu, *Chem. Commun.*, 2015, **51**, 4386–4389.
1155 A. H. Nadim, M. A. Al-Ghobashy, M. Nebsena and M. A. Shehata, *RSC Adv.*, 2015, **5**, 104981.
1156 P. Roy, L.-C. Ho, P. A. Prakash, Y.-S. Lin, M.-F. Huang and H.-T. Chang, *Sci. Lett. J.*, 2015, **4**, 120.
1157 J. S. Mu, J. Li, X. Zhao, E. C. Yang and X. J. Zhao, *RSC Adv.*, 2016, **6**, 35568–35576.
1158 X. P. Wang, C. Hou, W. Qiu, Y. P. Ke, Q. C. Xu, X. Y. Liu and Y. H. Lin, *ACS Appl. Mater. Interfaces*, 2017, **9**, 684–692.
1159 X. F. Yan, K. F. Gan, B. Z. Tian, J. L. Zhang, L. Z. Wang and D. L. Lu, *Res. Chem. Intermed.*, 2018, **44**, 1–11.

1160 A. Zeb, S. Sahar, U. Y. Qazi, A. H. Odda, N. Ullah, Y.-N. Liu, I. A. Qazi and A.-W. Xu, *Dalton Trans.*, 2018, **47**, 7344–7352.
1161 W. Wang, Q. Mao, H. H. He and M. H. Zhou, *Water Sci. Technol.*, 2013, **68**, 2367–2373.
1162 X. N. Duan, S. C. Corgie, D. J. Aneshansley, P. Wang, L. P. Walker and E. P. Giannelis, *ChemPhysChem*, 2014, **15**, 974–980.
1163 R. X. Huang, Z. Q. Fang, X. B. Fang and E. P. Tsang, *J. Colloid Interface Sci.*, 2014, **436**, 258–266.
1164 Y. L. Qin, M. C. Long, B. H. Tan and B. X. Zhou, *Nano-Micro Lett.*, 2014, **6**, 125–135.
1165 H. Wang, H. Jiang, S. Wang, W. B. Shi, J. C. He, H. Liu and Y. M. Huang, *RSC Adv.*, 2014, **4**, 45809–45815.
1166 W. Wang, Y. Liu, T. L. Li and M. H. Zhou, *Chem. Eng. J.*, 2014, **242**, 1–9.
1167 X. S. Wang, H. Huang, G. Q. Li, Y. Liu, J. L. Huang and D. P. Yang, *Nanoscale Res. Lett.*, 2014, **9**, 648.
1168 T. Zeng, X. L. Zhang, S. H. Wang, Y. R. Ma, H. Y. Niu and Y. Q. Cai, *Chem. – Eur. J.*, 2014, **20**, 6474–6481.
1169 X. L. Zhang, M. L. He, J. H. Liu, R. Liao, L. Q. Zhao, J. R. Xie, R. J. Wang, S. T. Yang, H. F. Wang and Y. F. Liu, *Chin. Sci. Bull.*, 2014, **59**, 3406–3412.
1170 R. Cheng, C. Cheng, G. H. Liu, X. Zheng, G. Q. Li and J. Li, *Chemosphere*, 2015, **141**, 138–143.
1171 G. F. Liu, N. Wang, J. T. Zhou, A. J. Wang, J. Wang, R. F. Jin and H. Lv, *RSC Adv.*, 2015, **5**, 95857–95865.
1172 M. Munoz, Z. M. de Pedro, J. A. Casas and J. J. Rodriguez, *Appl. Catal., B*, 2015, **176**, 249–265.
1173 Y. F. Qin, Z. Y. Qin, Y. N. Liu, M. Cheng, P. F. Qian, Q. Wang and M. F. Zhu, *Appl. Surf. Sci.*, 2015, **357**, 2103–2111.
1174 D. Wan, W. B. Li, G. H. Wang, K. Chen, L. L. Lu and Q. Hu, *Appl. Surf. Sci.*, 2015, **349**, 988–996.
1175 S. T. Yang, L. J. Yang, X. Y. Liu, J. R. Xie, X. L. Zhang, B. W. Yu, R. H. Wu, H. L. Li, L. Y. Chen and J. H. Liu, *Sci. China: Technol. Sci.*, 2015, **58**, 858–863.
1176 D. X. Nie, G. Y. Shi and Y. Y. Yu, *Chin. J. Anal. Chem.*, 2016, **44**, 179–184.
1177 H. Y. Xu, T. N. Shi, H. Zhao, L. G. Jin, F. C. Wang, C. Y. Wang and S. Y. Qi, *Front. Mater. Sci.*, 2016, **10**, 45–55.
1178 F. X. Chen, S. L. Xie, X. L. Huang and X. H. Qiu, *J. Hazard. Mater.*, 2017, **322**, 152–162.
1179 W. Chen, L. S. Xiong and F. X. Chen, *Micro Nano Lett.*, 2017, **12**, 711–713.
1180 D. Wan, W. B. Li, G. H. Wang, L. L. Lu and X. B. Wei, *Sci. Total Environ*, 2017, **574**, 1326–1334.
1181 D. Wan, G. H. Wang, W. B. Li and X. B. Wei, *Appl. Surf. Sci.*, 2017, **413**, 398–407.
1182 Q. Sun, Y. Hong, Q. H. Liu and L. F. Dong, *Appl. Surf. Sci.*, 2018, **430**, 399–406.
1183 X. K. Tang, Q. M. Feng, K. Liu, Z. S. Li and H. Wang, *J. Mater. Sci.*, 2018, **53**, 369–384.
1184 P. Janos, P. Kuran, M. Kormunda, V. Stengl, T. M. Grygar, M. Dosek, M. Stastny, J. Ederer, V. Pilarova and L. Vrtoch, *J. Rare Earths*, 2014, **32**, 360–370.
1185 P. Janos, J. Henych, O. Pelant, V. Pilarova, L. Vrtoch, M. Kormunda, K. Mazanec and V. Stengl, *J. Hazard. Mater.*, 2016, **304**, 259–268.
1186 S. Wang, L. Bromberg, H. Schreuder-Gibson and T. A. Hatton, *ACS Appl. Mater. Interfaces*, 2013, **5**, 1269–1278.
1187 J. B. Decoste and G. W. Peterson, *Chem. Rev.*, 2014, **114**, 5695–5727.
1188 Y. Y. Liu, S.-Y. Moon, J. T. Hupp and O. K. Farha, *ACS Nano*, 2015, **9**, 12358–12364.
1189 A. Atilgan, T. Islamoglu, A. J. Howarth, J. T. Hupp and O. K. Farha, *ACS Appl. Mater. Interfaces*, 2017, **9**, 24555–24560.
1190 Y. Q. Li, Q. Gao, L. J. Zhang, Y. S. Zhou, Y. X. Zhong, Y. Ying, M. C. Zhang, C. Q. Huang and Y. A. Wang, *Dalton Trans.*, 2018, **47**, 6394–6403.
1191 K. Herget, P. Hubach, S. Pusch, P. Deglmann, H. Goetz, T. E. Gorelik, I. y. A. Gural'skiy, F. Pfitzner, T. Link, S. Schenk, M. Panthoefer, V. Ksenofontov, U. Kolb, T. Opatz, R. Andre and W. Tremel, *Adv. Mater.*, 2017, **29**, 1603823.
1192 L. Z. Gao, Y. Liu, D. Kim, Y. Li, G. Hwang, P. C. Naha, D. P. Cormode and H. Koo, *Biomaterials*, 2016, **101**, 272–284.
1193 L. Z. Gao, K. M. Giglio, J. L. Nelson, H. Sondermann and A. J. Travis, *Nanoscale*, 2014, **6**, 2588–2593.
1194 Y. Liu, P. C. Naha, G. Hwang, D. Kim, Y. Huang, A. Simon-Soro, H.-I. Jung, Z. Ren, Y. Li, S. Gubara, F. Alawi, D. Zero, A. T. Hara, D. P. Cormode and H. Koo, *Nat. Commun.*, 2018, **9**, 2920.
1195 Z. W. Chen, H. W. Ji, C. Q. Liu, W. Bing, Z. Z. Wang and X. G. Qu, *Angew. Chem., Int. Ed.*, 2016, **55**, 10732–10736.
1196 C. W. Lien, Y. C. Chen, H. T. Chang and C. C. Huang, *Nanoscale*, 2013, **5**, 8227–8234.
1197 B. Lin, Q. Q. Sun, K. Liu, D. Q. Lu, Y. Fu, Z. A. Xu and W. Zhang, *Langmuir*, 2014, **30**, 2144–2151.
1198 P. F. Zhan, J. Y. Wang, Z. G. Wang and B. Q. Ding, *Small*, 2014, **10**, 399–406.
1199 Y. Y. Huang, F. Pu, J. S. Ren and X. G. Qu, *Chem. – Eur. J.*, 2017, **23**, 9156–9161.
1200 X. D. Lin, Y. Q. Liu, Z. H. Tao, J. T. Gao, J. K. Deng, J. J. Yin and S. Wang, *Biosens. Bioelectron.*, 2017, **94**, 471–477.
1201 V. Sharma and S. M. Mobin, *Sens. Actuators, B*, 2017, **240**, 338–348.
1202 C. H. Wang, J. Gao, Y. L. Cao and H. L. Tan, *Anal. Chim. Acta*, 2018, **1004**, 74–81.
1203 Y. H. Lin, C. Xu, J. S. Ren and X. G. Qu, *Angew. Chem., Int. Ed.*, 2012, **51**, 12579–12583.
1204 C. W. Lien, Y. T. Tseng, C. C. Huang and H. T. Chang, *Anal. Chem.*, 2014, **86**, 2065–2072.
1205 J. K. Nørskov, F. Studt, F. Abild-Pedersen and T. Bligaard, *Fundamental Concepts in Heterogeneous Catalysis*, John Wiley & Sons, Inc., Hoboken, New Jersey, 2014.
1206 A. J. Medford, A. Vojvodic, J. S. Hummelshøj, J. Voss, F. Abild-Pedersen, F. Studt, T. Bligaard, A. Nilsson and J. K. Nørskov, *J. Catal.*, 2015, **328**, 36–42.

1207 R. F. Parton, I. F. J. Vankelecom, M. J. A. Casselman, C. P. Bezoukhanova, J. B. Uytterhoeven and P. A. Jacobs, *Nature*, 1994, **370**, 541.
1208 Z. J. Zhang, Y. B. Liu, X. H. Zhang and J. W. Liu, *Nano Lett.*, 2017, **17**, 7926–7931.
1209 E. Golub, H. B. Albada, W.-C. Liao, Y. Biniuri and I. Willner, *J. Am. Chem. Soc.*, 2016, **138**, 164–172.
1210 Y. H. Hu, PhD thesis, Nanjing University, 2017.
1211 Y. Hu, X. J. Gao, Y. Zhu, F. Muhammad, S. Tan, W. Cao, S. Lin, Z. Jin, X. Gao and H. Wei, *Chem. Mater.*, 2018, **30**, 6431–6439.
1212 B. Jiang, D. Duan, L. Gao, M. Zhou, K. Fan, Y. Tang, J. Xi, Y. Bi, Z. Tong, G. F. Gao, N. Xie, A. Tang, G. Nie, M. Liang and X. Yan, *Nat. Protoc.*, 2018, **13**, 1506–1520.

